

Sheffield Hallam University

Shape distortion and air gap formation during continuous casting.

DELMONT, Andres Emilio.

Available from the Sheffield Hallam University Research Archive (SHURA) at:

<http://shura.shu.ac.uk/19549/>

A Sheffield Hallam University thesis

This thesis is protected by copyright which belongs to the author.

The content must not be changed in any way or sold commercially in any format or medium without the formal permission of the author.

When referring to this work, full bibliographic details including the author, title, awarding institution and date of the thesis must be given.

Please visit <http://shura.shu.ac.uk/19549/> and <http://shura.shu.ac.uk/information.html> for further details about copyright and re-use permissions.

SHEFFIELD ST 1W

794846601 0

TELEPEN



SHEFFIELD CITY
POLYTECHNIC LIBRARY
FOND STREET
SHEFFIELD S1 1WB

Sheffield City Polytechnic Library

REFERENCE ONLY

2055

Fines are charged at 50p per hour

16 FEB 2005

ProQuest Number: 10694430

All rights reserved

INFORMATION TO ALL USERS

The quality of this reproduction is dependent upon the quality of the copy submitted.

In the unlikely event that the author did not send a complete manuscript and there are missing pages, these will be noted. Also, if material had to be removed, a note will indicate the deletion.



ProQuest 10694430

Published by ProQuest LLC (2017). Copyright of the Dissertation is held by the Author.

All rights reserved.

This work is protected against unauthorized copying under Title 17, United States Code
Microform Edition © ProQuest LLC.

ProQuest LLC.
789 East Eisenhower Parkway
P.O. Box 1346
Ann Arbor, MI 48106 – 1346

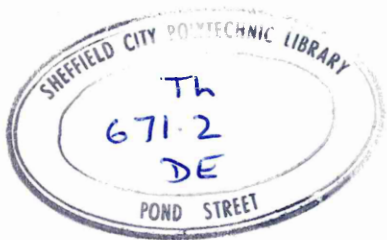
**SHAPE DISTORTION AND AIR GAP FORMATION
DURING CONTINUOUS CASTING**

by

Andres Emilio Delmont Mauri

This thesis is submitted in part fulfilment of the requirements for the Degree of Doctor of Philosophy of the Council for National Academic Awards. The work was carried out at Sheffield City Polytechnic, Department of Metals and Materials Engineering, in collaboration with British Steel Corporation.

February 1985



7948466-01

PREFACE

This thesis is submitted in part fulfilment of the requirements for the Degree of Doctor of Philosophy of the Council for National Awards. The research described was carried out during the period from January 1979 to January 1985 in the Department of Metals and Materials Engineering (formerly Department of Metallurgy) at the Sheffield City Polytechnic. No part of this dissertation has been submitted for a degree at any other University or College.

During the period of this work the author attended the following lectures which constituted part of the MSc in Metallurgical Process Management at the Sheffield City Polytechnic:

Module I	Process Metallurgy. Mechanical Metallurgy. Advanced Thermodynamics.
Module II	Computational Methods and Numerical Analysis. Accountancy. Micro-Economics and Financial Control.
Module III	High Strength Steels. Ironmaking. Heat treatment and transformations. Secondary Steelmaking. Oxygen Steelmaking. Metals and competitive Materials
Module IV	Case Studies in the subject areas of: Heat Treatment and Transformations. Ironmaking. Health & Safety in the Continuous Casting of Steels. (Appendix 3 of this dissertation)

The Candidate's performance during the above-mentioned courses has been satisfactorily assessed by means of specific assignments.

ACKNOWLEDGEMENTS

I would like to thank my supervisor Dr A W D Hills for the guidance he has given me during the course of this work. Especial thanks go to Ms L Pearse, Ms D Cosham, Ms P Oldfield, Mr R Day, Mr D Rimmer, Mr D Latimer, Mr B Taylor, Mr R Grant, Mr N Dziemidko, for their help and friendship. The suggestions and assistance of Mr M Muldownie, Mr R Daniel, Ms D Mullen, Mr J Bradshaw, Mr R Dimberline, Mr P Fletcher, Mr J Ross-Smith, Mr R Thomas, Mr B Palmer, Mr P Slingsby, Mr B Dodds, Mr G Gregory, Dr F B Pickering, Dr A J Fletcher and Dr G Briggs, from the Department of Metals and Materials Engineering, Dr A C Baker, from the Department of Mathematics, Statistics & Operational Research, Dr N W Taylor, from the Department of Civil Engineering, and Dr M S J Hashmi, from the Department of Mechanical and Production Engineering, are gratefully acknowledged. I would like to thank Dr I G Davies from the British Steel Corporation for his advice. Finally I would like to express my gratitude to my fellow students Mr J Soady, Mr A Bott, Ms M Staia, Mr J Duncombe, Mr H Cuicas and Mr M Simon for their advice and encouragement throughout this work.

I would like to acknowledge the Consejo Nacional de Investigaciones Cientificas y Technologicas for its financial support.

SHAPE DISTORTION AND AIR GAP FORMATION DURING CONTINUOUS CASTING

by Andres Emilio Delmont Mauri

ABSTRACT

A theoretical model has been developed which relates the build-up of stresses in the thin shell of steel solidifying in a continuously casting mould, to the shape distortion and the formation of an air gap. The work postulates that the behaviour of this shell can be analysed as that of a flexible structure formed by four elasto-perfectly plastic beams linked by rigid corners. This "box" represents the whole section of solidified shell at a given metallurgical height only if the section is totally detached from the mould. In general, it represents the detached corner portions alone. The rest of the shell is assumed to remain clamped against the mould wall by the metallostatic pressure. The thermal contraction of the neutral axis "filament" along the whole shell determines the amount of room which is available for the detached corner portion to distort, and thus also the size of the detached lengths of shell. The mechanical equilibrium of the structure is determined by the combined effect of temperature gradients and metallostatic pressure, by the rigidity condition imposed at the corner and by the flexural characteristics of the shell. The yield stress of the steel is assumed linearly dependent on temperature.

The analysis of the shape distortion and air gap formation was initially informed by the observed behaviour of a partial physical analogue constructed from bi-metallic strips linked by rigid corners. Thermal moments were induced by immersing this analogue in a water bath at controlled temperatures, and distributed loads were imposed through a system of pulleys. The elastic behaviour of this physical analogue was predicted using basic beam theory.

For the analysis of the deformation of a continuously cast structure, mathematical equations were derived which describe the overall moment and force equilibrium; the elastic and plastic stress distribution across the thickness of the shell; and the force and moment equilibrium within the cross-section of the shell. An equation was derived relating the curvature at any point along the shell to the moment at the corner of the structure. An iterative procedure was developed to determine the moment at the corner and a Runge-Kutta algorithm was incorporated to integrate the curvature equation. Further equations were derived which relate the deflection at the corner and the detached length on one side of the section, to the total length of the other side of the section.

Recent high temperature studies of the mechanical behaviour of steels have been analysed in terms of the theoretical model developed. The model is able to predict the extent and thickness of the air gaps forming in the corner regions during the casting of billets and slabs and also provides explanation for the formation of both internal and external off-corner cracks. It also demonstrates the theoretical basis behind the practically observed relationship between casting speed and crack formation.

TABLE OF CONTENTS

	Page
PREFACE	
ACKNOWLEDGEMENTS	
ABSTRACT	
LIST OF SYMBOLS	
LIST OF FIGURES	
LIST OF TABLES	
CHAPTER 1	
INTRODUCTION	1:1 to 1:4
CHAPTER 2	
LITERATURE REVIEW	
2.1 Gap formation in continuous casting.	2:1
2.2 Empirical evidence.	2:2
2.3 Theoretical models.	2:16
2.4 Mathematical models.	2:20
2.5 Mechanical properties of steels at high temperatures.	2:26 to 2:33
CHAPTER 3	
EXPERIMENTAL DEVELOPMENT OF BIMETALLIC STRUCTURE ANALOGUE	
3.1 Stages of development,	
Introduction.	3:1
Selection of the bimetal.	3:2
Rigid corner bimetallic structure.	3:9
The use of longer bimetallic strips.	3:18
3.2 Bimetallic structure analogue,	
Introduction.	3:47
Description of the apparatus.	3:48 to 3:57
(...)	

CHAPTER 4

DERIVATION OF THE EQUATIONS FOR THE MATHEMATICAL MODELING OF THE DEFORMATION OF A CONTINUOUSLY CAST STRUCTURE

4.1	Preliminary statement of the model.	4:1
4.2	The overall moment and force equilibrium equations.	4:11
4.3	The stress distribution across the thickness of the beams.	4:17
4.4	Plastic and elastic stress.	4:26
4.5	The cross-section force and moment equilibrium equations.	4:35
4.6	The curvature as a function of the moment at the corner.	4:38
4.7	The deflection of the structure.	4:46
4.8	The restraining presence of the mould.	4:52
4.9	Data used for the initial predictions.	4:60 to 4:63

CHAPTER 5

COMPUTER PROGRAM

5:1
to 5:17

CHAPTER 6

RESULTS

6.1	Preliminary analysis of the behaviour of the model.	6:1
6.2	Square billets within the mould.	6:17
6.3	Effect of halving the length of corner assumed rigid on the results predicted for billets within the mould.	6:42
6.4	Effect of reducing the assumed value of the quasi-static yield stress at 1000 degC on the results predicted for billets within the mould.	6:52
6.5	Effect of doubling the Young's modulus on the results predicted for billets within the mould.	6:60
6.6	Analysis of off-corner cracking in a slab	6:68

(...)

6.7	Analysis of crack progression within the mould during the casting of square billets.	6:74 to 6:88
CHAPTER 7		
	DISCUSSION	7:1
7.1	Distortion and stress distribution.	7:4
7.2	The formation and propagation of longitudinal off-corner cracks.	7:12
7.3	Characteristic behaviour of the model.	7:24
7.4	Effect of the assumptions made.	7:36
7.5	The bi-metallic strips analogue.	7:42
CHAPTER 8		
	CONCLUSIONS AND FURTHER WORK	8:1 to 8:3
REFERENCES		
APPENDIX 1		
	DERIVATION OF THE EQUATIONS FOR THE MATHEMATICAL MODELLING OF THE DEFORMATION OF THE BIMETALLIC STRUCTURE ANALOGUE.	
A1.1	Characteristics and thermal behaviour of bimetallic strips.	A1:3
A1.2	The effect of thermal stress upon the structure.	A1:10
A1.3	The effect of the load upon the structure.	A1:19 to A1:43
APPENDIX 2		
	BIMETALLIC STRIPS STRUCTURE MODEL COMPUTER PROGRAM	A2:1 to A2:8
APPENDIX 3		
	CASE STUDY: HEALTH & SAFETY IN THE CONTINUOUS CASTING OF STEEL	A3:1 to A3:16

LIST OF SYMBOLS

a	The length of the corner considered rigid, [m]
al	Coefficient of thermal expansion of the solid metal, [$^{\circ}\text{C}^{-1}$]
$c_1(u)$	Coefficient in the linear stress distribution function = to the stress at the cooling wall at position u, [N.m^{-2}]
$c_2(u)$	Coefficient in the linear stress distribution function = to the stress gradient between the cooling wall and the elastoplastic boundary at position u, [N.m^{-3}]
$c(u)$	Curvature of the beam at position u, [m^{-1}]
d_1 or d_2	Lengths of two filaments at different distances from cooling wall, [m]
E	Young's Modulus
f	Axial force per unit depth of solidified shell applied to a node, [N.m^{-1}]
ft	Transverse force per unit depth of solidified shell applied to a beam at the rigid corner, [N.m^{-1}]
g	Acceleration due to gravity, [m.s^{-2}]
k	Exponent to determine the sign of the plastic stress, [see page 4:26]
l	The length of the the solidified shell unsupported by the mould in half the length or width of the ingot cross section, [m]
m	Moment per unit depth of solidified shell applied at a node, [N]
meth	Metallurgical height - distance below metal meniscus, [m]
$m(u)$	Moment per unit depth of solidified shell in the solid shell at generic coordinate u, [N]
* a *	Generic corner node of the generic beam (a = 3), [(See Pages 4 13-15)]
* b *	Generic node at the rigid boundary of the generic beam (b = 2 or 4), [(See Pages 4 13-15)]

- * c * Generic node at the rigid boundary of the generic beam ($c = 1$ or 5), [(See Pages 4:13-15)]
- n(u) or n** Distance across the solidified shell from the cooling wall to the neutral axis at a position u , [m]
- p(u) or p** Distance across the solidified shell from the cooling wall to the elastoplastic boundary at a position u , [m]
- q** Liquid metal pressure exerted on solidified shell, [$\text{N}\cdot\text{m}^{-2}$]
- r(u) or r** Radius of curvature of the beam at position u measured from the cooling wall, [m]
- so** The stress in the solidified shell at the cooling wall, [$\text{N}\cdot\text{m}^{-2}$]
- s(u,v)** The stress in the solidified shell at a distance v from the cooling wall. [$\text{N}\cdot\text{m}^{-2}$]
- t** Thickness of solidified metal, [m]
- T** Temperature [$^{\circ}\text{C}$]
- T_c** The temperature of the cooling wall, [$^{\circ}\text{C}$]
- T_s** The solidification temperature, [$^{\circ}\text{C}$]
- T(v)** Temperature in the solidified shell at a distance v from the cooling wall, [$^{\circ}\text{C}$]
- u** Coordinate distance along the generic beam from the corner edge, [m]
- v** distance across the generic beam from the cooling wall, [m]
- w(u)** Deflection of the generic beam at position u , [m]
- x,y** Coordinates in a system whose origin lies in the corner when there is no distortion - distances towards the liquid core taken as positive, [m]
- Yo** Absolute magnitude of the yield stress of the solidified shell at the cooling wall, [$\text{N}\cdot\text{m}^{-2}$]
- Y(v)** Absolute magnitude of the yield stress of the solidified shell at a distance v from the cooling wall, [$\text{N}\cdot\text{m}^{-2}$]

Symbols used in **Appendix 1** are defined on page A1:4 and subsequently in the text.

ADIMENSIONAL VARIABLES

A	Length of the corner considered rigid, [See page 4 41]
Al	Coefficient of thermal expansion, [See page 4:41]
C	Curvature of beam [See page 4:46]
E*	Young's modulus, [See page 4:40]
F	Force, [See page 4:39]
L	Length of the unsupported shell, [See page 4:41]
M	Moment, [See page 4:39]
N	Position of the neutral axis, [See page 4:41]
P	Position of the elastoplastic boundary, [See page 4:41]
Q	Liquid metal pressure, [See page 4:40]
S	Stress, [See page 4:39]
So	Stress at the cooling wall, [-]
V	Distance from the cooling surface [See page 4 40]
U	Distance from the corner, [See page 4:41]
W	Deflection, [See page 4:46]
Y _p	Stress at the elastoplastic boundary, [-]

SUFFICES

1,2	Related to the two adjacent sides of an ingot when applied to 1, [-]
1 - 5	Related to the nodes * 1 * to * 5 *, [See Figure 6 on page 4:13]
a,b or c	Related to the nodes * a *, [* b * or * c *]
i	Related to the side i of an ingot, [-]
ii	Related to the adjacent side of the ingot, [-]

SUPERFIX

0,i	Superfix relating to the current iteration value of the corner moment - M_3 , [-]
-----	---

LIST OF FIGURES

The figures and pages in each chapter are numbered separately, the page numbers being a two part sequence. The first digit in the sequence represents the chapter number, the second one or two digits represents the page number in the chapter

Explicit reference to the chapter in which a figure appears is not made in this list of figures since the chapter reference is embedded in the page number.

Page	Figure:	
	No.	Title
2:3	1	Rate of heat transfer from ingot to mould.(4)
2:5	2	Contact sensor pattern and % contact time vs depth. (from L.S.Rudol, ref.11)
2:5	3	Variation in gap size along wide face d_1 and narrow face d_2 .
2:6	4	Mould heat flux as function of distance from top of mould for various casting speeds.(19)
2:9	5	Extent of solidification front non-uniformity over length of continuously cast strand.(17)
2:9	6	Coefficient of non-uniformity of thickness (17)
2:9	7	Coefficient of non-uniformity of thickness (17)
2:9	8	Effect of melt flow rate from steel casting nozzle.(17)
2:13	9	Location of thermocouples in copper mould (22)
2:13	10	Chemical analysis, mould-wall temperature and mould heat transfer for the heats investigated.(22)
2:14	11	Effect of carbon content on mould heat-transfer rate continuous casting.(22)
2:14	12	Temperature variation for the thermocouple located 1-1/2 in below the meniscus. (22)
2:15	13	Effect of carbon content on mould friction during continuous casting.(22)
2:15	14	As-cast surface on 0.10% and 0.40% carbon steels that have been shot-blasted.(22)
2:27	15	Reported mechanical properties of steel.(67)
2:31	16	Stress-strain curves for low carbon steel.(52)

- 2:31 17 Stress-strain curves for n.2 and n.3 high carbon steels.(52)
- 2:33 18 Dependence of tensile strength on temperature and carbon equivalent.(18)
- 2:33 19 Strain rate dependence of tensile strength at 1150°C for the steels listed in table 1.(52)
- 3:3 1 Comparative deflection curves for telcon medium to high activity bimetals.
- 3:8 2 Maximum loading stress curves.
- 3:9 3 Rigid corner bimetallic structure as assembled for experiment 1.
- 3:13 4 Measuring with a fixed ruler.
- 3:21 5 Bimetallic strip curved at room temperature.
- 3:23 6 Identification of the strips edge segments from where imprints were taken for the measurement of curvature.
- 3:29 7 Top view of the bimetallic strips structure used in experiment 4.
- 3:42 8 Deflection of the beam due to thermal stress experiment 4.
- 3:43 9 Deflection of the beam due to both thermal stress and loads at the long beam middle spar.
- 3:46 10 Predicted and experimental results model 2, experiment 4.
- 3:48 11 General view of the apparatus out of the water tank.
- 3:49 12 Top view of the bimetallic strips structure.
- 3:50 13 General view of the apparatus in the water tank.
- 3:51 14 Immersion heater disposition in the water tank
- 3:52 15 Detailed view of the pulley set up.
- 3:53 16 Disposition of thermometers.
- 3:54 17 Short beam pulley set up.
- 3:55 18 Bottom bar support.
- 3:56 19 V-shaped groove.

- 3:57 20 Corner supported on a low friction nylon bush.
- 4:2 1 Representation of the cross section of a continuously cast structure, perpendicular to the direction of casting at a given metallurgical height.
- 4:4 2 Corner section through a solidifying billet or slab.
- 4:10 3 Model representation of a quarter-section perpendicular to the direction of casting, of a continuously cast structure at a given metallurgical height.
- 4:10 4 Temperature distribution across the thickness of a beam.
- 4:10 5 Yield stress distribution across the thickness of a beam.
- 4:13 6 Overall equilibrium of the structure.
- 4:14 7 A generic beam.
- 4:15 8 A section of a generic beam.
- 4:23 9 Stress distribution at a generic cross-section.
- 4:24 10 Variation of the stress distribution.
- 4:25 11 Stress distribution and sign of the curvature in situations 10b and 10h.
- 4:34 12 Geometric relation between the length of filaments at different distances from the cooling wall.
- 6:6 1 Preliminary analysis of the behaviour of the model: reducing δ in the case of billets with $Q_{SYS} = 0.2 \times 10^{-8} \text{ N.m}^{-2}$
- 6:7 2 Preliminary analysis of the behaviour of the model: reducing δ in the case of billets with $Q_{SYS} = 0.3 \times 10^{-8} \text{ N.m}^{-2}$
- 6:8 3 Preliminary analysis of the behaviour of the model: reducing δ in the case of blooms.
- 6:9 4 Preliminary analysis of the behaviour of the model: Increasing the aspect ratio L_1/L_2 . (Short Face)
- 6:10 5 Preliminary analysis of the behaviour of the model: Increasing the aspect ratio L_1/L_2 . (Long Face)

- 6:11 6 Preliminary analysis of the behaviour of the model:
Decreasing the thickness t in the case of slabs
with $\Delta T = 250^\circ\text{C}$. (Short Face)
- 6:12 7 Preliminary analysis of the behaviour of the model:
Decreasing the thickness t in the case of slabs
with $\Delta T = 250^\circ\text{C}$. (Long Face)
- 6:13 8 Preliminary analysis of the behaviour of the model:
Decreasing the thickness t in the case of slabs
with $\Delta T = 300^\circ\text{C}$. (Short Face)
- 6:14 9 Preliminary analysis of the behaviour of the model:
Decreasing the thickness t in the case of slabs
with $\Delta T = 300^\circ\text{C}$. (Long Face)
- 6:15 10 Preliminary analysis of the behaviour of the model:
Decreasing the Young's modulus in the case of slabs
with $\Delta T = 300^\circ\text{C}$. (Short Face)
- 6:16 11 Preliminary analysis of the behaviour of the model:
Decreasing the Young's modulus in the case of slabs
with $\Delta T = 300^\circ\text{C}$. (Long Face)
- 6:39 12 Detached length vs billet quarter section length as
a function of casting speed and metallurgical
height.
- 6:40 13 Adimensional moment at the corner vs quarter
section length as a function of casting speed and
metallurgical height.
- 6:41 14 Adimensional moment at mid-face vs quarter section
length as a function of casting speed and
metallurgical height.
- 6:51 15 Effect of halving the rigid corner length on the
moment at the corner and the rigid boundary.
- 6:52 16 Effect of halving the corner length on the detached
length vs section.
- 6:59 17 Effect of reducing the yield stress on the moment.
- 6:67 18 Effect of doubling the Young's modulus on the
moment.
- 6:71 19 1300 mm x 300 mm slab cast at high speed.
- 6:72 20 1300 mm x 300 mm slab cast at intermediate speed.
- 6:79 21 Detached corner section for 200 mm square billet at
a metallurgical height of 0.1 m. cast at $0.06 \text{ m}\cdot\text{s}^{-1}$
: initial prediction.

- 6:80 22 Detached corner section for 200 mm square billet at a metallurgical height of 0.3 m. cast at 0.06 m.s^{-1} : initial prediction.
- 6:81 23 Detached corner section for 200 mm square billet at a metallurgical height of 0.6 m. cast at 0.06 m.s^{-1} : initial prediction.
- 6:82 24 Detached corner section for 250 mm square billet at a metallurgical height of 0.1 m. cast at 0.06 m.s^{-1} : initial prediction.
- 6:83 25 Detached corner section for 250 mm square billet at a metallurgical height of 0.3 m. cast at 0.06 m.s^{-1} : initial prediction.
- 6:84 26 Detached corner section for 250 mm square billet at a metallurgical height of 0.6 m. cast at 0.06 m.s^{-1} : initial prediction.
- 6:85 27 Detached corner section for 250 mm square billet at a metallurgical height of 0.6 m. but out of the mould cast at 0.06 m.s^{-1} : initial prediction.
- 6:86 28/29 Detached corner section for 166 mm square billet at metallurgical heights of 0.1 and 0.3 m. cast at 0.06 m.s^{-1} : initial prediction.
- 6:87 30 Detached corner section for 166 mm square billet at a metallurgical height of 0.6 m. cast at 0.06 m.s^{-1} : initial prediction.
- 6:88 31 Cross-section stress distribution: the formation of an off-corner crack in a 16.6 cm x 16.6 cm billet cast at high speed.
- 7:5 1 1300 mm x 300 mm slab cast at 0.03 m.s^{-1} at a metallurgical height of 0.1 m. thickness and lengths drawn to the same scale - entire quarter section.
- 7:6 2 1300 mm x 300 mm slab cast at 0.03 m.s^{-1} at a metallurgical height of 0.1 m. thickness and lengths drawn to the same scale - detached corner section.
- 7:16 3 Detached corner section for 250 mm square billet at a metallurgical height of 0.12 m cast at 0.06 m.s^{-1} : Initial prediction.
- 7:17 4 Detached corner section for 250 mm square billet at a metallurgical height of 0.2 m cast at 0.06 m.s^{-1} : Initial prediction.

- 7:18 5 Evolution of an internal crack in a 250 mm square billet cast at 0.06 m.s⁻¹.
- 7:22 6 Evolution of an internal crack at the mould exit in a 250 mm square billet cast at 0.06 m.s⁻¹.
- 7:34 7 Reported values of billet size in relation to casting speed, initial numerical predictions, and effect of adjustments.
- 7:35 8 Detached corner section for 150 mm square billet at a metallurgical height of 0.12 m cast at 0.06 m.s⁻¹: Predictions with the thickness adjusted to 0.6 it's liquidus value (with QSYS1000 degC = 6.5x10⁷ N.m⁻²).
- 7:36 9 Detached corner section for 122 mm square billet at a metallurgical height of 0.12 m cast at 0.06 m.s⁻¹: Predictions with the thickness adjusted to 0.6 it's liquidus value and QSYS1000 degC = 3.0x10⁷ N.m⁻².

- 7:18 5 Evolution of an internal crack in a 250 mm square billet cast at 0.06 m.s⁻¹.
- 7:22 6 Evolution of an internal crack at the mould exit in a 250 mm square billet cast at 0.06 m.s⁻¹.
- 7:34 7 Reported values of billet size in relation to casting speed, initial numerical predictions, and effect of adjustments.
- 7:35 8 Detached corner section for 150 mm square billet at a metallurgical height of 0.12 m cast at 0.06 m.s⁻¹: Predictions with the thickness adjusted to 0.6 it's liquidus value (with QSYS₁₀₀₀ degC = 6.5x10⁷ N.m⁻²).
- 7:36 9 Detached corner section for 122 mm square billet at a metallurgical height of 0.12 m cast at 0.06 m.s⁻¹: Predictions with the thickness adjusted to 0.6 it's liquidus value and QSYS₁₀₀₀ degC = 3.0x10⁷ N.m⁻².

LIST OF TABLES

The tables and pages in each chapter are numbered separately, the page numbers being a two part sequence. The first digit in the sequence represents the chapter number the second one or two digits represents the page number in the chapter.

Explicit reference to the chapter in which a table appears is not made in this list of figures since the chapter reference is embedded in the page number.

Page	Table: No.	Title
2:31	1	Chemical composition of the continuously cast slab samples tested.(52)
2:32	2	Change of 0.4% flow stress and tensile strength with test temperature.(52)
3:4	1	Instantaneous deflection constants for TELCON bi-metals.(TPIA, pg 31)
3:5	2	Mechanical properties of TELCON bi-metals. (TPIA, pg 12)
3:6	3	Fundamental characteristics of TELCON bi-metals. (TPIA, pg 14)
3:14	4	Experimental and theoretical results, experiment 1. (deflection of the long beam middle span)
3:16	5	Experimental and theoretical results, experiment 2. (deflection of the long beam middle span)
3:22	6	Characteristics of the bi-metallic strips curved at room temperature.(information provided by TELCON metals)
3:23	7	Local curvature of the strips edges.
3:30	8	Experiment 4 results (1 mm appreciation).
3:36	9	Experiment 4 results (0.5 mm appreciation).
3:41	10	Experiment 4 results: deflections.
6:21/22	1	A-D Characteristic results for billets in the mould: Casting speed = 0.01 m.s ⁻¹ Metallurgical height = 0.1 m
6:22/23	2	A-D Characteristic results for billets in the mould: Casting speed = 0.01 m.s ⁻¹ Metallurgical height = 0.3 m

- 6:24/25 3 A-D Characteristic results for billets in the mould:
Casting speed = 0.01 m.s^{-1}
Metallurgical height = 0.6 m
- 6:26/27 4 A-D Characteristic results for billets in the mould:
Casting speed = 0.03 m.s^{-1}
Metallurgical height = 0.1 m
- 6:28/29 5 A-D Characteristic results for billets in the mould:
Casting speed = 0.03 m.s^{-1}
Metallurgical height = 0.3 m
- 6:30/31 6 A-D Characteristic results for billets in the mould:
Casting speed = 0.03 m.s^{-1}
Metallurgical height = 0.6 m
- 6:32/33 7 A-D Characteristic results for billets in the mould:
Casting speed = 0.06 m.s^{-1}
Metallurgical height = 0.1 m
- 6:34/35 8 A-D Characteristic results for billets in the mould:
Casting speed = 0.06 m.s^{-1}
Metallurgical height = 0.3 m
- 6:36/37 9 A-D Characteristic results for billets in the mould:
Casting speed = 0.06 m.s^{-1}
Metallurgical height = 0.6 m
- 6:45/46 10 A-D Results using half Krishnamurthy's length
Casting speed = 0.06 m.s^{-1}
Metallurgical height = 0.1 m
- 6:47/48 11 A-D Results using half Krishnamurthy's length
Casting speed = 0.06 m.s^{-1}
Metallurgical height = 0.3 m
- 6:49/50 12 A-D Results using half Krishnamurthy's length
Casting speed = 0.06 m.s^{-1}
Metallurgical height = 0.6 m
- 6:54/55 13 A-D Results for a low yield stress steel
Casting speed = 0.06 m.s^{-1}
Metallurgical height = 0.1 m
- 6:56/57 14 A-D Results for a low yield stress steel
Casting speed = 0.06 m.s^{-1}
Metallurgical height = 0.3 m
- 6:58/59 15 A-D Results for a low yield stress steel
Casting speed = 0.06 m.s^{-1}
Metallurgical height = 0.6 m
- 6:61/62 16 A-D Results for a higher Young's modulus
Casting speed = 0.06 m.s^{-1}
Metallurgical height = 0.1 m

- 6:63/64 17 A-D Results for a higher Young's modulus
Casting speed = $0.06 \text{ m}\cdot\text{s}^{-1}$
Metallurgical height = 0.3 m
- 6:65/66 18 A-D Results for a higher Young's modulus
Casting speed = $0.06 \text{ m}\cdot\text{s}^{-1}$
Metallurgical height = 0.6 m
- 6:74 19 Relationship between section length, detached length and metallurgical height for a casting speed of $0.01 \text{ m}\cdot\text{s}^{-1}$.

CHAPTER 1 : INTRODUCTION

From its early days Continuous Casting has represented a challenge for Process Modelling. As with other important advances in Metallurgy, its implementation can be said to result from trial and error rather than from comprehensive theoretical understanding. Yet, much of the trial and error involved in the successful development of Continuous Casting has been based on physical and mathematical models.

The phenomena involved in the process are complex and the increased speed of solidification which results in the higher output of the continuous casting process has lead to a whole range of problems not previously encountered with ingot casting. Some of these problems are caused by intense stresses which develop within the solidifying shell during solidification. This current research investigation has focussed attention on the study of these stresses and the resulting deformation and overall mechanical behaviour of the solidifying shell in the early stages of solidification.

The great majority of mathematical models related to the Continuous Casting process have been primarily concerned with Heat Transfer. It is apparent, however, that any further development of these models requires analysis of the stresses involved in the process. This has proven to be particularly difficult in the early stages of solidification due to the lack of data on the mechanical properties of steel at high

temperature and the limited understanding of the complex behaviour of the solidifying shell. Although a number of models of increasing complexity have been developed, the mechanisms by which shape distortion and crack formation occur are still poorly understood.

A fundamental characteristic of the Continuous Casting strand of which the previous models do not take account is that the thin shells of metal solidifying along the four sides of the billet cross-section behave together as a flexible rectangular structure. Mechanical interactions between adjacent sides of this structure play an essential role in the development of the stresses within the solidifying shell. These interactions are particularly intense because the corners act effectively as rigid hinges.

The model that has been developed in this thesis analyses the equilibrium of forces and moments within this rectangular structure formed by the thin solidifying shells at a given metallurgical height. It assumes that the solidifying shells behave in essence as a "box" constructed from four elasto-perfectly plastic beams rigidly jointed at the corners.

Previous models (26,27,30) which have analysed the behaviour of the thin solidifying shells in terms of beam theory have assumed an elastic behaviour of the solid steel and have failed to consider the interaction between the sides of the billet. The beams representing the solidifying shell on each side of the slab are assumed to be either simply supported or

fixed at the ends

The predictions of these models are clearly restricted by the support assumptions made. A net inward dishing or outward bowing of the skin is predicted depending on which support assumption is made. The surface stresses predicted are either tensile or compressive along the whole beam.

The second chapter of the thesis contains a survey of both experimental and theoretical studies related to the behaviour of the solidifying metal within the mould of a continuous casting machine.

The next chapter describes a simple physical analogue constructed using bimetallic strips and rigid corners. The development of this physical analogue and of a mathematical model based on elastic beam theory to predict its behaviour played an essential role in the research providing a basic understanding. This elementary mathematical model is presented on appendix 1. The computer program developed to predict the deflection of the bimetallic strips structure is presented on appendix 2.

Chapter 4 is the central chapter of the thesis. It states the derivation of a mathematical model to analyse the equilibrium of forces and moments within the rectangular structure formed by the thin solidifying shells at a given metallurgical height. The computer program developed to predict the shape distortion of this structure and the distribution of stresses and moments is presented in the next chapter. The results are presented in

chapter 6 and discussed in chapter 7.

Finally the conclusions and propositions for further work are presented in chapter 8

CHAPTER 2 : LITERATURE REVIEW

2.1 GAP FORMATION IN CONTINUOUS CASTING

As a process, continuous casting seems to be nearer to an ideal continuous production with precise control than the traditional ingot casting. Better control is possible during the solidification process, the main variables being controlled in a continuous manner.

The high rates of heat transfer involved, however, give rise to phenomena of an intensity not seen before in solidification processes and small changes in the control variables produce quite distinct variations in the properties of the resulting material.

One such phenomenon is gap formation. It has been intensively studied both experimentally and theoretically but it is still not fully understood.

2.2 EMPIRICAL EVIDENCE

Although an important number of papers are related to different measurements of the gap formation, the information available is quite limited and no numerical data is given of the actual shape of the metal strand in or just below the mould zone.

Evidence has been given, however, that under certain circumstances, an air gap forms which varies in size in both longitudinal and transverse directions and which is not constant in time (for a given particular distance below the meniscus). The relation between the formation of this gap and its various causes has been roughly established.

The time at which gap forms can be measured in the case of ingot moulds by a method originally used by B.Matuschka (1), a wire is passed through the mould wall and the electrical resistance of the wire is measured between the ingot and a measuring point set in the mould wall. The air gap formation shows itself as a sudden increase in this resistance. Several authors (2,4) used this or similar methods. A.Diener et al (3), in a study of static casting, observed that the gap at the corners of the mould sets in quickly after the rising steel reaches the measuring position, well before the end of the casting, while gap formation in the middle of the sides follows much later and depends on the height of liquid steel above the measuring point and the length of the side.

Another method widely used is to place a number of thermocouples within the mould and record the variation of the temperature as solidification proceeds. The gap formation, or collapse is related to perceptible variations in the cooling rate (4,5,6,7,8,9). K.F.Behrens and H.Weingart (5), observed an interval of rapid temperature oscillation in their measurements, indicating that in that interval the solidified skin alternately separates from the mould and falls back onto it, i.e., when a gap forms there is a build-up of temperature in the solidified layer which raises its temperature and makes it easily deformable. This cycle is repeated until the ingot skin has attained adequate thickness and strength to resist the ferrostatic pressure.

Although these papers make quite wide interpretations of their results, their true significance is severely limited by the effect on the mechanical behaviour of the metal of factors which they do not take into account. Metal composition, as I will explain soon, is one of these factors.

Heat flow estimation methods have also been used. An example is the work developed by Mackenzie and Donald (4) who explain their result, i.e., the rapid fall observed in the rate of heat transfer to the mould (figure 1), as the separation of the ingot from the mould, being caused by expansion of the mould, contraction of the ingot or by both these factors.

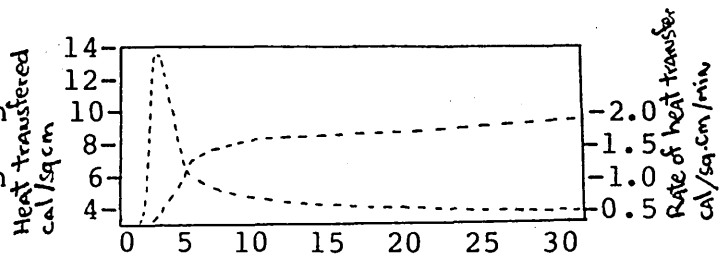


FIG 1: Rate of heat transfer from ingot to mould.(4)

In his M.Phil thesis at the Sheffield City Polytechnic (1978) Martinez-Fueyo (10), developed a direct observation method. He used a purpose built mould with one transparent glass wall and three metal walls with integrated cooling channels. It was observed that the air gap starts to form at the corners of the cast progressing towards the center when it is cooled uniformly and at relatively high rates. Pure tin and 50% lead tin alloy at some 20 C and 50 C respectively above the solidus arrests were used in these experiments.

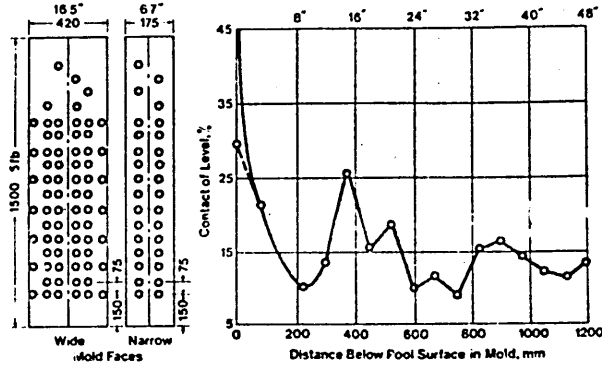
If gap formation has been observed in ingot solidification, and a lot of valuable information can be deduced from this, gap formation in Continuous Casting is much more pronounced as is the deformation of the metal. In continuous casting, solidification times are measured in minutes compared with the hours of conventional casting.

The measurement methods used in Continuous Casting are in general similar to the methods used for ingot solidification measurements, although problems due to the reciprocating movement of the mould have to be solved and no explanation of how this is done has been found in the literature. It is also possible (11) to make direct measurements of the dimensions of the cast structure as it comes out of the mould. But, reading the papers, it is difficult to assess the reliability of the results given.

In the early 70's, L.S.Rudoi (12) placed a network of sensors in a vertical slab casting mould to estimate the degree of

contact between the mould walls and the metal surfaces adjacent to them. Overall results are given which show that the degree of contact is intermittent and that there is a net decrease of contact from top to bottom (figure 2). It is interesting to notice that the main decrease is in the first 200mm below the pool

surface and, in 1200mm of "sensible" distance, contact is not completely lost. No detailed information on transverse differences in the degree of contact



is given, but the initial decrease is probably related to contraction at the corners.

FIG 2: Contact sensor pattern and % contact time vs depth. (from L.S.Rudoi, ref.11)

More interesting is the instrumented-mould study carried out by Roztkov et al (12) which measured the variation in gap

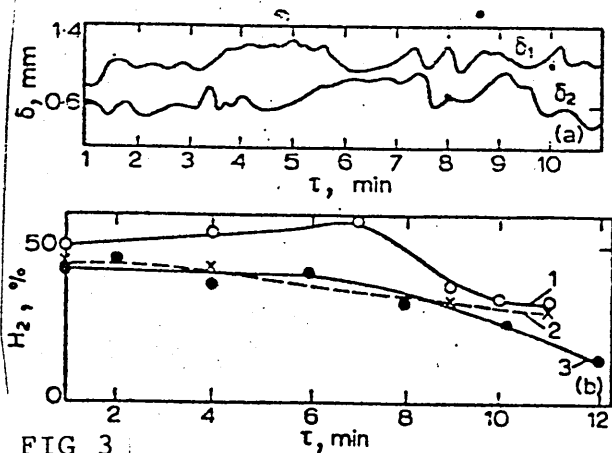


FIG 3
 a Variation in gap size along wide face δ_1 and narrow face δ_2 ; b hydrogen content of gap along (1) narrow and (2) wide face with (3) average for nine heats (12)

width as a function of time and shows quite unstable behaviour. Gap variations of 0.6-1.2mm and 0.2-0.8mm for the wide and narrow faces, respectively, of a 250x360mm slab lubricated with paraffin (figure 3) were reported. Sampling

tests confirmed the presence of CO₂, O₂, CO, N₂ and H₂ in the gases. In a related study, Akimenko et al (14) observed that the composition of hydrogen in the gas is a maximum as the lubricant is first introduced, 45-55%, but that the average composition during casting is closer to 10-20%.

Although the influence of the hydrogen atmosphere in the gap on the heat transfer, and thus on the mechanical behaviour of the metal, is not made evident from these papers, but rather accepted as a fact, several other papers show how important it is and its importance is readily accepted in today's industrial practice. Charles R. Taylor, in a 1975 review on continuous casting (21), refers to some measurements made by Volk and Wunnenberg from Mannesman in a mould specially designed for the purpose of the mean heat flux in the interface at different levels. This mould has 8 different horizontal channels of water.

Measuring the water flow and the change in temperature (in a similar way as has been done for ingot moulds), they estimated the heat flux in each of 8 levels. As could be expected the heat flux varied with depth and they also found that the relation between heat flux and depth varied with the casting speed (figure 4).

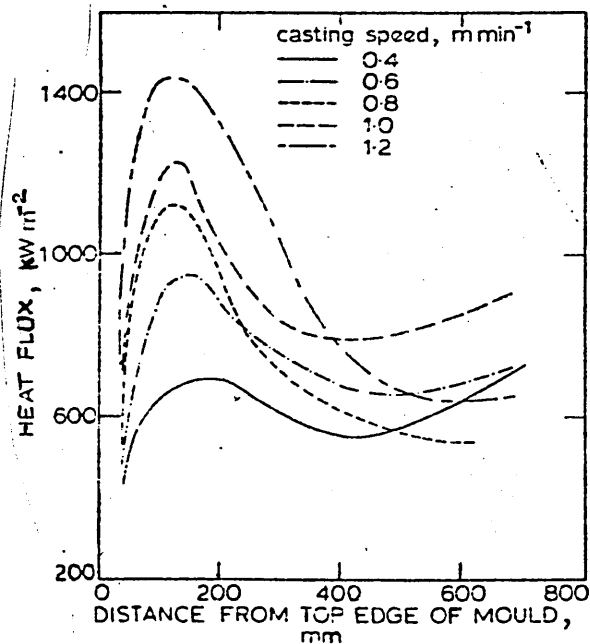


FIG 4: Mould heat flux as function of distance from top of mould for various casting speeds.(19)

The increase in heat transfer towards the bottom of the mould is related to the influence of the gas atmosphere in the gap. Jacobi (16), investigated the influence of different gas atmospheres, reporting that high levels of H₂ will result in faster cooling rates.

Taylor relates the presence of hydrogen in the bottom part of the mould with the dissociation of water coming up from the top sprays of the secondary cooling zone.

Klipov et al (16), report a higher upper-mould heat flux with oil than with mould powder which is probably also due to an hydrogen-rich atmosphere resulting from the breakdown of the oil. The injection of hydrogen into the gap increases the heat transfer rates as K.Cliff & R.Dain (17) have shown. However, because the presence of hydrogen is normally related to breakdown of the lubricant film, erratic variations in temperature can be produced.

Now, observing fig. 3, which reviews Rozhkov et al work (13), the oscillations in gap thickness shown do not seem to be related to any oscillation in the level of hydrogen present. There is, however, a net variation of the hydrogen content in the 12min period considered and it could be said that a general pattern can be observed in the variation of the gap thickness which follows the pattern of the curve of hydrogen content. The actual oscillation of the gap thickness, which seems quite important, has, however, no relation with the registered levels of hydrogen. It could be argued that not

enough samples were taken, but this is not the explanation.

V.A.Ul'yanov et al published a paper on the non-uniformity of the solidification front in continuous casting strands (19), which gives further clues. There is a strong interdependence between the width of the gap, its non-uniformity and the non-uniformity of the solidification front. One of the factors which affect uniformity is the disturbing effect of the stream of molten metal. Depending on the casting method and the flow rate of the molten metal, the flow currents extend to a depth of 1-2m, while the zone of maximum rates of the circulating currents, which wash the shell being formed, are found at a distance of 0.3-0.8m from the meniscus (that is, in Soviet practice). In this zone, the solidification front is subjected to melting and erosion, with particular intensity,. Non-uniformity of the solidification front occurs as a result of non-alignment between the molten stream and the technological axis of the machine (figures 5,6,7,8 on the next page).

Another major reason for the non-uniformity of solidification is the non-uniformity of the heat extraction around the perimeter of a continuous casting strand, which is, of course not only related to the gap formation but also to:

- * non-uniform shrinkage of individual regions of the solidifying shell.
- * appearance of additional thermal resistances in the form of lubricant, oxides, slag particles.
- * distortion of the mould.

(...)

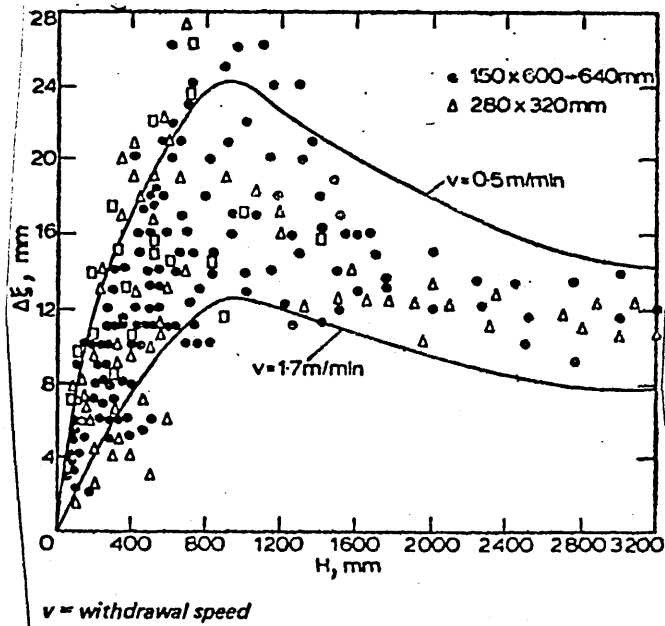


FIG 5:
Experimental (shown by symbols) and calculated data (upper and lower curves) on extent of solidification-front non-uniformity over length of continuously cast strand (17)

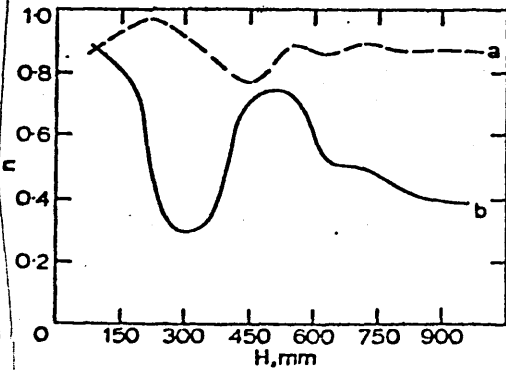
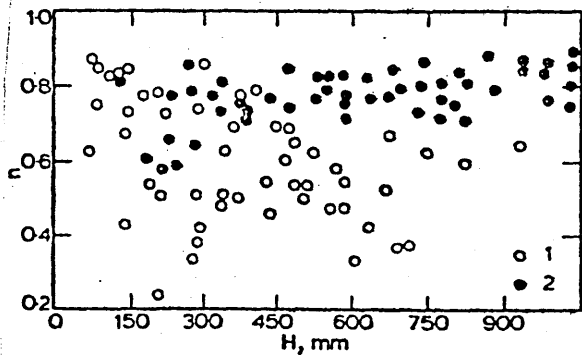


FIG 6:
Coefficient of non-uniformity of thickness $n = \xi_{min}/\xi_{av}$ of solidified shell at wide faces of rectangular strand with non-alignment between stream of molten metal and technological axis of machine (17)



1, casting without slag, metal feed by open stream;
2, casting with slag, metal feed by immersed pouring

FIG 7:
Coefficient of non-uniformity of thickness n of solidified shell of rectangular strand (17)

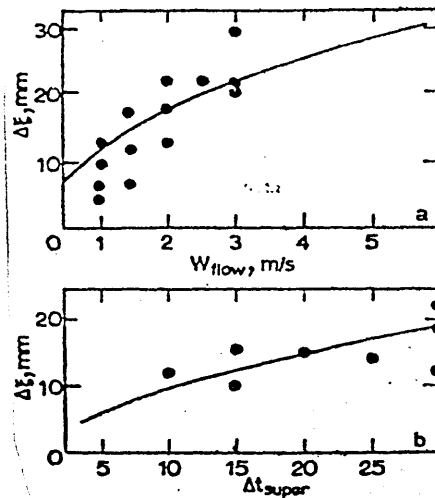


FIG 8:
Effect of flow rate of melt w_{flow} from steel casting nozzle (a) and of superheat of melt Δt_{super} in mould (b) on maximum degree of solidification-front non-uniformity $\Delta \xi$ (17)

- * thermal stresses and coarse scratches or dents in the walls (which will deform both or one of the mould and the strand).
- * locally varying heat fluxes (associated with the water cooling channels).
- * varying flow rates of the water in these water cooling channels.
- * non-optimal withdrawal speed.

It has been said (16) that data from numerous experimental investigations and from mathematical modelling indicates that raising the withdrawal speed for 600-640x150mm strands from 0.5 to 1.1 m/min reduces " Δ_{MAX}^s ", the maximum non-uniformity, (see figure 6) by a factor of 1.5-2, while a further increase from 1.1 to 1.7 m/min reduces " Δ_{MAX}^s " by only 5-10%.

There is a close relationship between the casting speed and the breakdown of the lubricant, as H.Takeuchi et al point out (17). Data collected by Gray & Marston, Wyckaert and H.Nakata (referred by 17) show that the velocity of casting corresponding to a minimum incidence of cracking varies inversely with the viscosity of the lubricant used. A.W.D.Hills points out a relationship between the lubricant viscosity, the casting speed and the lubricant thickness (18).

Further information on the causes of the non-uniformity of the solidification front is given by Singh and Blazek (22) as the

result of the important experimental work they carried out.

A total of 30 heats was cast on a bench-scale caster with steels of 10 different carbon contents (see figures 9 & 10). The mold was stationary. Most of the necessary technical data is given.

To study the macroscopic solid-liquid interface of the solidifying skin, unsolidified steel was emptied from the casting by means of a controlled breakout technique. This technique consisted of burning a hole in the solidified steel skin 1.8m below the mold. After the unsolidified steel flowed out, the shell was withdrawn and cut longitudinally to permit examination of the solidified skin. Transverse and longitudinal sections were taken from the completely solid sections of the billets and etched with hot HCl to reveal the grain structure. The outer surface was shot blasted to remove scale, so that the surface roughness could be examined and the surface could be rated for pinholes.

The technique of controlled breakouts (22,23) seems to give the best results for measuring the shell thickness. However, since a finite time elapses while the unsolidified steel is being emptied, the thickness measured is always bigger than the original and this difference increases towards the point where it is being emptied. It should be possible to recognise or estimate this latter skin, although no mention is made of such an estimate in the literature. In any case the errors involved seem to be smaller than those produced by the other

The most interesting result reported by Singh and Blazek (22) is their observation of the change in behaviour that occurs on approaching the 0.1 carbon content in the steel (figures 11, 12, 13, 14). This could explain the differences in results found in comparing previous measurements, which in fact become meaningless when the carbon content is not specified.

The effect of mould reciprocation has, in general, been avoided in the available literature, although some reference is found in USSR articles in relation to the development of special mould designs to "...avoid skin defects and improve the heat transfer uniformity." (24,25).

The results found by Singh and Blazek for the effect of carbon content on friction in the mould vary greatly and do not seem very reliable (figure 13). Other conditions, not taken into account, might have changed. But it does seem that this factor does not determine the roughness observed at 0.1C which contrasts with the relative smoothness observed at other carbon contents (figure 14).

Singh and Blazek suggest that the solidified skin is stressed between the shrinking forces due to the change of state (solid more dense than liquid) and the ferrostatic pressure, and it has to wrinkle to be able to release the stresses. However, this is still not a satisfactory explanation.

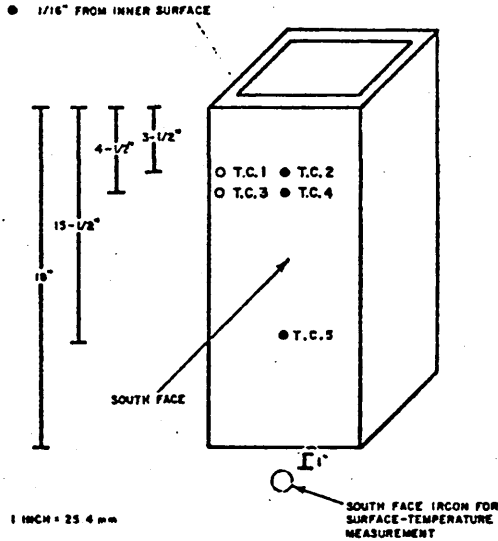


FIG 9: Locations of thermocouples in Cu mould to measure the temperature and location of ircon to measure exit temperature on the south face of the billet.(22)

Heat No.	Composition,* wt %			Comments**	Temperature, F				Temp, F. at Mold Exit (South Face)	Mold Heat Transfer, kBtu/(hr)(ft ²)
	C	Mn	Si		TC1	TC2	TC3	TC4		
ST 781	0.69	0.88	0.30		234	307	204	267	2242	532
ST 782	0.69	0.89	0.30		238	283	252	271	2089	528
ST 784	0.11	0.90	0.30		184	219	180	207	2414	434
ST 785	0.27	0.86	0.28		194	291	173	262	2387	504
ST 786	0.20	0.93	0.33		216	267	200	246	2318	487
ST 787	0.12	0.90	0.32		178	205	166	208	2423	411
ST 788	0.42	0.88	0.29		212	316	194	243	2417	542
ST 789	0.20	0.97	0.32		189	266	179	254	2365	488
ST 790	0.27	0.83	0.32		193	273	197	284	2316	534
ST 791	0.41	0.94	0.33		212	289	194	271	2245	518
ST 792	0.89	0.89	0.30		246	280	233	266	2145	524
ST 793	0.89	0.92	0.38		243	274	235	254	2224	506
ST 794	0.20	0.90	0.39		189	251	184	254	2310	503
ST 796	0.11	0.84	0.29	E.R.	205	235	248	285	2354	487
ST 797	0.066	0.90	0.33		213	249	205	234	2397	475
ST 798	0.12	0.89	0.33	0.98% Cr	190	214	188	203	2471	413
ST 799	0.12	0.89	0.33	1.03% Ni	184	215	188	221	2436	471
ST 800	0.003	0.84	0.31		218	264	207	258	2345	469
ST 802	0.085	0.91	0.36		214	252	210	255	2305	505
ST 803	0.69	0.86	0.32	E.R.	55	48	104	104	2064	567
ST 804	0.14	0.89	0.31	0.023% Al S.T.	202	233	201	227	2417	436
ST 805	0.003	0.85	0.34				206	219	2390	505
ST 806	0.69	0.91	0.34	0.30% S	216	282	197	261	2152	511
ST 808	0.69	0.91	0.34	0.30% S	259	42	259	274	2145	504
ST 810	0.70	0.86	0.32	E.R.	73	76	227	263	2042	615
ST 812	0.11	0.90	0.36	S.T.	167	202	183	214	2122	472
ST 813	1.84	0.96	0.36		253	272	249	263	1935	523
ST 814	1.50	0.91	0.36		247	267	241	255	1881	514
ST 815	1.96	0.86	0.87		197	267	196	250	1902	527
ST 831	0.096	0.89	0.35	0.30% S	231	291	230	283	1908	541

* P and S were both <0.01% for all heats.

** E.R. = elevated ceramic reservoir
S.T. = submerged tube.

FIG 10: Chemical analysis, mould-wall temperature, and mould heat transfer for the Heats investigated. (22)

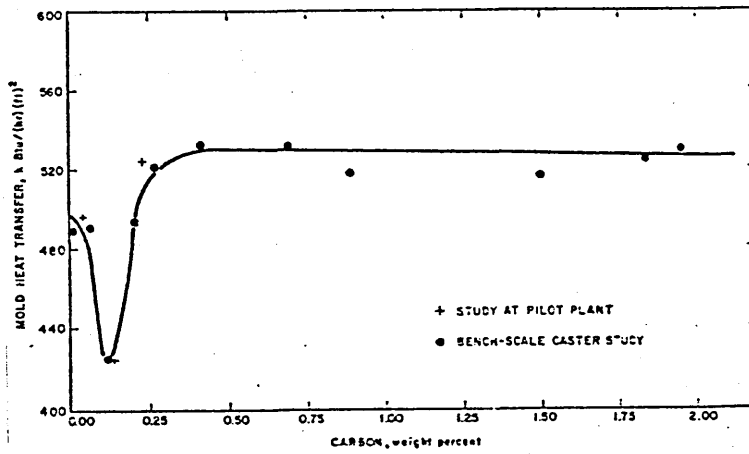


FIG 11: Effect of carbon content on mould heat-transfer rate during continuous casting (22).

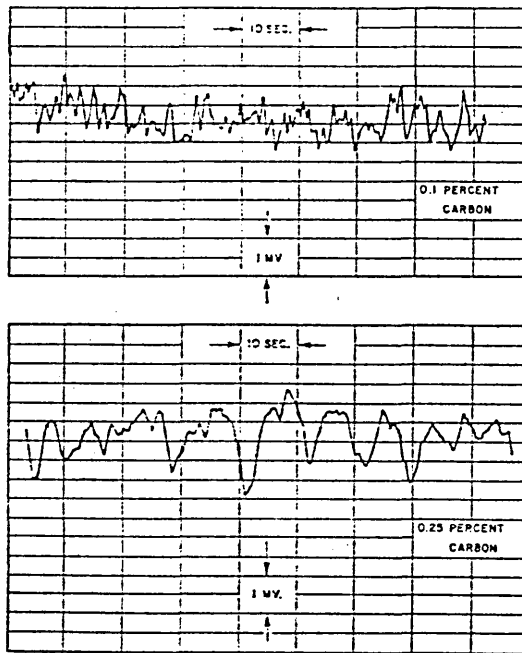


FIG 12: Temperature variation for the thermocouple located 1-1/2 in below the meniscus in the center of the south face for 0.1 & 0.25% carbon steels.(22)

Fig. 7—Effect of carbon content on mold friction during continuous casting.

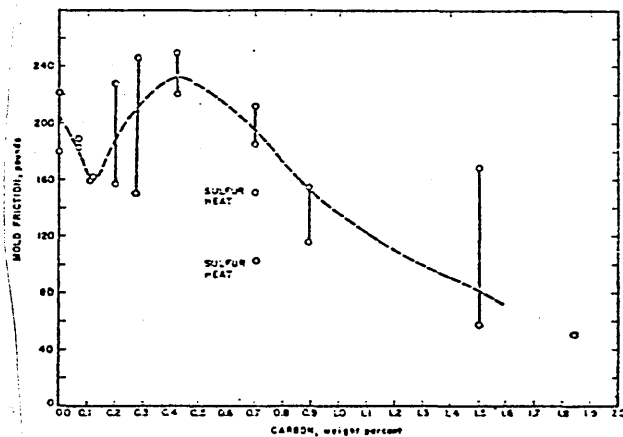


FIG 13: Effect of carbon content on mould friction during continuous casting. (22)

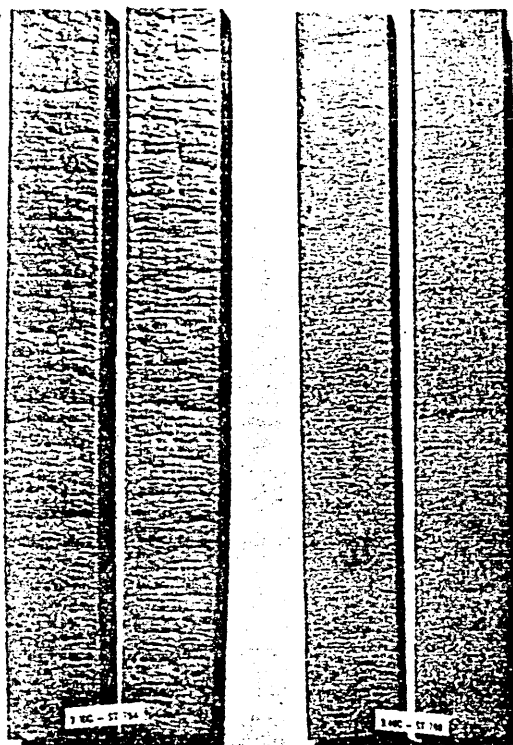


FIG 14: As-cast surface of 0.10% and 0.40% carbon steels that have been shot-blasted.(22)

2.3 THEORETICAL MODELS

Several theoretical models have been developed to describe the behaviour of the metal surface during solidification. The lack of data has made it difficult to achieve satisfactory descriptions, but some growth of understanding of the phenomenon involved has been achieved. I want to describe here briefly the main models that have been put forward and give some opinion on them.

The model developed by Savage (26) in 1962 consists of 4 beams simply supported with the Young's modulus being taken as constant up to the melting point of the steel. Purely elastic behaviour of each of these beams is assumed. The beams tend to bow concavely towards the liquid core under the action of the thermal stresses originating from the temperature gradient throughout the shell. However, the beams cannot bow until the ferrostatic pressure is overcome by thermal stresses in the solidified shell and the time when this occurs is taken as the time at which the air-gap forms. The model first assumes the modulus of elasticity to be independent and then dependent of temperature.

Tien and Koump (27) advanced Savage's model (26). By assuming the solidified skin to be an assembly of four separate beams, each behaving elastically, they calculated the stress distribution and the distortion of the solidified shell. The calculations were carried out for an exponential decrease of

the beam surface temperature and for different thicknesses of the beam. Their model assumes a linear temperature dependent Young's modulus which is nil at the melting point of the material. They consider two cases: a simple supported beam and a built-in beam. They found, for both cases, a time dependent displacement.

For simple supported beams the displacement changes from a positive to a negative value and remains negative thereafter, i.e., the beam changes from a convex to a concave shape as solidification proceeds.

For a built-in beam the displacement is always positive, i.e., the shape of the beam is convex towards the liquid core as solidification proceeds. The final shape of the simply supported beam that this model predicts agrees with that of Savage (26).

Weiner and Boley (28) assume that the solidified layer does not bend, and that there are no external forces, either in the axial direction or at the corners. The yield condition is assumed to be independent of plastic strain following idealised plastic theory and as the elastic portion of the strain is included in the analysis, they named their model as Elasto-Perfectly Plastic.

The temperature distribution in the solidified layer was taken to be given by the Neumann solution, with a constant external surface temperature. This implied that at the start of solidification there is an immediate temperature drop at

the external surface from the melting temperature down to this constant surface temperature, a situation that does not occur in practice since the surface temperature does not drop suddenly, but gradually.

Richmond and Tien (29) introduce creep behaviour: when the material is subjected to a constant force and its temperature is raised to a high level, the elongation of the material will be observed to increase continuously with time. Elastic behaviour is also considered as part of the mechanical process, a temperature dependent Young's modulus being used.

Their model leads to non-linear differential equations for which an analytical solution is only available for very slow solidification. In this case the stress resulted to be uniform through the ingot skin at all times, beginning with a compressive value and becoming less compressive as solidification proceeds.

Oeters and Sardeman (30) consider mould deformation as a relevant process in the case of continuous casting although they do not consider it relevant in the case of ingot casting. The gap is considered into two parts, one due to the deformation of the solidified layer and one due to the deformation of the mould. The solidifying metal can be deformed by the ferrostatic pressure, not the mould. Contraction of the metal during solidification is neglected as it is said to be completely obliterated by the ferrostatic pressure. (This may be so in ingot casting depending on the rate of solidification

and the composition of the steel, but it is certainly not the case for continuous casting).

The solidified layer is assumed to behave as 4 stressed beams (behaving purely elastically) with fixed ends. It further considered that: "...any yielding occurring at the highest temperatures may possibly be compensated for by increased strength in the lower temperature regions near to the surface of the ingot." (In fact, they assume this to be so, which is an inconsistency since there can be no yielding in a beam that behaves elastically).

Several mathematical models (26,...,48) have been developed to analyse heat transfer and, in some cases, stresses in the continuous casting process.

The relevance of these models to predict how the solidification proceeds is limited by the lack of understanding of the processes involved, which still leaves many questions without satisfactory answer, and also by the inherent complexity of the heat conduction problem.

Many assumptions have to be made about heat transfer across the air gap between the slab surface and the mould wall and about mechanical and thermal properties of the metal at temperatures near to the solidification temperature.

Heat transfer analysis

The analysis of heat transfer is in itself complex because of the presence of a phase transformation.

The solidification front is not simply the locus of points where the temperature is equal to the temperature of solidification it is also a boundary across which the properties of the material change abruptly. Unless a gradual transition from one phase to the other can be assumed, the differential equation describing the heat transfer has to be formulated with the solidification front as one of its boundaries. This

is a major complication because the position of the solidification front has to be predicted by the differential equation itself.

A boundary of this sort is known as a free boundary, in opposition to a fixed boundary which is specified beforehand.

The external surface of the solidified metal is the second boundary of the differential equation. It can be made a fixed boundary by taking it as the origin of the system of reference used. The distance between this surface and the surface of the mould is external to the range of the differential equation and so the fact that it cannot be specified beforehand will not affect the problem in the same way as the fact that the position of the solidification front cannot be specified beforehand.

Several mathematical treatments have been developed to tackle a problem of the kind given here by the heat equation and its boundary conditions (45). In general, these treatments transform the differential equation into an integral equation and then solve this later equation with the use of numerical methods. Analytical solutions have only been found for some ideal situation. In the particular case of the continuous casting solidification, in which the free boundary coincides initially with the fixed boundary, mainly two alternative mathematical treatments have been used:

1.- The integral profile method,

This method has been extensively used in the form presented by

Hills (32,33). The differential equation is transformed into an integral equation incorporating the free boundary condition and the integral of the temperature across the solidified layer. The integral of the temperature is then estimated by the use of an approximated auxiliary function and in this way the problem is reduced into a system of non linear ordinary differential equations which can be solved by a marching technique.

2.- The finite differences method,

The differential equation and its boundary conditions are approximated by difference equations. The method uses a grid with a variable time step to ensure that the boundary nodes coincide with the free boundary. This is done by selecting a space step first and then finding the appropriate time step through an iterative process of solving simultaneously the difference equations given (32,37,45).

Stress analysis

The mathematical methods used for the analysis of the stresses within the solidified metal have varied very much because of the various theoretical models of mechanical behaviour (see section 2.3).

The finite-element method is at present the most commonly used technique (37,38,39,46,47,48). The fact that this technique was originally developed for the analysis of structures seems to have misled many authors into believing that the structural

analysis of the solidifying shell had been overcome. But the finite-element method has serious limitations. Its application to non-elastic structures requires great care and substantial computation time.

The complex nature of thermomechanical behaviour in the early stages of solidification in the continuous casting process has required certain simplifications to be introduced in all models.

Few authors have attempted to deal with the actual bending of the solidifying skin, the example set by Weiner & Boley (28) of considering only an idealised situation in which there is no bending was followed in most later models.

Savage (26), Tien & Koump (27) and Oeters & Sardeman (30) analysed the behaviour of the thin solidifying shells in terms of beam theory. They assumed an elastic behaviour of the solid steel with constant or linearly dependent Young's modulus and failed to consider the interaction between the sides of the slab. The beams representing the solidifying shell on each side of the slab are assumed to be either simply supported or fixed at the ends.

The predictions of these models are clearly restricted by the support assumptions made. A net inward dishing or outward bowing of the skin is predicted depending on which support assumption is made. The surface stresses predicted are either tensile or compressive along the whole beam.

The increasing complexity of the models found in the literature has been primarily focussed on the elasto plastic behaviour of the steel at high temperature. Thus Weiner & Boley (28) assume an elasto-perfectly plastic behaviour but restrict their analysis to the consideration of a square cross-section and neglect the melt pressure to avoid bending and rotation of the corner. Richmond & Tien (29) assume a non-linear viscous behaviour but consider that the pressure of the melt and the viscous response of the solidifying skin "...insures contact between the skin and the mold wall and also a lateral compressive stress in the skin, thus preventing bending".

Recent models based on the finite elements method fail to consider bending, effectively assuming that the cooling face remains in contact with the mould. This idealization of the problem is necessary because the numerical techniques used were originally developed for the analysis of structures fundamentally different from that formed by the solidifying shells and these techniques become extremely difficult to operate under conditions significantly different from those for which they were developed.

The model developed by Grill, Brimacombe & Weinberg (37), and later modified by Sorimachi & Brimacombe (38) is based on the modified pure tangent stiffness approach originally formulated by Yamada, Yoshimura & Sakuray (49). This approach was developed for problems in which the plastic deformation is contained and for which the overall distortion of the body is

of the order of $1/E$ times the mean stress. In order to apply this method, then, it is necessary to assume that the distortions of the solidifying shell are vanishingly small - effectively to assume that the shell remains in contact with the mould wall.

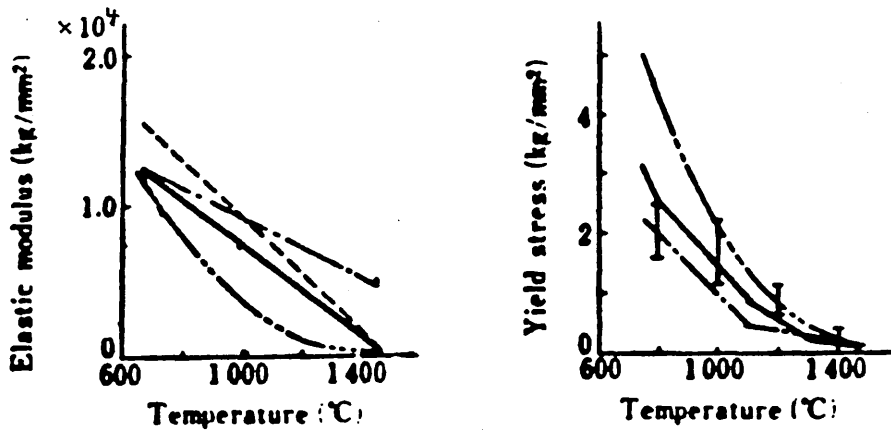
Grill, Sorimachi and Brimacombe (39), attempted to extend this approach to treat distortion within the mould but ran into a number of problems. They used load increments that caused a fixed number of elements to yield each time in order to reduce the overall computation time but even then found that the load analysis was too expensive to operate at every time interval used in the thermal analysis. Knothe and Muller (50), however, in a general discussion of the Yamada's modification to the tangent stiffness approach, showed that even for load increments small enough to cause the yielding of a single element only, the finite element solution will drift above the upper bound solution.

Very little information on the mechanical properties of steel or indeed of metals in general near their solidification temperatures is available.

P.J. Wray and M.F.Holmes (51) documented the plastic deformation of austenitic iron, represented by a zone refined iron an electrolytic iron, an Fe-0.05C alloy, and an Fe-5.2Mn alloy, for the temperature range 950 to 1350 deg C and the strain-rate range 2.8×10^{-3} to 2.3×10^{-4} (1/sec.). Their documentation is restricted to initial periods of strain usually less than 0.10 due to the intrusion of recrystallization during deformation. It is also restricted because they had to use specimens that were possibly unrepresentative of a polycrystalline aggregate in order to maintain the initial structure as an invariant for tests at different temperatures. On the basis of their results, Wray and Holmes found that chemical composition appeared to influence the plastic-flow behaviour of austenitic iron primarily through its effect on the grain structure. The large-grained zone refined iron was found to be relatively weak and the difference in behaviour between the Fe-0.05C alloy and the Fe-5.2Mn alloy was found to be small.

Sorimachi and Brimacombe (38) infer the data used in their model of stresses in the continuous casting of steel from the values reported by Wray and Holmes (51) for austenitic iron.

The lack of data is reflected on wide variations on the values used in different models, as is illustrated in figure 15 (67). Kojima et al (67) refer to this wide dispersion, which they relate to variations in measuring methods, to justify the use of mean values based on the data referred for the modelling of bulging of slabs in the secondary cooling zone. It must be observed, however, that only two of Kojima's references correspond to experimental results. It is interesting to note that the only Young's modulus curve presented which corresponds to experimental measurements differs from the other curves in that it shows a rapid decrease of the Young's modulus which tends to stabilise after about 1000 degC.



Kojima (assumed)
 Sorimachi (assumed)
 Fekete (assumed)
 Puhringer (experimental)
 Kinoshita (experimental)

FIG 15 Mechanical properties of steel (67)

More recently, the tensile properties of continuously cast carbon steels at elevated temperatures up to their melting points were investigated by H.Kitaoka, K.Kinoshita and T.Emi (52). Strength and ductility of steel solidifying in a continuous casting machine was investigated for low, medium and high carbon steel slab specimens reheated on an Instron type testing machine up to their melting points.

Table 1 presents the chemical composition of the continuously cast slab tested.

The stress-strain curves obtained for sample No. 1 and for samples No. 2 and No. 3 are given (figures 16 and 17). It can be noticed from these figures that the amount of work hardening decreases significantly with increasing temperatures, suggesting that the assumption of elasto-perfect plasticity represents a good approximation of reality. It can also be noticed that the variation of the Young's modulus with temperature appears to be negligible in these figures.

Table 2 shows the change of the 0.4% flow stress and of the tensile strength. A variation of the order of 100% on the values of the tensile strength reported for different steels at each temperature can be appreciated in this table. The difference between corresponding values of 0.04% flow stress and tensile strength is also of the order of 100% at 1000 degC and above.

Figure 18, illustrates the dependence of tensile strength on temperature and carbon equivalent. It shows the quasi-linear

variation of the tensile strength with temperature

The stress values given in figures 16 and 17 and in table 2 correspond to a strain rate of 10^{-4} sec^{-1} . The effect of the strain rate on the values of the tensile strength was tested at 1150 degC and at 1200 degC. The authors indicate that the results obtained, shown in figure 19, follow the same relationship between stress at a quasi-static strain rate and the strain rate reported by Jonas et al (53) for various materials, which include carbon and alloy steels, at lower temperatures (up to 1100 degC).

$$\text{stress}(\text{strain rate}) = \text{stress}(\text{QSSR}) (\text{strain rate}/\text{QSSR})^{0.2} \quad 1$$

where.

$$\text{QSSR} = 6 \times 10^{-4} \text{ sec}^{-1}$$

is the usually assumed quasi-static strain rate (53)

The stress rate referred to in this equation is the average rate of strain, such as has been used in nearly all experiments on dynamic plasticity. It is interesting to note that although the strain rate has a significant effect on the magnitude of the stresses, it has no effect on the Young's modulus (55).

The same type of equation is used in the model developed by Sorimachi and Brimacombe (38) assuming a constant strain rate of 10^{-3} m.s^{-1} .

The measurements made by Kitaoka et al (52) represent an important advance in that they cover a whole range of steels and can be related to specific characteristics of these steels. Still, the determination of the mechanical properties of steels solidifying in a continuously casting mould by experimental methods which rely on reheating cold specimens is limited. This is illustrated by the investigations undertaken by Weinberg (70) which show important differences in the results obtained after preheating the steel to near its melting point prior to testing.

The results of these measurements can only be taken as an indication of what the mechanical properties of continuously cast steels might actually be while they are solidifying in the mould.

Table 1 : Chemical composition of the continuously cast slab samples tested (52)

(%)

Steel	C	Si	Mn	P	S	Al _{tot}	N	Cr	Nb	V
No.1	0.035	0.019	0.25	0.016	0.015	0.048	0.0040	—	—	—
No.2	0.40	0.26	1.37	0.019	0.008	0.012	0.0068	—	—	—
No.3	0.89	0.27	0.46	0.014	0.008	0.001	0.0058	0.18	—	—
No.4	0.94	0.22	0.38	0.014	0.003	—	0.0039	1.16	—	—
No.5	0.08	0.25	1.61	0.020	0.004	0.037	—	0.004	0.037	0.052
No.6	0.13	0.21	0.62	0.021	0.011	0.002	—	—	—	—
No.7	0.18	0.21	0.68	0.027	0.014	0.003	—	—	—	—

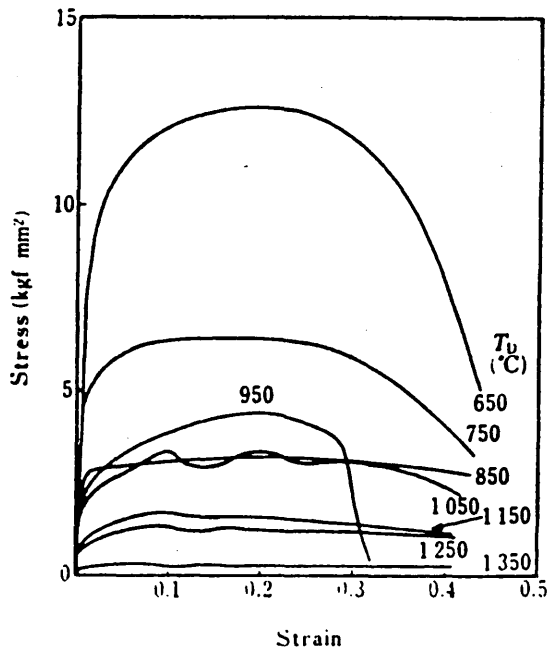


FIG 16: Stress-strain curves for No.1 low carbon steel (52)

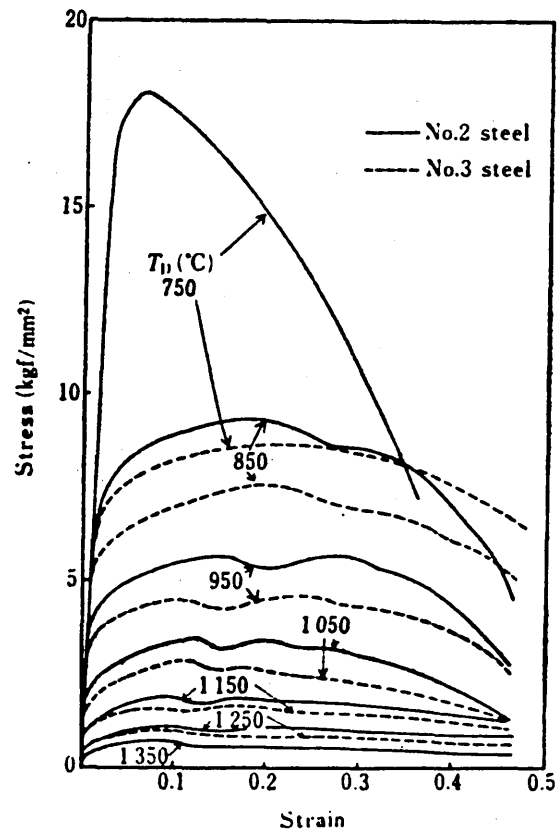


FIG 17: Stress-strain curves for No.2 and No.3 high carbon steel (52)

Table 2 : Change of 0.4% flow stress and tensile strength with test temperature.(52)

(kgf/mm²)

Steel	Stress	T _D (°C)									
		650	750	850	950	1050	1150	1250	1350	1400	1450
No. 1	$\sigma_{0.004}$	2.5	2.2	1.7	1.6	1.5	1.0	0.7	0.3	0.4	—
	σ_{TS}	12.7	6.5	3.2	4.5	3.4	1.7	1.4	0.6	0.5	—
No. 2	$\sigma_{0.004}$	3.2	2.4	2.3	1.8	1.7	0.9	0.6	0.4	0.3	0.3
	σ_{TS}	30.8	17.6	9.3	5.7	3.5	1.9	1.2	0.7	0.5	0.4
No. 3	$\sigma_{0.004}$	2.3	2.2	2.1	1.3	1.2	0.9	0.5	0.2	—	—
	σ_{TS}	20.3	8.6	7.6	4.5	2.8	1.6	1.0	0.3	—	—
No. 4	$\sigma_{0.004}$	2.8	2.2	1.8	1.9	1.1	1.1	0.6	0.2	—	—
	σ_{TS}	24.6	9.5	8.9	4.4	2.9	1.7	1.0	0.3	—	—

Steel	Stress	T _D (°C)									
		700	800	900	1000	1100	1200	1300	1400	1450	1470
No. 5	$\sigma_{0.004}$	2.8	3.1	2.1	2.4	2.3	1.1	0.6	0.4	—	—
	σ_{TS}	25.1	13.4	9.9	6.4	3.9	2.4	1.3	0.8	—	—
No. 6	$\sigma_{0.004}$	2.7	2.4	1.4	2.0	1.4	0.9	0.9	0.4	0.3	0.2
	σ_{TS}	14.9	6.9	5.4	4.6	3.2	2.0	1.3	0.8	0.6	0.5
No. 7	$\sigma_{0.004}$	2.6	2.7	2.3	1.7	1.2	1.0	0.7	0.5	0.3	0.2
	σ_{TS}	18.4	7.2	6.4	4.1	3.0	2.2	1.3	0.9	0.6	0.4

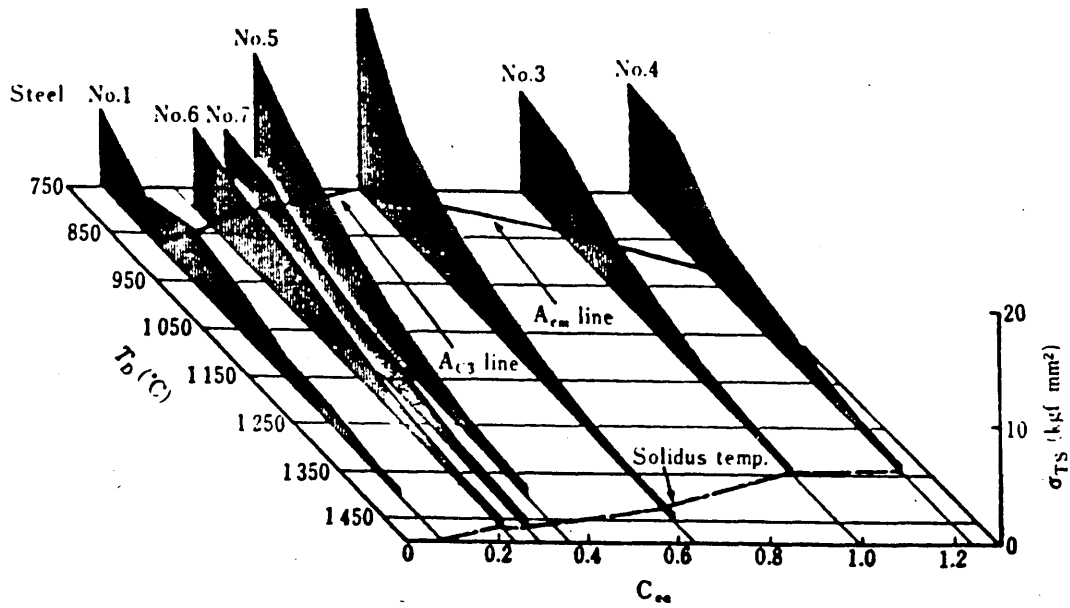


FIG 18 Dependence of tensile strength on temperature and carbon equivalent. (52)

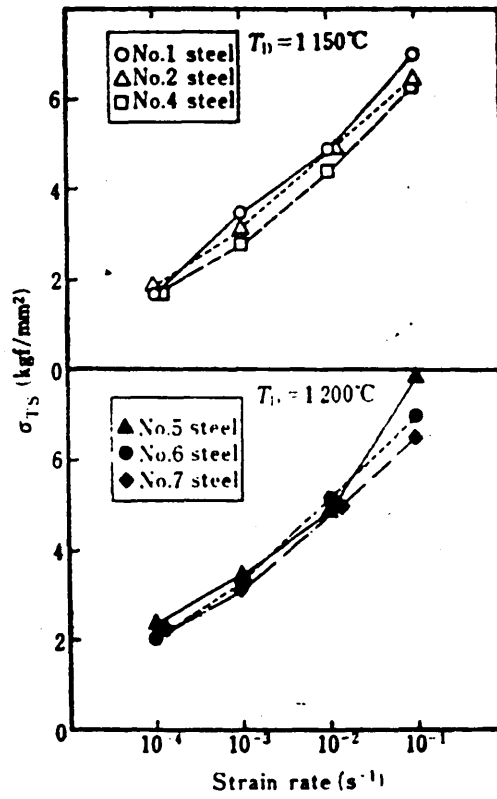


FIG 19 Strain rate dependence of tensile strength at 1150 degC and 1200 degC for the steels listed in table 1.

CHAPTER 3 : EXPERIMENTAL DEVELOPMENT OF BIMETALLIC STRUCTURE ANALOGUE

3.1 STAGES OF DEVELOPMENT

INTRODUCTION

The previous analysis has already identified the main area of interest of the research as the study of the continuous casting solidifying shell as a structure of four beams joined together by rigid corners.

The aim of the experimental work was to develop a physical analogue of this structure, that is, to construct a simple structure and subject it to factors analogous to those found in continuous casting. In this way the behaviour of the structure forming in the real process could be visualised and familiarity with its likely structural behaviour be achieved.

If an horizontal cross section of a continuously cast strand is considered, it appears that a rectangular box structure formed by four bimetallic strips and four corners provides a suitable analogy.

The use of bimetallic strip allows the development of thermo-mechanical behaviour analogous to some extent to that shown by rapidly solidifying metal shells. Some type of distributed load can provide an effect analogous to that of the liquid steel pressure acting upon the solidifying shell.

SELECTION OF THE BIMETAL

The bimetal TELCON 200 was selected because of its high strip deflection constant,

$$K_s = 3/4 (\alpha - \beta) = 19.3 \times 10^{-6} \text{ [1/deg C]}$$

where " α " and " β " are the coefficient of thermal expansion of the high and low expansion sides respectively.

Bimetal TELCON 200 is based on a comparatively recent innovation in the high expansion alloy field: the development of high manganese copper-nickel alloy with an expansion coefficient of about 29×10^{-6} [1/deg C]. This alloy when combined with a standard low expansion alloy, produces a thermostatic bimetal with approximately 50% higher thermal activity than standard high sensitivity bimetals.

Figure 1 shows the comparative deflection curves for medium to high activity TELCON bimetals, which are typical bimetals.

High activity bimetals have the further advantage of having a stable deflection constant over the range from 25 to 100 DegC or up to 150 DEG C for type 200 (Table 1).

It was assumed intuitively that the higher the bimetal deflection constant the greater would be the deflection produced experimentally. This proved to be right, although it later became apparent that there were other factors that had to be taken into account in selecting the most suitable bimetal.

Table 2 presents the mechanical properties and table 3 other fundamental characteristics of the TELCON bimetals.

FIGURE 1 : COMPARATIVE DEFLECTION CURVES FOR TELCON MEDIUM TO HIGH ACTIVITY BIMETALS.

TYPES 200, 160, 140, E140, 400, E400

(Telcon bimetals, publication TPlA, pg. 29)

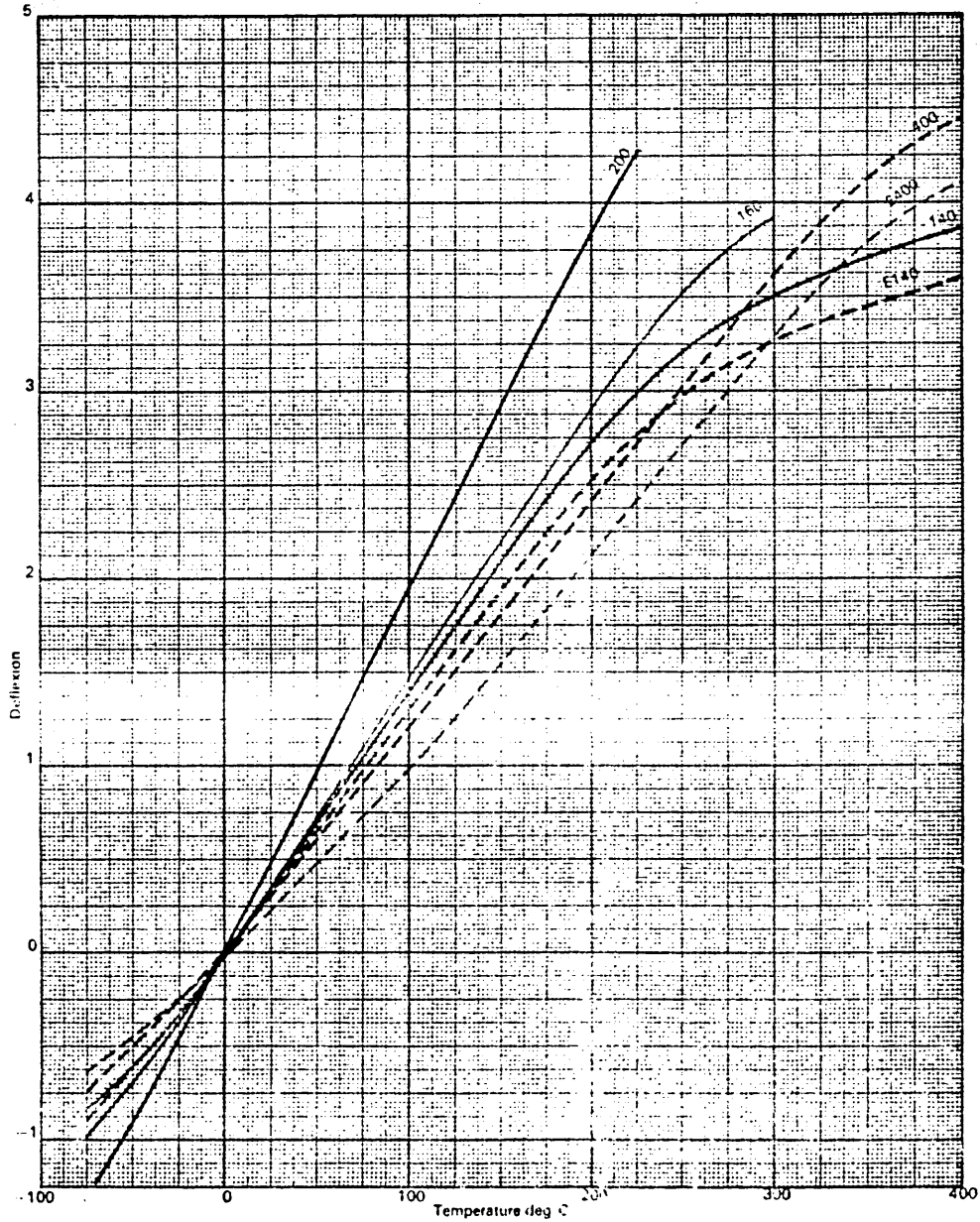


TABLE 1 : INSTANTANEOUS DEFLECTION CONSTANTS FOR TELCON BIMETALS.

(Telcon bimetals, publication TPlA, pg 31)

TYPE	Temperature deg C																
	-75	-50	-25	0	25	50	75	100	125	150	175	200	225	250	275	300	325
200	15.8	17.7	18.6	19.1	19.3	19.3	19.3	19.3	19.3	19.3	19.0	18.9	14.6	9.5			
160	11.2	12.3	13.5	14.5	14.8	14.8	14.8	14.8	14.8	14.7	14.3	13.6	12.4	10.5	7.5	5.1	
140	9.8	10.3	11.7	13.6	14.0	14.0	14.0	14.0	14.0	13.9	13.2	11.6	9.2	7.2	5.7	4.55	3.85
E140	10.7	11.7	12.4	12.9	13.1	13.1	13.1	13.1	12.9	12.6	11.9	10.8	9.1	7.2	5.5	4.3	3.55
400	9.4	9.7	10.3	11.2	11.6	11.9	11.9	11.9	11.9	12.0	12.0	12.1	12.1	12.1	12.0	11.6	10.6
E400	6.7	7.6	8.5	9.4	9.8	10.2	10.6	11.0	11.2	11.4	11.5	11.6	11.7	11.7	11.7	11.3	10.4
15	7.7	8.1	8.6	9.0	9.4	9.5	9.5	9.2	8.6	7.5	6.0	4.55	3.4	2.75	2.5	2.4	
188	6.7	6.9	7.5	8.7	9.3	9.2	9.0	8.8	8.3	7.6	6.4	4.75	3.0	2.8	2.5	2.4	2.35
75	4.1	4.8	5.4	5.8	6.1	6.4	6.6	6.9	7.2	7.5	7.7	8.0	8.1	8.0	7.8	7.2	6.6
41	3.3	3.7	3.95	4.1	4.15	4.2	4.2	4.1	4.0	3.8	3.7	3.6	3.5	3.3	3.0	2.7	2.3

TABLE 2 : MECHANICAL PROPERTIES OF TELCON BIMETALS.

(Telcon bimetals, publication TPLA, pg 12)

Type	Component alloys LE HE	Modulus of elasticity		Ultimate tensile strength		Specific gravity	Typical hardness HV	
		kgf/mm ²	lbf/in ²	kgf/mm ²	tonf/in ²		HE	LE
200	36 Ni Mn/Cu/Ni	13 500	19.0 × 10 ⁴	70	45	7.8	230	210
160	36 Ni Ni/Mn/Fe	16 000	22.5 × 10 ⁴	70	45	8.0	230	210
140	38 Ni Ni/Mn/Fe	16 000	22.5 × 10 ⁴	70	45	8.0	230	210
E140	36 Ni Ni/Cr/Fe	17 000	24.0 × 10 ⁴	80	50	8.0	260	220
400	42 Ni Ni/Mn/Fe	16 000	23.0 × 10 ⁴	70	45	8.0	230	220
E400	42 Ni Ni/Cr/Fe	17 000	24.5 × 10 ⁴	80	50	8.0	260	220
15	36 Ni Ni	18 500	26.0 × 10 ⁴	70	45	8.6	210	210
188	Ni/Fe/Cr Ni/Fe/Cr	17 500	25.0 × 10 ⁴	80	50	8.0	250	230
75	58 Ni Ni/Mn/Fe	17 500	25.0 × 10 ⁴	70	45	8.3	230	220
41	Ni Ni/Cr/Fe	19 500	28.0 × 10 ⁴	70	45	8.6	250	200

The Modulus of Elasticity of type 200 is significantly lower than the Moduli of Elasticity of the other types which means that the forces and bending moments necessary to deflect it are significantly lower. On one hand, this is an interesting characteristic of type 200 as it means that it is more sensible to the forces and bending moments. On the other hand, working with small loads made friction forces in the experimental apparatus relatively more significant.

TABLE 3 : FUNDAMENTAL CHARACTERISTICS OF TELCON BIMETALS.
 (Telcon bimetals, publication TPlA, pg 14)

Type	Deflexion constant per deg C (20-100 deg C)	Range of maximum Sensitivity	Useful deflexion Range	Modulus of elasticity		Electrical resistivity @ 20 deg C	Stabilising heat treatment deg C for 1 hour
		deg C	deg C	kgf/mm ²	mi-crohm m		
200	19.3 × 10 ⁻⁶	-25 to 200	-75 to 260	13500		1.11	260
160	14.8 × 10 ⁻⁶	0 to 180	-75 to 320	16000		0.78	350
*140	14.0 × 10 ⁻⁶	0 to 175	-75 to 350	16000		0.76	350
E140	13.1 × 10 ⁻⁶	-25 to 150	-75 to 400	17000		0.78	350
*400	11.8 × 10 ⁻⁶	0 to 310	-75 to 400	16000		0.70	350
E400	10.5 × 10 ⁻⁶	70 to 310	-75 to 400	17000		0.68	350
15	9.3 × 10 ⁻⁶	-10 to 110	-75 to 250	18500		0.16	350
188	8.8 × 10 ⁻⁶	0 to 130	-75 to 400	17500		0.87	350
75	6.5 × 10 ⁻⁶	125 to 300	-75 to 400	17500		0.46	350
41	4.1 × 10 ⁻⁶	-25 to 150	-75 to 400	19500		0.16	350

(NOTE ON HEAT TREATMENT: Following recommendations of the manufacturer, all bimetallic strips were heat treated to release the stresses induced during the manufacture. This heat treatment consists simply of heating the piece parts to the temperature recommended in this table and maintaining the temperature for one hour. The parts being treated must be packed in such a manner that they are free to deflect during the heat treatment cycle.)

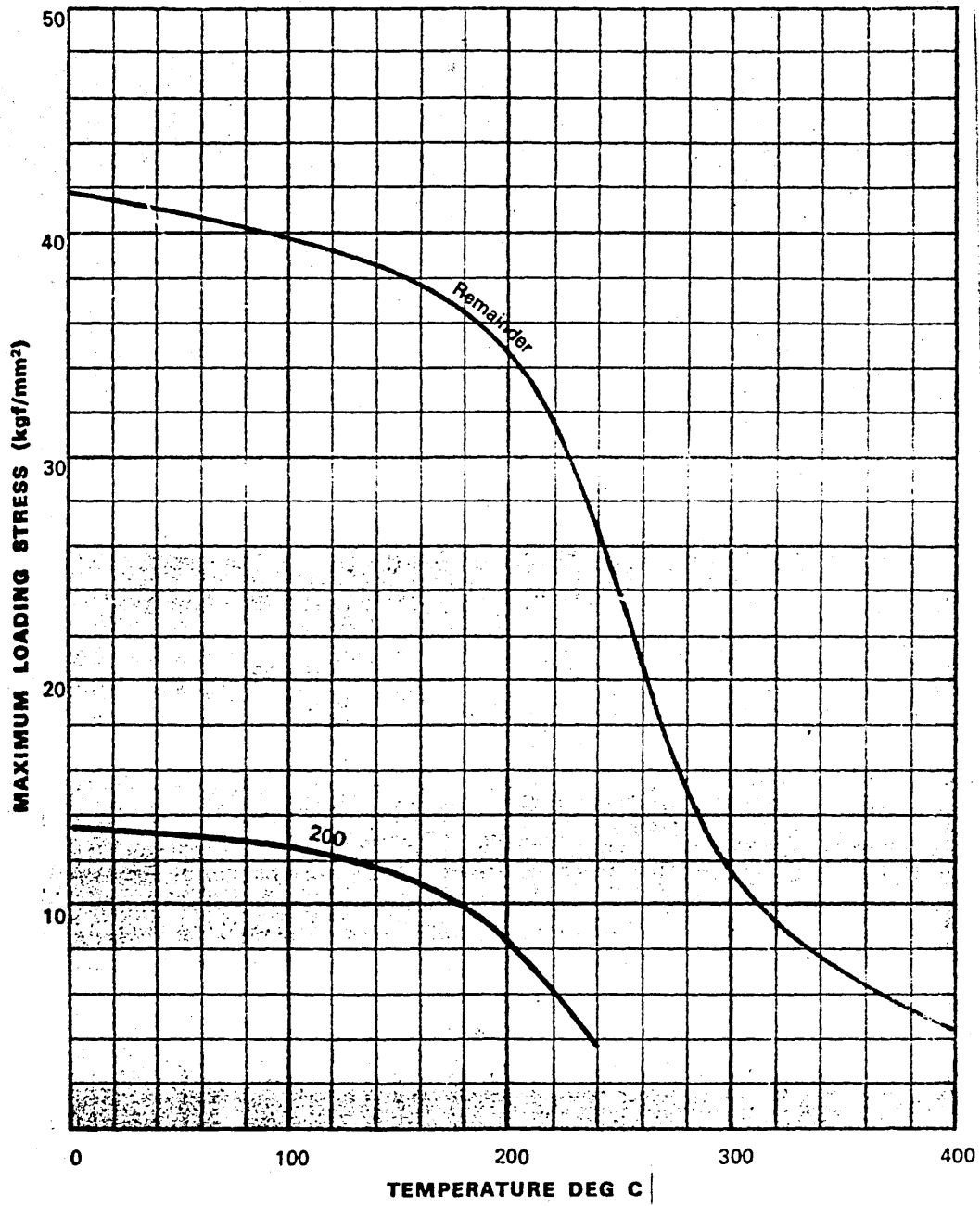
Another important factor to take into account is that the high deflection constant of bimetal TELCON 200 is achieved at the cost of an inherent weakness, the Maximum Loading Stress which it is able to withstand at a given temperature is significantly lower than for other bimetals (figure 2). This Maximum Loading Stress given in figure 2 is related to the internal stresses which develop in the bimetal and which have a particularly significant effect at the bonding between the two components . It is a safe margin, determined empirically by the manufacturer, to ensure that no permanent set (no "plastic deformation") of the bimetal occurs.

But this weakness of type 200 is compensated by the fact that lower loads (and bending moments) are involved in its deflection.

Four TELCON 200 bimetallic strips, flat at room temperature, 300mm x 35mm x 1mm , were ordered from the manufacturer to provide the sides of the box analogue structure.

FIGURE 2 : MAXIMUM LOADING STRESS CURVES

(Telcon bimetals, publication TPlA, pg 33)



RIGID CORNER BIMETALLIC STRUCTURE

The first rigid corners were constructed using angle sections of extruded aluminium together with aluminium plates, which were held with nuts and bolts. Figure 3 shows these first rigid corners and the assembled structure (with dimensions corresponding to the structure used in the first experiment). Each end of each bimetallic strip is clamped between a plate and one face of the angle section and positioned between the four bolts so that the strip lies horizontally with its longitudinal axis at the required height (32mm from the surface on which the structure rests).

Each corner is provided with a foot made by grinding a weld into an inverted cone shape. The assembled structure can thus rest upon a smooth surface with the corners free to rotate and slide as the structure deforms.

Since the corners are free to slide, no more than a slight tension on the bolts is sufficient to prevent the strip being pulled out of the clamp. However, it is also necessary to restrain the bimetallic strips from twisting and bending about their horizontal axes, so the aluminium used both for the angle and the plates has to be thick enough and the bolts have to be kept well tightened.

**EXPERIMENT 1 : EFFECT OF THE TEMPERATURE CHANGE ON A
STRUCTURE WITH DIFFERENT MOMENTS OF INERTIA IN
EACH PAIR OF OPPOSING SIDES.**

A rigid corner bimetallic structure with the following dimensions was assembled for this experiment (see figure 3), where,

CORNERS : Internal side width, 35mm
(Aluminium) Length (height) 56mm
Thickness, 3mm
Internal plates dimensions, 30mm x 56mm x 3mm

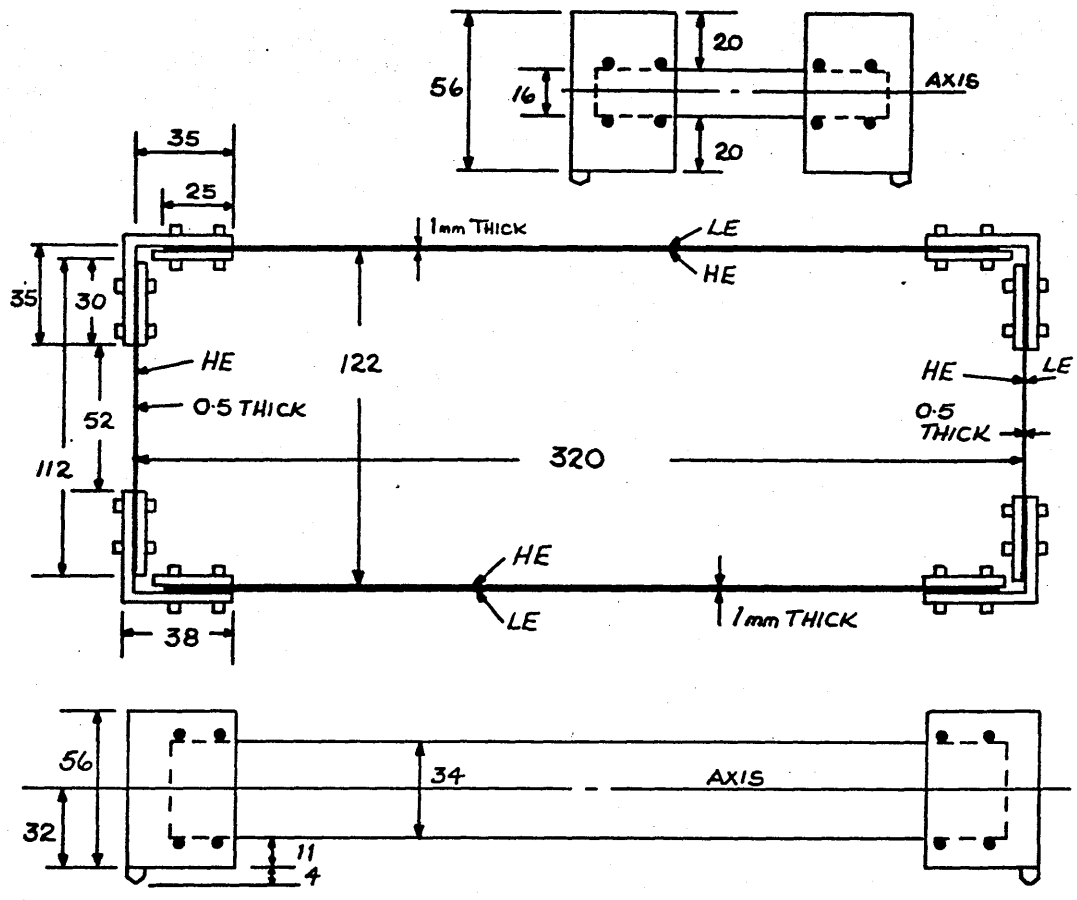
BIMETAL STRIPS : 2 x (112mm x 16mm x 0.5mm)
(TELCON 200*) 2 x (300mm x 34mm x 1.0mm)
flat at (20 ± 5) deg C

OVERLAP AT CORNER : ov = 30mm for the short strip.
ov = 25mm for the long strip.

The structure was immersed in water in a standard insulated tank 300mm x 900mm x 300mm. The water level was maintained at least 150mm over the top of the structure, that is, at least 210mm high.

Two 350W stirring immersion heaters were used to control the temperature of the tank. They had to be left on overnight to reach a temperature of 90 deg C. Measurements were then taken by cooling down the water to the desired temperature. Measurements were also taken increasing the water temperature to the desired temperature. No difference was detected between "cooling-down" and "heating-up" measurements.

FIGURE 3 : RIGID CORNER BIMETALLIC STRUCTURE AS ASSEMBLED FOR EXPERIMENT 1



KEY.

- HE.. HIGH EXPANSION
- LE. LOW EXPANSION.

ALL DIMENSIONS ARE IN MM.

The water temperature was monitored at different locations to detect temperature gradients. A PVC sheet helped to minimize heat escape by evaporation from the upper surface of the tank, while allowing the structure to be observed. It was possible to minimize the temperature gradients by raising the water temperature so that all thermometers would read at least 2 deg C more than the desired temperature and then leaving the temperature to stabilise after turning off the heater. In this way the temperature difference over the height of the bath could be kept below under 1 deg C, while temperature differences within the immediate vicinity of the structure were negligible.

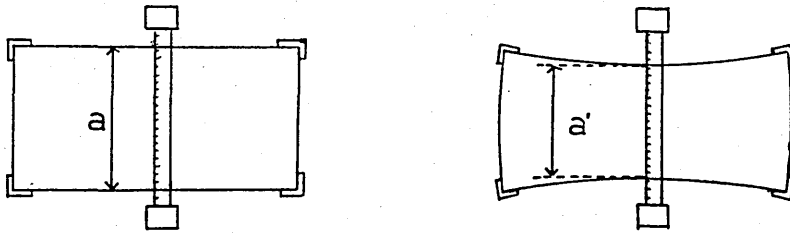
Various direct methods, using reference grids on top or under the structure, have been tried to measure the deflection.

None of them was satisfactory, several problems developing:

- * the deflections involved were small.
- * water vapour from the bath tended to obscure direct observation.
- * the water surface distorted direct readings.
- * it was difficult to keep the water clear.

Some measurements were, however, made. The contraction of the minimum distance between the two long beams (along the transversal median line of the rectangle) was measured using a ruler fixed slightly above the top of the long strips on two steel bars (aprox. 50mm from the bottom). The bars were welded upon a plate to increase their stability.(See fig. 4).

FIGURE 4 : MEASURING WITH A FIXED RULER.



The contraction of the distance between the long beams is given by,

$$\Delta a = a - a'$$

where,

a is the distance between the long beams at $T_0 = 20 \text{ deg C}$

a' is the distance between the long beams at T

The deflection of a long beam, at mid-span, was then assumed to be,

$$v(160) = \frac{a - a'}{2}$$

Measurements were taken at 20 deg C, 40 deg C and 60 deg C twice after "heating-up" and 6 times after "cooling-down". The results obtained were reproducible to within 1mm. The averages of the 8 sets of measurements are presented in table 4 . They are compared with the results predicted by the first and the final theoretical models.

The reading error estimate is based upon the fact that for each measurement of a' two readings had to be made on the ruler scale,

$$a' = r' - r''$$

so that the error on a' is twice the basic reading error ϵ_r ,

$$\epsilon_{a'} = 2 \epsilon_r$$

and it was difficult to estimate the position of each strip in relation to the ruler within less than $\pm 2\text{mm}$.

TABLE 4 : EXPERIMENTAL AND THEORETICAL RESULTS, EXPERIMENT 1
(deflection at the long beam middle span)

T	$a = a - a'$	$v(160)$ EXPERIMENT	$v(160)$ FIRST MODEL	$v(160)$ FINAL MODEL
[deg C]	[mm]	[mm]	[mm]	[mm]
20 ± 1	12 ± 4	6 ± 2	3.3	6.5
40 ± 1	22 ± 4	11 ± 2	6.6	13.0
60 ± 1	42 ± 4	21 ± 2	10.0	19.5

At the time of these initial experiments, only the first theoretical model of the physical analog was completed (with its limitations).

The difference between experimental and theoretical results was attributed to two possible reasons:

- 1.- lack of effective rigidity at the corners due to play in the corner clamp.
- 2.- limitations of the theoretical model.

The possibility that the first reason was correct was reinforced by the observation of a slight bending of the holding plates after several experimental runs. But after replacing the 1.5mm thick plates originally used with 3mm plates, the results remained within the same range but no bending of the plate could be detected. Later results confirmed that the difference between the experimental and theoretical results was not due to experimental errors but to limitations in the first theoretical model. Indeed, these measurements showed that the lack of rigidity of the corner was negligible.

The measurement technique used limited the analysis of the deflection of the beams to the mid-span deflection of the long beams, that is, to the maximum deflection within the structure. Attempts were made to measure the short beam mid-span deflection, but they were abandoned as no significant change could be measured between one temperature and another.

**EXPERIMENT 2 : EFFECT OF THE TEMPERATURE CHANGE ON A
STRUCTURE WITH CONSTANT MOMENTS OF INERTIA.**

Experiment 1 was repeated using strips of different length, two short and two long ones as before, but of otherwise equal characteristics (same thickness, width, components),

CORNERS : Internal side width, 35mm
(Aluminium) Length (height), 56mm
Thickness, 3mm
Internal plates dimensions, 30mm x 56mm x 3mm

BIMETAL STRIPS : 2 x (112mm x 34mm x 1.0mm)
(TELCON 200) 2 x (300mm x 34mm x 1.0mm)
flat at (20 ± 5) deg C

OVERLAP AT CORNER : ov = 30mm for the short strip.
ov = 25mm for the long strip.

The general set up of the experiment and the measurement technique used were the same as in the first experiment.

TABLE 5 : EXPERIMENTAL AND THEORETICAL RESULTS, EXPERIMENT 2
(deflection at the long beam middle span)

T	a = a - a'	v(160) EXPERIMENT	v(160) FIRST MODEL	v(160) FINAL MODEL
[deg C]	[mm]	[mm]	[mm]	[mm]
0 ± 1	0 ± 2	0 ± 1	0.0	0.0
0 ± 1	0 ± 2	0 ± 1	0.0	0.0
0 ± 1	0 ± 2	0 ± 1	0.0	0.0

No deflection could be detected. This result agrees with the predictions of both the first and final theoretical models.

The deflection of the structure is independent of the relative lengths of the bimetallic strips as the bending moment induced in both is constant over their length and all their other characteristics are equal.

The result confirmed that lack of rigidity at the corners was negligible and that the absence of agreement between the results predicted by the first model and those obtained in the first experiment was due to the limitations of the theoretical model. Limitations of the measurement technique had already been taken into account in the error estimate of the results.

THE USE OF LONGER BIMETALLIC STRIPS

After these first attempts to develop a physical analogue of continuous casting, it became evident that both the techniques used to measure deflection and the mathematical model of the analogue had to be improved a great deal to approach a satisfactory starting point.

The structure itself was unsatisfactory.

Although measurement techniques and mathematical modelling could be improved a lot it was already apparent from the simple observation of the behaviour of the structure under temperature changes and under its simple handling (pulling out the strips with the hands) that the variations in curvature along the strips remained very small.

One of the aims of the research is to develop some understanding of the curvature variations along the deforming faces resulting in significant changes of concavity along the long face of a continuously cast slab. It was not clear, at first, if a purely elastic deformation along the faces could account for such a final shape, but the analogue structure had already shown that elastic deformation by itself could lead to similar shapes from the combination of thermal and mechanical loads. However the results also showed the necessity of amplifying the effects obtained before firm conclusions could be drawn.

Whereas the thermally induced bending moment on a bimetallic strip is constant, the bending moment arising from a mechanical load is not since its magnitude is related to the relative distance from the supports as much as to distance from the points of application of the load.

The bending moment resulting from the superposition of thermal and mechanical loads is thus not constant along any of the beams.

Thus in practice, variable moments, similar to those found in continuous casting, can be developed within the physical analogue, even though its deflections are purely elastic. There is, however, no direct relation between the non-uniformity of the moments within the analogue, due to the mechanical loading, and the non-uniformity of the moments within the continuous casting shell which involve plasticity and variable thermal loading as well as mechanical loading.

Increasing the lengths of the bimetallic strips in the analogue structure, without altering their other characteristics, would amplify both the overall deflections and the variations in curvature caused by the non uniform moments.

CURVATURE OF THE STRIPS AT ROOM TEMPERATURE

New bimetallic strips were obtained having the same thickness as the previous strips, but being longer and wider (Table 1). The other important difference was that they were not flat at room temperature. (figure 5).

This allowed meaningful measurements to be made at room temperature on the combined effects on the structure of mechanical and thermal loads, assuming that the curvature at room temperature was in fact due to a thermal effect, there being a certain higher temperature at which the strips were flat (experiment 4).

The curvature of the strips was measured geometrically from the imprint of their edges.

There is a variation of curvature within each strip (Table 6) which consists mainly of a regular increase of the radius of curvature along the length of the strip due to the fact that the strips are finished and packed in rolls. There is also some twisting of the strips, which manifest in different curvatures of the top and bottom edges of a given length. However, the effect of this twisting is less than the length variation and negligible at the center lines where the deflection measurements were later taken with the final apparatus.

Both curvature variations are diminished when the strips are assembled into the structure and are too small to induce a relevant built up of stresses.

FIGURE 5 : BIMETALLIC STRIP CURVED AT ROOM TEMPERATURE USED.

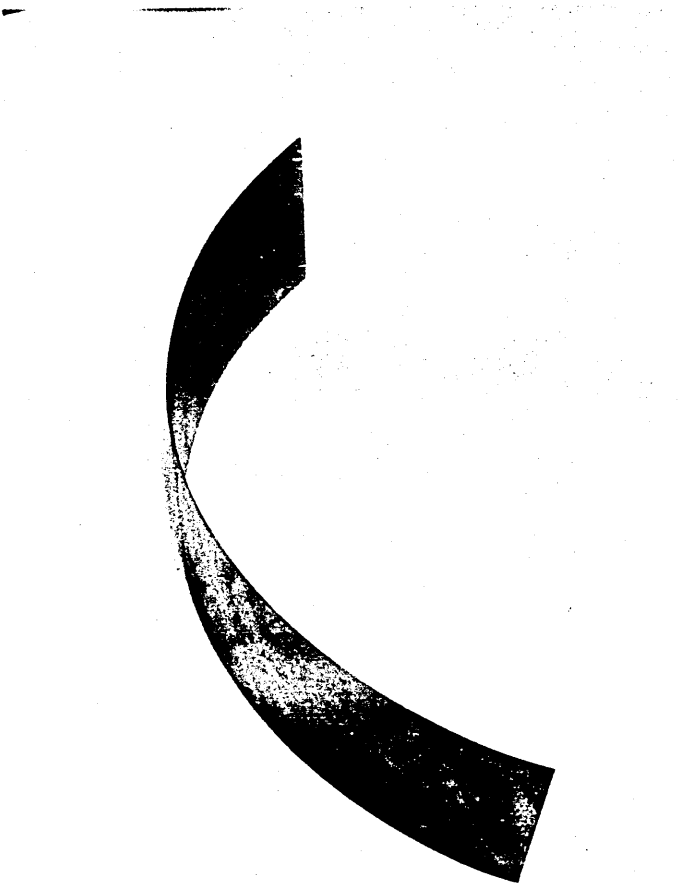


TABLE 6 : CHARACTERISTICS OF THE BIMETALLIC STRIPS CURVED AT ROOM TEMPERATURE USED

(Information provided by Telcon metals)

Type: TELCON 200

Components alloys, L.E. : 36 Ni

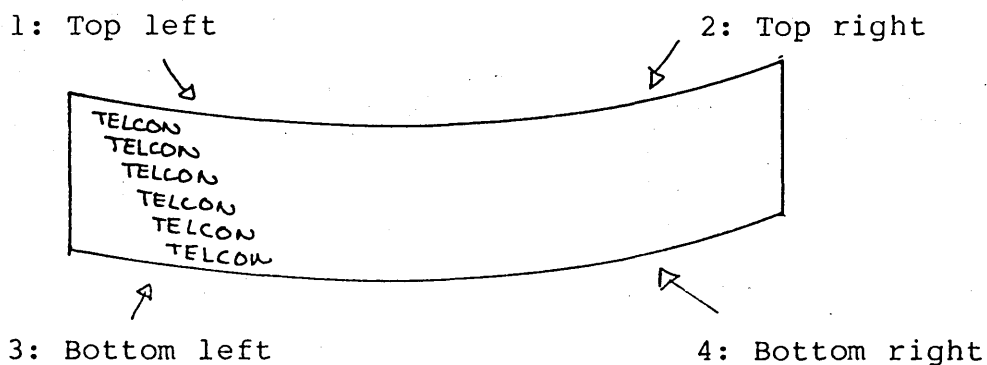
H.E. : Mn/Cu/Ni

Modulus of elasticity:	13500	[kgf/mm]
Ultimate tensile strength:	70	[kgf/mm]
Specific gravity:	7.8	
Typical hardness (HV),	L.E. : 210	
	H.E. : 230	
Deflection constant (20-100 deg C):	19.3	$\times 10^{-6}$ [1/deg C]
Specific deflection (20-100 deg C):	0.212	$\times 10^{-6}$ [1/deg C]
Range of maximum sensitivity:	-25 to 200	[deg C]
Useful deflection range:	-75 to 260	[deg C]
Stabilising heat treatment:	260 deg C for one hour	

Dimensions:	short strips	long strips
	[mm]	[mm]
length	214	502
width	120	116
thickness	1.0	0.5

Curvature at room temperature: (260 20) [mm]

FIGURE 6 : IDENTIFICATION OF THE STRIPS EDGE SEGMENTS FROM WHERE IMPRINTS WERE TAKEN FOR THE MEASUREMENT OF CURVATURE.



The "TELCON LE" labels, printed on the strips to identify their low expansion side, also identify unambiguously the edge segments considered.

TABLE 7 : LOCAL CURVATURE OF THE STRIPS EDGES

STRIP	DIMENSION	CURVATURE AT EDGE SEGMENT:			
		1	2	3	4
		[mm]	[mm]	[mm]	[mm]
A	1mmx120mmx214mm	250	265	245	273
B	1mmx120mmx214mm	243	265	245	285
C	.5mmx116mmx502mm	238	262	243	269
D	.5mmx116mmx502mm	247	263	246	263

EXPERIMENT 3 : LONGER AND WIDER BIMETALLIC STRIPS

This was an attempt to repeat the previous experiments with the new longer and wider bimetallic strips. The assembled structure had the following characteristics,

CORNERS : External side width, 25mm
 (Aluminium) Length (height), 150mm
 Thickness, 3mm
 External plates dimensions, 25mm x 130mm x 3mm

BIMETAL STRIPS : 2 x (100mm x 120mm x 1.0mm)
 (TELCON 200) 2 x (300mm x 120mm x 1.0mm)
 flat at (20 ± 5) deg C

OVERLAP AT CORNER : ov = 25mm for all strips.

The general set up of the experiment was similar to the one used in the first experiment, although a bigger and non insulated water tank (600mm x 600mm x 600mm) had to be used as well as an extra 500W immersion heater.

Several attempts were made to obtain a homogeneous temperature distribution around the structure during heating-up. A propeller stirrer was used in different orientations with different orientations for the immersion heaters, but a temperature difference of up to 10 deg C remained within the vicinity of the structure. This induced a twisting of the bimetallic strips.

A more homogeneous temperature distribution was obtained by cooling down the water slowly from 80 deg C to 30 deg C. Hot water was extracted from the top of the tank, while cold water was introduced at the bottom (far from the

structure), very slowly, using 8 rubber hoses (10mm internal diameter) (4 to extract the water, 4 to introduce it) Cooling from 80 degC to 30 deg C took about 3 hours. In this way, the maximum temperature gradient within the vicinity of the structure was reduced to less than 4 deg C for any temperature.

A high depth of water had to be maintained to minimize the temperature gradients and this made the observation of distortion very difficult.

The corners were a further problem as they lacked the rigidity which had been achieved for the narrow strips used in the first and second experiments.

New corners were made out of pairs of aluminium plates, bent to form right angles, which fitted together to hold the bimetallic strips. These proved to be much more rigid than the previous system and was found to be satisfactory.

EXPERIMENT 4: COMBINED EFFECT OF CENTRAL LOAD AND T VARIATION

The structure assembled for this experiment had the following characteristics,

CORNERS : INTERNAL ALUMINIUM ANGLES,
 External side width (section 1) 35.5mm
 External side width (section 2) 35.0mm
 Length (height) 170.0mm
 Thickness 3.0mm
 EXTERNAL ALUMINIUM ANGLES,
 Internal side width (both sections) 36.0mm
 Length (height) 150.0mm
 Thickness 3.0mm

BIMETALLIC STRIPS : 2 x (502mm x 116mm x 0.5mm)
 2 x (214mm x 120mm x 1.0mm)
 Radius of curvature at (20 ± 5) deg C = (255 ± 15) mm
 (with low expansion side, inside the curve)

OVERLAP AT CORNERS : ov = 35mm, both long and short strips

ASSEMBLED WITH LOW EXPANSION SIDES FACING OUTWARDS

It was assembled in a way similar to that used in the previous experiments, but with the low expansion sides facing outwards so that, if not restrained by the corners, all strips would bend outwards (the curvature being convex outwards).

Once assembled, the short strips force the long strips inwards (see figure 7). This is because the short strips are stronger than the long ones as they are thicker while being roughly of the same width. Their length is irrelevant.

The structure was placed upon a small square table and subjected to loads pulling the strips outwards from their middle span. Simple pulleys made from machined cast aluminium were used, held at an angle by a standard vice. Balance plates

and weights were attached to embroidery thread which was found to have the strength and flexibility required. The thread was simply looped around the strips and held with a simple knot. The weights involved were enough to ensure that the thread remained at the middle of each strip.

The top edges of the strips were marked with slight indentations at mid-span and at 20mm intervals from their joint with each corner, up to the point nearest to the middle of the span. The corners' top edges were also marked 20mm from the joints, that is at 16mm from the corner origin (figure 7).

The structure had to be very carefully adjusted so that opposite strips had the same length.

The distance between each pair of opposite marks was then measured directly with a ruler.

Balance plates were attached to the free ends of the threads and loaded with weights so as to increase equally the loads until the distance between the middle span marks on the long strips was equal to the original distance between the corner marks, at 16mm from the corner origin, before weights were added.

The results obtained are presented on table 8 and plotted on figure 7.

$L_1 = 268\text{mm}$ is half the length of the long beams. 1

$L_2 = 140\text{mm}$ is half the length of the short beams. 2

$l^T(x)$ is the distance between the two long beam opposite marks distant x from their respective corner origin when the structure has no load. 3

$l(x)$ is the similar distance when the structure is loaded. 4

$s^T(y)$ and $s(y)$ are the corresponding distances for the short beams. 5

The final load on each plate was,

$$F = (650 \pm 25) \text{ grs} \quad 6$$

The error is estimated from the fact that,

$$l(268) = 272\text{mm} \quad \text{for} \quad F = 638 \text{ grs} \quad 7$$

$$l(268) = 274\text{mm} \quad \text{for} \quad F = 672 \text{ grs} \quad 8$$

and that a $\pm 1\text{mm}$ error bound was assumed for the distance measurements.

The distance between all the other opposite marks was then measured with 650 gr loading on both plates. The structure was quite stable and no change on the measured distances could be detected even after perturbing sensibly the table upon which the structure was laid.

The loads were withdrawn, and the initial measurements were repeated obtaining the same results as initially. The loads were then replaced to take the measurements again. No variation was found. Such an agreement ^{between} ~~been~~ two sets of measurements showed that no further measurements were necessary to ensure that the experiment could be reproduced.

FIGURE 7 : TOP VIEW OF THE BIMETALLIC STRIPS STRUCTURE USED IN EXPERIMENT 4.

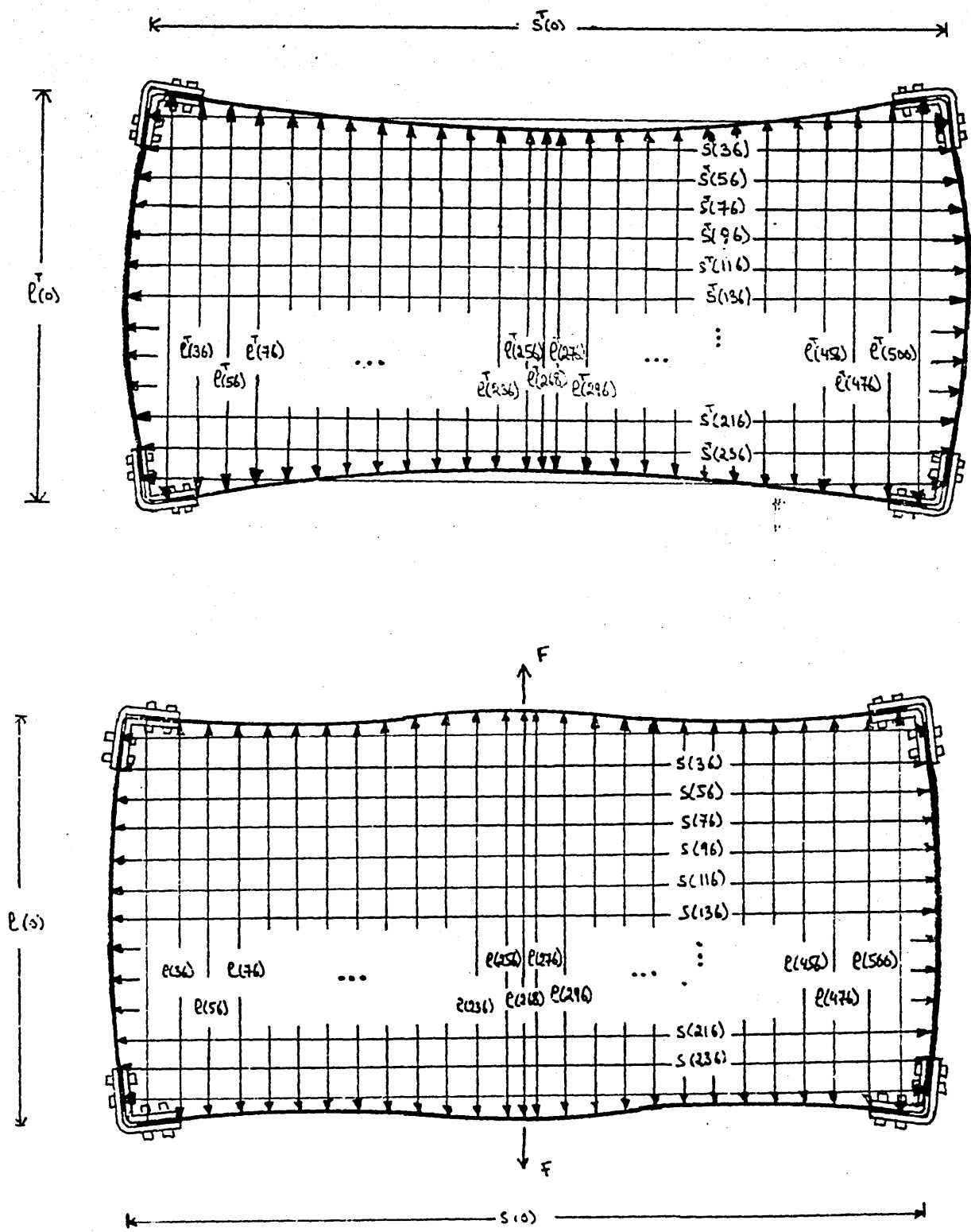


TABLE 8 : EXPERIMENT 4 RESULTS

(1mm appreciation)

Long beam, ($L_1 = 268\text{mm}$)

x [mm]	$l^T(x)$ [mm]	$l^T(536-x)$ [mm]	$d^T(x)$ [mm]	$l(x)$ [mm]	$l(536-x)$ [mm]	$d(x)$ [mm]
16	273	273	136.5	273	273	136.5
36	266	266	133.0	268	268	134.0
56	260	260	130.0	264	264	132.0
76	254	254	127.0	262	262	131.0
96	250	251	125.0	261	261	130.5
116	246	247	123.0	262	261	131.0
136	242	242	121.0	263	263	131.5
156	237	237	118.5	264	264	132.5
176	234	233	117.0	266	266	133.0
196	232	230	115.5	268	267	134.0
216	229	228	114.0	270	270	135.0
236	227	226	113.0	272	272	136.0
256	225	224	112.0	272	273	136.0
268	223	223	111.5	273	273	136.5

Short beam, ($L_2 = 140\text{mm}$)

y [mm]	s(x) [mm]	s(280-x) [mm]	d(x) [mm]	s(x) [mm]	s(280-x) [mm]	d(x) [mm]
16	536	536	268.0	535	535	267.0
36	543	543	271.5	542	542	271.0
56	549	550	275.0	547	548	274.0
76	556	556	278.0	553	553	276.5
96	559	560	280.0	558	558	279.0
116	562	562	281.0	559	559	279.5
136	563	563	281.5	560	560	280.0
140	563	563	281.5	560	560	280.0

INTERPRETATION OF THE RESULTS

The median lines, or symmetry axis, represent a suitable reference system to analyse the deformation of the structure.

As in previous analysis, it is assumed that the structure is, and remains symmetrical. The measurements taken show that the irregularities observed in the shape of the strips are smoothed out on the structure.

It can be observed that,

$$\forall x < 268\text{mm} \quad l_x^T(x) = l^T(536\text{mm} - x) \pm 3\text{mm} \quad 9$$

$$l(x) = l(536\text{mm} - x) \pm 3\text{mm} \quad 10$$

$$\forall y < 140\text{mm} \quad s^T(y) = s^T(280\text{mm} - y) \pm 3\text{mm} \quad 11$$

$$s(y) = s(280\text{mm} - y) \pm 3\text{mm} \quad 12$$

That is, the structure remains symmetrical up to a $\pm 3\text{mm}$ error bound.

It is assumed that the built of moments from this smoothing is negligible as the initial irregularities observed on the bimetallic strips curvature before assembling the structure were not very significant.

Then, assuming symmetry, a quarter section of the structure is analysed.

Let,

$d_x^T(x)$ the distance from the short beams axis of symmetry to 13
the long beam mark at a distance x from the corner when
there is no load.

$d_x(x)$ the similar distance when the structure is loaded. 14

$dy^T(y)$ and $dy(y)$ the corresponding distances for the short 15
beam.

these distances related to the axis of symmetry are taken as
half the average values of the measured distances, that is,

$\forall x < 268\text{mm}$ on the long beam,

$$d_x^T(x) = \frac{l^T(x) + l^T(536\text{mm} - x)}{4} \quad 16$$

$$d_x(x) = \frac{l(x) + l(536\text{mm} - x)}{4} \quad 17$$

$\forall y < 140\text{mm}$ on the short beam,

$$dy^T(y) = \frac{s^T(y) + s^T(280\text{mm} - y)}{4} \quad 18$$

$$dy(y) = \frac{s(y) + s(280\text{mm} - y)}{2} \quad 19$$

These calculated values are affected both by the error due to
irregularities along the beams,

$$\text{ERROR BOUND(irregularities)} = \pm 3 \text{ mm} \quad 20$$

and by the error inherent to the measurement technique

adopted

$$\text{ERROR BOUND(ruler)} = \pm 1 \text{ mm} \quad 21$$

These errors affect directly the measured distances, then,

$$\text{ERROR BOUND(measured distances)} = \pm 4 \text{ mm} \quad 22$$

but the double average made in relation with the two symmetrical axis to obtain the analytical distances makes,

$$\text{E.B.}(analytical \text{ distances}) = 1/4 \text{ E.B.}(measured \text{ distances}) \quad 23$$

$$\text{E.B.}(analytical \text{ distances}) = 1/4 \text{ E.B.}(measured \text{ distances}) \quad 24$$

This is the error bound of $d_x^T(x)$, $d_x(x)$, $dy^T(y)$ and $dy(y)$.

ROTATION OF THE CORNER

When there is no load, the slope of the long beam corner section is given by,

$$\text{slope}(T,L) = \frac{d_x^T(36\text{mm}) - d_x^t(16\text{mm})}{20\text{mm}} \quad 25$$

$$\text{slope}(T,L) = \frac{133\text{mm} - 136.5\text{mm}}{20\text{mm}} \quad 26$$

$$\text{slope}(T,L) = - 0.18 \quad 27$$

and the slope of the short beam corner section is given by,

$$\text{slope}(T,s) = \frac{d_y^T(36\text{mm}) - d_y^T(16\text{mm})}{20\text{mm}} \quad 28$$

that is,

$$\text{slope}(T,s) = \frac{271.5\text{mm} - 268\text{mm}}{20\text{mm}} \quad 29$$

$$\text{slope}(T,s) = + 0.18 \quad 30$$

When the structure is loaded, the slope of the long beam corner section is given by,

$$\text{slope}(TL,L) = \frac{d_x^T(36\text{mm}) - d_x^T(16\text{mm})}{20\text{mm}} \quad 31$$

that is,

$$\text{slope}(TL,L) = \frac{134\text{mm} - 136.5\text{mm}}{20\text{mm}} \quad 32$$

$$\text{slope}(TL,L) = - 0.13 \quad 33$$

and the slope of the short beam corner section is given by,

$$\text{slope}(TL,s) = \frac{d_y^T(36\text{mm}) - d_y^T(16\text{mm})}{20\text{mm}} \quad 34$$

$$\text{slope}(TL,s) = \frac{271\text{mm} - 268\text{mm}}{20\text{mm}} \quad 35$$

$$\text{slope}(TL,L) = + 0.15 \quad 36$$

Before the mechanical loads were placed, the corner was effectively rigid and we obtained,

$$\text{slope}(T,L) = - \text{slope}(T,s) \quad 37$$

But after the loads were placed it was found that,

$$\text{slope(TL,L)} \neq - \text{slope(TL,s)} \quad 38$$

$$\text{slope(TL,L)} = - \text{slope(TL,s)} + 0.02 \quad 39$$

There is an apparent lack of rigidity at the corner, but it is necessary to take into account the error bounds on the values obtained.

Within the corner sections there are no irregularities, and the main source of error is the limited appreciation of the ruler used. With a 1mm appreciation ruler, the error in the analytical distances is estimated to be of the order of $\pm 0.25\text{mm}$.

Still, the possible error on the slope is,

$$\text{E.B.}[\text{slope}] = \frac{2 \times \text{E.B.}[dz(z)]}{20\text{mm}} \quad 40$$

$$\text{E.B.}[\text{slope}] = 0.025 \quad 41$$

Which means that the difference on the slopes obtained would be negligible given the measurement and calculation errors. However, if a better ruler is used, one with an 0.5mm appreciation, the error on the calculated distances from the axis of symmetry can be reduced to $\pm 0.0125\text{mm}$.

The experiment was repeated and more careful measurements were made, with an 0.5mm appreciation ruler, for the marks next to the corner (16mm, 36mm, 56mm).

The following results were obtained,

TABLE 9 : EXPERIMENT 4 RESULTS (0.5mm appreciation)

Long beam,

x	$l^T(x)$	$l^T(536-x)$	$d^T(x)$	$l(x)$	$l(536-x)$	$d(x)$
[mm]	[mm]	[mm]	[mm]	[mm]	[mm]	[mm]
16	273.0	273.0	136.5	273.5	273.5	136.75
36	266.5	266.5	133.25	268.0	268.0	134.0
56	260.0	260.0	130.0	264.0	264.0	132.0

Short beam,

y	$s^T(x)$	$s^T(280-x)$	$d^T(x)$	$s(x)$	$s(280-x)$	$d(x)$
[mm]	[mm]	[mm]	[mm]	[mm]	[mm]	[mm]
16	536.0	536.0	268.0	535.5	535.5	267.75
36	542.5	542.5	271.25	541.0	541.0	270.5
56	549.5	549.5	275.25	547.75	548.75	273.75

Therefore,

$$\text{slope}(T,L) = \frac{d_x^T(36\text{mm}) - d_x^T(16\text{mm})}{20\text{mm} - (d_x^T(36\text{mm}) - d_x^T(16\text{mm}))} = - (0.16 \pm 0.01) \quad 42$$

$$\text{slope}(T,s) = \frac{d_y^T(36\text{mm}) - d_y^T(16\text{mm})}{20\text{mm} - (d_y^T(36\text{mm}) - d_y^T(16\text{mm}))} = - (0.16 \pm 0.01) \quad 43$$

$$\text{slope}(TL,L) = \frac{d_x(36\text{mm}) - d_x(16\text{mm})}{20\text{mm} - (d_x(36\text{mm}) - d_x(16\text{mm}))} = - (0.14 \pm 0.01) \quad 44$$

$$\text{slope}(TL,s) = \frac{d_y(36\text{mm}) - d_y(16\text{mm})}{20\text{mm} - (d_y(36\text{mm}) - d_y(16\text{mm}))} = - (0.14 \pm 0.01) \quad 45$$

It appears, then, that there is no significant lack of rigidity at the corner.

POSITION OF THE CORNER

Let,

p_x^T and p_y^T be the coordinates of the corner of the structure 46
subjected only to thermal stress in relation to the
flat strips structure.

p_x and p_y the corresponding coordinates of the corner of the 47
structure subjected both to thermal stress and
mechanical load.

The position of the corner can be calculated by extrapolation,

Long beam, without mechanical load, #

$$d_x^T(0) = d_x^T(16\text{mm}) + \text{slope}(T,L) \times 16 \text{ mm} \quad 48$$

that is, using equation 42,

$$d_x^T(0) = 139.0 \text{ mm} \quad 49$$

Therefore,

$$p_x^T(0) = L_1 - d_x^T(0) \quad 50$$

$$p_x^T(0) = 1.0 \text{ mm} \quad 51$$

Short beam, without mechanical load,

$$d_y^T(0) = d_y^T(16\text{mm}) + \text{slope}(T,s) \times 16 \text{ mm} \quad 52$$

that is, using equation 43,

$$d_y^T(0) = 265.5 \text{ mm} \quad 53$$

Therefore,

$$p_Y^T(0) = L_1 - d_Y^T(0) \quad 54$$

$$p_X^T(0) = 2.5 \text{ mm} \quad 55$$

Long beam, with mechanical load,

$$d_X(0) = d_X(16\text{mm}) + \text{slope(TL,L)} \times 16 \text{ mm} \quad 56$$

that is, using equation 44,

$$d_X(0) = 139.0 \text{ mm} \quad 57$$

Therefore,

$$p_X(0) = L_2 - d_X(0) \quad 58$$

$$p_X(0) = 1.0 \text{ mm} \quad 59$$

Short beam, with mechanical load,

$$d_Y(0) = d_Y(16\text{mm}) + \text{slope(TL,s)} \times 16 \text{ mm} \quad 60$$

that is, using equation 43,

$$d_X(0) = 265.5 \text{ mm} \quad 61$$

Therefore,

$$p_Y(0) = L_1 - d_Y^T(0) \quad 62$$

$$p_X^T(0) = 2.5 \text{ mm} \quad 63$$

DEFLECTION OF THE STRUCTURE

Figure 8 shows the deflection of the structure due to the thermal stress as measured.

At about 50 deg C, the bimetallic strips of the structure are flat, and it is only in this situation that the distances measured along the beam agree precisely with the projected distances.

Knowing the position of the corner, and of the reference marks in relation to the medians, it is possible to express the position of the reference marks in relation to the x, y reference system of axis parallel to that defined by the flat beam structure but with the displaced corner as origin.

Let,

$v(x)$ be the deflection at a distance x from the corner along 64 the long beam in relation to the corner reference system.

$v(y)$ be the deflection at a distance y from the corner along 65 the short beam in relation to the corner reference system.

the superfix T shall denote, as previously, the values which correspond to the structure subjected to thermal stresses alone.

The absence of superfix denotes, as previously, the values which correspond to the structure subjected to both thermal

and mechanical loads.

We shall also use now the superfix L , to denote the values which correspond to the structure subjected to mechanical loads alone. These are calculated using the principle of superposition.

$$\forall x < L_1,$$

$$v^T(x) = - l^T(x)/2 + L_2 \quad 66$$

$$v(x) = - l(x)/2 + L_2 \quad 67$$

$$v^L(x) = v(x) - v^T(x) \quad 68$$

$$\forall y < L_2,$$

$$v^T(y) = - s^T(y)/2 + L_1 \quad 69$$

$$v(y) = - s(y)/2 + L_1 \quad 70$$

$$v^L(y) = v(y) - v^T(y) \quad 71$$

The calculated deflections corresponding to the results of experiment 4 are presented on table 10 (next page).

These deflections are plotted assuming the distance along the beam to be approximately equal to the projected distances along the axis whose origin is the displaced corner and which is parallel to the flat strips position (figure 8 and 9).

TABLE 10: EXPERIMENT 4 RESULTS: DEFLECTIONS

long beam, ($L_1=268\text{mm}$, $L_2=140\text{mm}$, $d_x(0)=139.5\text{mm}$, $d_x(0)=138.5\text{mm}$)

x [mm]	$v^T(x)$ [mm]	$v^T(536-x)$ [mm]	$v(x)$ [mm]	$v(536-x)$ [mm]	$v^L(x)$ [mm]	$v^L(536-x)$ [mm]
16	3.5	2.5	3.25	2.25	- 0.25	- 0.25
36	6.75	5.75	6.0	5.0	- 0.75	- 0.75
56	10.0	9.0	8.0	7.0	- 2.0	- 2.0
76	13.0	12.0	9.0	8.0	- 4.0	- 4.0
96	15.0	14.0	9.5	8.5	- 5.5	- 5.5
116	17.0	16.0	9.0	8.0	- 8.0	- 8.0
136	19.0	18.0	8.5	7.5	- 10.5	- 10.5
156	21.5	20.5	8.0	7.0	- 13.5	- 13.5
176	23.0	22.0	7.0	6.0	- 16.0	- 16.0
196	24.5	23.5	6.0	5.0	- 18.5	- 18.5
216	26.0	25.0	5.0	4.0	- 21.0	- 21.0
236	27.0	26.0	4.0	3.0	- 23.0	- 23.0
256	28.0	27.0	4.0	3.0	- 24.0	- 24.0
268	28.5	27.5	3.5	2.5	- 25.0	- 25.0

Short beam, ($L = 140\text{mm}$, $L = 268\text{mm}$, $d_y(0)=265.0\text{mm}$, $d_y(0)=265.5\text{mm}$)

y [mm]	$v^T(y)$ [mm]	$v^T(280-y)$ [mm]	$v(y)$ [mm]	$v(280-y)$ [mm]	$v^L(y)$ [mm]	$v^L(280-y)$ [mm]
16	0.00	- 2.50	0.25	- 2.25	0.25	0.25
36	- 3.25	- 5.75	- 2.50	- 5.50	0.75	0.75
56	- 6.75	- 9.25	- 5.75	- 8.25	1.0	1.0
76	- 9.5	- 12.0	- 8.5	- 11.0	1.0	1.0
96	- 12.0	- 14.5	- 11.0	- 13.5	1.0	1.0
116	- 13.0	- 15.5	- 11.5	- 14.0	1.5	1.5
136	- 13.5	- 16.0	- 12.0	- 14.5	1.5	1.5
140	- 13.5	- 16.5	- 12.0	- 14.5	1.5	2.0

FIGURE 8 : DEFLECTION OF THE BEAM DUE TO THERMAL STRESS

EXPERIMENT 4

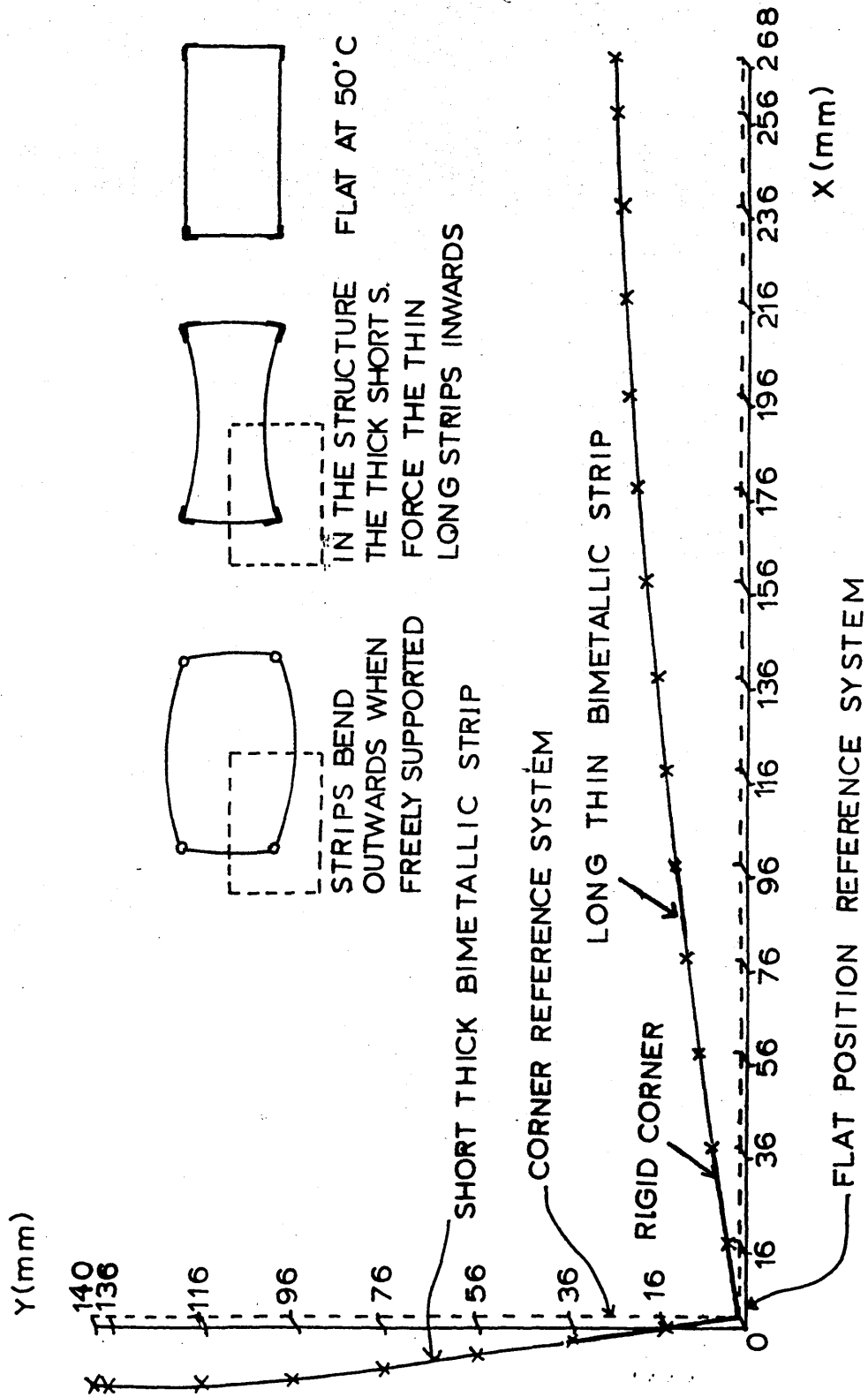
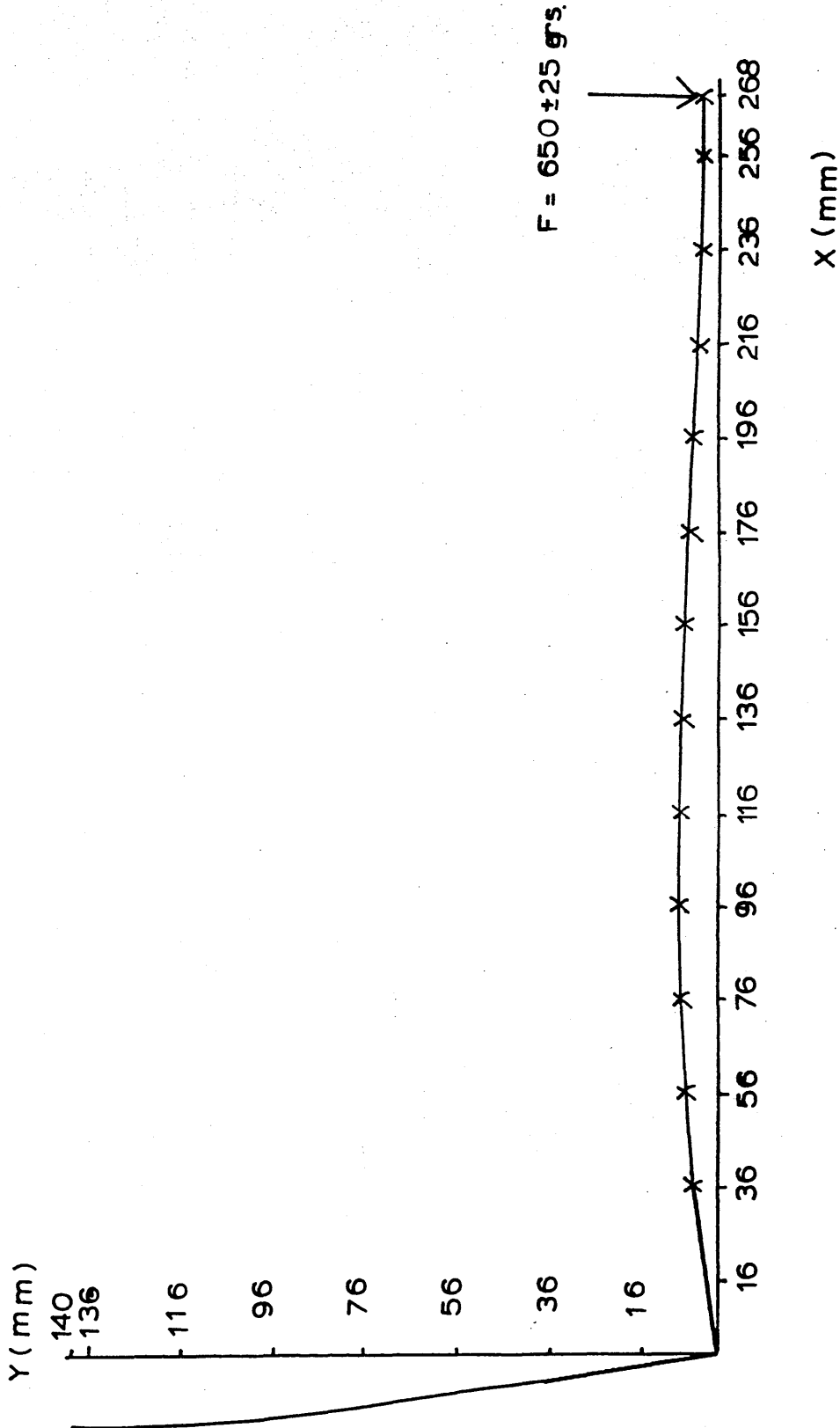


FIGURE 9 : DEFLECTION OF THE BEAM DUE TO BOTH THERMAL STRESS AND LOADS AT THE LONG BEAMS MIDDLE SPAN

EXPERIMENT 4



PREDICTED AND EXPERIMENTAL RESULTS

Table 11 and figure 10 compare the measured results with those predicted by model 2.

Model 2 was designed to predict first the force necessary to have a nil deflection at the long beams middle span and then to calculate the deflection of the whole structure under this load. The deviation of nearly 1mm in the calculated deflection at middle span can be reduced by an iteration to adjust the value of the necessary load in relation with the calculated deflection at middle span.

On the other hand, given the difficulty in measuring the distance between two opposite corner origins, the distance between two opposite 16mm marks on the long beams was taken as the basis of the experimental "nil deflection at middle span" criteria,

$$l(268) = l(16) = 273 \text{ mm} \quad 72$$

instead of,

$$l(268) = l(0) = 278 \text{ mm} \quad 73$$

value which was not measured, but extrapolated.

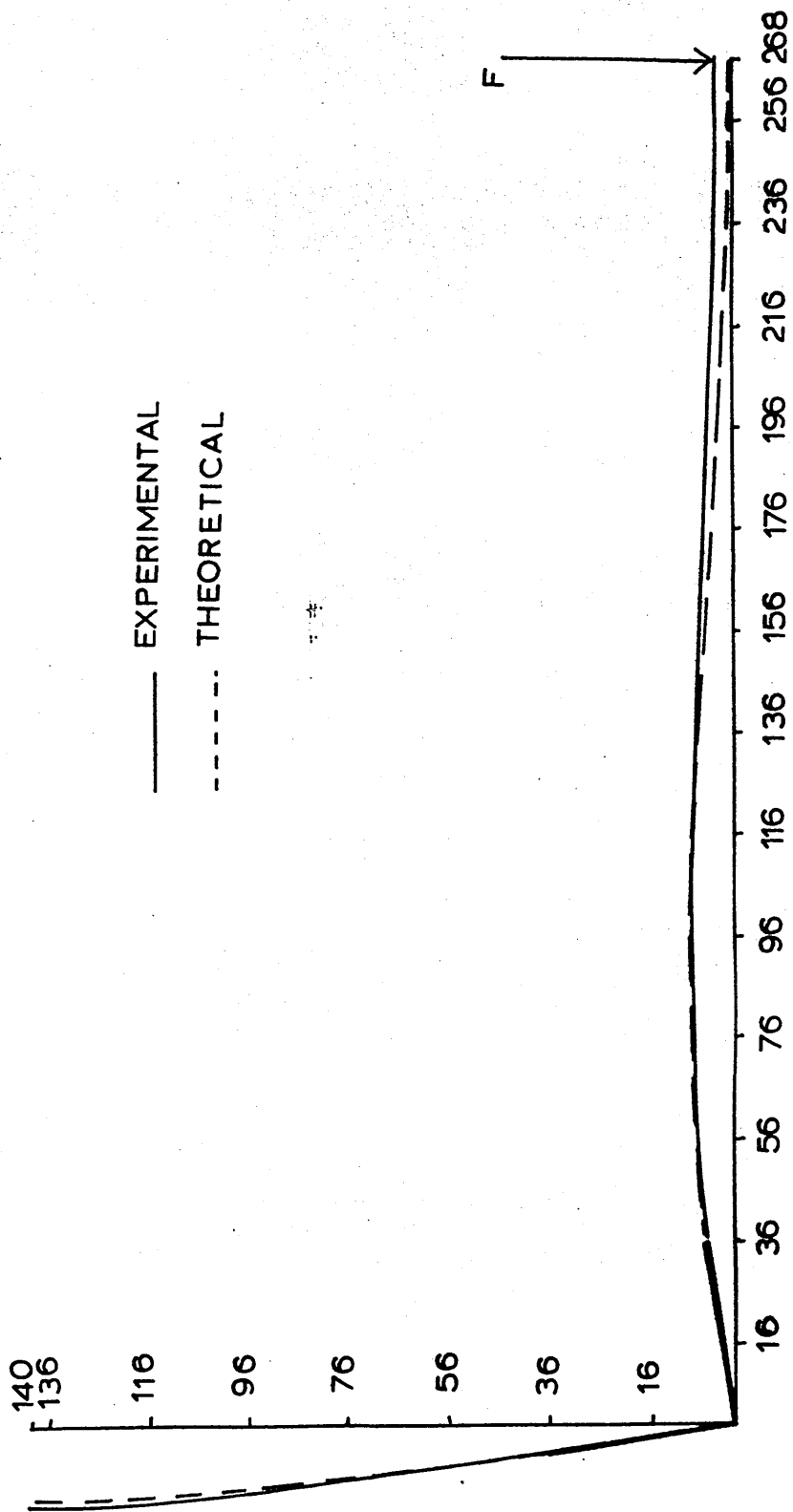
Model 2, then, was predicting fairly well and the agreement could be improved but the attention was focussed in making the model more related to the uniformly distributed load found in continuous casting. On the experimental side as well, the path was paved to look for a better analogy.

TABLE 11 : PREDICTED AND EXPERIMENTAL RESULTS

Long beam, x [mm]	MODEL 2 PREDICTED DEFLECTION [mm]	F= 674grs DEFLECTION [mm]	EXP.4 MEASURED DEFLECTION [mm]	F=(650 25)grs DEFLECTION [mm]
0		0		0
16		2.4		2.25
36		5.5		5.0
56		7.5		7.0
76		8.5		8.0
96		8.7		8.5
116		8.2		8.0
136		7.2		7.5
156		5.9		7.0
176		4.3		6.0
196		2.7		5.0
216		1.3		4.0
236		0.1		3.0
256		- 0.6		3.0
268		- 0.7		2.5
Short beam,				
0		0		0
16		- 2.4		- 2.25
36		- 5.5		- 5.0
56		- 8.2		- 8.25
76		- 10.4		- 11.0
96		- 12.1		- 13.5
116		- 13.1		- 14.0
136		- 13.4		- 14.5
156		- 13.5		- 14.5

FIGURE 10 : PREDICTED AND EXPERIMENTAL RESULTS

MODEL 2, EXPERIMENT 4



3.2 BIMETALLIC STRUCTURE ANALOGUE

INTRODUCTION

The apparatus developed as a result of the experimental work is described by means of a sequence of commented photographs.

The system of pulleys used to amplify the deflection represents a major improvement of the previous methods used to measure the deflection which relied on the use of a ruler. It also allowed a direct visualization of the evolution of the deflection.

The experiments carried out with this apparatus verified once again that the deflection of the bimetallic strips analogue can be predicted quite accurately with the mathematical model developed for this purpose.

Having completed this analogue, a basic intuitive knowledge of structural behaviour had been achieved together with a knowledge of the basic elements of structural analysis. The task of modelling the behaviour of the solidifying shell in the early stages of the continuous casting process taking into account plasticity could not wait any longer.

The physical analogue was instrumental in designing the model described in the next chapter as a basic reference to which it was necessary to come back many times to check the coherence of the model. The very basic characteristics of the structure considered are clearly illustrated by the analogue.

DESCRIPTION OF THE APPARATUS

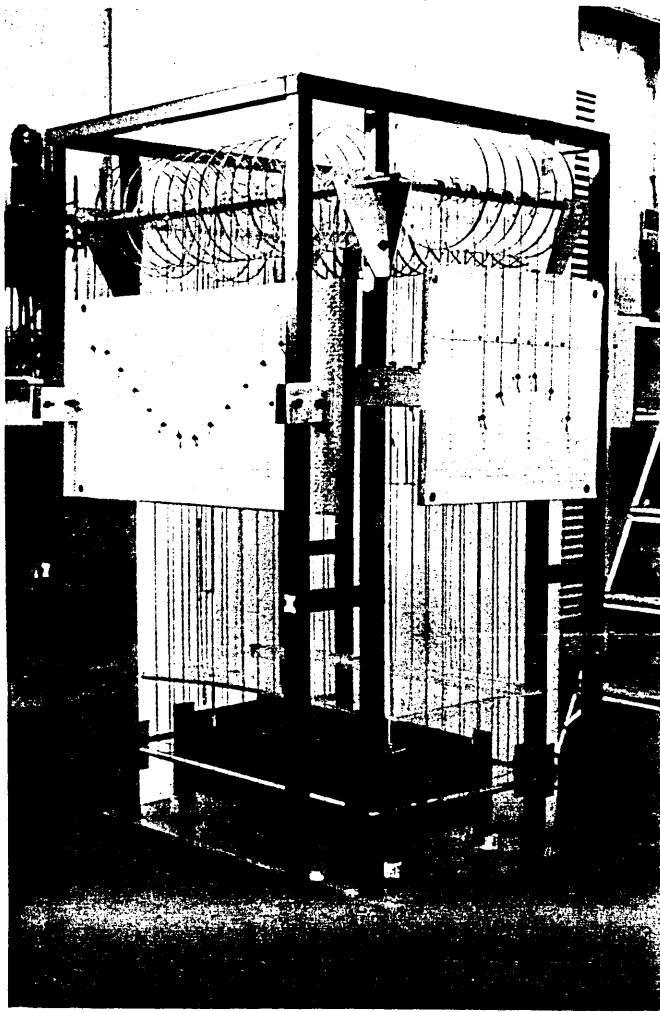


FIGURE 11: GENERAL VIEW OF THE APPARATUS OUT OF THE WATER TANK

The bimetallic strips can be seen resting on top of the bottom plate. Embroidery threads attached to the bimetallic strips and to the corner at regular intervals transmit the deflection to a set of pulleys which can be seen at the top. The pulleys amplify ten times the deflection which can then be read on the charts. The perplex plate seen on top of the structure is at water level when the apparatus is placed in the water tank, it minimizes heat flow while allowing a good vision of the bimetallic strips structure.

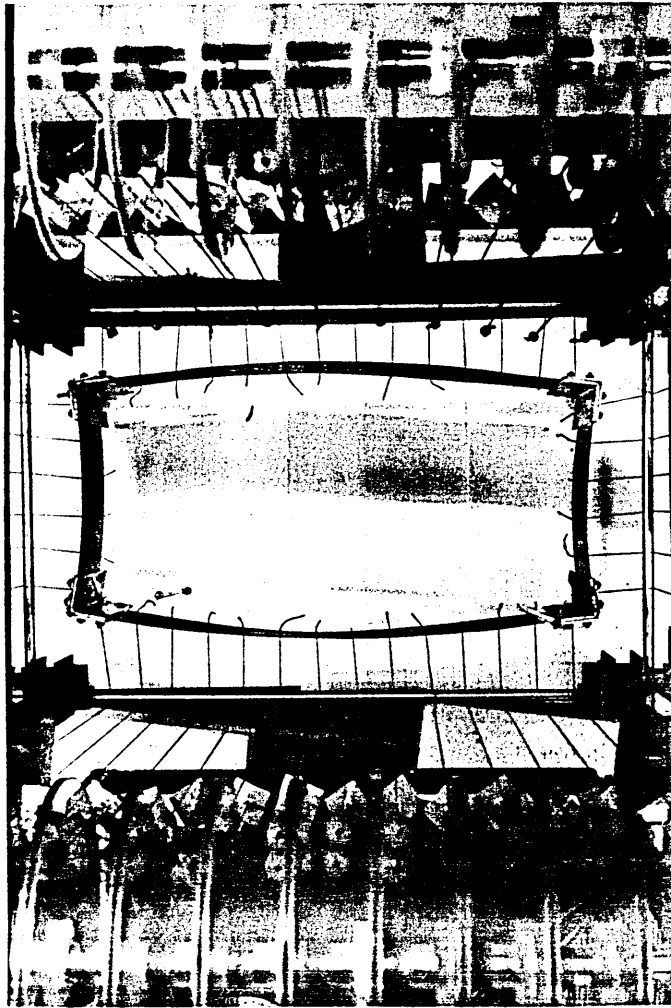


FIGURE 12 : TOP VIEW OF THE BIMETALLIC STRIPS STRUCTURE

The embroidery threads are attached to the bimetallic strips at half height and at 36mm intervals. One thread is attached to each side of the corner at 18mm ($36\text{mm}/2$) from the corner origin. The joint between the corner side and the adjacent bimetallic strip is then at 18mm from the nearest threads. The number of threads attached to each beam is even so that when a quarter symmetrical section is considered the last threads are also at 18mm from the symmetry axis. This improves the analogy with a uniformly distributed load.

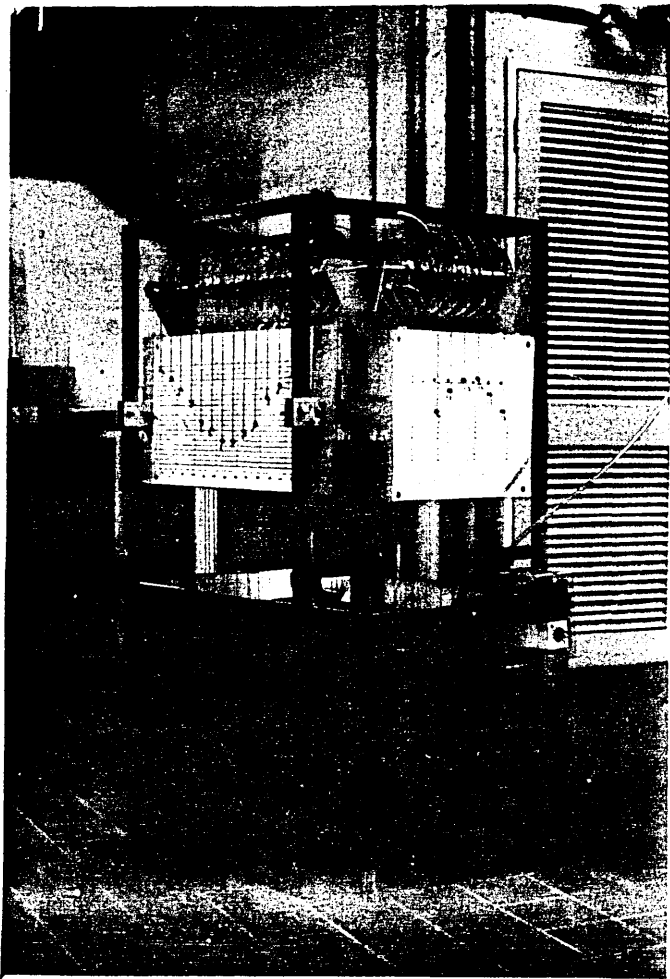


FIGURE 13 : GENERAL VIEW OF THE APPARATUS IN THE WATER TANK

When the apparatus is placed in the water tank, the structure is immersed in the water up to the level shown by the perplex plate in figure 1 and enough space is left for the heating element of the immersion heater to fit under the bottom plate (figure 4). The deflections shown are the actual results obtained after all the markers had been placed in their zero position with the water bath at about 50 deg C, when the bimetallic strips are flat, and water was subsequently cooled to 20 deg C.

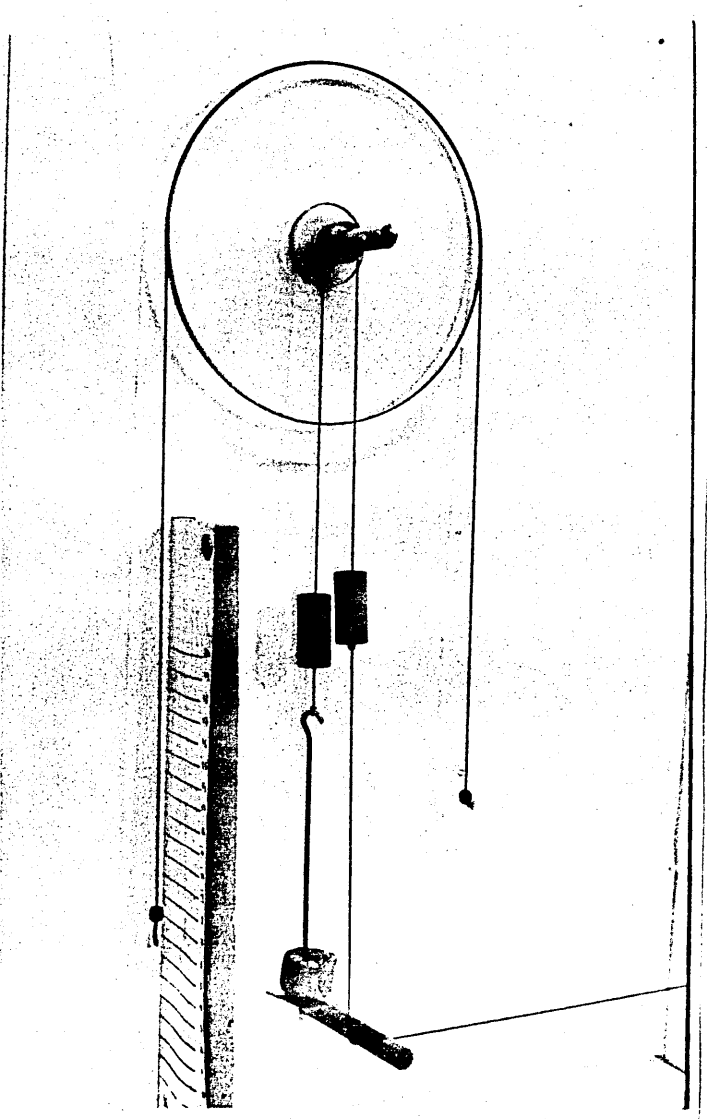


FIGURE 15 : DETAILED VIEW OF THE PULLEY SET UP

Each pulley is double, with a small pulley 15mm diameter attached to a 150mm diameter pulley. The thread turns twice around the pulleys to ensure a good grip. Two equal weights along the transmitting thread at each side of the small pulley keep the thread tight.



FIGURE 16 : DISPOSITION OF THERMOMETERS

Up to five thermometers with 110 deg C scale were used to control the temperature gradients. In this picture the middle one is placed just under the bimetallic strip while the other two are at the level of the top edge of the strips. The thermometers were fitted through purpose drill holes on the perplex insulating plate. Temperature gradients were not a problem while heating, but cooling had to be done very slowly to keep the temperature difference from top to bottom of the bimetallic strips below some 5 deg C and even 10 deg C.

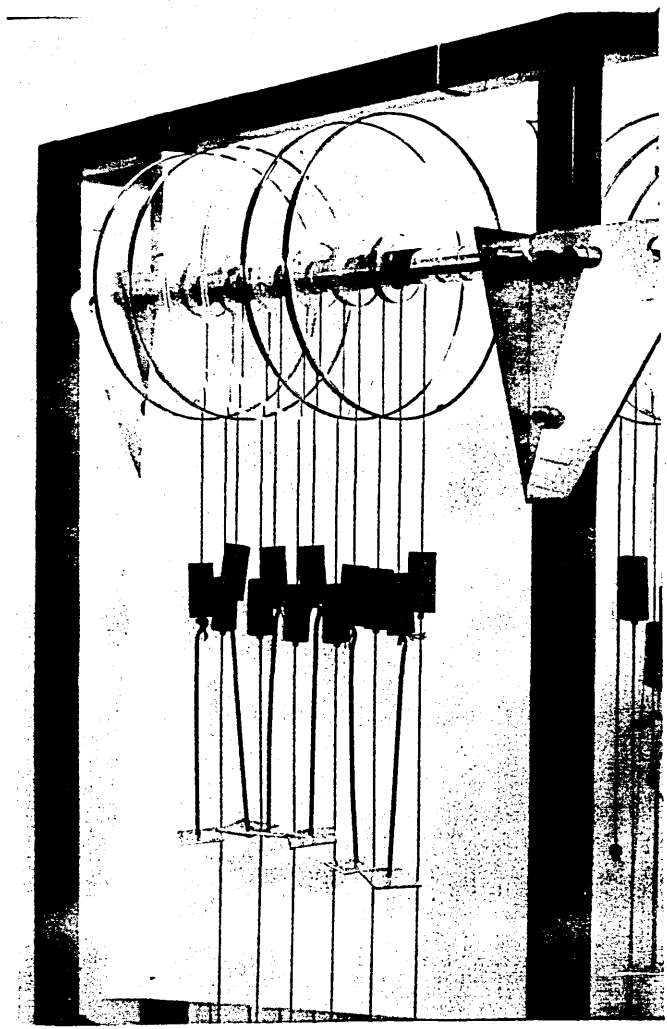


FIGURE 17 : SHORT BEAM PULLEYS SET UP

Six pulleys were used to amplify the deflection of the short beam. Another six pulleys were set up for the opposite short beam (shown here) so as to be able to apply a symmetrical load. The plates to carry the loads are seen here. The actual loads can be seen in figure 5. The steel bar which holds the pulleys is fixed, and so is the corresponding bottom steel bar, to ensure that all threads go up and down vertically.

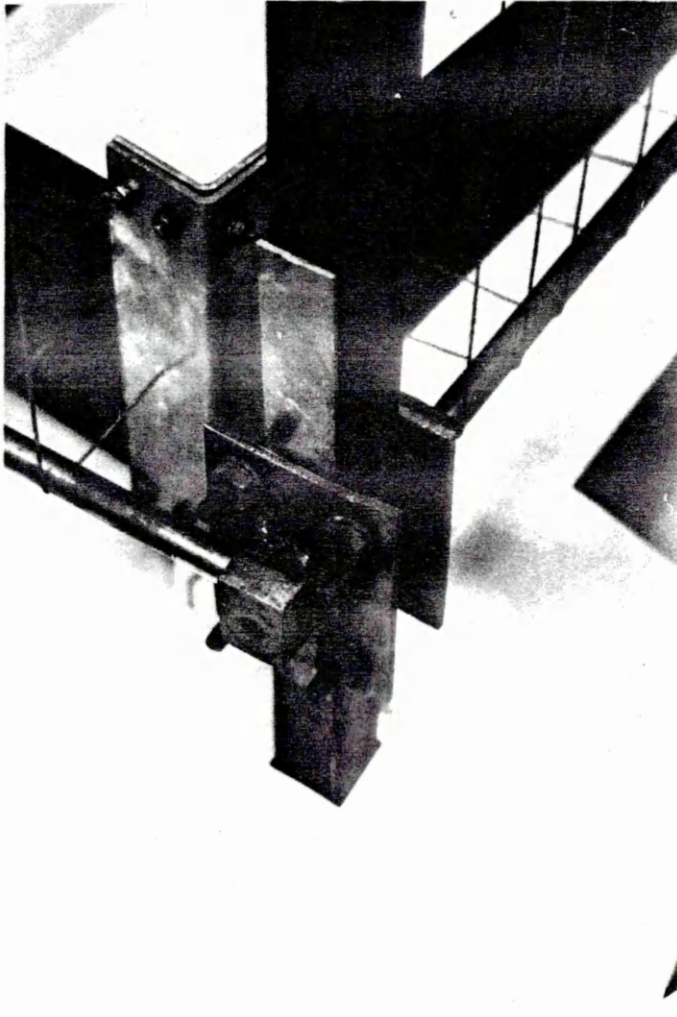


FIGURE 18 : BOTTOM BAR SUPPORT

Can be adjusted to fit different structures. Depending on the width of the bimetallic strips, the support have to raised or lowered to level with the bimetallic strips middle height.

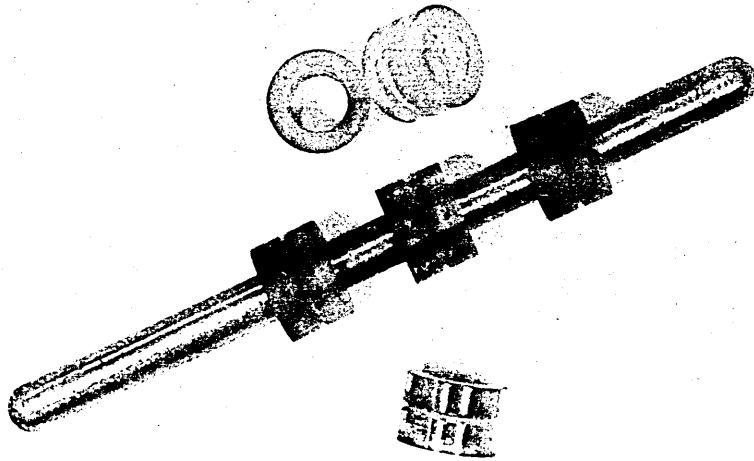


FIGURE 19 : V-SHAPE GROOVE

These pulleys were first used, but it was realised that the threads have to go twice round the pulleys to ensure a good grip and so a u-shape groove is necessary. The bigger pulleys could be machined to expand the v-shape grooves into the u-shape, but the small pulleys had to be discarded and remade.

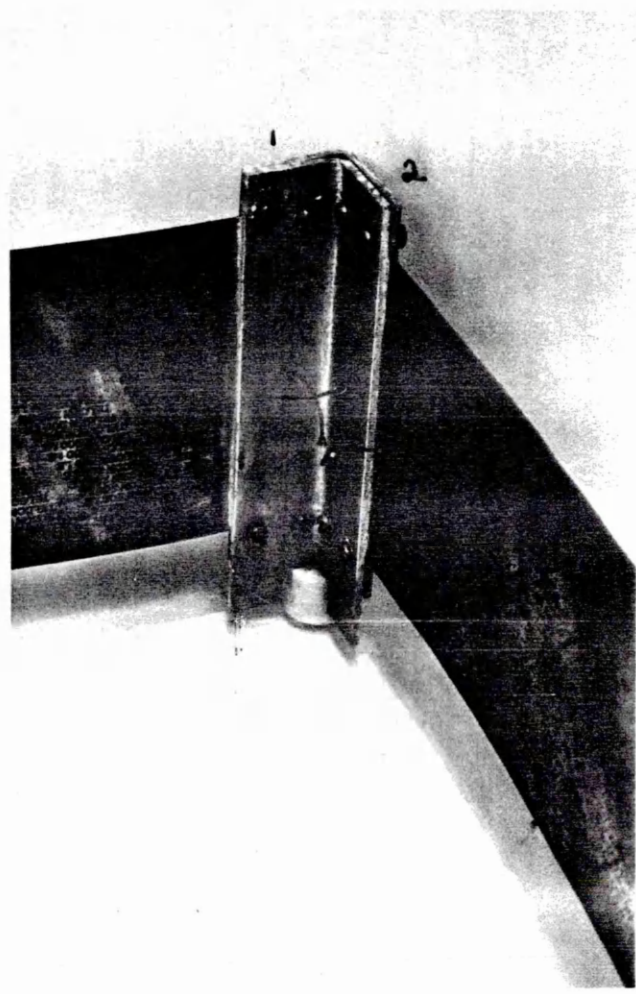


FIGURE 20 : CORNER SUPPORTED ON A LOW FRICTION NYLON BUSH

DIMENSIONS	INTERNAL ANGLE [mm]	EXTERNAL ANGLE [mm]
External side width (sec.1)	35.5	39.0
External side width (sec.2)	35.0	36.0
Internal side width (sec.1)	32.5	36.0
Internal side width (sec.2)	32.0	36.0
Height	170.0	150.0
Thickness	3.0	3.0

4.1 PRELIMINARY STATEMENT OF THE MODEL

Figure 1 represents the cross-section, perpendicular to the direction of casting at a metallurgical height $meth$, of a continuously cast structure.

t , is the thickness of the solidifying layer.

q , is the liquid metal pressure.

a , is the length of corner considered rigid.

$2x_1$, is the length of the cross-section.

$2x_2$, is the width of the cross-section.

As the whole structure is subjected to a rapid extraction of heat within the mould region, the heat transfer in the direction of casting is negligible compared with the heat transfer directed towards the exterior of the structure (that is, within the plane perpendicular to the direction of casting). The stresses which develop during the process reflect this as they reflect the fact that the downwards movement of the structure diminishes the vertical component of the metal pressure so that only the horizontal component of the liquid metal pressure upon the solid layer is important.

The cross-section can be considered as a unit length structure on its own. It is in the deformation of this structure that we

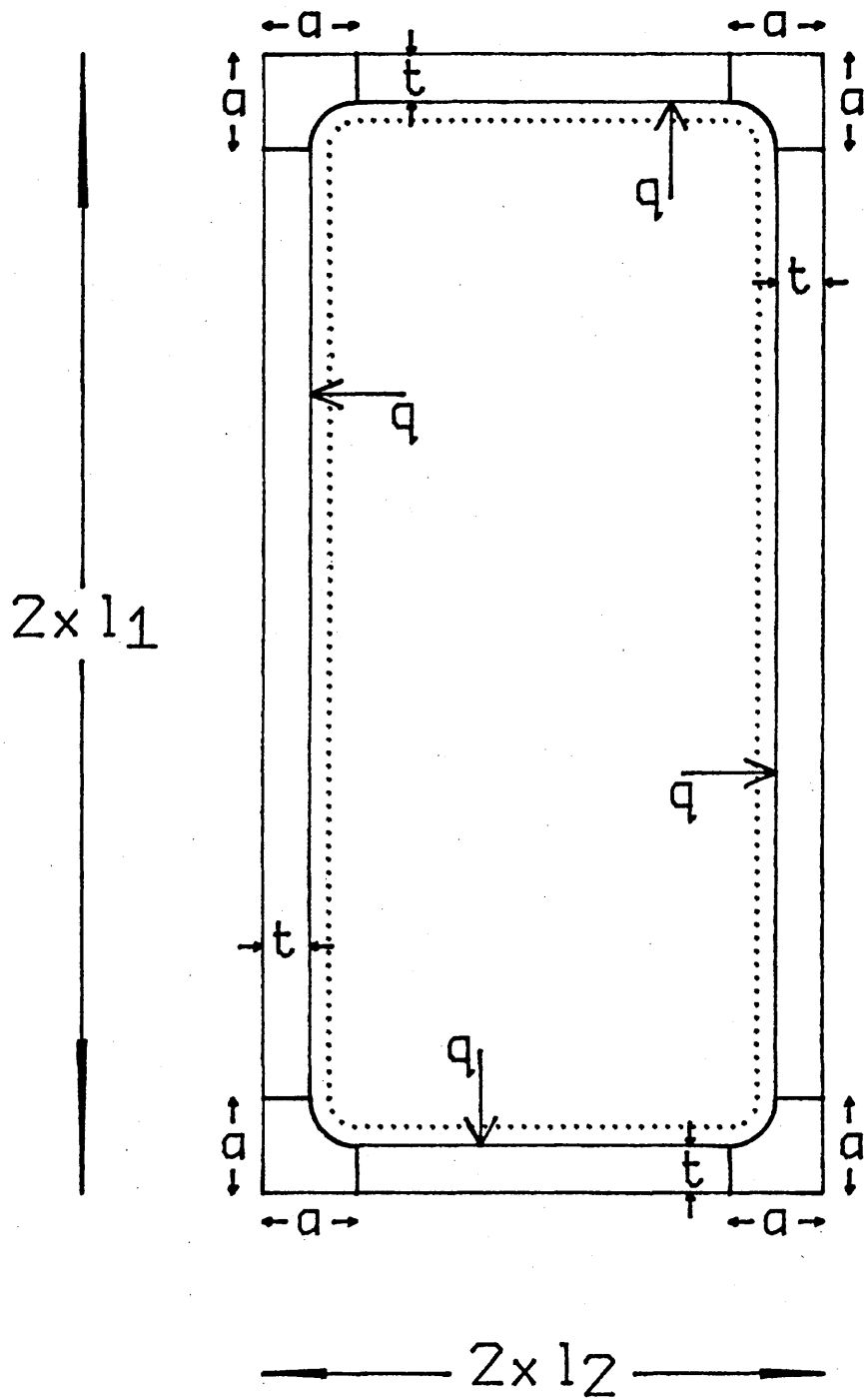


Fig. 1 : REPRESENTATION OF THE CROSS SECTION OF A CONTINUOUSLY CAST STRUCTURE, PERPENDICULAR TO THE DIRECTION OF CASTING AT A GIVEN METALLURGICAL HEIGHT **metH**.

structural analysis, it is a box formed by four beams joined together at the corners. Heat is extracted in two directions in the vicinity of the corners, making the solid layer thicker there and the corners can be considered as rigid joints; they are significantly more rigid than the beams. Any variation in the thickness of the solid layer outside the corner region is neglected, so that t is considered to be constant at a given metallurgical height.

Based on the approach developed by K.V. Krishnamurthy (1969) for the study of solidification of metals with two dimensional heat flow, it is possible to associate a specific length to the corner region and it is this length that is considered rigid.

Krishnamurthy's model is based on the idea that the solidification process is only affected by the two dimensional heat flow within a finite region close to the edge. This model is illustrated in figure 2, which represents a section through part of a billet or slab. The edge affected region is a square prism whose side a grows as solidification proceeds, although one edge of the prism remains anchored to the edge of the structure.

Outside of the corner region, the iso-thermal surfaces, and the solidification front in particular, are planes parallel to the sides of the billet. Here, the solidification process is uni-directional and the existing integral profile solution

the isothermal surfaces are curved, their distribution and in particular the length of the corner can be found using Krishnamurthy's model.

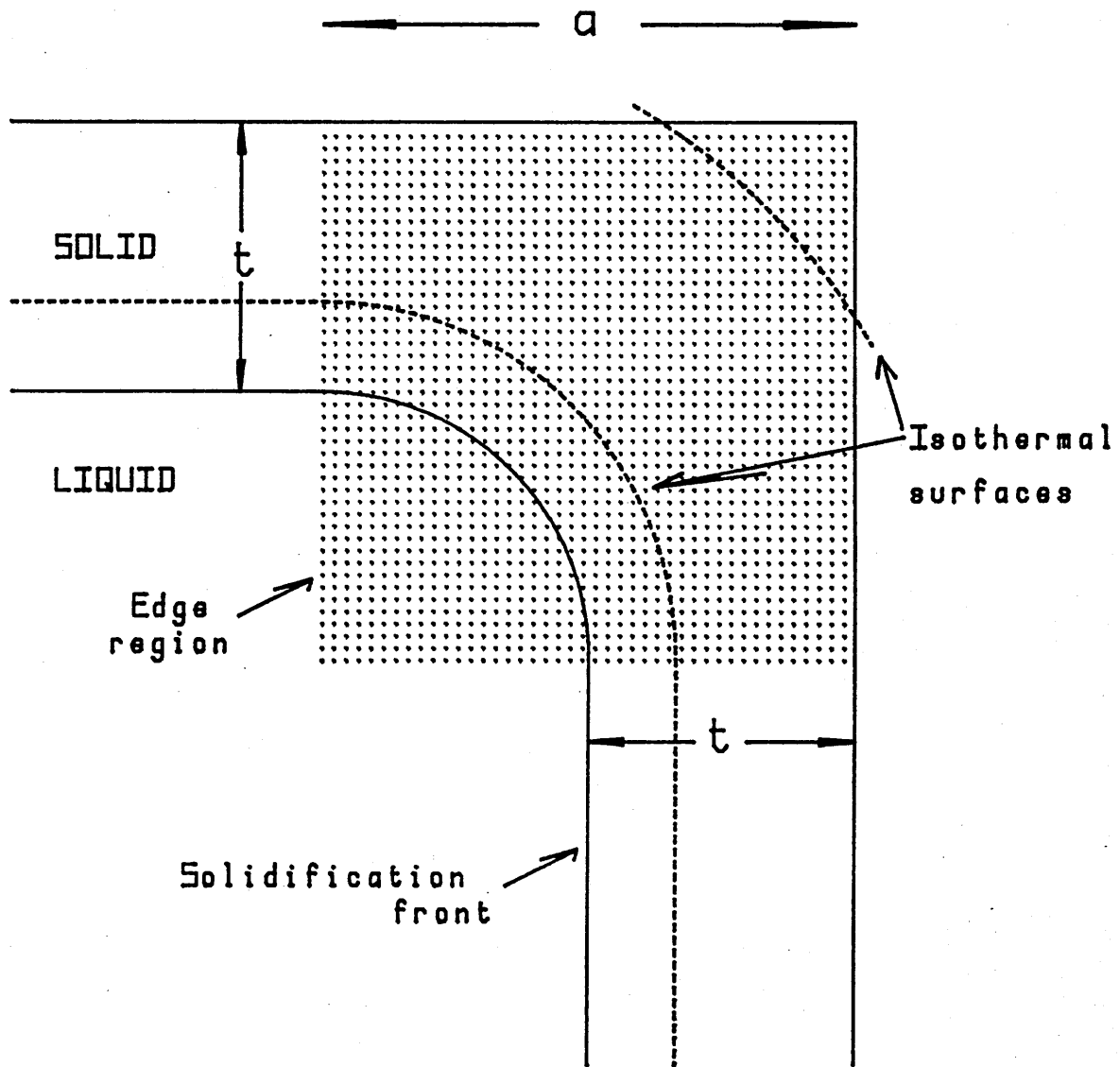


Fig. 2 : CORNER SECTION THROUGH A SOLIDIFYING BILLET OR SLAB
(taken from K.V. Krishnamurthy, 1969)

mechanical conditions are symmetrical, the analysis can be restricted to a quarter-section; the slope of the deflection is nil at the mid points of the beams span and these represent planes of symmetry.

We shall therefore concentrate our attention on this particular structure, comprising two beams, half the size of those considered originally, and rigidly joined at the corner. The corner region is represented as a small rigid length a in each beam, these lengths being rigidly bound together at right angles.

As shown in figure 6, five nodes, or critical points, must be considered :

- *1*, at the end of the long beam.
- *2*, at the boundary between the rigid and non rigid sections of the long beam.
- *3*, at the edge of the corner.
- *4*, at the boundary between the rigid and non rigid sections of the short beam.
- *5*, at the end of the short beam.

The structure has only one degree of freedom at each one of nodes *1* and *5* , it is only free to move in the direction perpendicular to the beam at each one of these nodes.

node *1*.

f_5 , is the axial force per unit length applied to the beam at node *5*.

m_1 , is the moment per unit length applied to the beam at node *1*.

m_5 , is the moment per unit length applied to the beam at node *5*.

q , is the metalostatic pressure.

T_s , is the solidification temperature.

T_c , is the temperature of the cooling wall.

The x,y reference system which coincides with the cooling wall when there is no distortion and has its origin at the edge of the corner is chosen as the basic reference system. However, distances which characterise the state of the structure at a particular cross-section (such as the position of the neutral axis, the position of the elastoplastic boundary within the beam and the radius of curvature) are measured from the cooling wall along the line defined by the cross-section in the x,y plane (the perpendicular to the cooling wall at x or y). Because much of the analysis which follows is independent of the specific beam being considered, a generic distance from the edge of the corner, u , is adopted, although the specific values of the variables dependent upon this distance will also depend on the specific beam being considered.

- 1.- Deflections are assumed to remain small.
- 2.- The thickness of the beams is assumed to be small compared to their length.
- 3.- Cross-sections remain plane and perpendicular to the cooling wall during the bending process.

This allows, among other things, to approximate any distance along the cooling wall by its projection along the corresponding axis of the x,y reference system.

l_1 , is the length of the long beam.

l_2 , is the length of the short beam.

$w(u)$, is the deflection at u . that is, the distance from the point $(u,0)$ if $u=x$, or $(0,u)$ if $u=y$, of the x,y reference system to the cooling wall (along the perpendicular to the u axis).

$n(u)$, is the position of the neutral axis at u , measured from the point corresponding to u on the cooling wall.

$p(u)$, is the position of the elastoplastic boundary at u , measured from the point corresponding to u on the cooling wall.

It is assumed that there is only one plastic region and one elastic region, and therefore only one elastoplastic boundary, within any particular cross-section.

$r(u)$, is the beam's radius of curvature at u , measured from the point corresponding to u on the cooling wall.

the point corresponding to u on the cooling wall.

$T(v)$, is the temperature at a distance v from the cooling wall.

$Y(v)$, is the absolute magnitude of the yield stress at a distance v from the cooling wall.

Both the temperature and the absolute magnitude of the yield stress are constant in respect to u as the iso-thermal lines are assumed parallel to the cooling wall, within the non-rigid sections of the beams.

$s(u,v)$, is the stress at a distance v from the cooling wall, within the cross-section at u .

To complete this preliminary statement of the model, two further basic assumptions are introduced : both the temperature and the yield stress are assumed to be linearly distributed across the section. These assumptions simplify considerably the model and are considered to be justified given the present knowledge on the behaviour of metals at high temperatures. The fundamental approach of the model would not have to be changed in order to account for the non linearity of the temperature and stress distribution across the section, but such a sophistication of the model would increase the complexity of the mathematical techniques required to infer the deflection of the structure and the distribution of stresses within it from the basic equations describing its behaviour.

by a linear model is considered the most appropriate.

LINEAR TEMPERATURE DISTRIBUTION.

The temperature is assumed to vary linearly across the thickness of the beams (and constant along them), (Fig.4)

$$T(v) = T_c + \frac{v}{t} (T_s - T_c) \quad 1$$

LINEAR YIELD STRESS DISTRIBUTION.

The absolute magnitude of the yield stress of the metal is also assumed to vary linearly across the beam, with temperature, from a value Y_0 at the cooling wall to a value nil at the solidification front, (Fig.5)

$$Y(v) = \pm \frac{Y_0}{t} (t - v) \quad 2$$

The Yield stress is assumed to have the same magnitude in compression and in tension.

The fundamental parameters of the model, and the basic assumptions in which it relies, have now been introduced. We are now going to identify the basic equations which describe the behaviour of the structure. In the next section, we are going to look at the structure from an overall perspective, focussing our attention on its overall equilibrium and inferring the equations which describe it. Then, in sections 4.3, 4.4 and 4.5, we shall consider what happens within a particular cross section of the beams.

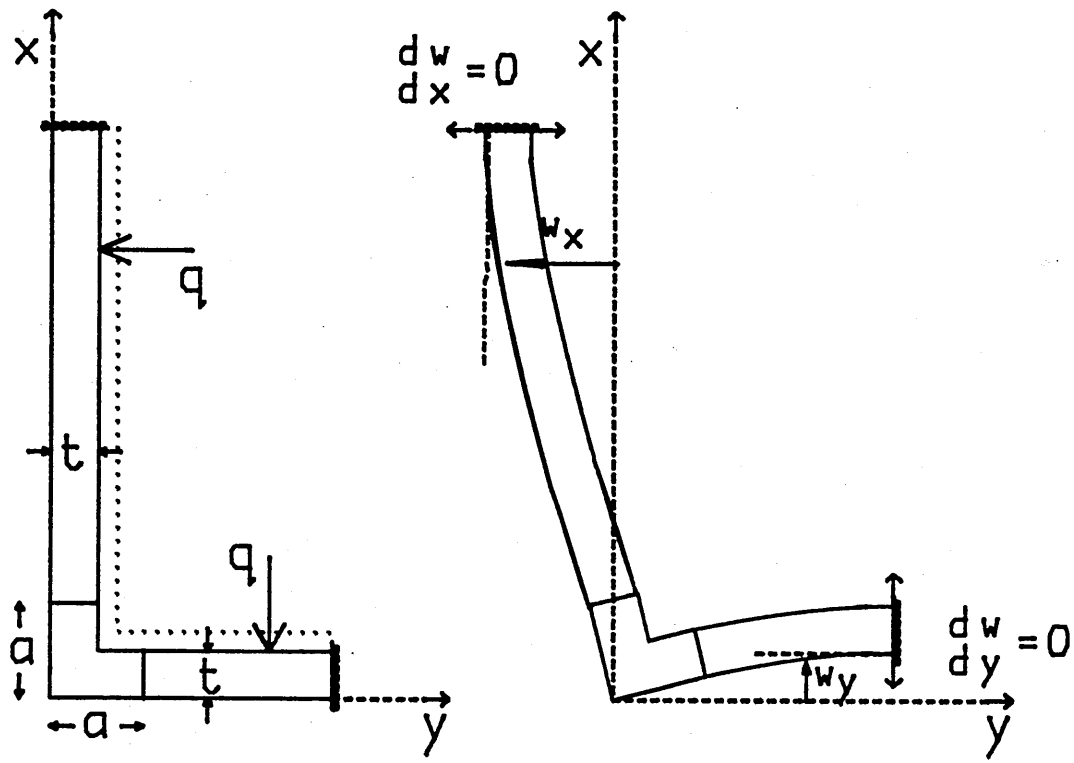


Fig. 3: MODEL REPRESENTATION OF A QUARTER-SECTION, PERPENDICULAR TO THE DIRECTION OF CASTING, OF A CONTINUOUSLY CAST STRUCTURE AT A GIVEN METALLURGICAL HEIGHT meth.

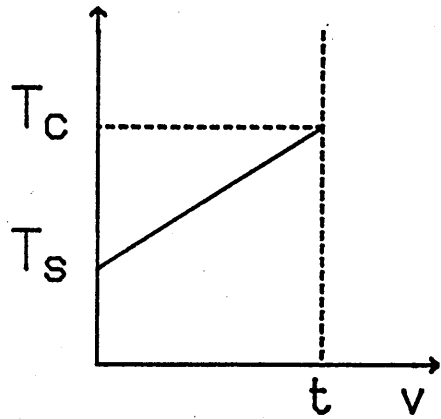


Fig. 4: TEMPERATURE DISTRIBUTION ACROSS THE THICKNESS OF A BEAM.

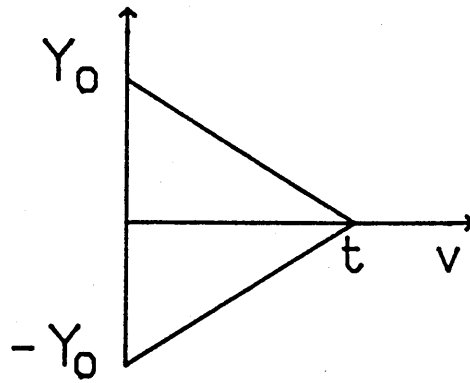


Fig. 5: YIELD STRESS DISTRIBUTION ACROSS THE THICKNESS OF A BEAM.

The equilibrium of the structure is considered first from an overall perspective as represented in figure 6. We shall not consider yet the temperature distribution and the stress distribution across the section of the beam. A consequence of the assumption of a linear temperature distribution is that the thermal gradient across the thickness of the beam will not by itself produce a moment of forces. In other words, the stresses caused by the non linearity of the temperature distribution are being neglected.

The temperature does affect the overall moment and force equilibrium of the structure by determining the unstressed length of the beam filaments in relation to their distance from the cooling wall, and therefore determining the actual magnitude of the stress as a function of the distance to the cooling wall. But the overall moment and force equilibrium equations can be stated without any explicit reference to the temperature and stress distribution.

Later, in section 4.3 ("The stress distribution across the thickness of the beams"), in section 4.4 ("Plastic and elastic stresses") and in section 4.5 ("The cross-section force and moment equilibrium equations"), we shall consider explicitly what happens within the thickness of the beams.

Let us now, therefore, focuss our attention in the overall equilibrium of the structure.

structure.

It is assumed that,

$$| w(x) | \ll x \quad \text{for any } x \text{ in the interval } (0, l_2) \quad 1$$

$$| w(y) | \ll y \quad \text{for any } y \text{ in the interval } (0, l_1) \quad 2$$

Deflexions are considered positive towards the liquid core (in agreement with the x, y reference system adopted).

Anticlockwise moments are considered positive.

Resolving the equilibrium of forces vertically,

$$f_1 = - q l_2 \quad 3$$

and horizontally,

$$f_5 = - q l_1 \quad 4$$

Where, f_1 and f_5 are the force per unit length applied upon the beam at nodes *1* and *5* respectively.

The equilibrium of moments at any node leads to,

$$m_1 + m_5 - \frac{1}{2} q (l_1^2 - l_2^2) = 0 \quad 5$$

The moments $w(l_1) f_5$ and $w(l_2) f_1$ are neglected, as the deflections are assumed to remain small.

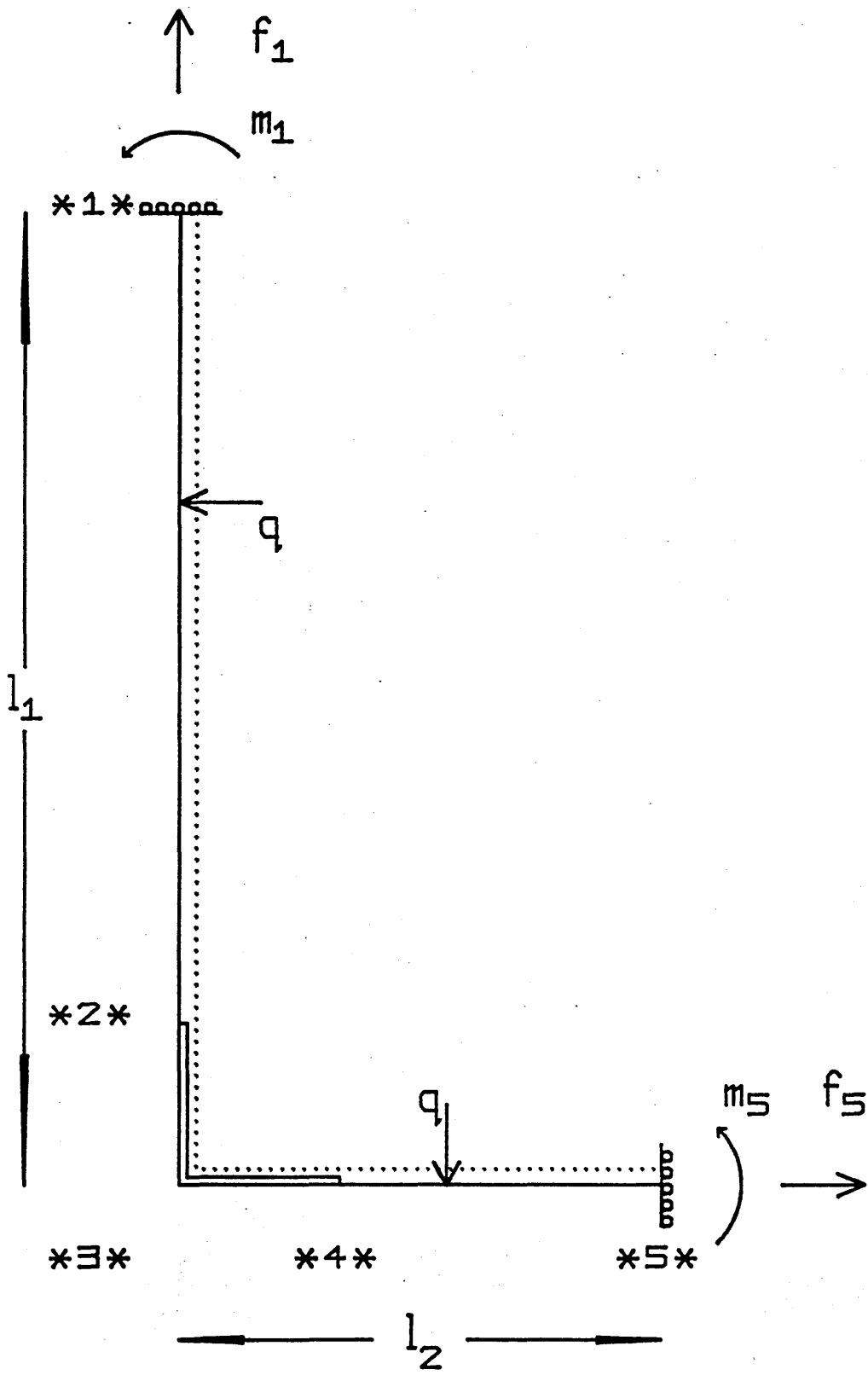


Fig. 6 : OVERALL EQUILIBRIUM OF THE STRUCTURE

c, and length l_i .

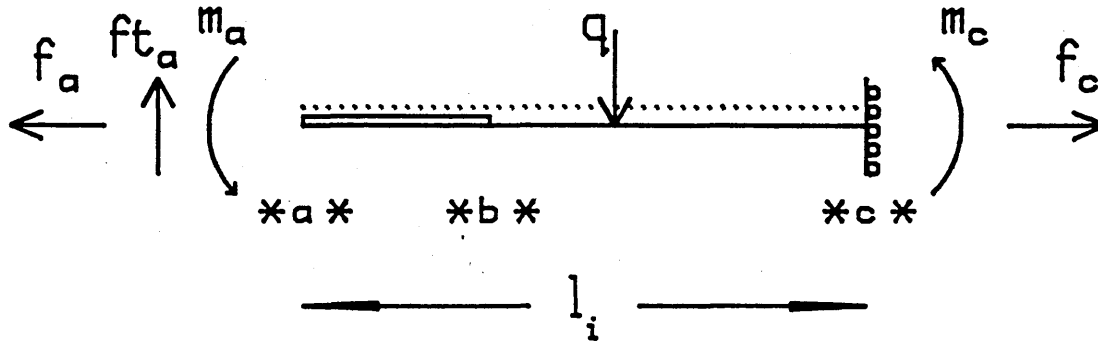


Fig. 7

This beam is representative of both the long and the short beam. m_a , f_a and ft_a are the moment, the axial force and the transverse force that the other beam applies upon the one considered at the corner (node *a* in this representation). m_c and f_c are the moment and the axial force applied upon the beam considered at node *c* .

Resolving the vertical equilibrium of forces,

$$ft_a = -q l_i \quad 6$$

the horizontal equilibrium of forces,

$$f_a = -f_c \quad 7$$

And the moment equilibrium around any node,

$$m_a + m_c + \frac{1}{2} q l_i^2 = 0 \quad 8$$

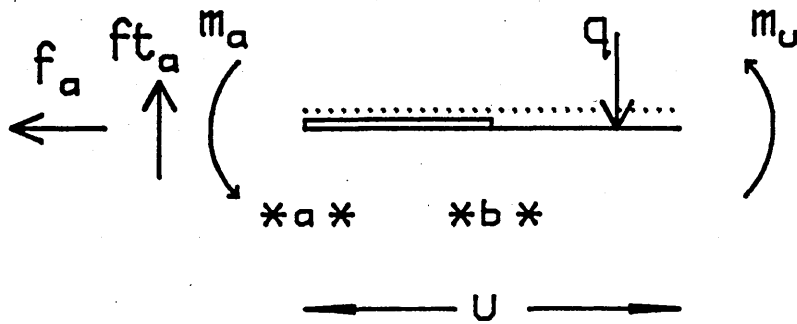


Fig. 8

we have,

$$m_a + m(u) - \frac{1}{2} q u^2 + q l_i u = 0 \quad 9$$

That is,

$$m(u) = - m_a + \frac{1}{2} q u^2 - q l_i u \quad 10$$

We also have,

$$m_a = m_3 \quad 11$$

m_a is the moment at the corner in this generic representation which is valid for both beams.

For the short beam, we have,

$$m(x) = - m_3 + \frac{1}{2} q x^2 - q l_2 x \quad 12$$

and for the long beam,

$$m(y) = - m_3 + \frac{1}{2} q y^2 - q l_1 y \quad 13$$

x,y reference system chosen (Fig.6); but we are now considering the long beam "from behind the page". This point of view is quite convenient because it allows a generic consideration of the beams, where only some parameter magnitudes change. In equations 11 and 12, only the magnitude of the length changes. The magnitude and the sign of the other parameters, including m_3 are the same for both beams. It is essential to remember, however, that this generic representation has a direct correspondance with the x,y reference system chosen, only in the case of the short beam.

We can write, using equations 10 and 11,

$$m(u) = - m_3 + \frac{1}{2} q u^2 - q l_i u \quad 14$$

The axial force at u is, using equation 7,

$$f(u) = - f_a = f_c \quad 15$$

That is, from equations 3 and 4,

$$f(u) = - q l_{ii} \quad 16$$

where l_{ii} is the length of the other beam.

The pressure q can be calculated given the metallurgical height and the density of the liquid metal,

$$q = \rho H \times (\text{density of the liquid metal}) \times g \quad 17$$

where g is the aceleration of gravity.

We shall now consider what happens within the thickness of the beams.

Figure 9 on page 4-23 represents the stress distribution at a generic cross-section u . Figures 10a to 10i on page 4-24 illustrate the range of variation of the cross-section stress distribution which is allowed within the model.

These figures give a fair approximation of the picture provided by the model on the behaviour of the stresses within the cross-section. As a simple geometrical representation of the basic relations involved, they opened the way for the conclusive assembling of the model.

The distance from the cooling wall is plotted, on the vertical axis of the triangle, against stress. The sides of the triangle correspond to the yield stress of the metal given by equation 4.1.2. The oblique straight line which intersects the triangle corresponds to the stress distribution in the elastic portion of the cross-section. The elastic stress distribution is linear as a direct consequence of our linearization assumptions, in particular of the way the strain is considered within the model (see 4.4).

At the elastoplastic boundary p , the Yield stress curve and the elastic stress curve intersect. The stress at this point can be negative, i.e. compressive, as in figure 9. But it can also be positive, i.e. tensile, as in figures 10a to 10g.

It is assumed that only one elastoplastic boundary occurs, and this is equivalent to the requirement that the absolute value

at most equal to, Y_0 ,

$$|s_0| < Y_0 \quad \text{or} \quad |s_0| = Y_0 \quad 1$$

The situation where $s_0 = -Y_0$ is illustrated in figure 10a, and that where $s_0 = +Y_0$ is illustrated in figure 10i. These are the two limiting situations being considered within the model, any further bending of the beam shall be considered to cause total plasticity at the cross-section. It is an approximation, "on the safe side", similar to those made in the design of structures to limit the risk of plastic deformation.

The stress at the elastoplastic boundary $Y(p)$, is also bounded,

$$|Y(p)| < Y_0 \quad 2$$

The neutral axis n , is not bounded. It can be located within the beam, as in figures 10a to 10c and 10g to 10i. But there is no reason to assume this must be so.

The position of the neutral axis n , the position of the elastoplastic boundary p , the stress at the cooling wall s_0 , the stress at the elastoplastic boundary $Y(p)$, the curvature c , and the moment m ; all depend upon the distance of the cross-section from the edge of the corner and upon the beam being considered. But for the cross-section analysis which follows it is not necessary to make this dependence explicit as this analysis concerns relations between these variables

At equilibrium under a given temperature and load distribution, the cross-section stress distribution is uniquely determined by a set of basic relations which describe the state of the cross-section :

- 1.- The stress in the elastic portion of the cross-section is given by Hooke's law.
- 2.- Within the plastic portion of the cross-section, the stress is equal to the Yield stress.
- 3.- The elastic stress curve and the plastic stress curve intersect at the elastoplastic boundary.
- 4.- The sum of the stresses within the cross-section at u is equal to the axial force at u .
- 5.- The sum of the moments within the cross-section at u is equal to the net moment at u .

The first of these relations, is the only one to involve directly the curvature (in terms of which the strains, and therefore the stresses, can be geometrically expressed). But in order to determine the curvature it is necessary to establish its relationship with the equilibrium conditions at the cross-section (that is, express it in terms of the axial force and the net moment acting upon the cross-section), and then to use the overall equilibrium conditions of the structure established in (4.2).

The axial force can be determined independently at any cross-section as it is constant in each beam, f_1 within the long

know already that the axial force is tensile in both beams. Therefore all cross-sections within the structure are in net tension, the difference between the positive and negative areas under the stress curve is always positive (and constant within each beam). This provides an essential basis to draft the possible stress distribution as in figure 10 using the fourth condition.

If the neutral axis is at the solidification front, then the situation of the cross-section must be as depicted in fig.10g,

$$\int \sigma_n = t \frac{3}{4} \quad \int \sigma_p = t \frac{3}{4} \quad \text{and} \quad \int \sigma_o = 2 \frac{f}{t} \frac{3}{4} \quad 3$$

This is in fact the only situation in which the beam is perfectly elastic (in theory, within our approximations),

$$\int \sigma_n = t \frac{3}{4} \quad \int \sigma_p = 0 \frac{3}{4} \quad 4$$

The moment, in this case, can be calculated geometrically from figure 10g. It will always be positive.

$$M_{\text{perfectly elastic}} = \frac{1}{2} s_o t \left(\frac{1}{2} t - \frac{1}{3} t \right) \quad 5$$

$$M_{\text{perfectly elastic}} = \frac{1}{12} s_o t^2 \quad 6$$

The curvature is not necessarily positive in this situation as the beam is affected by thermal contraction. The layers of metal will have contracted more towards the cooling surface and the resulting curvature might well be negative.

function of the moment,

$$m(u_1) > m(u_2) \quad \Leftrightarrow \quad c(u_1) > c(u_2) \quad 7$$

If the moment increases, the cross-section stress distribution will move from the Fig.10g situation towards those depicted in figures 10h and 10i. The curvature increases.

If the moment decreases, the cross-section stress distribution will move from the Fig.10g situation towards those depicted in figures 10f to 10a. The curvature will decrease (although it will increase in absolute magnitude as soon as it becomes negative).

The sign of the plastic stress can be determined both in terms of the moment and in terms of the curvature. Figure 10g represents the situation where the plastic stress is nil, and where its sign changes. Therefore, using eqs. 6 & 3, we have,

$$Y(p) > 0 \quad \Leftrightarrow \quad m < \frac{1}{12} s_0 t^2 = \frac{1}{6} f t \quad 8$$

Alternatively, if $c_{\text{perfectly elastic}}$ is the curvature corresponding to the situation depicted in Fig.10g, we have,

$$Y(p) > 0 \quad \Leftrightarrow \quad c < c_{\text{perfectly elastic}} \quad 9$$

At situation 10e the elastic stress is constant (the neutral axis is at infinity). The area defined by the stress curve above $\frac{1}{2} t$ is smaller than the area defined by the stress curve below $\frac{1}{2} t$ because in the plastic region the stress decreases.

situation. The moment, however, will be nil in a situation relatively close to situation 10e.

On the other hand, the situation where the curvature is nil can be expected to be relatively close to the situation where the moment is nil.

Outside a certain range, the curvature and the moment will have the same sign. Figure 11 (page 4-25) represents the stress distribution and the sign of the curvature, which is assumed to be equal to that of the moment, in situations 10b and 10h. The actual magnitude of the curvature in figure 11 is arbitrary, we are not yet in a position to calculate it. The stress distribution is given by the triangular figures as in figure 10. It is also illustrated by a series of lines within the beam itself whose length is proportional to the stress. The position of the neutral axis and that of the elasto-plastic boundary are clearly identified.

The dotted area in figure 11 represents the plastic region.

It was important to gain a preliminary global understanding of what happens within the thickness of the beams. Now, a more detailed consideration of the stresses, both plastic and elastic, can be undertaken. This is done in the next section.

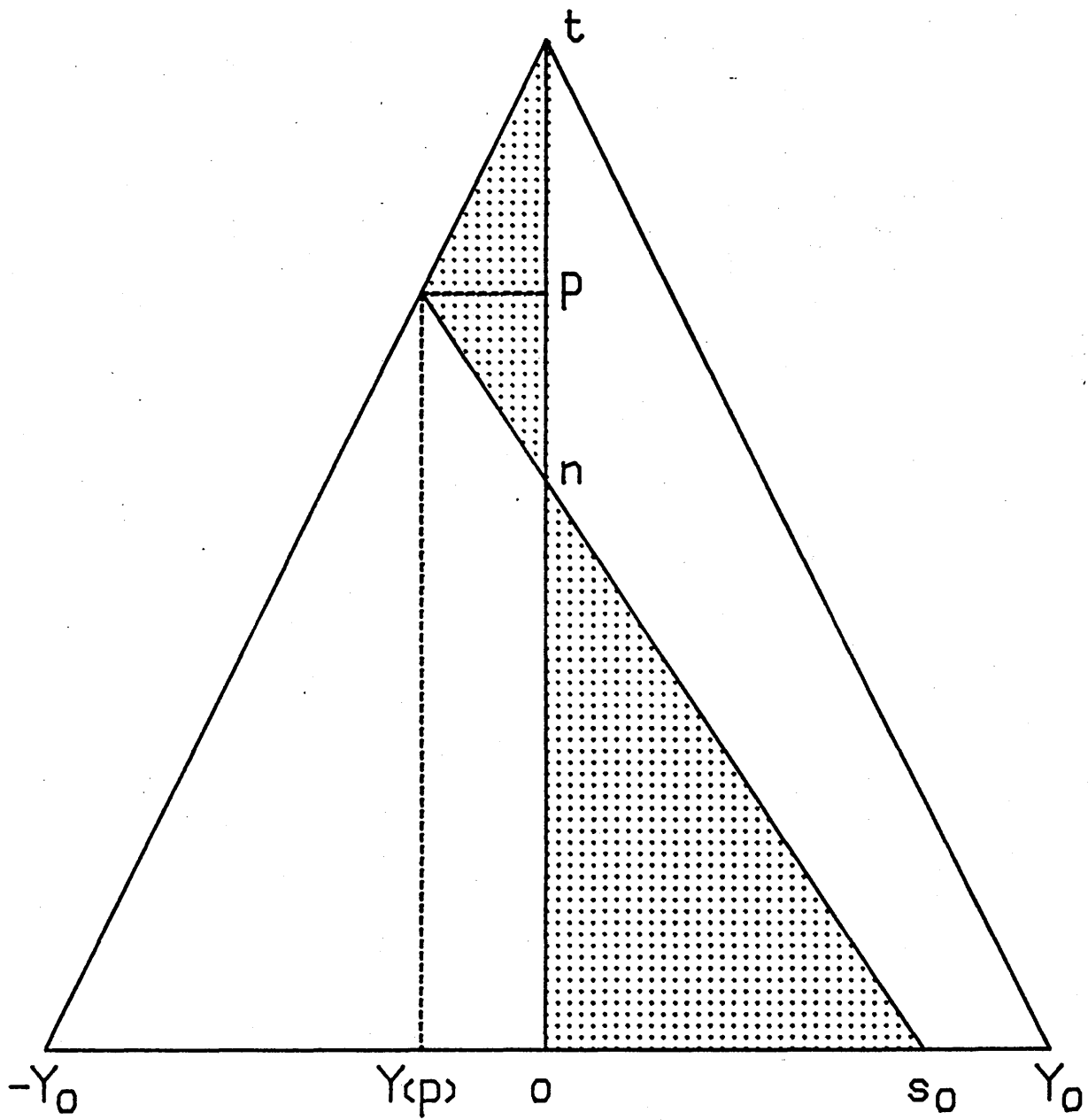
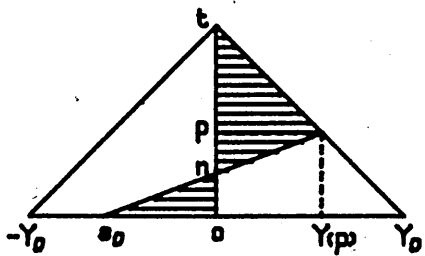
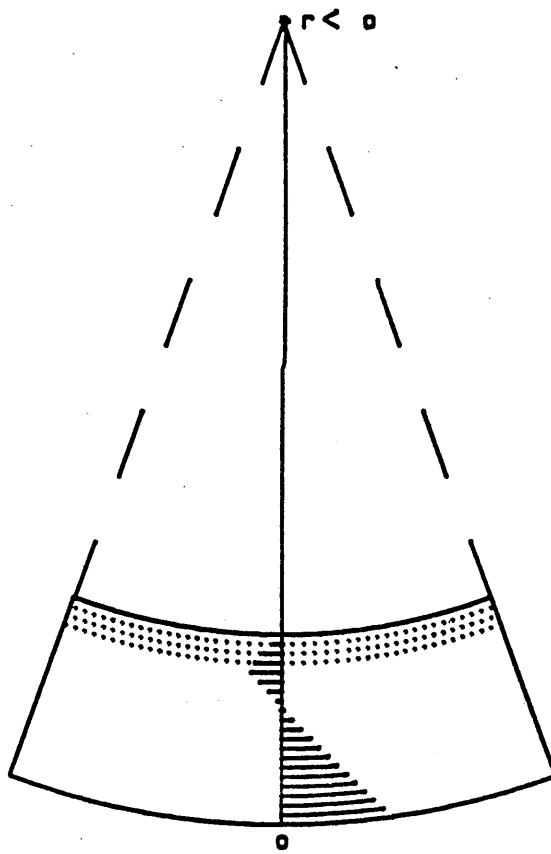


Fig.9 : STRESS DISTRIBUTION AT A GENERIC CROSS-SECTION



Situation 10b



Situation 10h

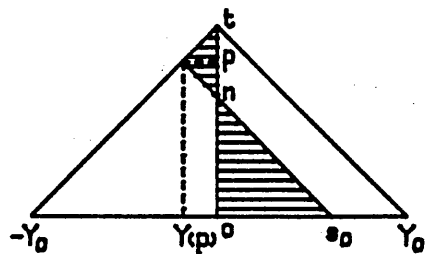
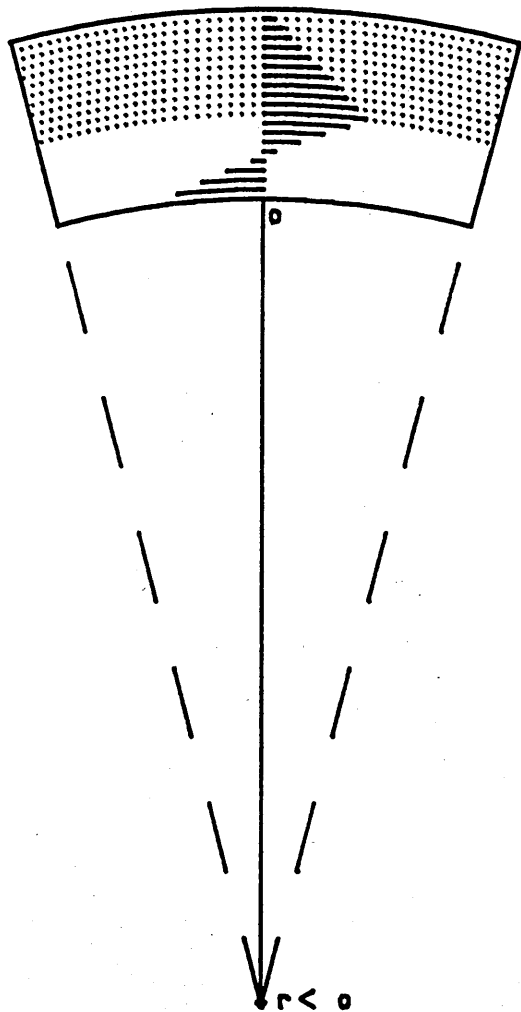


Fig.11 STRESS DISTRIBUTION AND SIGN OF THE CURVATURE IN SITUATIONS 10b AND 10h (Fig.10).

PLASTIC STRESS

Within the plastic portion of the beam the stress is equal to the Yield stress of the metal.

Using equation 4.1.2, we have,

for any (u,v) such that $a < u < l_i$ and $p < v < t$,

$$s(u,v) = \pm \frac{Y_0}{t} (t - v) \quad 1$$

The sign of the plastic stress can be determined in terms of the moment or in terms of the curvature using eq. 4.3.8 or eq. 4.3.9 ,

for any (u,v) such that $a < u < l_i$ and $p < v < t$,

$$s(u,v) = (-1)^K \frac{Y_0}{t} (t - v) \quad 2$$

where, using eq. 4.3.8,

$$\begin{aligned} K = 1 & \quad \text{if} \quad m > \frac{1}{6} f t \\ K = 2 & \quad \text{if} \quad m < \frac{1}{6} f t \end{aligned} \quad 3$$

or, alternatively, using eq. 4.3.9,

$$\begin{aligned} K = 1 & \quad \text{if} \quad c > c_{\text{perfectly elastic}} \\ K = 2 & \quad \text{if} \quad c < c_{\text{perfectly elastic}} \end{aligned} \quad 4$$

Equations 3 and 4 are equivalent.

Therefore, at the elastoplastic boundary,

$$Y(p) = (-1)^K \frac{Y_0}{t} (t - p) \quad 5$$

where K can be defined by eq.3 or by eq.4 .

for any (u,v) such that $a < u < l_i$ and $p < v < t$,

$$s_{(u,v)} = \frac{Y(p)}{t - p} (t - v)$$

6

ELASTIC STRESS

Lets consider, at a distance u from the edge of the corner, an infinitesimal section of the beam, $\frac{1}{2}u$, as illustrated in figure 12. Within this small section the curvature can be assumed to be constant.

$l_{(u,v)}$, is the length of the filament at a distance v from the cooling wall.

It is assumed that,

l_0 , is the original length at which all filaments within the section have solidified.

If the neutral axis is within the beam, the filament at a distance n from the cooling wall has the size which corresponds to its temperature because the stress is nil at the neutral axis. The strain on this filament is due solely to thermal contraction,

$$\text{strain}_{(u,n)} = - \alpha_l (T_s - T(n))$$

7

where, α_l is the coefficient of thermal expansion of the metal in $[1/\text{degC}]$.

have,

$$\text{strain}_{(u,n)} = - \alpha l [T_S - T_C - \frac{\rho}{\epsilon} (T_S - T_C)] \quad 8$$

$$\text{strain}_{(u,n)} = - \alpha l (1 - \frac{\rho}{\epsilon}) (T_S - T_C) \quad 9$$

Therefore the length of the filament at the neutral axis is,

$$l_{(u,n)} = l_0 [1 - \alpha l (1 - \frac{\rho}{\epsilon}) (T_S - T_C)] \quad 10$$

The assumption that cross-sections remain plane and perpendicular to the cooling wall during the bending process implies a geometrical relation between the length of any two filaments.

Taking the neutral axis as one of them,

$$l_{(u,v)} = l_{(u,n)} \frac{r - v}{r} \quad 11$$

Using eq. 10 to replace $l_{(u,n)}$ in eq. 11,

$$l_{(u,v)} = l_0 [1 - \alpha l (1 - \frac{\rho}{\epsilon}) (T_S - T_C)] \frac{r - v}{r} \quad 12$$

The strain at a distance v from the cooling wall is by the definition of strain,

$$\text{strain}_{(u,v)} = \frac{l_{(u,v)} - l_0}{l_0} \quad 13$$

Therefore, using eq. 12 to replace $l_{(u,v)}$ in eq. 13,

$$\text{strain}_{(u,v)} = [1 - \alpha l (1 - \frac{\rho}{\epsilon}) (T_S - T_C)] \frac{r - v}{r} - 1 \quad 14$$

That is,

$$\text{strain}_{(u,v)} = \frac{1}{r} \frac{1}{n} [n - v - a l (1 - \frac{p}{t}) (T_s - T_c) (r - v)] \quad 15$$

In the elastic portion of the beam Hooke's law applies, the stress is given by,

$$s_{(u,v)} = E [\text{strain}_{(u,v)} + a l (T_s - T(v))] \quad 16$$

That is, using equations 15 and 4.1.1,

for any (u,v) such that $a < u < l_i$ and $0 < v < p$,

$$s_{(u,v)} = \frac{E}{r} \frac{1}{n} [n - v - a l (1 - \frac{p}{t}) (T_s - T_c) (r - v) + a l (1 - \frac{v}{t}) (T_s - T_c) (r - n)] \quad 17$$

That is, for any (u,v) such that $a < u < l_i$ and $0 < v < p$,

$$s_{(u,v)} = E \frac{1}{r} \frac{1}{n} [1 + a l (T_s - T_c) (\frac{r}{t} - 1)] \quad 18$$

This equation can also be written in terms of the curvature,

for any (u,v) such that $a < u < l_i$ and $0 < v < p$,

$$s_{(u,v)} = E \frac{1}{r} \frac{1}{c} [c + a l (T_s - T_c) (\frac{1}{t} - c)] \quad 19$$

where,

$$c = \frac{1}{r} \quad 20$$

We have, in particular, at the cooling wall,

$$s_o = s_{(u,0)} = E \frac{1}{r} \frac{1}{c} [c + a l (T_s - T_c) (\frac{1}{t} - c)] \quad 21$$

and at the elastoplastic boundary, where the elastic stress is equal to the plastic stress,

$$Y(p) = s_{(u,p)} = E \frac{n-p}{1-cn} [c + al (T_S - T_C) (\frac{1}{t} - c)] \quad 22$$

These equations, both for the strain and the stress, still hold when the neutral axis is outside the beam. The concept of a neutral axis, in that case, is simply a convenient way to express the relation between the strains and between the stresses within the beam, although it is then hypothetical to talk about strain or stress at the neutral axis.

There is an indeterminacy when n tends to $\pm\infty$, but it can be overcome, now that the basic relation concerning the elastic stress has been established, using the condition that the plastic stress is equal to the elastic stress at the elastoplastic boundary to relate the curvature to p , and avoid n .

From eq. 5 and eq. 22 we have,

$$(-1)^K \frac{Y_0}{t} (t - p) = E \frac{n - p}{1 - cn} [c + al (T_S - T_C) (\frac{1}{t} - c)] \quad 23$$

where K is given by eq. 3, in terms of the moment, or by eq. 4, in terms of the curvature.

Therefore,

$$\begin{aligned} & (-1)^K \frac{Y_0}{t} (t - p) + E p [c + al (T_S - T_C) (\frac{1}{t} - c)] \\ & = n \left\{ (-1)^K \frac{Y_0}{t} (t - p) c + E [c + al (T_S - T_C) (\frac{1}{t} - c)] \right\} \quad 24 \end{aligned}$$

$$n = \frac{(-1)^K \frac{Y_0}{t} (t - p) + E p [c + a l (T_S - T_C) (\frac{1}{t} - c)]}{(-1)^K \frac{Y_0}{t} (t - p) c + E [c + a l (T_S - T_C) (\frac{1}{t} - c)]} \quad 25$$

Replacing n in equation 21 and simplifying the resulting equation we obtain,

$$s_0 (1 - c p) = (-1)^K \frac{Y_0}{t} (t-p) + E p [c + a l (T_S - T_C) (\frac{1}{t} - c)] \quad 26$$

that is,

$$\begin{aligned} s_0 - (-1)^K \frac{Y_0}{t} (t - p) - E p a l (T_S - T_C) \frac{1}{t} \\ = s_0 c p + E p c [1 - a l (T_S - T_C)] \end{aligned} \quad 27$$

and we have,

$$c = \frac{s_0 - (-1)^K \frac{Y_0}{t} (t - p) - E p a l (T_S - T_C) \frac{1}{t}}{s_0 p + E p [1 - a l (T_S - T_C)]} \quad 28$$

As the stress is assumed to be linearly distributed, it can be expressed in terms of the stress at the cooling wall, s_0 , and the stress at the elastoplastic boundary, $Y(p)$. This will simplify the evaluation of the cross-section force and moment equilibrium equations (section 4.5).

For any (u, v) such that $a < u < l_i$ and $0 < v < p$,

$$s(u, v) = c_1(u) + c_2(u) v \quad 29$$

$$s(u,0) = s_0 = c_1(u) \quad 30$$

and, at the elastoplastic boundary, where the elastic stress is equal to the plastic stress,

$$s(u,p) = Y(p) = c_1(u) + c_2(u) p \quad 31$$

Therefore,

$$c_1(u) = s_0 \quad 32$$

$$c_2(u) = \frac{Y(p) - s_0}{p} \quad 33$$

and we have,

for any (u,v) such that $a < u < l_i$ and $0 < v < p$,

$$s(u,v) = s_0 + \frac{Y(p) - s_0}{p} v \quad 34$$

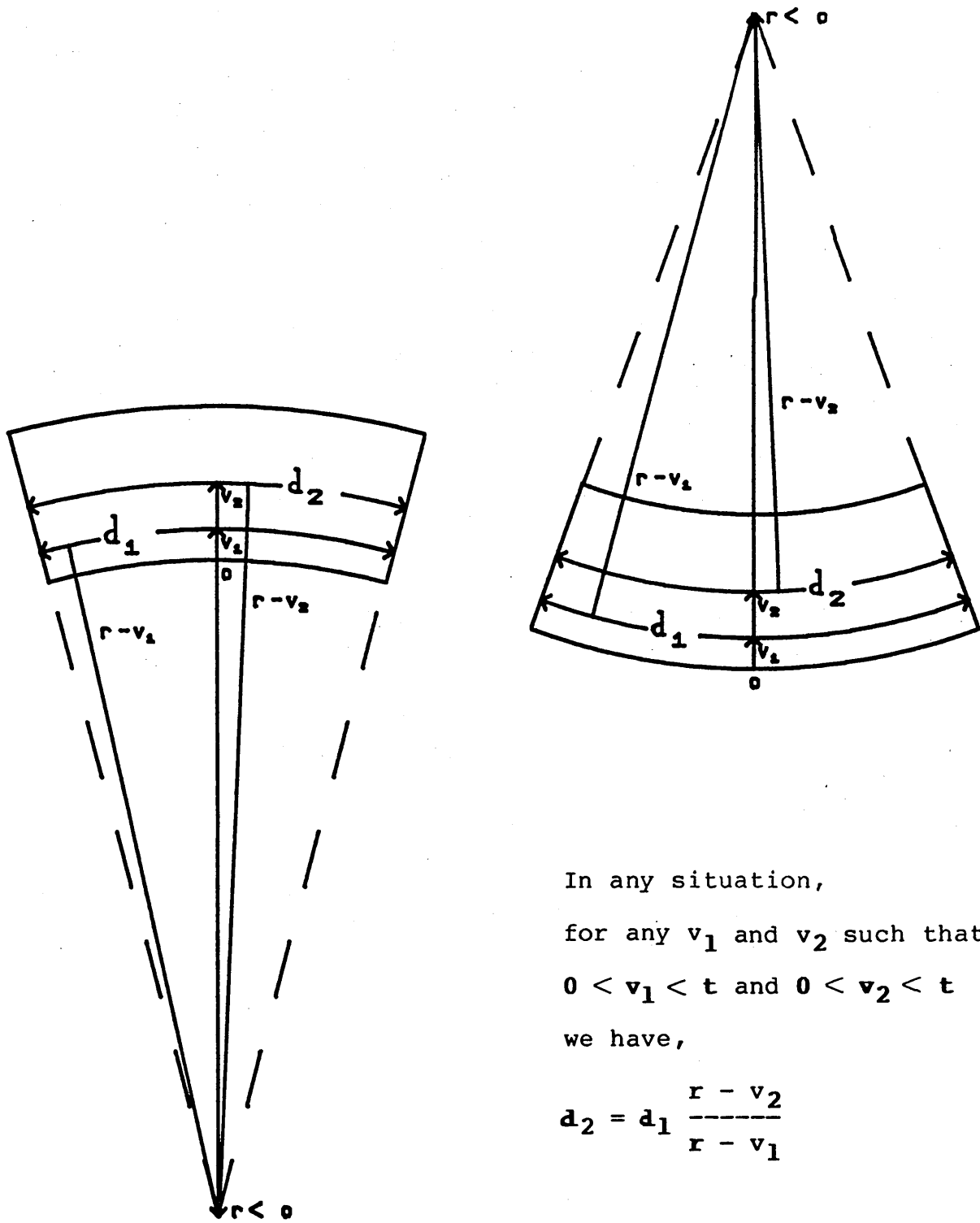
In this section, the basic equations of the plastic and elastic stress have been established.

Equation 5, combined with equation 3 which determines the sign as a function of the stress at the cooling wall, gives the stress at the elastoplastic boundary in terms of its position, the stress at the cooling wall (for the sign), and of otherwise known quantities.

cooling wall as a function of the curvature, of the position of the elastoplastic boundary, of the moment (for the sign of the plastic stress which is required in this equation), and of otherwise known quantities. It could be combined with equation 4 to determine the sign of the plastic stress, although there is no contradiction in using again equation 3 to determine this sign even if it does so as a function of the stress at the cooling wall itself. Under our linear assumptions, the value of the stress at the cooling wall together with the value of the stress at the elastoplastic boundary determine the value of the stress in the elastic region (eq. 34).

But, as we shall soon see, equation 28 is useful as an expression for the curvature (as it is written) rather than as an expression for the stress at the cooling wall. In the next section we shall infer an appropriate expression for the stress at the cooling wall in terms of the force and the moment.

Having established the basic equations describing the overall equilibrium of the structure in section 4.2, and the basic equations for the elastic and plastic stress in this section, we shall now consider further what happens within the thickness of the beam in order to establish the equations which describe the equilibrium of the cross-section.



In any situation,
 for any v_1 and v_2 such that,
 $0 < v_1 < t$ and $0 < v_2 < t$
 we have,

$$d_2 = d_1 \frac{r - v_2}{r - v_1}$$

Fig.12 GEOMETRICAL RELATION BETWEEN THE LENGTH OF FILAMENTS AT DIFFERENT DISTANCE FROM THE COOLING WALL.

At equilibrium, the sum of the stresses across the thickness of the beam must be equal to the net force applied upon the section,

$$f = \int_0^t s(u,v) dv \quad 1$$

Using eq. 4.4.34 for the elastic stress and eq. 4.4.6 for the plastic stress,

$$f = \int_0^p \left(s_0 + \frac{Y(p) - s_0}{p} v \right) dv + \int_p^t \frac{Y(p)}{t-p} (t-v) dv \quad 2$$

Integrating,

$$f = s_0 p + \frac{1}{2} \frac{Y(p) - s_0}{p} p^2 + \frac{Y(p)}{t-p} \left(t^2 - \frac{1}{2} t^2 - t p + \frac{1}{2} t^2 \right) \quad 3$$

$$f = \frac{1}{2} s_0 p + \frac{1}{2} Y(p) p + \frac{1}{2} Y(p) (t-p) \quad 4$$

That is,

$$f = \frac{1}{2} s_0 p + \frac{1}{2} Y(p) t \quad 5$$

Replacing $Y(p)$ using eq. 4.4.5 ,

$$f = \frac{1}{2} s_0 p + (-1)^K \frac{1}{2} Y_0 (t-p) \quad 6$$

where K is given by eq. 4.4.3 or by eq. 4.4.4 .

the beams must be equal to the net moment,

$$m = \int_0^t s(u,v) \left(\frac{1}{2} t - v\right) dv \quad 7$$

That is, using eq. 4.4.34 for the elastic stress and eq. 4.4.6 for the plastic stress,

$$m = \int_0^p \left(s_0 + \frac{Y(p)-s_0}{p} v \right) \left(\frac{1}{2} t - v\right) dv + \int_p^t \frac{Y(p)}{t-p} (t-v) \left(\frac{1}{2} t - v\right) dv \quad 8$$

$$m = \int_0^p \left(\frac{1}{2} s_0 t - s_0 v + \frac{1}{2} \frac{Y(p)-s_0}{p} t v - \frac{Y(p)-s_0}{p} v^2 \right) dv + \frac{Y(p)}{t-p} \int_p^t \left(\frac{1}{2} t^2 - \frac{3}{2} t v + v^2 \right) dv \quad 9$$

Integrating,

$$m = \frac{1}{2} s_0 t p - \frac{1}{2} s_0 t^2 + \frac{1}{4} Y(p) t p - \frac{1}{4} s_0 t p - \frac{1}{3} Y(p) p^2 + \frac{1}{3} s_0 p^2 + \frac{Y(p)}{t-p} \left(\frac{1}{2} t^3 - \frac{3}{4} t^3 + \frac{1}{3} t^3 - \frac{1}{2} t^2 p + \frac{3}{4} t p^2 - \frac{1}{3} p^3 \right) \quad 10$$

That is,

$$m = \frac{1}{4} s_0 t p - \frac{1}{6} s_0 p^2 + \frac{1}{4} Y(p) t p - \frac{1}{3} Y(p) p^2 + \frac{Y(p)}{t-p} \left(\frac{1}{12} t^3 - \frac{1}{2} t^2 p + \frac{3}{4} t p^2 - \frac{1}{3} p^3 \right) \quad 11$$

$$m = s_0 \left(\frac{1}{4} t p - \frac{1}{6} p^2 \right) + (-1)^K \frac{Y_0}{t} (t-p) \left(\frac{1}{4} t p - \frac{1}{3} p^2 \right) \\ + (-1)^K \frac{Y_0}{t} \left(\frac{1}{12} t^3 - \frac{1}{2} t^2 p + \frac{3}{4} t p^2 - \frac{1}{3} p^2 \right) \quad 12$$

where K is given by eq. 4.4.3 or by eq. 4.4.4 .

$$m = s_0 \left(\frac{1}{4} t p - \frac{1}{6} p^2 \right) \\ + (-1)^K \frac{Y_0}{t} \left(\frac{1}{4} t^2 p - \frac{1}{3} t p^2 - \frac{1}{4} t p^2 + \frac{1}{3} p^3 \right) \\ + \frac{1}{12} t^3 - \frac{1}{2} t^2 p + \frac{3}{4} t p^2 - \frac{1}{3} p^2 \quad 13$$

which simplifies to,

$$m = s_0 \left(\frac{1}{4} t p - \frac{1}{6} p^2 \right) + (-1)^K \frac{Y_0}{t} \left(\frac{1}{12} t^3 - \frac{1}{4} t^2 p + \frac{1}{6} t p^2 \right) \quad 14$$

That is,

$$m = s_0 \left(\frac{1}{4} t p - \frac{1}{6} p^2 \right) + (-1)^K Y_0 \left(\frac{1}{12} t^2 - \frac{1}{4} t p + \frac{1}{6} p^2 \right) \quad 15$$

where K is given by eq. 4.4.3 or by eq. 4.4.4 .

Equation 6, for the axial force, and equation 15, for the moment, complete the basic equations of the model. It is now a question of inferring from them suitable expressions for the deflection of the structure and the stress distribution. In the next section, we shall introduce adimensional variables which will simplify the manipulation of these equations and the basic parameters of the model will be related to the moment at the corner.

We are now in a position to express the curvature as a function of the moment at the corner on the basis of the equations which have been established. The following equations lead to such an expression,

$$m = -m_3 + \frac{1}{2} q u^2 - q l_i u \quad 4.2.14$$

$$f = -q l_{ii} \quad 4.2.16$$

$$K = 1 \quad \text{if} \quad m > \frac{1}{6} f t \quad 4.4.3$$

$$K = 2 \quad \text{if} \quad m < \frac{1}{6} f t$$

$$c = \frac{s_0 - (-1)^K \frac{Y_0}{E} (t - p) - E p a l (T_s - T_c) \frac{1}{E}}{s_0 p + E p [1 - a l (T_s - T_c)]} \quad 4.4.28$$

$$f = \frac{1}{2} s_0 p + (-1)^K \frac{1}{2} Y_0 (t - p) \quad 4.5.6$$

$$m = s_0 \left(\frac{1}{4} t p - \frac{1}{6} p^2 \right) + (-1)^K Y_0 \left(\frac{1}{12} t^2 - \frac{1}{4} t p + \frac{1}{6} p^2 \right) \quad 4.5.15$$

In order to gain a better picture of the relation between the various parameters involved it is convenient to substitute adimensional variables for those used up to now.

Situation 10g in Figure 10 with $s_0 = Y_0$ represents the hypothetical limiting situation between perfect elasticity and

perfect plasticity. This situation can not occur in practice, nor can it occur within this model, as it implies the moment to be constant and different from nil along the whole structure. But it provides some basis to situate the values of the force and moment within reasonable limits.

The axial force and the moment corresponding to this situation can be calculated geometrically,

$$f_{\text{unit}} = \frac{1}{2} Y_0 t \quad 1$$

$$m_{\text{unit}} = \frac{1}{12} Y_0 t^2 \quad 2$$

Force and moment magnitudes are related to these specific values through the use of the following adimensional variables which have unit value in this particular situation,

Adimensional force :

$$F = \frac{f}{\frac{1}{2} Y_0 t} \quad 3$$

Adimensional moment :

$$M = \frac{m}{\frac{1}{12} Y_0 t^2} \quad 4$$

The magnitude of the stress is bounded by the magnitude of the yield stress at the cooling wall,

Adimensional stress :

$$S = \frac{s_0}{Y_0} \quad 5$$

In particular,

the adimensional stress at the cooling wall is,

$$S_o = \frac{s_o}{Y_o} \quad 6$$

the adimensional stress at the elastoplastic boundary is,

$$Y_p = \frac{Y(p)}{Y_o} \quad 7$$

and the adimensional yield stress at the cooling wall is,

$$l = \frac{Y_o}{Y_o} \quad 8$$

The same parameter, although not limiting, is used to define :
Adimensional Young's Modulus :

$$E^* = \frac{E}{Y_o} \quad 9$$

Adimensional liquid metal pressure :

$$Q = \frac{q}{Y_o} \quad 10$$

The adimensional distances, both from the cooling wall and from the corner, are defined in relation to the thickness of the beam,

Adimensional distance from the cooling wall surface :

$$U = \frac{u}{t} \quad 11$$

In particular,

the adimensional neutral axis position is,

$$N = \frac{n}{t} \quad 12$$

the adimensional elastoplastic boundary position is,

$$P = \frac{p}{t} \quad 13$$

the adimensional thickness of the beams is,

$$l = \frac{t}{t} \quad 14$$

Adimensional distance from the corner :

$$V = \frac{v}{t} \quad 15$$

In particular,

the adimensional length of the corner is,

$$A = \frac{a}{t} \quad 16$$

the adimensional lengths of the beams are,

$$L_1 = \frac{l_1}{t} \quad ; \quad L_2 = \frac{l_2}{t} \quad 17$$

Finally,

Adimensional coefficient of thermal expansion :

$$Al = al (T_S - T_C) \quad 18$$

The six equations brought together at the beginning of this section to describe the model at its current stage of development gain simplicity when written in terms of the adimensional variables just introduced,

$$M = - M_3 + 6 Q U^2 - 12 Q L_i U \quad 19$$

$$F = - 2 Q L_{ii} \quad 20$$

$$K = 1 \quad \text{if} \quad M > F \quad 21$$

$$K = 2 \quad \text{if} \quad M < F$$

$$C = \frac{S_0 - (-1)^K (1 - P) - E^* P A1}{S_0 P + E^* P (1 - A1)} \quad 22$$

$$F = S_0 P + (-1)^K (1 - P) \quad 23$$

$$M = S_0 (3 P - 2 P^2) + (-1)^K (1 - 3 P + 2 P^2) \quad 24$$

From eq. 23, we have,

$$S_0 = \frac{F - (-1)^K (1 - P)}{P} \quad 25$$

Replacing S_0 in eq. 22, we have,

$$C = \frac{F - (-1)^K (1 - P) - (-1)^K (1 - P) P - E^* P^2 A1}{P [F - (-1)^K (1 - P) + E^* P (1 - A1)]} \quad 26$$

$$C = \frac{F - (-1)^K + P^2 [(-1)^K - E^* A1]}{P [F - (-1)^K] + P^2 [(-1)^K + E^* (1 - A1)]} \quad 27$$

Replacing now S_0 in eq. 24, using again eq.25, we have,

$$M = [F - (-1)^K (1 - P)] (3 - 2 P) + (-1)^K (1 - 3 P + 2 P^2) \quad 28$$

$$M = 3 F - 2 F P - 2 (-1)^K + 2 (-1)^K P \quad 29$$

$$P = \frac{M - 3 F + 2 (-1)^K}{- 2 F + 2 (-1)^K} \quad 30$$

Equation 27, with P given by equation 30, determines the curvature in terms of the moment and the force at U,

C =

$$\frac{[F - (-1)^K] [-2F + 2(-1)^K]^2 + [M - 3F + 2(-1)^K]^2 [1 - E^* A1]}{[F - (-1)^K] [M - 3F + 2(-1)^K] [-2F + 2(-1)^K] + [M - 3F + 2(-1)^K]^2 [1 + E^* (1 - A1)]} \quad 31$$

The adimensional Young's modulus, E^* , and the adimensional coefficient of thermal expansion, $A1$, are assumed to be known. The axial force, F , is constant within each beam and can be calculated using equation 20. The moment at U, M , is given by equation 19 as a function of the moment at the corner M_3 , of the adimensional length of the beam, L_{ij} , of the adimensional position, U , and of the adimensional pressure of the liquid metal, Q . Of these variables, only M_3 is unknown.

The adimensional metalostatic pressure, Q , can be calculated, given the metallurgical height and the density of the liquid metal, using equation 4.2.17 and equation 10.

Equation 31, therefore, gives the curvature as a function of the moment at the corner, M_3 , and of otherwise known quantities.

In the same way, equation 30 gives the adimensional position of the elato-plastic boundary, P , as a function of the moment at the corner, M_3 , and of known quantities.

A similar expression can be inferred for the adimensional position of the neutral axis, N :

Writing equation 4.4.25 in adimensional terms,

$$N = \frac{(-1)^K (1 - P) + E^* P [C + A1 (1 - C)]}{(-1)^K (1 - P) C + E^* [C + A1 (1 - C)]} \quad 32$$

That is, replacing P , using equation 30,

$$N = \frac{(-1)^K [(-2F+2(-1)^K)-(M-3F+2(-1)^K)]+E^*(M-3F+2(-1)^K)[C-A1(1-C)]}{(-1)^K [(-2F+2(-1)^K)-(M-3F+2(-1)^K)]C+E^*(-2F+2(-1)^K)[C-A1(1-C)]} \quad 33$$

For the adimensional stress at the cooling wall, S_o :

Replacing P in equation 25, using equation 30, we have,

$$S_o = \frac{(F - (-1)^K) (-2 F + 2 (-1)^K) + (-1)^K (M - 3 F + 2 (-1)^K)}{M - 3 F + 2 (-1)^K} \quad 34$$

that is,

$$S_0 = \frac{-2F^2 + (-1)^K (F + M)}{M - 3F + 2(-1)^K} \quad 35$$

And for the adimensional stress at the elasto-plastic boundary, Y_p :

Writing equation 4.4.5 in adimensional terms,

$$Y_p = (-1)^K (1 - P) \quad 36$$

and replacing P , using equation 30,

$$Y_p = (-1)^K \frac{-M + F}{-2F + 2(-1)^K} \quad 37$$

We have therefore inferred a series of expressions which relate the fundamental parameters of the structure to the moment at the corner, M_3 . This moment is determined by the boundary conditions stated in section 4.1:

- 1.- the beams are rigidly bound together at right angles (at node *3*).
- 2.- the derivative of their deflection is nil at their other boundary (nodes *1* and *5*).

In the next section we are going to use these conditions to integrate the curvature, which is the second derivative of the deflection, as it is given by equation 31.

4.7 THE DEFLECTION OF THE STRUCTURE

Let, the adimensional deflection be defined as,

$$W = \frac{w}{t} \quad 1$$

The curvature is the second derivative of the deflexion, therefore using equation 4.6.31,

$$C = \frac{d^2W}{dU^2} = \frac{[F-(-1)^K] [-2F+2(-1)^K]^2 + [M-3F+2(-1)^K]^2 [1-E^*A1]}{[F-(-1)^K] [M-3F+2(-1)^K] [-2F+2(-1)^K] + [M-3F+2(-1)^K]^2 [1+E^*(1-A1)]} \quad 2$$

where M is given by equation 4.6.19,

$$M = -M_3 + 6 Q U^2 - 12 Q L_i U \quad 3$$

F, is given by equation 4.6.20,

$$F = -2 Q L_{ii} \quad 4$$

K, is given by equation 4.6.21,

$$K = 1 \quad \text{if} \quad M > F \quad 5$$

$$K = 2 \quad \text{if} \quad M < F$$

And Q can be calculated using equation 4.2.17,

$$q = \text{meth} \times (\text{density of the liquid metal}) \times g \quad 6$$

and the definition of adimensional liquid metal pressure, given by equation 4.6.10,

$$Q = \frac{q}{\gamma_0} \quad 7$$

These equations are valid for both beams.

$$L_i = L_1 \quad \text{for the long beam} \quad 8$$

$$L_i = L_2 \quad \text{for the short beam}$$

$$L_{ii} = L_2 \quad \text{for the long beam} \quad 9$$

$$L_{ii} = L_1 \quad \text{for the short beam}$$

Under equilibrium conditions, at a given metallurgical height,

*.- the pressure Q is constant.

*.- the axial force F is constant within each beam.

$$F = - 2 Q L_2 \quad \text{for the long beam} \quad 10$$

$$F = - 2 Q L_1 \quad \text{for the short beam} \quad 11$$

*.- the moment M , and therefore the sign of the plastic stress and the curvature, depends on both the beam and the distance from the corner U ,

$$M = - M_3 + 6 Q U^2 - 12 Q L_1 U \quad \text{for the long beam} \quad 12$$

$$M = - M_3 + 6 Q U^2 - 12 Q L_2 U \quad \text{for the short beam}$$

*.- the moment at the corner M_3 must be the same for both beams.

*.- the derivative of the deflection must satisfy,

$$\frac{dW}{dU} \text{ (at } U=A, \text{ long beam)} = - \frac{dW}{dU} \text{ (at } U=A, \text{ short beam)} \quad 13$$

$$\frac{dW}{dU} \text{ (at } U=L_1, \text{ long beam)} = 0 \quad ; \quad \frac{dW}{dU} \text{ (at } U=L_2, \text{ short beam)} = 0 \quad 14$$

*.- at the corner origin the deflexion is nil,

$$W \text{ (at } U=0, \text{ both beams)} = 0 \quad 15$$

Assuming an initial value for the moment at the corner, M_3^0 , the curvature functions defined by the previous equations for each beam can be integrated numerically from $U=A_i$, up to $U=L_i$. A fourth order Runge-Kutta algorithm is suitable for this.

This gives, for each beam and for the assumed value of M_3^0 , the value of the difference between the derivative of the deflection at the two integration boundaries.

For the long beam, we have,

$$\int_{A_1}^{L_1} \frac{d^2w}{dU^2} (M_3 = M_3^0) dU = \frac{dw}{dU} (M_3 = M_3^0, U=L_1) - \frac{dw}{dU} (M_3 = M_3^0, U=A_1) \quad 16$$

and for the short beam,

$$\int_{A_2}^{L_2} \frac{d^2w}{dU^2} (M_3 = M_3^0) dU = \frac{dw}{dU} (M_3 = M_3^0, U=L_2) - \frac{dw}{dU} (M_3 = M_3^0, U=A_2) \quad 17$$

As the derivative of the deflection is nil at both $U = L_1$ and $U = L_2$ (equation 14), we have,

for the long beam,

$$\int_{A_1}^{L_1} \frac{d^2w}{dU^2} (M_3 = M_3^0) dU = - \frac{dw}{dU} (M_3 = M_3^0, U=A_1) \quad 18$$

and for the short beam,

$$\int_{A_2}^{L_2} \frac{d^2w}{dU^2} (M_3 = M_3^0) dU = - \frac{dw}{dU} (M_3 = M_3^0, U=A_2) \quad 19$$

The value of M_3 is then iterated,

$$M_3^{i+1} = M_3^i + \Delta M_3^i \quad \text{if} \quad \frac{dW}{dU}(M_3=M_3^i, U=A_2) < - \frac{dW}{dU}(M_3=M_3^i, U=A_1) \quad 20$$

$$M_3^{i+1} = M_3^i - \Delta M_3^i \quad \text{if} \quad \frac{dW}{dU}(M_3=M_3^i, U=A_2) > - \frac{dW}{dU}(M_3=M_3^i, U=A_1)$$

where,

$$\Delta M_3^i = | M_3^i - M_3^{i-1} | \quad 21$$

and,

$$\Delta M_3^0 = \frac{1}{2} M_3^0 \quad 22$$

until,

$$\frac{dW}{dU}(M_3=M_3^i, U=A_2) + \frac{dW}{dU}(M_3=M_3^i, U=A_1) < \text{a given error bound} \quad 23$$

Having identified the value of the moment at the corner, the value of the derivative of the deflection can be obtained at any point of the intervals (A_1, L_1) and (A_2, L_2) ,

For the long beam, we have, for any U such that $A_1 < U < L_1$,

$$\int_{A_1}^U \frac{d^2W}{dU^2}(M_3) dU = \frac{dW}{dU}(M_3, U) - \frac{dW}{dU}(M_3, A_1) \quad 24$$

and for the short beam, for any U such that $A_2 < U < L_2$,

$$\int_{A_2}^U \frac{d^2W}{dU^2}(M_3) dU = \frac{dW}{dU}(M_3, U) - \frac{dW}{dU}(M_3, A_2) \quad 25$$

The integration can be carried out further to obtain the deflection at any point of these intervals,

For the long beam, for any U such that $A_1 < U < L_1$,

$$\int_{A_1}^U \frac{dW}{dU}(M_3) dU = W(M_3, U) - W(M_3, A_1) \quad 26$$

and for the short beam, for any U such that $A_2 < U < L_2$,

$$\int_{A_2}^U \frac{dW}{dU}(M_3) dU = W(M_3, U) - W(M_3, A_2) \quad 27$$

The deflection at the boundary between the rigid and non-rigid portions of the beams can be obtained directly because the rigid portion will remain flat. The corner rotates as a whole without deforming. The angle of rotation is given by the derivative of the deflection at the boundary.

Therefore, we have,

$$W(M_3, A_1) = A_1 \frac{dW}{dU}(\text{at } A_1) \quad 28$$

$$W(M_3, A_2) = A_2 \frac{dW}{dU}(\text{at } A_2) \quad 29$$

The derivative of the deflection at the rigid/non-rigid boundaries is in fact the same, but for the sign, for both beams (as stated in equation 14).

It must be remembered that we are working with a generic beam (see section 4.2, fig 7). This generic representation has a direct correspondance with the X, Y reference system (which

coincides with the cooling wall when there is no distortion and has its origin at the edge of the corner) only in the case of the short beam. It must be remembered that we are looking at the long beam "from behind the page" (section 4.2).

Within the X,Y reference system, the moment at the corner has opposite signs for each beam. The "generic" sign is true only of the short beam. In general, all the moments obtained within the generic representation of the long beam will acquire an opposite sign within the X,Y reference system, while the short beam moments will keep their sign.

All distances, and their derivatives, keep their sign when transferred from the "generic" representation to the X,Y reference system chosen.

The equations derived in this chapter, up to this point, are the basic equations of the model.

They allow us to predict the mechanical equilibrium of a structure which comprises two lengths of solidifying shell rigidly joined at the corner and supported only by axial forces applied at the ends.

This structure was originally taken to correspond to a whole quarter of the section of a continuously cast billet or slab totally detached from the mould at a given metallurgical height.

However, it is now possible to relate the structure considered to the corner portion of the solidifying shell which is

detached from the mould at a given metallurgical height. This corner portion is not necessarily the whole of the quarter section.

The slope of the deflection of the two detached lengths of shell are parallel to the mould at $x=L_1$ and at $x=L_2$, as are the axial forces applied at these points by the remaining lengths of shell.

At the present stage of development of the model presented in this thesis it is assumed that the taper is not significant enough to generate an additional moment affecting the equilibrium of the detached corner portion. Under this assumptions therefore the overall moment equilibrium equations derived in section 4.2 need not to be altered and all the equations derived up to now apply.

The computer program presented in chapter 5 was developed in several stages. In a first stage, it was constructed without taking into account the presence of the mould and used in a preliminary analysis of the possible behaviour of detached corner portions of the solidifying shell. The results of this preliminary analysis are presented in the first section of chapter six. This was the basis for a further development of the model which considered the restraining presence of the mould.

Up till now, the analysis has considered the deformation of two lengths of solidifying shell rigidly joined at the corner and supported only by axial forces applied at the ends.

This occurs within the mould because the shells contract as they cool and thus pull the corner of the solidifying structure inwards from the corner of the mould while the rest of the solidifying shell remains flat against the mould wall, clamped by the metallostatic pressure.

In the absence of additional moments (which could arise, for instance, if the taper is very significant) the detached corner portion increases without contacting the mould at intermediate points until one face (or both in the case of a square billet) is completely detached from the mould.

Under these circumstances it is the contraction of one side of the structure that makes space available for the deflection of the other. At any given metallurgical height and with any given thermal state in the solidifying shells, the length of unsupported shell (beam) along one side of the structure is determined by the space made available for its deflection by the contraction of the entire supported and unsupported length of the adjacent side and by the reduction of this space due to the taper.

A suitable iterative algorithm would therefore allow prediction the behaviour of any slab or billet section.

At this stage of development of the model, however, a different approach is adopted in order to generate results which allow the analysis of trends in the behaviour of continuously cast billets and slabs. This approach, which consists in using the detached lengths rather than the total section lengths as the independent variables, was used to generate a comprehensive set of results which allow to predict the mechanical behaviour of any particular continuously cast billet in the mould. In the case of slabs it was used to generate predictions, for a metallurgical height of **0.1 m**, corresponding to a particular slab continuously cast at different speeds. In the absence of overall results for slabs, these predictions involved a basic trial and error iteration.

As in previous sections, a quarter section of the slice of billet or slab at a certain metallurgical height is considered. Now, however, we shall focuss our attention on the deformation of the corner portion of the solidifying shell which is detached from the mould. This corner portion not necessarily being the whole of the quarter section.

The remaining of the solidifying shell within the quarter section is assumed to be clamped against the wall of the mould by the ferrostatic pressure. The detached corner portion is assumed to be supported only by axial forces applied by the remaining solidifying shell at distances L_1 and L_2 from the corner. If, under specified conditions, the billet or slab considered is totally detached from the mould, then L_1 and L_2 are the dimensions of the quarter section. However, if the billet or slab is not totally detached, then L_1 or/and L_2 are distances from the corner to the points of attachment with the mould such that any point along the surface of the solidifying shell nearer to the corner than these points is detached from the mould and any such point further from the corner than these points is in contact with the mould.

The slope of the deflection of the detached lengths of shell are parallel to the mould at $x=L_1$ and at $x=L_2$, as are the axial forces applied at these points by the remaining lengths of shell.

Let,

$l_{\text{total } i}$, be half the total length of face i of the slab or billet.

The contraction of this total length of shell on one side of the quarter section considered, $\Delta l_{\text{total } i}$, is taken as the thermal contraction in the length of the neutral axis - no stress acts along the neutral axis which therefore suffers no elastic or plastic deformation. The position of the neutral axis within the shell section where it lies flat against the mould is taken as its position at the end of the detached shell length. The temperature there, and hence the thermal contraction of this supported length, can be simply determined from the temperature distribution assumed across the shell section.

Calculation of the thermal contraction of the neutral axis in the detached length of shell is considerably more complicated because the position of the neutral axis varies in this section as the balance of thermal and mechanical load varies along its length. A first order approximation to the thermal contraction of this length can be simply obtained, however, by assuming that it also deforms as if the neutral axis remained in the position it occupies in the supported length.

The contraction of the total length of shell, $\Delta l_{\text{total } i}$, is therefore given by:-

$$\Delta l_{\text{total } i} = - \alpha l (T_s - T(n_i)) l_{\text{total } i} \quad 1$$

Using the assumption of a linear temperature distribution across the shell stated in equation 4.1.1, we have,

$$\Delta l_{\text{total } i} = - \alpha l (T_s - t_c) (t - n_i) l_{\text{total } i} / t \quad 2$$

This equation can be written in adimensional terms using equations 4.6-12/17/18

$$\Delta L_{\text{total } i} = - \alpha l (1 - N_i) L_{\text{total } i} \quad 3$$

The corner gap distance, G_i , that is the distance between face i and the mould at the corner edge, is determined by the contraction of the adjacent length of shell, $\Delta L_{\text{total } ii} < 0$, and by the taper of face i of the mould at the metallurgical height considered, $0 < \text{TAPER } i < - \Delta L_{\text{total } ii}$,

$$G_i = - \Delta L_{\text{total } ii} - \text{TAPER } i > 0 \quad 4$$

That is, using equation 3,

$$G_i = \alpha l (1 - N_{ii}) L_{\text{total } ii} - \text{TAPER } i \quad 5$$

The deflections are measured from the corner reference system adopted. Therefore, the negative deflections (towards the mould) must be smaller in magnitude than the corner gap of the face considered, while positive deflections do not need to be restricted by the corner gap. That is,

for any x such that $0 < x < L_i$,

$$- W(x) < G_i \quad 6$$

Under the assumptions made, this occurs if, and only, the deflection at the end of the detached length of shell of the face i considered is smaller in magnitude than the corner gap,

$$- W(L_i) < G_i \quad 7$$

We are now in a position to define $L_{ac\ ii}(W(L_i))$, the total length of face ii required to accommodate the deflection of face i at L_i :

$$L_{ac\ ii}(W(L_i)) = \frac{TAPER\ i - W(L_i)}{Al(1 - N_{ii})} \quad 8$$

$L_{ac\ ii}(W(L_i))$, could actually have a negative value if the deflection at L_i is positive. The physical meaning of defining the accommodating length in this way will be made clear briefly.

Replacing $L_{ac\ ii}(W(L_i))$, as given by equation 8, for $L_{total\ ii}$ in equation 5, and reordering, it follows that,

$$-W(L_i) = G_i \quad 9$$

The accommodating total length defined is therefore that which accommodates exactly the deflection of the adjacent length of shell.

We also have,

$$\text{for any } L_{total\ ii} > L_{ac\ ii} \\ \frac{TAPER\ i - W(L_i)}{Al(1 - N_{ii})} < L_{total\ ii} \quad 10$$

$$-W(L_i) < Al(1 - N_{ii}) L_{total\ ii} - TAPER\ i < G_i \quad 11$$

The inequalities can be reversed, that is,

$$\text{for any } L_{total\ ii} < L_{ac\ ii} \\ -W(L_i) > G_i \quad 11$$

The total length can not be smaller than the accommodating length.

Therefore, using the definition of the detached lengths, we have,

$$L_{\text{total } ii} \neq L_{\text{ac } ii} (W_i) \Leftrightarrow L_{\text{total } i} = L_i \quad 12$$

$$L_{\text{total } i} \neq L_{\text{ac } i} (W_{ii}) \Leftrightarrow L_{\text{total } ii} = L_{ii} \quad 13$$

For a square billet: the total lengths, the taper on each mould face and the adjacent detached lengths are equal.

Therefore equations 12 and 13 imply,

$$L_{\text{total}} = L \quad \text{if} \quad L_{\text{ac}} (W(L)) < L \quad 14$$

$$L_{\text{total}} = L_{\text{ac}} (W(L)) \quad \text{if} \quad L_{\text{ac}} (W(L)) > L \quad 15$$

At the present stage of development of the model presented in this thesis only one situation is considered for slabs and blooms within the mould. That is, when both the minimum length calculated are bigger than the detached lengths of the other face,

$$L_{\text{ac } i} (W(L_2)) > L_i \quad \text{and} \quad L_{\text{ac } ii} (W(L_1)) > L_{ii} \quad 16$$

In this situation, which appears to be the prevalent situation for slabs and blooms in the mould, the assumption that there are no additional moments than those established by the equilibrium of the detached lengths of shell holds and we have,

$$L_{\text{total } i} = L_{\text{min } i} \quad 17$$

$$L_{\text{total } ii} = L_{\text{min } ii} \quad 18$$

4.9 DATA USED FOR THE INITIAL PREDICTIONS

COEFFICIENT OF THERMAL EXPANSION

$$\alpha_1 = 0.18 \times 10^{-4} \text{ degC}^{-1}$$

This value corresponds to austenitic steel, a small variation could be expected depending on the presence of alloying elements but this has been neglected at this stage.

DENSITY OF THE MOLTEN METAL

$$\text{DENSITY(molten steel)} = 7.5 \times 10^3 \text{ kg.m}^{-3}$$

The same value was used for all predictions.

MODULUS OF ELASTICITY

$$E = 7 \times 10^9 \text{ N.m}^{-2}$$

This value was derived from the data reported by Kitaoka et al (52). Previous models (35-38,67) have assumed a linear dependence of the Young's modulus with temperature leading to an average above 1000 degC which is an order of magnitude higher. As it was pointed out in the Literature Survey, Section 2.5, experimental results related to steels indicate values of the Young's modulus of the order of magnitude of that adopted.

The effect of using higher values of the Young's modulus was investigated (Section 6.5).

YIELD STRESS, QUASI-STATIC YIELD STRESS AND STRAIN RATE

The yield stress at the surface, Y_s , is determined as a function of the surface temperature, T_c , from the quasi-static yield stress at 1000 degC, $QSYS(1000 \text{ degC})$, and an estimated mean strain rate, $EMSR$.

The following equation, given by Jonas et al (53), is used,

$$Y_0(T_c) = QSYS(T_c) (EMSR / QSSR)^{0.2}$$

where,

$$QSSR = 0.0006 \text{ s}^{-1}$$

is the quasi-static strain rate (53-55).

The estimated mean strain rate is taken as constant pending further development of the model at a value which is said to be characteristic in continuous casting moulds (38),

$$EMSR = 0.006 \text{ s}^{-1}$$

In fact the value used in previous models (35-38,47,48,67) is 0.001 s^{-1} , but then the quasi-static strain rate used is 0.0001 s^{-1} which results in the same ratio in equation 1, which is similar to the equations used in those models.

The quasi-static yield stress at the cooling wall temperature T_c , used in equation 1, is derived by linear interpolation,

$$QSYS(T_c) = QSYS(1000 \text{ degC}) (T_s - T_c)/(T_s - 1000 \text{ degC}) \quad 2$$

The values of the quasi-static yield stress at 1000 degC used range between 2.4 and $6.5 \times 10^7 \text{ N.m}^{-2}$, which corresponds to the range of values reported by Kitaoka for the tensile strength and the flow stress at 0.004% strain of various steels.

**THICKNESS OF THE SHELL,
TEMPERATURE DIFFERENCE ACROSS THE SHELL AND CASTING SPEED**

Two logarithmic functions of the solidification time determine the thickness of the solidifying shell, t , and the temperature difference across the shell, delT ,

$$\text{delT} = 96.93 \quad \text{Log}(0.6 \text{ TIME} + 1) \quad [\text{deg C}] \quad 3$$

and,

$$t = 0.00977 \quad \text{Log}(0.15 \text{ TIME} + 1) \quad [\text{ m }] \quad 4$$

These functions were established on the basis of typical predictions of heat transfer models (59,67).

The solidification time is calculated from values of the casting speed, $\text{CS} [\text{m.s}^{-1}]$, and of the metallurgical height, $\text{meth} [\text{m}]$,

$$\text{TIME} = \text{meth} / \text{CS} \quad 5$$

RIGID CORNER LENGTH

The length of solidified shell considered rigid in the corner region, A , is calculated by a logarithmic function of the solidification time established on the basis of the results reported by Krishnamurthy (60),

$$A = t (3.159 - \log(0.1 \text{ TIME} + 1))$$

6

```

PROGRAM LUCIA
C   GOING DOWN THE MOULD TO ESTIMATE TOTAL LENGTH
C.....
CDETERMINATION OF THE DEFLECTION OF A CONTINUOUSLY CAST STRUCTURE
C.....
C LAST MODIFIED ON: 25/02/85 DO LOOP          7,8,9 CONTINUE
C
C           GOING DOWN THE MOULD
C           26/02/85 CASTING SPEED AND LENGTH DO-LOOPS
C           28/02/85 ADDED CORNER AS FUNCTION OF TIME
C           new functions: t=t(time), delT=delT(time), QSYS=QSYS(delT)
C           ^QF"DECE" TO MODIFY PRINTED DATE!
C MAJOR MODIFICATIONS:
C10/12/84: CONSTRUCTED ON THE BASIS OF NOV17 SINGLE BEAM PROGRAM
C           TO GIVE THE DEFLECTION WITH RESPECT TO X,Y REF.SYSTEM
C           AND TO ITERATE M3 WITH LITTLE INTERVENTION.
C.....
C
REAL*8 X,Y,DERY,PRMT,L,SL1,SL2,MAXM3,MINM3,F2,G,DT
REAL*8 G,HEIGHT,DMS,HEIGHT,QSYS,QSSR,EMSR,YS,TIME,CASP
REAL*8 LENGTH,DETACH,SECTIO,CN,CW
DIMENSION PRMT(21),Y(2),DERY(2),AUX(8,4),KW(2,2,2)
DIMENSION CN(2),CW(2),LENGTH(2),DETACH(2),SECTIO(2)
EXTERNAL FCT,OUTP
C
C STAGE FLAG, PRMT(20):(INITIAL, LONG BEAM) STAGE = (1)
C                   (INITIAL, SHORT BEAM) STAGE = (2)
C ^QF"*ST" FINDS    (PRINTER, LONG BEAM) STAGE = (3)
C STAGE DEPENDENCE (PRINTER, SHORT BEAM) STAGE = (4)
C                   (PLOTTER, LONG BEAM) STAGE = (5)
C                   (PLOTTER, SHORT BEAM) STAGE = (6)
C AFFECTS:
C MAIN PROGRAM: (1) ITERATES M3
C               (1)&(2) NDIM=1          DERY(1)=1
C               (3)TO(6) NDIM=2  Y(2)=0.D0 DERY(1)=.5 DERY(2)=.5
C               (3) PRINTS DATA AND FINAL RESULTS TITLES.
C ALSO DEFINES THE LENGHT OF THE GENERIC
C BEAM, AND THAT OF THE "OTHER" BEAM,
C (1),(3),(5) =" PRMT(2)=L1 , PRMT(6)=L2
C (2),(4),(6) =" PRMT(2)=L2 , PRMT(6)=L1
C
C DRKGS: ONLY THROUGH INTEGRATION PARAMETERS GIVEN BY MAIN PROGRAM
C [ NDIM=1 OR 2, Y(2) GIVEN OR NOT, DERY(1)=1 OR .5 ]
C PRMT(2) IS THE UPPER BOUND OF INTEGRATION.
C
C FCT: (1)&(2) JUMPS LINE WHICH GIVES DERY(2) THE DERIVATIVE AT U.
C ALSO THROUGH VALUES OF PRMT(2) AND PRMT(6) GIVEN BY MAIN PR.
C
C OUTP: (1) PRINTS THE ITERATION STEP AND M3
C       (2) PRINTS DW/DU AT L1 AND AT L2 ON THE SCREEN
C       (3) PRINTS THE LONG BEAM RESULTS
C       (4) PRINTS THE SHORT BEAM RESULTS, REQUESTS PAPER TRANSFER
C           FROM PRINTER TO PLOTTER.
C       (5) PLOTS DEFLECTED LONG BEAM.
C       (6) PLOTS DEFLECTED SHORT BEAM.
C

```

```

C 26/2/85 MODIFICATION:
C CASTING SPEED DO-LOOP:
    DO 9 KCS=1,10
C     KCS=2
C
C
C 26/2/85 MODIFICATION:
C LENGTH DO-LOOP
    DO 8 KKL=1,10
    DO 7 KLE=1,2
C     KLE=2
C
C 25/2/85 MODIFICATION:
C METALLURGICAL HEIGHT DO-LOOP
C     DO 7 KDT=3,6,3
    KDT=1
C
C
C ADDITIONAL PARAMETERS USED,
C CASTING SPEED [m/sec]:
    CASP=0.03D0-KCS*0.01D0
C QSYS AT 1000 degC [N/m**2],
C AS GIVEN BY KITAOKA ET AL (1980),
    QSYS=30000000.D0
C METALLURGICAL HEIGHT, [m]
    HEIGHT=KDT*0.1D0
C TIME ELAPSED FROM BEGINNING OF SOLIDIFICATION,
    TIME=HEIGHT/CASP
C
C 25/2/85 MODIFICATION: t and delT are calculated on the basis of
C logarithmic functions which aproximate
C experimental results given by:
C Gautier et al.(1970) & Brimacombe (1976).
C
C THICKNESS OF THE SOLIDIFIED METAL [m]:
C
    G=0.00977D0*DLOG(0.15D0*TIME+1.D0)
C
C TEMPERATURE DIFFERENCE ACROSS THE THICKNESS (TS-TC) [degC],
C modification Time=time/2 to raise surface temperature
    DT=96.93D0*DLOG(0.6D0*TIME+1.D0)
C     DT=106.35D0*DLOG(0.7D0*TIME+1.D0)
C
C LENGTH OF CORNER CONSIDERED RIGID [m]:
    PRMT(1)=G*(3.159D0-DLOG(0.1D0*TIME+1))
C
C COUNTER:
C
    PRMT(20)=1.D0
C
C VALUE OF THE DERIVATIVE OF THE DEFLECTION. INITIALLY TAKEN AS 0
C FOR THE FIRST INTEGRATION DONE WITHIN A REFERENCE SYSTEM WHICH
C ROTATES WITH THE CORNER,
C
    PRMT(19)=0.D0

```

```

C LENGTH OF THE WALLS (BEAMS) [m]
C TAKEN AS A FUNCTION OF G AS A FIRST APROXIMATION OF GAP
C FORMATION WITHIN THE MOULD.
C PRMT(6)=5.D0*KLE*0.001D0
C PRMT(6)=0.098D0+(KKL+KLE)*0.001D0
C PRMT(6)=0.15D0
C PRMT(2)=0.095D0+KKL*0.001D0
C PRMT(6)=G*KLE+PRMT(1)
C PRMT(2)=G*KLE+PRMT(1)
C
C COEFFICIENT OF LINEAR THERMAL EXPANSION [1/degC]:
C PRMT(7)=0.000018D0
C
C DENSITY OF THE MOLTEN METAL [Kg/m**3]:
C DMS=7500.D0
C
C LIQUID METAL PRESSURE [N/m ] (NEGATIVE BY SIGN CONVENSON):
C PRMT(8)=-DMS*HEIGHT*9.80665D0
C
C MODULUS OF ELASTICITY OF THE METAL AT HIGH TEMPERATURES,
C ASSUMED CONSTANT [N/m ] (INFERED FROM KITAOKA ET AL,1980):
C PRMT(9)=7000000000.D0
C
C QUASI-STATIC YIELD STRESS AT THE COOLING WALL TEMPERATURE
C QSYS [N/m ] CALCULATED FROM QSYS AT 1000 degC and DT :
C QSYS=QSYS*DT/450.D0
C
C QUASI-STATIC STRAIN RATE, QSSR [1/seg]:
C QSSR=.0006D0
C
C ESTIMATED MEAN STRAIN RATE, EMSR [1/seg]:
C EMSR=.006D0
C
C EFFECTIVE YIELD STRESS AT THE COOLING WALL TEMPERATURE GIVEN
C THE HIGH STRAIN RATE, USING JONAS ET AL (1969) EQUATION,
C YS [N/m ]:
C YS=(EMSR/QSSR)**.2D0*QSYS
C
C KT=DT
C WRITE(2,215) PRMT(7),PRMT(9),PRMT(2),PRMT(6),PRMT(1),G,KT,
C 2 HEIGHT,QSYS,EMSR
C 215 FORMAT(/14X,'DATA: AL',7X,
C 3'E L1 L2 A t delT meth QSYS EMSR'
C 4/15X,'dim.',2E8.2,2F5.3,2F5.3,I5,F5.3,E10.3,F6.4)
C
C ... TRANSLATE INTO ADIMENSIONAL VARIABLES ...
C
C ADIMENSIONAL CORNER LENGHT AND LOWER BOUND OF RK INTEGRATION,
C PRMT(1)=PRMT(1)/G
C
C ADIMENSIONAL LENGHT OF THE BEAM CONSIDERED AND UPPER BOUND OF
C RK INTEGRATION,
C PRMT(2)=PRMT(2)/G
C

```

```

C ADIMENSIONAL INITIAL INCREMENT OF THE INDEPENDENT VARIABLE
C (INITIAL RK STEP),
  PRMT(3)=0.1D0
C
C ADIMENSIONAL UPPER ERROR BOUND FOR RK INTEGRATION. IF ABSOLUTE
C ERROR IS GREATER THAN PRMT(4), INCREMENT GETS HALVED.
C IF INCREMENT IS LESS THAN PRMT(3) AND ABSOLUTE ERROR LESS THAN
C PRMT(4)/50, INCREMENT GETS DOUBLED.
  PRMT(4)=.0005
C
C PRMT(5) IS NOT AN INPUT PARAMETER, SUBROUTINE DRKGS INITIALIZES
C PRMT(5)=0. THE SUBROUTINE DRKGS IS TERMINATED WHEN THE UPPER
C BOUND OF THE INTEGRATION IS REACHED AND SUBROUTINE OUTP SETS
C PRMT(5)=1.
C
C ADIMENSIONAL LENGHT OF THE JOINT BEAM,
  PRMT(6)=PRMT(6)/G
C
C ADIMENSIONAL COEFFICIENT OF LINEAR THERMAL EXPANSION,
  PRMT(7)=PRMT(7)*DT
C
C ADIMENSIONAL LIQUID METAL PRESSURE,
  PRMT(8)=PRMT(8)/YS
C
C ADIMENSIONAL MODULUS OF ELASTICITY,
  PRMT(9)=PRMT(9)/YS
C
C INITIAL M3 GUESS
  PRMT(11)=0.34D0
C INITIAL M3 ITERATION LIMITS,
  MAXM3=1.2D0
  MINM3=-1.0D0
C ITERATION ERROR
  ERIT=.0001
C
C INITIAL NUMBER OF STEPS IN BETWEEN PRINTING (SEE PRMT(3)&(4))
  PRMT(21)=10.
  K=1
C   ^CONTROL TO REPEAT ONLY ONCE WHEN IMPROVING ACCURACY.
C COMES BACK HERE TO PREPARE FOR A NEW INTEGRATION DURING THE
C M3 ITERATION.
C
  1 CONTINUE
C
C ADIMENSIONAL AXIAL FORCE WITHIN THE BEAM CONSIDERED,
C*STAGE DEPENDENT PARAMETER (PRMT(6) VALUE DEPENDS ON BEAM)
  PRMT(10)=-2*PRMT(8)*(PRMT(6)-1)
C
C INPUT VECTOR OF INITIAL VALUES (USED & DESTROYED BY DRKGS)
C   Y(1) IS THE SLOPE OF THE DEFLECTION AT THE RIGID/NON RIGID
C   BOUNDARY REQUIRED BY DRKGS FOR THE INTEGRATION. FOR
C   THE INITIAL INTEGRATION OF THE CURVATURE (STAGE 1),
C   A REFERENCE SYSTEM WHICH ROTATES WITH THE CORNER IS
C   ADOPTED AND THIS SLOPE IS TAKEN AS NIL. THE VALUE OF
C   THIS SLOPE FOR THE X,Y REFERENCE SYSTEM USED LATER

```

```

C      IS OBTAINED BY THIS FIRST INTEGRATION AND STORED IN
C      PRMT(19) SO THAT IT CAN BE USED IN STAGES 2 AND 3.
C      Y(2) IS THE ACTUAL DEFLECTION AT THIS BOUNDARY. IT IS NOT
C      NEEDED FOR THE FIRST INTEGRATION AND IT IS CALCULATED
C      FROM THE KNOWN VALUE OF THE SLOPE AFTERWARDS.
C
C*STAGE DEPENDENT PARAMETERS:(REDEFINED AFTER ST(2))
C
C      Y(1)=0.D0
C
C      INPUT VECTOR OF ERROR WEIGHTS (USED & DESTROYED BY DRKGS)
C      (THE SUM OF ITS COMPONENTS MUST BE EQUAL TO 1. LATER ON
C      DERY IS THE VECTOR OF DERIVATIVES, WHICH BELONG TO
C      FUNCTION VALUES Y AT A POINT X.)
C*STAGE DEPENDENT PARAMETERS:(REDEFINED AFTER ST(2))
C
C      DERY(1)=1.
C
C      INPUT VALUE WHICH SPECIFIES THE NUMBER OF EQUATIONS IN THE
C      SYSTEM:
C*STAGE DEPENDENT PARAMETER:(REDEFINED AFTER ST(2))
C      NDIM=1
C
C      TOTAL NUMBER OF RK STEPS COMPLETED (ACCUMULATIVE COUNTER)
C      THAT IS, NUMBER OF TIMES OUTP HAS BEEN CALLED SINCE INTEGRATION
C      IS STARTED.
C      PRMT(12)=IDINT(PRMT(1))+PRMT(2)-IDINT(PRMT(2))
C
C      ACCUMULATIVE RK STEP COUNTER FOR PRINTING DECISION. INITIALLY
C      SET C TO #NECESSARY FOR PRINTING - 1, SO THAT IT PRINTS THE
C      INITIAL C VALUES.
C      PRMT(13)=PRMT(21)-1.D0
C
C      CALL DRKGS(PRMT,Y,DERY,NDIM,IHLF,FCT,OUTP,AUX,KW)
C
C      123 CONTINUE
C      WRITE(3,102) PRMT(11),Y(1),PRMT(20)
C      102 FORMAT(1X,'M3= ',F11.7/1X,/1X,'Y(1)= ',F7.3/1X,'ST= ',F3.1/)
C
C      SWAP BEAM LENGTHS,
C      L=PRMT(2)
C      PRMT(2)=PRMT(6)
C      PRMT(6)=L
C
C      IF(PRMT(20).EQ.1.) SL1=-Y(1)
C      IF(PRMT(20).EQ.2.) SL2=Y(1)
C
C*STAGE JUNCTION: ITERATE M3 ONLY IF AT ST(2)
C
C      IF(PRMT(20).NE.2.) GO TO 2
C      ERR=DABS(SL1-SL2)
C      IF(ERR.LT.ERIT) GO TO 3
C      IF(SL1.LT.SL2) MINM3=PRMT(11)
C      IF(SL1.GT.SL2) MAXM3=PRMT(11)
C      PRMT(11)=(MINM3+MAXM3)/2

```

```

PRMT(20)=1.
GO TO 1
C
2 CONTINUE
PRMT(20)=2.
C
C short cut used in the case of billets when it is not necessary
C to repeat the integration. (stage 2 is jumped).
C
IF (PRMT(2).EQ.PRMT(6)) GO TO 123
GO TO 1
C
3 CONTINUE
PRMT(19)=SL1
WRITE(3,100) PRMT(19)
100 FORMAT(1X,'THE ITERATION IS COMPLETED, PREPARE PRINTER'/
1 1X,'DW/DU(A2)=' ,F7.4/)
PRMT(20)=3.
C
C ...PREPARE FOR RK INTEGRATION... STAGE 3
C
C*STAGE CHANGE, BEAM LENGTHS ALREADY SWAPED,
C
C*STAGE CHANGE, AXIAL FORCE FOR THE BEAM CONSIDERED
PRMT(10)=-2*PRMT(8)*(PRMT(6)-1)
C*STAGE 3 TO 6, ERROR WEIGHTS
DERY(1)=.5D0
DERY(2)=.5D0
C*STAGE 3 TO 6, INITIAL VALUES DW/DU(A1)=Y(1), W(A1)=Y(2)
Y(1)=PRMT(19)
Y(2)=PRMT(1)*Y(1)
C*STAGE 3 TO 6, # OF EQUATIONS (NDIM IS NOT DESTROYED BY DRKGS)
NDIM=2
C
C*STAGE 3: PRINTS DATA
F2=-2*PRMT(8)*(PRMT(2)-1)
WRITE(2,105) PRMT(7),PRMT(9),PRMT(2),PRMT(6),PRMT(1),YS,
1 PRMT(3),PRMT(10),PRMT(8),PRMT(4),F2,PRMT(11),ERIT
105 FORMAT(14X,'adim.',2E8.2,2F5.1,F5.2,' 1.',11X,'YS=',E8.3/
4 22X,'RKstep =',F7.5,16X,'F1 =',E8.2,2X,' Q = ',E8.2/
5 22X,'RKerror =',F7.5,16X,'F2 =',E8.2,2X,'M3 = ',F6.4/
6 22X,'ITerror =',F7.5)
C
C*STAGE 3: PRINTS LONG BEAM TABLE TITLES
WRITE(2,130)
39X IF N NOT PRINTED
130 FORMAT(31X,'DETACHED SECTION 1 :')
WRITE(2,140)
140 FORMAT(31X,'X',4X,'C',3X,'DW/DX',3X,'W',4X,'M',4X,'S0',3X,'P',
1 4X,'YP',4X,'N'/)
C
C TOTAL NUMBER OF RK STEPS COMPLETED (ACCUMULATIVE COUNTER)
C THAT IS, NUMBER OF TIMES OUTP HAS BEEN CALLED SINCE INTEGRATION
C IS STARTED.
PRMT(12)=IDINT(PRMT(1))+PRMT(2)-IDINT(PRMT(2))

```

```

C
C ACCUMULATIVE RK STEP COUNTER FOR PRINTING DECISION. INITIALLY SET
C TO #NECESSARY FOR PRINTING - 1, SO THAT IT PRINTS THE INITIAL
C VALUES.
  PRMT(21)=10.
  PRMT(13)=PRMT(21)-1.D0
C
C ... RK INTEGRATION ...      STAGE 3
C
  CALL DRKGS(PRMT,Y,DERY,NDIM,IHLF,FCT,OUTP,AUX,KW)
C
  CW(1)=Y(2)
  CN(1)=PRMT(18)
C
C
C ...PREPARE FOR RK INTEGRATION... STAGE 4
C
C*STAGE CHANGE, SWAP BEAM LENGTHS,
  L=PRMT(2)
  PRMT(2)=PRMT(6)
  PRMT(6)=L
C*STAGE CHANGE, AXIAL FORCE FOR THE BEAM CONSIDERED
  PRMT(10)=-2*PRMT(8)*(PRMT(6)-1)
C*STAGE 3 TO 6, ERROR WEIGHTS
  DERY(1)=.5D0
  DERY(2)=.5D0
C*STAGE 3 TO 6, INITIAL VALUES DW/DU(A1)=Y(1), W(A1)=Y(2)
  Y(1)=-PRMT(19)
  Y(2)=PRMT(1)*Y(1)
C
  WRITE(2,150)
C
  39X IF N NOT PRINTED
150 FORMAT(/31X,'DETACHED SECTION 2 :')
  IF(PRMT(20).EQ.3.) PRMT(20)=4.
  IF(PRMT(20).EQ.1.) PRMT(20)=2.
C
C TOTAL NUMBER OF RK STEPS COMPLETED (ACCUMULATIVE COUNTER)
C THAT IS, NUMBER OF TIMES OUTP HAS BEEN CALLED SINCE INTEGRATION
C IS STARTED.
  PRMT(12)=IDINT(PRMT(1))+PRMT(2)-IDINT(PRMT(2))
C
C ACCUMULATIVE RK STEP COUNTER FOR PRINTING DECISION. INITIALLY SET
C TO #NECESSARY FOR PRINTING - 1, SO THAT IT PRINTS THE INITIAL
C VALUES.
  PRMT(13)=PRMT(21)-1.D0
C
C ... RK INTEGRATION ...      STAGE 4
C
  CALL DRKGS(PRMT,Y,DERY,NDIM,IHLF,FCT,OUTP,AUX,KW)
C
C
C

```

```

C      CW(2)=Y(2)
      CN(2)=PRMT(18)
C
C CALCULATE AND PRINT TOTAL LENGTH
C
      LENGTH(1)=CW(2)/(CN(1)-1)/PRMT(7)
      LENGTH(1)=LENGTH(1)*G
      DETACH(1)=PRMT(6)*G
      SECTIO(1)=DETACH(1)
      IF(LENGTH(1).GT.DETACH(1)) SECTIO(1)=LENGTH(1)
C
      LENGTH(2)=CW(1)/(CN(2)-1)/PRMT(7)
      LENGTH(2)=LENGTH(2)*G
      DETACH(2)=PRMT(2)*G
      SECTIO(2)=DETACH(2)
      IF(LENGTH(2).GT.DETACH(2)) SECTIO(2)=LENGTH(2)
      WRITE(2,178) LENGTH(1),LENGTH(2),SECTIO(1),SECTIO(2),DETACH(1),
1      DETACH(2)
178 FORMAT(36X,' MINL1(W2)  :',F5.3,8X,' MINL2(W1)  :',F5.3
1/30X,' SECTION LENGTH 1  :',F5.3,2X,' SECTION LENGTH 2  :',F5.3
2/30X,' DETACHED LENGTH 1  :',F5.3,2X,' DETACHED LENGTH 2  :',F5.3//)
C
C End of quick tables do-loop :
C
      7 CONTINUE
      8 CONTINUE
      9 CONTINUE
      WRITE(3,500)
500 FORMAT(1X,'I HAVE FINISH THE TABLE, LETS GET ON WITH THAT PLOT',
1' NOW.'/1X,'0.- READ ME FIRST, WAIT FOR * READY? *.'//
2 1X,'1.- CHECK THE PEN IS IN PS1, TURN PLOTTER ON.'//
3 1X,'2.- PRINTER LOCAL, TRANFER PAPER TAKING OUT PERFORATED ',
4'SIDES.'/1X,'3.- CHART LOAD, PAUSE, SMOOTH PAPER.')
      WRITE(3,505)
505 FORMAT(1X,'4.- PRINTER OFF, SWAP INTERFACES.'//1X,
5 '* READY ? * ... YES=1 ...'//)
51 CONTINUE
      READ(3,510) KREADY
510 FORMAT(1X,I1)
      IF(KREADY.NE.1) GO TO 51
      WRITE(3,515)
515 FORMAT(1X,'* SURE ? * ... ITS BEEN A LOT OF WORK, YOU KNOW.')
52 CONTINUE
      READ(3,520) KREADY
520 FORMAT(1X,I1)
      IF(KREADY.NE.1) GO TO 52
      WRITE(3,525)
525 FORMAT(1X,'* I DARE TO ASK YOU ONCE MORE * ... FOR OUR OWN SAKE')
53 CONTINUE
      READ(3,530) KREADY
530 FORMAT(1X,I1)
      IF(KREADY.NE.1) GO TO 53
C
      PRMT(20)=5.

```

```

C
C ...PREPARE FOR RK INTEGRATION... STAGE 5
C
C*STAGE CHANGE, SWAP BEAM LENGTHS,
    L=PRMT(2)
    PRMT(2)=PRMT(6)
    PRMT(6)=L
C*STAGE CHANGE, AXIAL FORCE FOR THE BEAM CONSIDERED
    PRMT(10)=-2*PRMT(8)*(PRMT(6)-1)
C*STAGE 3 TO 6, ERROR WEIGHTS
    DERY(1)=.5D0
    DERY(2)=.5D0
C*STAGE 3 TO 6, INITIAL VALUES DW/DU(A1)=Y(1), W(A1)=Y(2)
    Y(1)=PRMT(19)
    Y(2)=PRMT(1)*Y(1)
C
C*STAGE 5: INITIATE KW(I,J,N) AND PLOT THE CORNER ...
C
C I = COOLING FACE (1) or SOLIDIFICATION FRONT (2).
C J = OLD,i.e.,lower within long beam,(1) or NEW,upper,(2).
C N = X coordinate (1) or Y coordinate (2).
C
C SCALE: 1 ADIMENSIONAL 'U' UNIT = 300 PLOTTER UNITS
C         1 ADIMENSIONAL 'V' UNIT = 600 PLOTTER UNITS
C
C U, distance from the edge of the corner,
C     A = PRMT(1) ; L1 = PRMT(2) ; RKstep = PRMT(3) = .1 = 30
C     W = Y(2) , the deflection which is plotted from the axis,
C         is MAGNIFIED TEN TIMES
C V, distance from the cooling wall,
C     P = PRMT(15) ; t = 1 = 600 ; N = PRMT(18) only when t .
C
C the corner is drawn as a square of sides 'A', the corner length,
C which is originally in 'U' units. It is assumed that, 2 t ~ A .
C
C the edge of the corner is (COOLING FACE, OLD, X and Y),
    KW(1,1,1)=6000
    KW(1,1,2)=1500
C the top left vertex is (COOLING FACE, NEW, X and Y),
    KW(1,2,1)=6000+Y(2)*3000
    KW(1,2,2)=1500+PRMT(1)*300
C the lower right vertex is for the purpose of STAGE 5, plotting
C the long beam, (SOLIDIFICATION FRONT, OLD, X and Y).
    KW(2,1,1)=6000+PRMT(1)*300
    KW(2,1,2)=1500-Y(2)*3000
C and the top right vertex is (SOLIDIFICATION FRONT, NEW, X and Y),
    KW(2,2,1)=6000+PRMT(1)*300+Y(2)*3000
    KW(2,2,2)=1500+PRMT(1)*300-Y(2)*3000
C
C
    WRITE(2,540) KW(1,2,1),KW(1,2,2),KW(1,1,1),KW(1,1,2),
    1 KW(2,1,1),KW(2,1,2),KW(2,2,1),KW(2,2,2),KW(1,2,1),KW(1,2,2)
540 FORMAT(1X,'SP1;VS1;PA',I5,',',I5,',';PD;PA',I5,',',I5,',';PA',
    1 I5,',',I5,',';PA',I5,',',I5,',';PA',I5,',',I5,',';PU;VS10;')
C
C

```

```

C TOTAL NUMBER OF RK STEPS COMPLETED (ACCUMULATIVE COUNTER)
C THAT IS, NUMBER OF TIMES OUTP HAS BEEN CALLED SINCE INTEGRATION
C IS STARTED.
    PRMT(12)=IDINT(PRMT(1))+PRMT(2)-IDINT(PRMT(2))
C
C ACCUMULATIVE RK STEP COUNTER FOR PRINTING DECISION. INITIALLY SET
C TO NIL AS THE INITIAL VALUES ARE ALREADY PLOTTED.
    PRMT(21)=1.
    PRMT(13)=0.
C new RKstep, to slow down the computer and give time to the plotter,
    PRMT(3)=0.1
    PRMT(4)=0.0005
C
C ... RK INTEGRATION ...          STAGE 5
C
    CALL DRKGS(PRMT,Y,DERY,NDIM,IHLF,FCT,OUTP,AUX,KW)
C
    PRMT(20)=6.
C
C ...PREPARE FOR RK INTEGRATION... STAGE 6
C
C*STAGE CHANGE, SWAP BEAM LENGTHS,
    L=PRMT(2)
    PRMT(2)=PRMT(6)
    PRMT(6)=L
C*STAGE CHANGE, AXIAL FORCE FOR THE BEAM CONSIDERED
    PRMT(10)=-2*PRMT(8)*(PRMT(6)-1)
C*STAGE 3 TO 6, ERROR WEIGHTS
    DERY(1)=.5D0
    DERY(2)=.5D0
C*STAGE 3 TO 6, INITIAL VALUES DW/DU(A1)=Y(1), W(A1)=Y(2)
    Y(1)=-PRMT(19)
    Y(2)=PRMT(1)*Y(1)
C
C*STAGE 6: INITIATE KW(I,J,N) AND PLOT THE CORNER ...
C
C the edge of the corner is (COOLING FACE, OLD, X and Y),
    KW(1,1,1)=6000
    KW(1,1,2)=1500
C the top left vertex is (SOLIDIFICATION FRONT, OLD, X and Y)(ST6),
    KW(2,1,1)=6000-Y(2)*3000
    KW(2,1,2)=1500+PRMT(1)*300
C the lower right vertex is for the purpose of STAGE 6, plotting
C the short beam, (COOLING FACE, NEW, X and Y).
    KW(1,2,1)=6000+PRMT(1)*300
    KW(1,2,2)=1500+Y(2)*3000
C and the top right vertex is (SOLIDIFICATION FRONT, NEW, X and Y),
    KW(2,2,1)=6000+PRMT(1)*300-Y(2)*3000
    KW(2,2,2)=1500+PRMT(1)*300+Y(2)*3000
C
    WRITE(2,600) KW(1,2,1),KW(1,2,2)
    600 FORMAT(1X,'PU;PA',I5,',',I5,',';')
C

```

```

C TOTAL NUMBER OF RK STEPS COMPLETED (ACCUMULATIVE COUNTER)
C THAT IS, NUMBER OF TIMES OUTP HAS BEEN CALLED SINCE INTEGRATION
C IS STARTED.
    PRMT(12)=IDINT(PRMT(1))+PRMT(2)-IDINT(PRMT(2))
C
C ACCUMULATIVE RK STEP COUNTER FOR PRINTING DECISION. INITIALLY SET
C TO NIL, SO THAT IT DOES NOT PLOT THE INITIAL VALUES.
    PRMT(13)=0.
C
C ... RK INTEGRATION ...          STAGE 6
C
    CALL DRKGS(PRMT,Y,DERY,NDIM,IHLF,FCT,OUTP,AUX,KW)
C
999 CONTINUE
    STOP
    END
C
C
C RUNGE KUTTA TO SOLVE THE DIFFERENTIAL EQUATIONS:
C
    SUBROUTINE DRKGS(PRMT,Y,DERY,NDIM,IHLF,FCT,OUTP,AUX,KW)
C
C
    DIMENSION Y(2),DERY(2),AUX(8,2),A(4),B(4),C(4),PRMT(21),KW(2,2,2)
    REAL*8 PRMT,Y,DERY,AUX,A,B,C,X,XEND,H,AJ,BJ,CJ,R1,R2,
1DELT
    DO 1 I=1,NDIM
1  AUX(8,I)=.0666666666666666667D0*DERY(I)
    X=PRMT(1)
    XEND=PRMT(2)
    H=PRMT(3)
    PRMT(5)=0.D0
    CALL FCT(X,Y,DERY,PRMT)
C
C    ERROR TEST
    IF(H*(XEND-X)) 38,37,2
C
C    PREPARATION FOR THE RUNGE KUTTA METHOD
2  A(1)=.5D0
    A(2)=.2928932188134525D0
    A(3)=1.7071067811865475D0
    A(4)=.1666666666666666667D0
    B(1)=2.D0
    B(2)=1.D0
    B(3)=1.D0
    B(4)=2.D0
    C(1)=.5D0
    C(2)=.2928932188134525D0
    C(3)=1.7071067811865475D0
    C(4)=.5D0
C
C    PREPARATION FOR THE FIRST RUNGE KUTTA STEP
    DO 3 I=1,NDIM
    AUX(1,I)=Y(I)
    AUX(2,I)=DERY(I)

```

```

    AUX(3,I)=0.D0
3  AUX(6,I)=0.D0
    IREC=0
    H=H+H
    IHLF=-1
    ISTEP=0
    IEND=0
C
C    START OF A RUNGE KUTTA STEP
4  IF((X+H-XEND)*H) 7,6,5
5  H=XEND-X
6  IEND=1
C
C    RECORDING THE INITIAL VALUES OF THIS STEP
7  CALL OUTP(X,Y,DERY,IREC,NDIM,PRMT,KW)
    IF(PRMT(5)) 40,8,40
8  ITEST=0
9  ISTEP=ISTEP+1
C
C    START OF INNERMOST RUNGE KUTTA LOOP
    J=1
10  AJ=A(J)
    BJ=B(J)
    CJ=C(J)
    DO 11 I=1,NDIM
        R1=H*DERY(I)
        R2=AJ*(R1-BJ*AUX(6,I))
        Y(I)=Y(I)+R2
        R2=R2+R2+R2
11  AUX(6,I)=AUX(6,I)+R2-CJ*R1
    IF(J-4) 12,15,15
12  J=J+1
    IF(J-3) 13,14,13
13  X=X+.5D0*H
14  CALL FCT(X,Y,DERY,PRMT)
    GO TO 10
C    END OF INNERMOST RUNGE KUTTA LOOP
C
C    TEST OF ACCURACY
15  IF(ITEST) 16,16,20
C    IN CASE ITEST=0 THERE IS NO POSSIBILITY FOR TESTING OF ACCURACY
16  DO 17 I=1,NDIM
17  AUX(4,I)=Y(I)
    ITEST=1
    ISTEP=ISTEP+ISTEP-2
18  IHLF=IHLF+1
    X=X-H
    H=.5D0*H
    DO 19 I=1,NDIM
        Y(I)=AUX(1,I)
        DERY(I)=AUX(2,I)
19  AUX(6,I)=AUX(3,I)
    GO TO 9
C
C    IN CASE ITEST=1 TESTING OF ACCURACY IS POSSIBLE

```

```
20 IMOD=ISTEP/2
   IF(ISTEP-IMOD-IMOD) 21,23,21
21 CALL FCT(X,Y,DERY,PRMT)
   DO 22 I=1,NDIM
   AUX(5,I)=Y(I)
22 AUX(7,I)=DERY(I)
   GO TO 9
```

C

C COMPUTATION OF TEST VALUE DELT

```
23 DELT=0.D0
   DO 24 I=1,NDIM
24 DELT=DELT+AUX(8,I)*DABS(AUX(4,I)-Y(I))
   IF(DELT-PRMT(4)) 28,28,25
```

C

C ERROR IS TOO GREAT

```
25 IF(IHLF-10) 26,36,36
26 DO 27 I=1,NDIM
27 AUX(4,I)=AUX(5,I)
   ISTEP=ISTEP+ISTEP-4
   X=X-H
   IEND=0
   GO TO 18
```

C

C RESULT VALUES ARE GOOD

```
28 CALL FCT(X,Y,DERY,PRMT)
   DO 29 I=1,NDIM
   AUX(1,I)=Y(I)
   AUX(2,I)=DERY(I)
   AUX(3,I)=AUX(6,I)
   Y(I)=AUX(5,I)
29 DERY(I)=AUX(7,I)
   CALL OUTP(X-H,Y,DERY,IHLF,NDIM,PRMT,KW)
   IF(PRMT(5)) 40,30,40
30 DO 31 I=1,NDIM
   Y(I)=AUX(1,I)
31 DERY(I)=AUX(2,I)
   IREC=IHLF
   IF(IEND) 32,32,39
```

C

C INCREMENT GETS DOUBLED

```
32 IHLF=IHLF-1
   ISTEP=ISTEP/2
   H=H+H
   IF(IHLF) 4,33,33
33 IMOD=ISTEP/2
   IF(ISTEP-IMOD-IMOD) 4,34,4
34 IF(DELT-.02D0*PRMT(4)) 35,35,4
35 IHLF=IHLF-1
   ISTEP=ISTEP/2
   H=H+H
   GO TO 4
```

C

C

```

C     RETURNS TO CALLING PROGRAM
36  IHLF=11
    CALL FCT(X,Y,DERY,PRMT)
    GO TO 39
37  IHLF=12
    GO TO 39
38  IHLF=13
39  CALL OUTP(X,Y,DERY,IHLF,NDIM,PRMT,KW)
40  RETURN
    END

```

```

C
C
C
C

```

```

C SUBROUTINE FCT,
C

```

```

    SUBROUTINE FCT(X,Y,DERY,PRMT)
    REAL*8 X,Y,DERY,PRMT
    DIMENSION Y(2),DERY(2),PRMT(21)

```

```

C
C

```

```

    WRITE(3,100) X
100 FORMAT(10X,'X= ',F9.6/)

```

```

C
C

```

```

    EVALUATE THE MOMENT AT X,
    PRMT(14)=-PRMT(11)+6*((X-2*PRMT(2))*X+PRMT(2))*PRMT(8)

```

```

C
C

```

```

    SIGN OF PLASTIC STRESS,
    NS=2
    IF(PRMT(14).GT.PRMT(10)) NS=1

```

```

C
C

```

```

    ELASTO/PLASTIC BOUNDARY
    PRMT(15)=(PRMT(14)-3*PRMT(10)+(-1)**NS*2)/2/((-1)**NS-PRMT(10))

```

```

C
C

```

```

    CURVATURE (DDW/DXX) AT X,
    DERY(1)=(PRMT(10)+((-1)**NS-PRMT(9))*PRMT(7))*PRMT(15)*PRMT(15)
    1-(-1)**NS)
    2/PRMT(15)
    3/(PRMT(9)*(1-PRMT(7))*PRMT(15)+PRMT(10)-(-1)**NS*(1-PRMT(15)))

```

```

C
C

```

```

    DW/DX AT X,
    IF(PRMT(20).GT.2.) DERY(2)=Y(1)

```

```

C
C

```

```

    RETURN
    END

```

```

C
C

```

```

C SUBROUTINE TO PRINT THE RESULTS:
C

```

```

    SUBROUTINE OUTP(X,Y,DERY,IHLF,NDIM,PRMT,KW)
    REAL*8 X,Y,DERY,PRMT,V,EQ,LIM
    DIMENSION Y(2),DERY(2),PRMT(21),V(3),EQ(3),KW(2,2,2)

```

```

C
C

```

```

    PRMT(13)=PRMT(13)+1.

```

```

C
C

```

```

    WRITE(3,301) PRMT(13),PRMT(12)
301 FORMAT(20X,'(13)= ',F5.1,'(12)=',F5.1/)
    IF((PRMT(12).GT.PRMT(2)).AND.((X+0.095D0).GT.PRMT(2))) GO TO 4

```

```

      IF(PRMT(13).LT.PRMT(21)) GO TO 99
      PRMT(13)=0.D0
      WRITE(3,302) X,PRMT(2)
302  FORMAT(20X,'X/L=',F6.2,'/',F6.2)
      1 PRMT(12)=PRMT(12)+1.D0
      IF(PRMT(20).LE.2.) GO TO 5
C  AUXILIARY VARIABLES
      V(1)=PRMT(9)*(DERY(1)*(1-PRMT(7))+PRMT(7))
      V(2)=PRMT(9)*(1-PRMT(7))
      V(3)=1-PRMT(15)
C
C  EVALUATE THE MOMENT AT X,
      PRMT(14)=-PRMT(11)+6*((X-2*PRMT(2))*X+PRMT(2))*PRMT(8)
C
C  SIGN OF PLASTIC STRESS,
      NS=2
      IF(PRMT(14).GT.PRMT(10)) NS=1
C
C  STRESS AT THE COOLING SURFACE,
      PRMT(16)=(PRMT(10)-(-1)**NS*(1-PRMT(15)))/PRMT(15)
C
C  STRESS AT THE ELASTO/PLASTIC BOUNDARY,
      PRMT(17)=(-1)**NS*V(3)
C
C  NEUTRAL AXIS,
C      PRMT(18)=V(1)+(-1)**NS*DERY(1)*V(3)
C      PRMT(18)=PRMT(16)+1-PRMT(15)
C      PRMT(18)=PRMT(16)-PRMT(17)
      IF(PRMT(18).EQ.0.) GO TO 2
C      PRMT(18)=(V(1)*PRMT(15)+(-1)**NS*V(3))/PRMT(18)
      PRMT(18)=PRMT(15)*PRMT(16)/PRMT(18)
      GO TO 3
      2 CONTINUE
      PRMT(18)=10**33
      3 CONTINUE
C
C  The following variables were used to verify that the basic
C  equations were properly satisfied.
C
C      EQ(1)=PRMT(15)-(V(1)*PRMT(18)-(-1)**NS*(1-DERY(1)*PRMT(18)))
C      1      /(V(1)-(-1)**NS*(1-DERY(1)*PRMT(18)))
C      EQ(2)=PRMT(10)-PRMT(16)*PRMT(15)-(-1)**NS*(1-PRMT(15))
C      EQ(3)=PRMT(14)-PRMT(16)*PRMT(15)*(3-2*PRMT(15))
C      1      -(-1)**NS*(1-PRMT(15)*(3-2*PRMT(15)))
      IF(PRMT(20).LT.5.) WRITE(2,105) X,DERY(1),Y(1),Y(2),PRMT(14),
      1 PRMT(16),PRMT(15),PRMT(17),PRMT(18)
105  FORMAT(29X,F5.1,F6.3,F5.2,F6.2,4F5.2,E9.3)
110  FORMAT(2X,'eq.16 = ',E7.1,' eq.17 = ',E7.1,' eq.18 = ',E7.1/)
      GO TO 5
      4 PRMT(5)=1.
      GO TO 1
      5 CONTINUE
      IF(PRMT(20).GT.2.) GO TO 8
      WRITE(3,115) PRMT(12)
115  FORMAT(1X,'(12)= ',F5.1/)

```

```

8 CONTINUE
  IF(PRMT(20).GT.5.) GO TO 9
  IF(PRMT(20).LT.5.) GO TO 99
C   COOLING WALL,
    KW(1,1,1)=KW(1,2,1)
    KW(1,1,2)=KW(1,2,2)
    KW(1,2,1)=6000+Y(2)*3000
    KW(1,2,2)=X*300+1500
C   SOLIDIFICATION FRONT,
    KW(2,1,1)=KW(2,2,1)
    KW(2,1,2)=KW(2,2,2)
    KW(2,2,1)=KW(1,2,1)+600
    KW(2,2,2)=KW(1,2,2)
C   ELASTOPLASTIC BOUNDARY, distance P from cooling wall,
    KP=PRMT(15)*600
    WRITE(2,500) KW(1,2,1),KW(1,2,2)
    LIM=600-2*Y(2)*3000
    IF(KW(2,2,2).GE.LIM) WRITE(2,510) KW(2,1,1),KW(2,1,2),
1   KW(2,2,1),KW(2,2,2),KW(1,2,1),KW(1,2,2),KP,KW(2,2,1),
2   KW(2,2,2)
    WRITE(2,515) KW(1,2,1),KW(1,2,2)
500  FORMAT(1X,'PD;PA',I5,',',I5,',';PU;')
510  FORMAT(1X,'PA',I5,',',I5,',';PD;PA',I5,',',
1   I5,',';PU;PA',I5,',',I5,',';PR',I5,',0;LT1,0.2;PD;PA',I5,',',I5,
2   ',;LT;PU;')
515  FORMAT(1X,'PA',I5,',',I5,',';')
    GO TO 99
9 CONTINUE
C   COOLING WALL,
    KW(1,1,1)=KW(1,2,1)
    KW(1,1,2)=KW(1,2,2)
    KW(1,2,1)=6000+X*300
    KW(1,2,2)=1500+Y(2)*3000
C   SOLIDIFICATION FRONT,
    KW(2,1,1)=KW(2,2,1)
    KW(2,1,2)=KW(2,2,2)
    KW(2,2,1)=KW(1,2,1)
    KW(2,2,2)=KW(1,2,2)+600
C   ELASTOPLASTIC BOUNDARY,
    KP=PRMT(15)*600
    WRITE(2,610) KW(1,2,1),KW(1,2,2),KW(2,1,1),KW(2,1,2),KW(2,2,1),
1   KW(2,2,2),KW(1,2,1),KW(1,2,2),KP,KW(2,2,1),KW(2,2,2),
2   KW(1,2,1),KW(1,2,2)
610  FORMAT(1X,'PD;PA',I5,',',I5,',';PU;PA',I5,',',I5,',';PD;PA',I5,',',
1   I5,',';PU;PA',I5,',',I5,',';PR0',I5,',';LT1,0.2;PD;PA',I5,',',I5,
2   ',;LT;PU;PA',I5,',',I5,',';')
99 CONTINUE
    RETURN
    END

```

INTRODUCTION

Basic theory of the bending of beams is used in the analysis of the deformation of the bimetallic structure analogue. A comprehensive account of this theory can be found in any basic structural analysis textbook. Two main references have been used in the present work :

- * E.H.Brown, "Structural Analysis", Longmans, 1967
- * R.C.Coates, M.G.Coutie & F.K.Kong, "Structural Analysis".

Under the experimental conditions to which it is subjected, the bimetallic structure analogue constructed can be assumed to behave elastically. This allows use of the principle of superposition which states that the effects of different external loads or conditions are additive. The deflection due to the thermal stress and the deflection due to the load are calculated independently and then simply added together to obtain the deflection due to the combined effect of thermal stress and load. Furthermore, each beam is considered independently and the effect of their interaction is analysed separately. The resulting deflection of the structure is then obtained by adding two magnitudes obtained independently.

Double symmetry of the structure is assumed, and thus the analysis is restricted to a quarter section with the condition

that the curvature of the deflection is nil at the open end of the beams (which corresponds to the middle of the physical analogue beams or bimetallic strips).

The analysis of the thermal behaviour of the bimetallic strips is based on the work done by P.Martin and N.Yarworth, "An Introduction to the Theory and Use of Thermostatic Bimetals", published by Telcon Metals Ltd., Manor Royal, Crawley, Sussex, England.

CHAPTER 6 :
THE RESULTS FROM THE COMPUTER PROGRAM

Results are presented in this section obtained using the computer program described in the previous chapter applied to billets of square cross section and to slabs. Section 6.1 presents investigations into the sensitivity of the model to the values of the parameters involved and considers completely unsupported sections.

Section 6.2 presents results obtained for square billets within the mould and sections 6.3, 6.4 and 6.5 report investigations into the effect on these results of changing, respectively, the rigid corner length, the quasi-static yield stress at the cooled surface and the Young's Modulus.

Except for the preliminary sensitivity analysis, the results are presented in terms of computer print out for typical results and graphs and charts demonstrating the significant trends that were discovered.

6.1 : PRELIMINARY ANALYSIS OF THE BEHAVIOUR OF THE MODEL

The initial work with the computer programme was an investigation of the sensitivity of the model. The results are shown in figures 1 to 11 on pages 6:6-16 in terms of the stress distribution across the cross section of hypothetical solidifying shells at the rigid boundary and at the mid-face position for a metallurgical height of 0.6 m (i.e., at the bottom of most continuous casting machine moulds).

Billets of small cross-section were considered initially followed by billets of increasing size and then by slabs, once again of increasing size but also of increasing aspect ratio. For billets 160 mm square, the temperature difference across the thickness of the shell was varied from 100 C to 300° C for quasi-static surface yield stresses of $2 \times 10^7 \text{ N.m}^{-2}$ (Figure 1, page 6:6) and $3 \times 10^7 \text{ N.m}^{-2}$ (Figure 2, page 6:7). In both cases, increasing the temperature difference rotates the elastic stress distribution line anti-clockwise so as to decrease the tension or to decrease the compression at the solidification front. The effect of the increase in the quasi-static yield stress is to decrease the adimensional magnitude of the stresses at all points in the shell.

The case of blooms 600 mm square is considered in figure 3 (page 6:8) for a quasi-static yield stress of $3 \times 10^7 \text{ N.m}^{-2}$ and temperature differences varying from 150 C to 350' C. The

thickness of the solidified shell had to be increased from the 10 mm considered in the previous case to 15 mm. If this had not been done, the adimensional stress at the surface would have dropped, within the temperature range considered, below -1. The stresses within the section were considerably higher in this case than in the previous case but the basic trends were the same. Because the section was longer, however, greater differences were predicted between the stresses at the corner and at the mid-face and the stress distribution at the rigid boundary always showed tensile plasticity at the solidification front.

The next investigation carried out involved varying the aspect ratio of a slab over the range $L_1/L_2 = 1$ to 5, whilst maintaining the sum $L_1 + L_2 = 1200$ mm (see figures 4 and 5, pages 6:9,10). The thickness of the beams was fixed at 20 mm for a temperature difference of 250' C and a quasi static yield stress at the cooled surface of 3×10^7 N.m⁻². The effect of increasing the aspect ratio was to rotate the elastic stress distribution line clockwise in both the short and long faces at the rigid boundary and at the middle of the short face, but anti-clockwise at the mid-face for the long face.

For an aspect ratio $L_1/L_2 = 5$, the adimensional stress at the surface dropped below -1. At the time this preliminary investigation was carried out, such a value was considered to indicate break-out. The actual stress distributions predicted are not presented for this aspect ratio, however,

since they indicate the existence of a second plastic region at the cooled surface. The model is currently constructed assuming one plastic region so that the stress distributions in this case have little relationship to reality, The model indicates situations in which the second plastic region will appear but does not predict accurate stress distributions under these conditions. The break-out criteria had to be reconsidered later when further results proved it inadequate. (see chapter 7).

As a follow-up to the previous result and to continue investigation into the behaviour of the model, the thickness of the shells of the **1000mmx200mm** slab considered to break-out in the previous investigation was varied from **25mm** to **21mm**. The other parameters were maintained at the same values. Figure 6 (page 6:11), for the short face, and figure 7 (page 6:12), for the long face, show the stress distributions predicted for each thickness at the rigid boundary and at the mid-face. The effect of decreasing the thickness was similar to the effect of increasing the aspect ratio observed previously - rotation of the elastic stress distribution line clockwise in both the short and long faces at the rigid boundary, clockwise at the middle of the short face but anti-clockwise at the middle of the long face. For **t = 21mm**, the adimensional stress at the surface is very close to the critical value of **-1** along the whole of the short beam, it is below **-0.5** at the rigid boudary of the long beam and it increases along the long beam to a value close to **1**.

The investigation was then repeated with a temperature difference of **300°C**. The same trends can be observed as the thickness of the beams is reduced (figures 8 and 9, pages 6:13,14). Increasing the temperature difference always caused an anticlockwise rotation in the elastic stress distribution line and a consequent reduction in the stress levels in the short beam. Although the magnitudes of the stresses at the rigid boundary of the long beam are also reduced, the stresses at the mid-face of the long beam are magnified. Plasticity at the cooled face tended to appear first at the middle of the long solidifying shell as the thickness approached 21 mm (figure 8) whereas it had first appeared in the rigid boundary of the short solidifying shell when the temperature difference was **250°C**, the thickness of the shell approaching the same value.

The next investigation (figures 10 & 11, pages 6:15,16) considered the effect of reducing the Young's modulus whilst keeping the other parameters constant. The same **1000mmx200mm** slab was assumed under conditions similar to those considered in the first case of the previous investigation except that the Young's modulus (in N.m^{-2}) was decreased from **3.0×10^{10}** to **1.0×10^{10}** in steps of **0.5×10^{10}** . The effect of reducing the Young's modulus was to rotate the elastic stress line clockwise in both the short and long faces at the rigid boundary and at the middle of the short face as was observed when reducing the thickness of the beams. This time, however, the effect on the elastic stress line in the middle of the long face was to rotate it clockwise also.

FIGURE 1 : PRELIMINARY ANALYSIS OF THE BEHAVIOUR OF THE MODEL:
 REDUCING ΔT IN THE CASE OF BILLETS
 WITH $Q_{SYS} = 0.2 \times 10^{-8} \text{ N.m}^{-2}$.

DATA:	AL	E	L1	L2	A	t	ΔT	meth	Q_{SYS}	EMSR
	.18E-04	.3E+11	.08	.08	.020	.010	*	.6	.2E+08	06
	'C ⁻¹	N.m ⁻²	m	m	m	m	'C	m	N.m ⁻²	N.m ⁻²

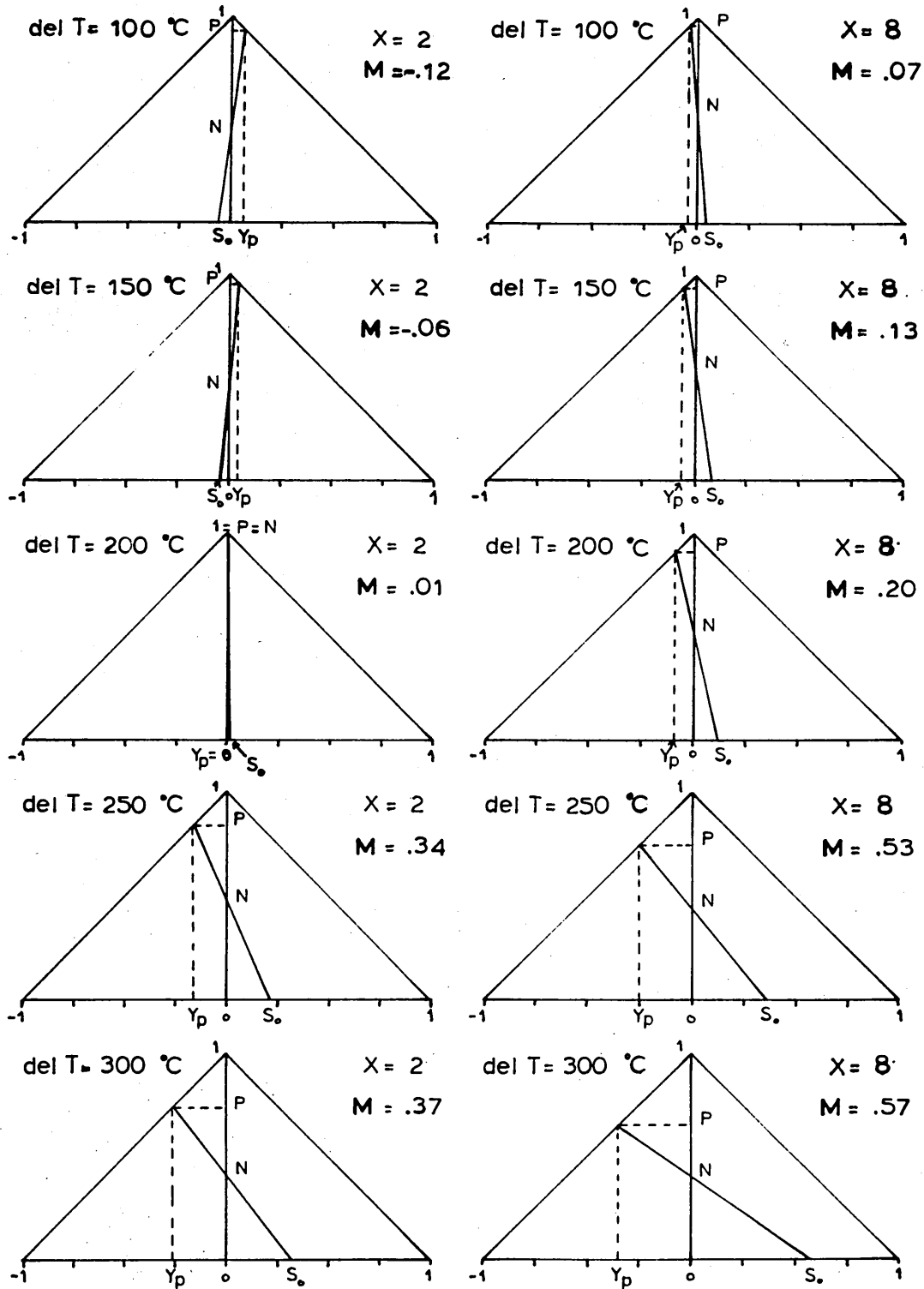


FIGURE 2 : PRELIMINARY ANALYSIS OF THE BEHAVIOUR OF THE MODEL:
 REDUCING ΔT IN THE CASE OF BILLETS
 WITH $Q_{SYS} = 0.3 \times 10^{-8} \text{ N.m}^{-2}$.

DATA:	AL	E	L1	L2	A	t	ΔT	meth	Q_{SYS}	EMSR
	.18E-04	.3E+11	.08	.08	.020	.010	*	.6	.3E+08	.06
	'C ⁻¹	N.m ⁻²	m	m	m	m	'C	m	N.m ⁻²	N.m ⁻²

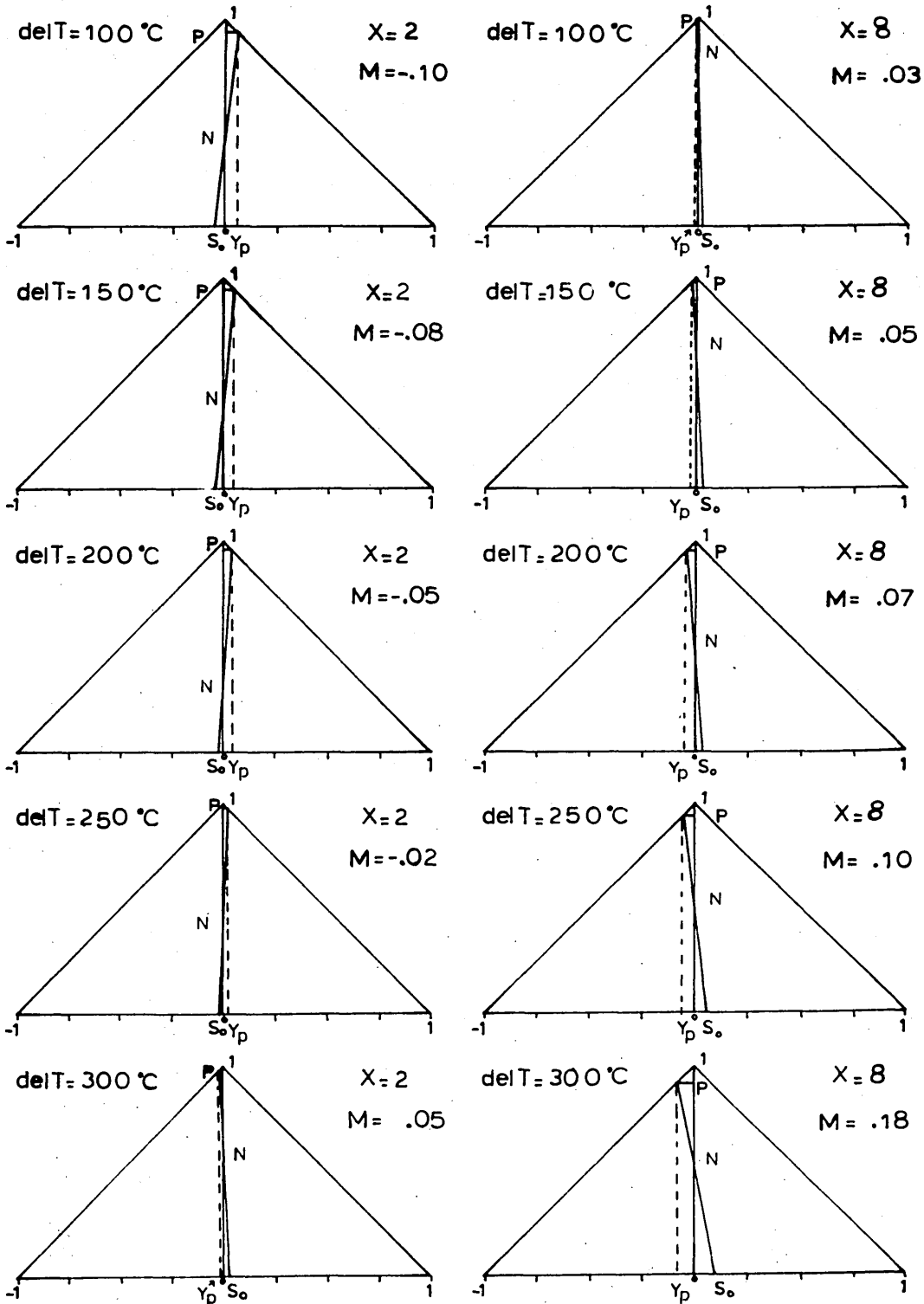


FIGURE 3 . PRELIMINARY ANALYSIS OF THE BEHAVIOUR OF THE MODEL:
REDUCING δT IN THE CASE OF BLOOMS

DATA:	AL	E	L1	L2	A	t	δT	meth	QSYS	EMSR
	.18E-04	.3E+11	.30	.30	.030	.015	*	.6	.2E+08	.06
	'C ⁻¹	N.m ⁻²	m	m	m	m	'C	m	N.m ⁻²	N.m ⁻²

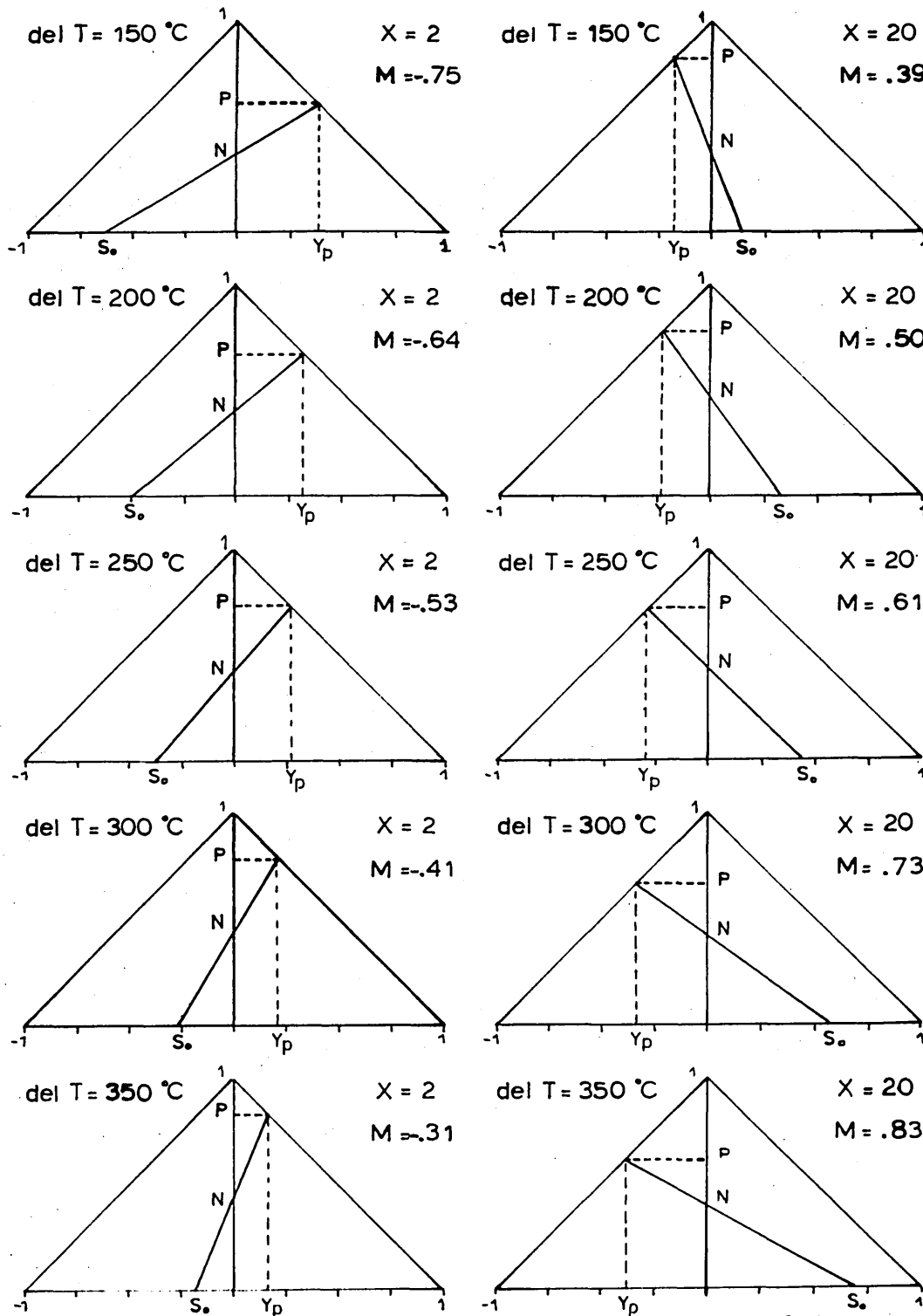


FIGURE 4 : PRELIMINARY ANALYSIS OF THE BEHAVIOUR OF THE MODEL:
 INCREASING THE ASPECT RATIO L_1/L_2 .
 (SHORT FACE)

DATA: AL E L1+L2 A t delT meth QSYS EMSR
 .18E-04 .3E+11 .60 .040 .020 250 .6 .3E+08 .06
 'C⁻¹ N.m⁻² m m m 'C m N.m⁻² N.m⁻²

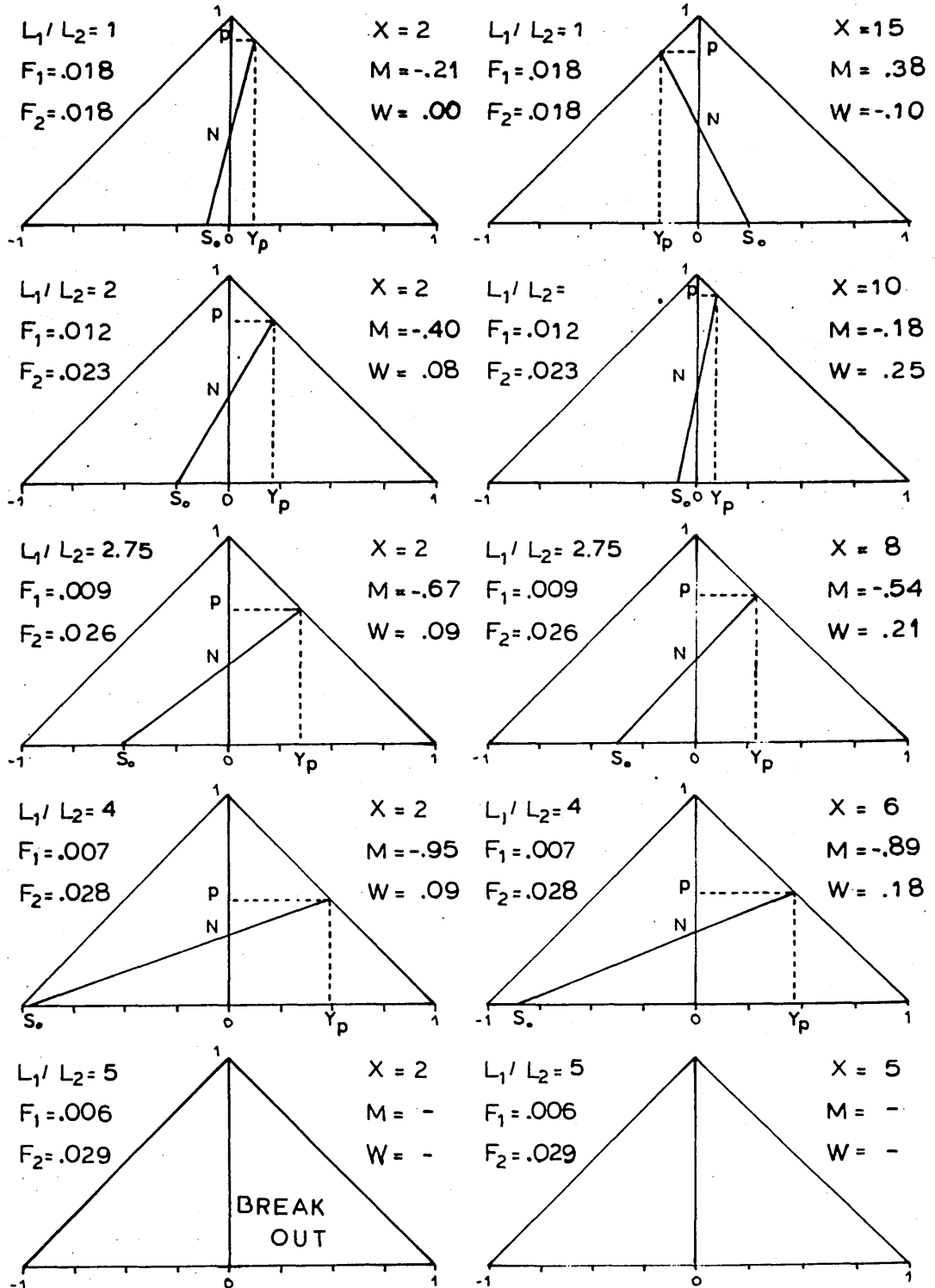


FIGURE 5 : PRELIMINARY ANALYSIS OF THE BEHAVIOUR OF THE MODEL:
INCREASING THE ASPECT RATIO L_1/L_2 .
(LONG FACE)

DATA: AL E L1+L2 A t delT meth QSYS EMSR
 .18E-04 .3E+11 .60 .040 .020 250 .6 .3E+08 .06
 'C⁻¹ N.m⁻² m m m 'C m N.m⁻² N.m⁻²

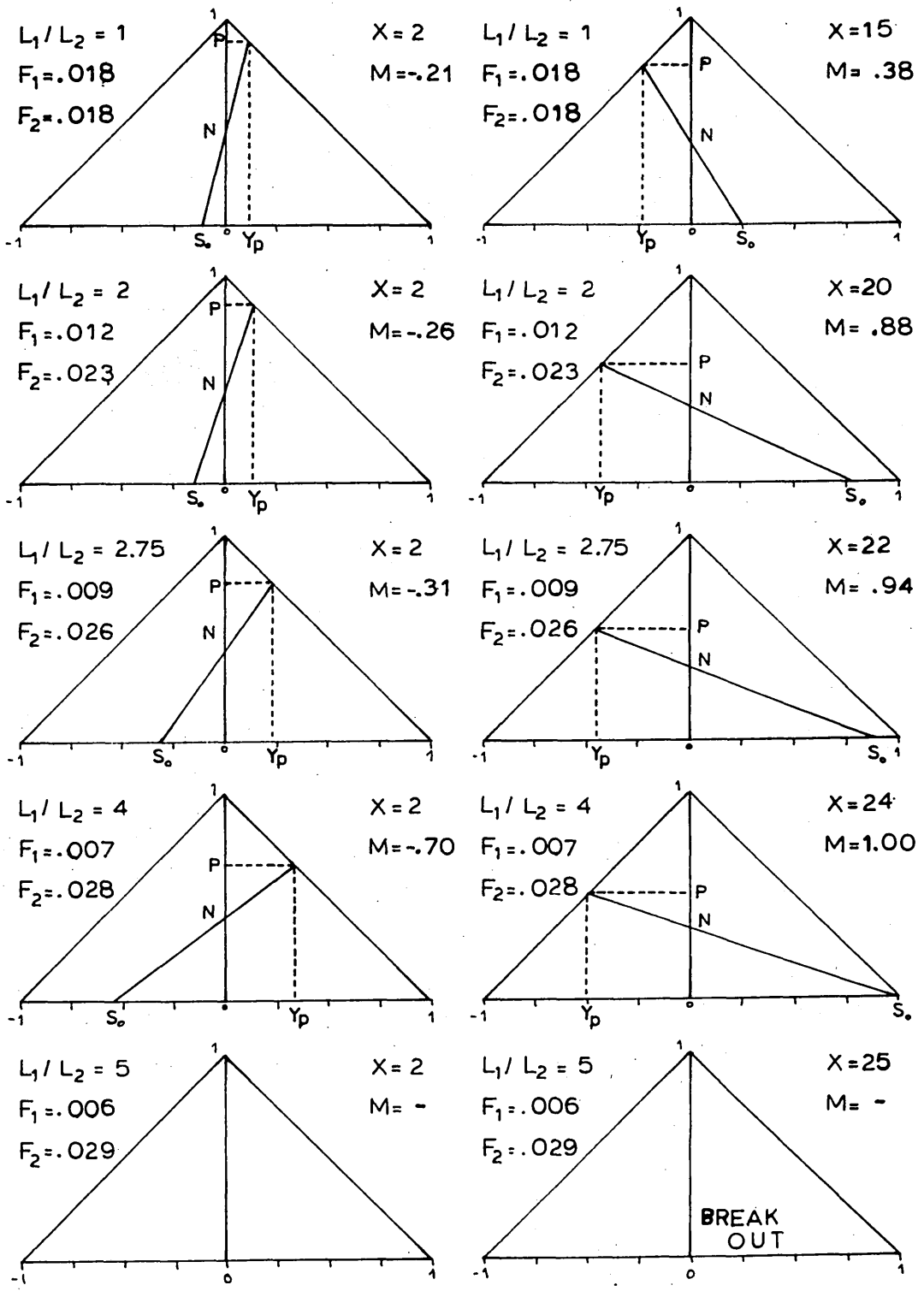


FIGURE 6 : PRELIMINARY ANALYSIS OF THE BEHAVIOUR OF THE MODEL:
 DECREASING THE THICKNESS t IN THE CASE OF SLABS
 WITH $\Delta T = 250^\circ\text{C}$. (SHORT FACE)

DATA: AL E L1 L2 A t ΔT meth QSYS EMSR
 .18E-04 .3E+11 .50 .10 2xt * 250 .6 .3E+08 .06
 'C⁻¹ N.m⁻² m m m m 'C m N.m⁻² N.m⁻²

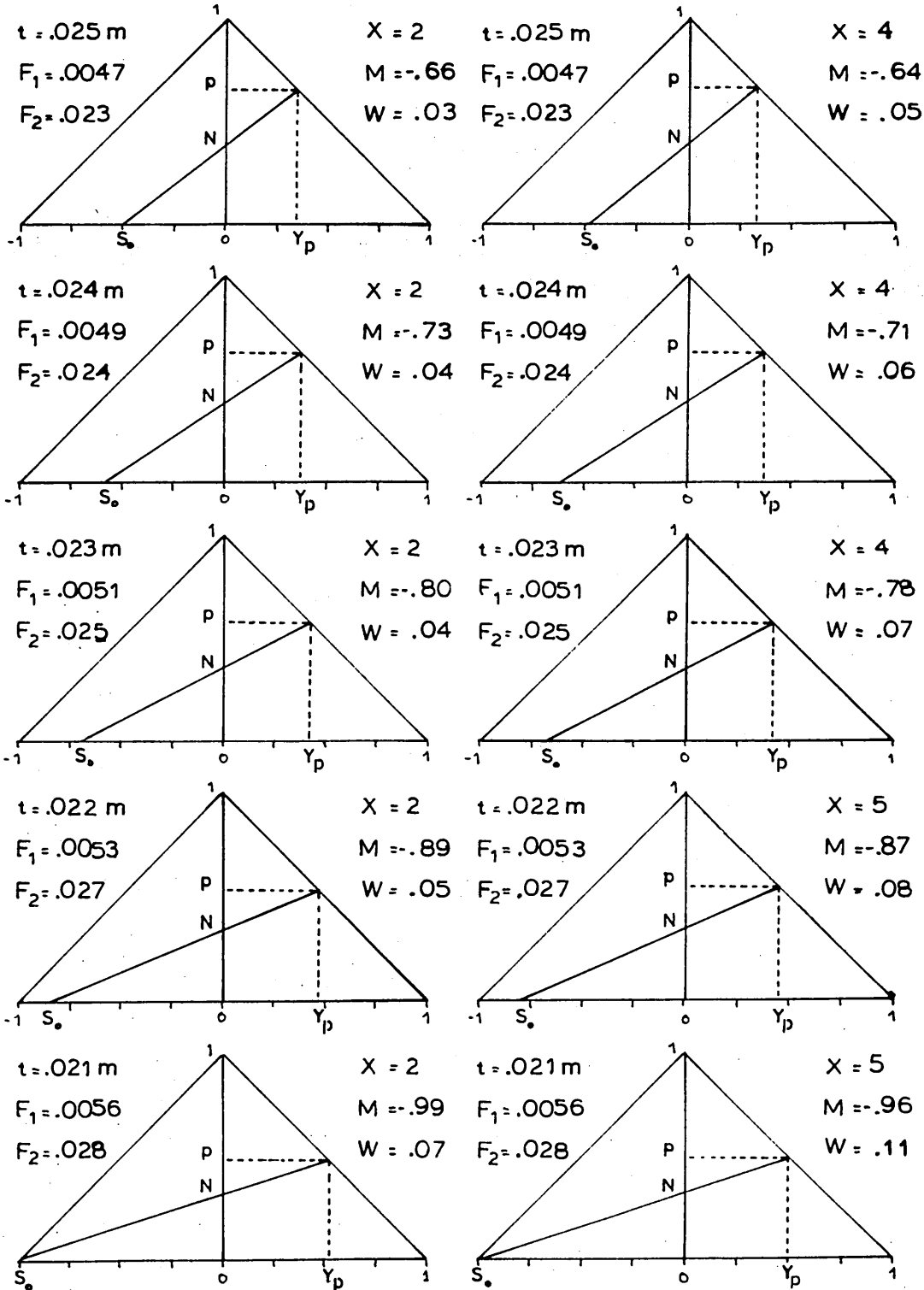


FIGURE 7 : PRELIMINARY ANALYSIS OF THE BEHAVIOUR OF THE MODEL:
 DECREASING THE THICKNESS t IN THE CASE OF SLABS.
 WITH $\Delta T = 250^\circ\text{C}$. (LONG FACE)

DATA:	AL	E	L1	L2	A	t	ΔT	meth	QSYS	EMSR
	.18E-04	.3E+11	.50	.10	2xt	*	250	.6	.3E+08	.06
	'C ⁻¹	N.m ⁻²	m	m	m	m	'C	m	N.m ⁻²	N.m ⁻²

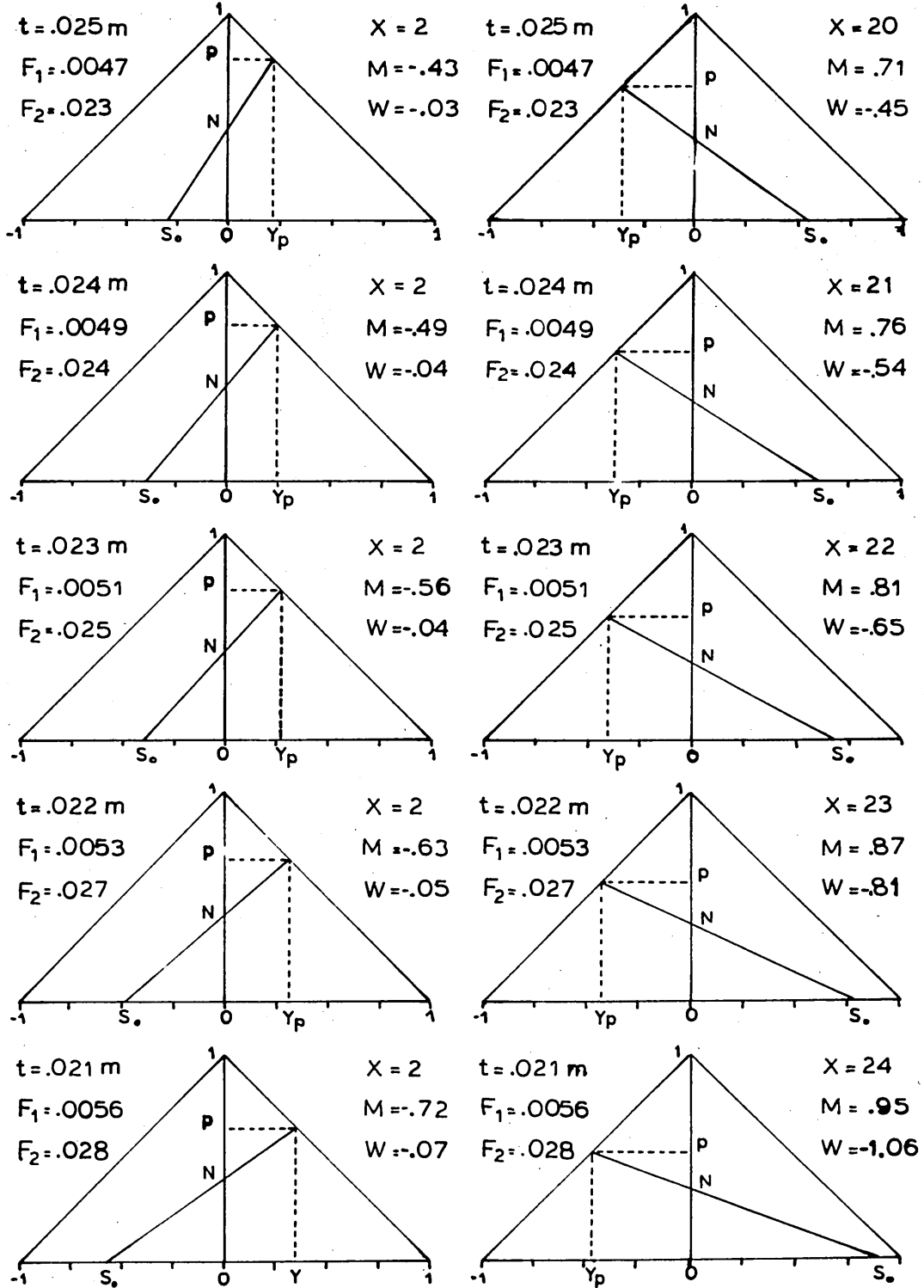


FIGURE 8 : PRELIMINARY ANALYSIS OF THE BEHAVIOUR OF THE MODEL:
 DECREASING THE THICKNESS t IN THE CASE OF SLABS
 WITH $\Delta T = 300^\circ C$. (SHORT FACE)

DATA: AL E L1 L2 A t ΔT meth QSYS EMSR
 .18E-04 .3E+11 .50 .10 2xt * 300 .6 .3E+08 .06
 'C⁻¹ N.m⁻² m m m m 'C m N.m⁻² N.m⁻²

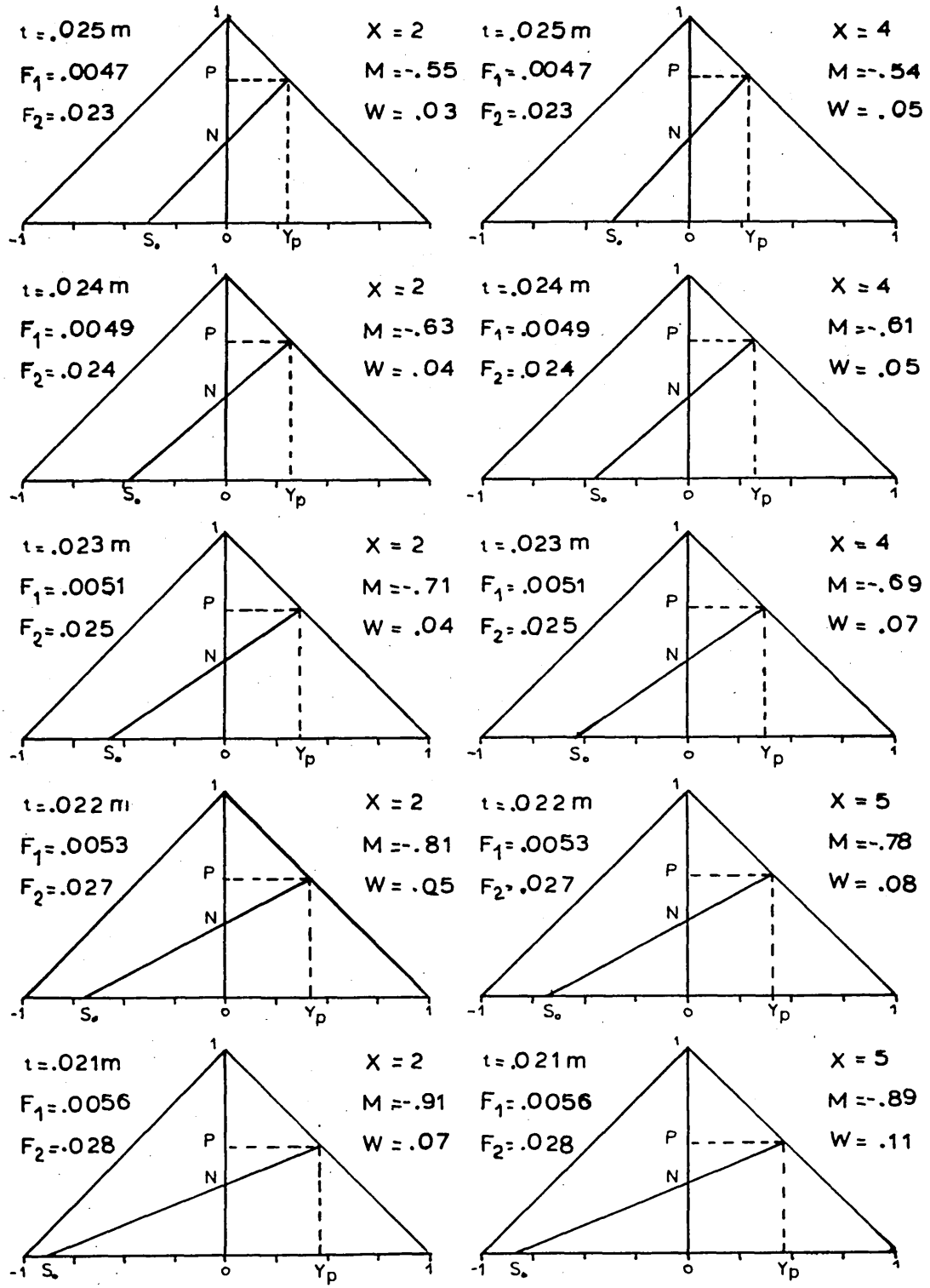


FIGURE 9 : PRELIMINARY ANALYSIS OF THE BEHAVIOUR OF THE MODEL:
 DECREASING THE THICKNESS t IN THE CASE OF SLABS.
 WITH $\Delta T = 300^\circ\text{C}$. (LONG FACE)

DATA: AL E L1 L2 A t ΔT meth QSYS EMSR
 .18E-04 .3E+11 .50 .10 2xt * 300 .6 .3E+08 .06
 'C⁻¹ N.m⁻² m m m m 'C m N.m⁻² N.m⁻²

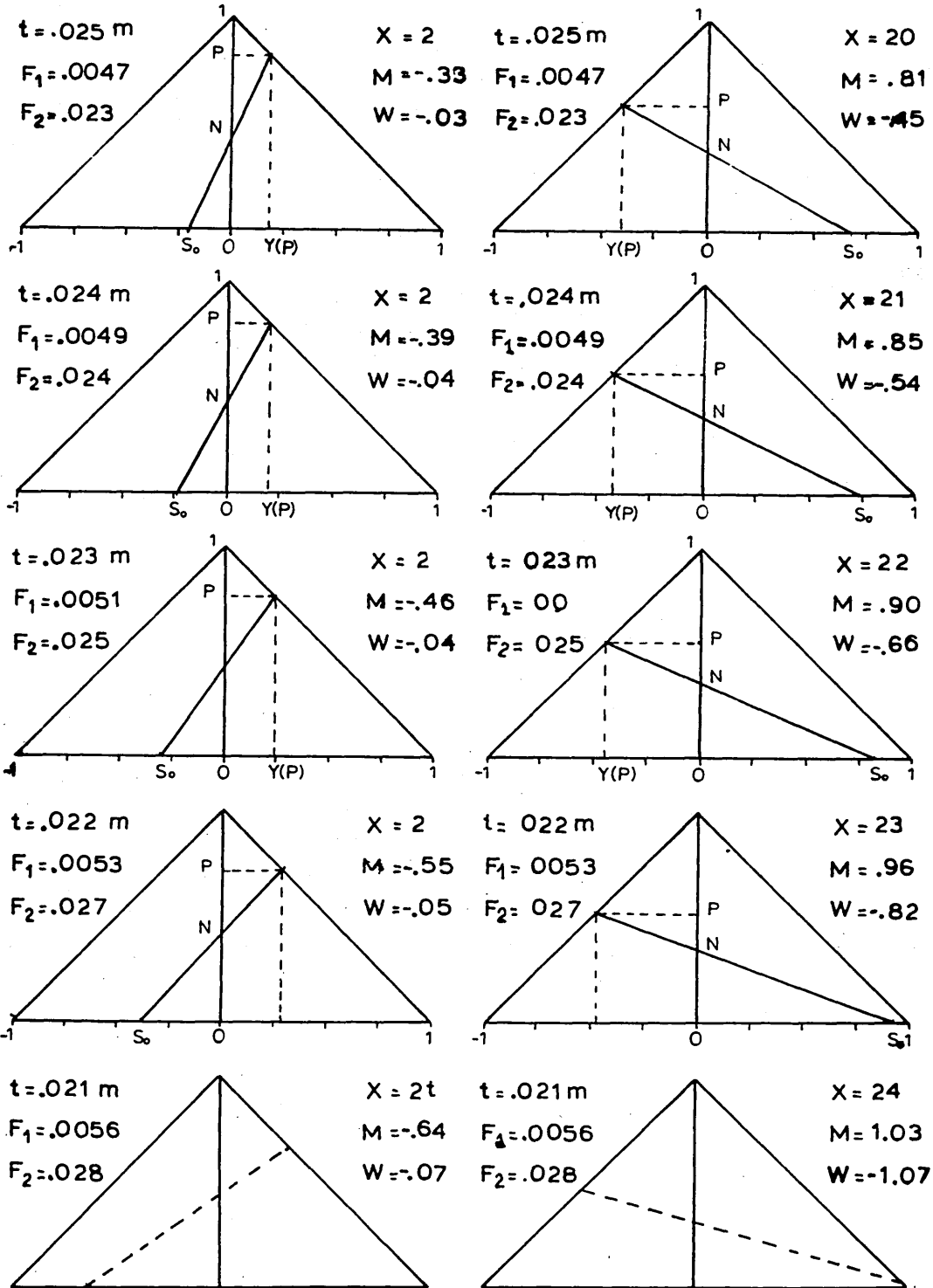


FIGURE 10 : PRELIMINARY ANALYSIS OF THE BEHAVIOUR OF THE MODEL:
 DECREASING THE YOUNG'S MODULUS IN THE CASE OF SLABS
 WITH $\Delta T = 300^{\circ}C$. (SHORT FACE)

DATA: AL E L1 L2 A t ΔT meth QSYS EMSR
 .18E-04 * .50 .10 .050 .025 300 .6 .35E+08 .06
 'C⁻¹ N.m⁻² m m m m 'C m N.m⁻² N.m⁻²

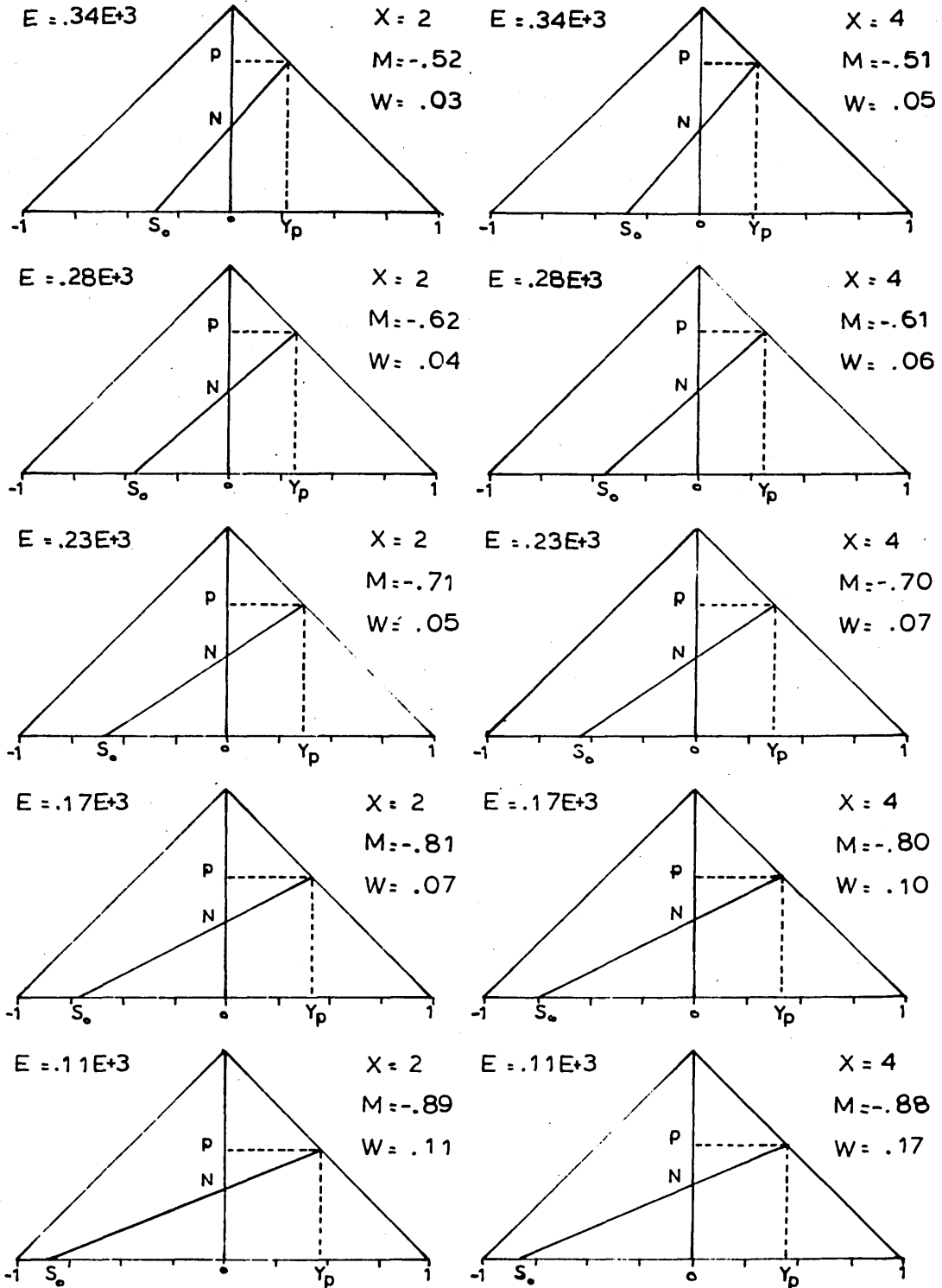
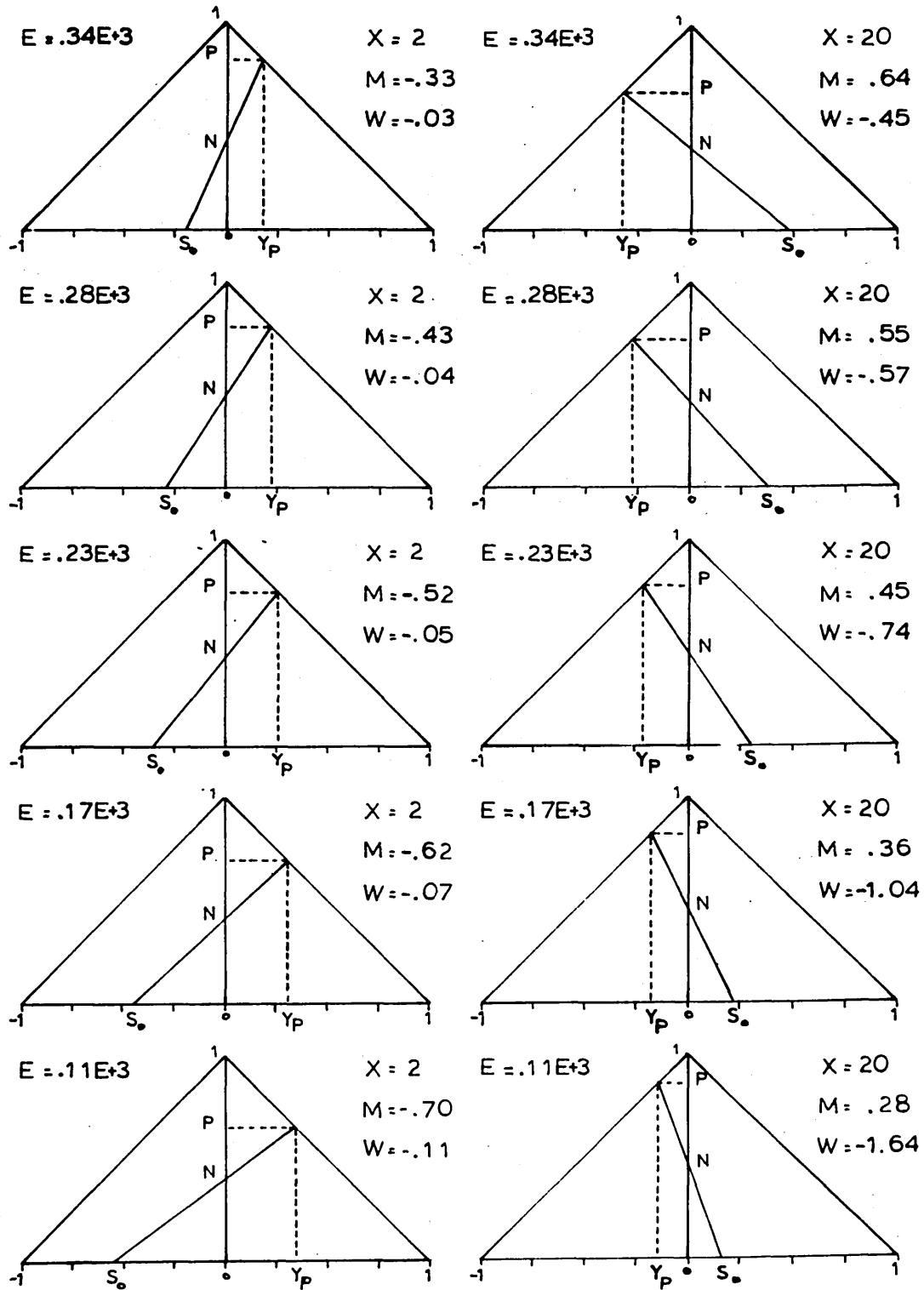


FIGURE 11 : PRELIMINARY ANALYSIS OF THE BEHAVIOUR OF THE MODEL:
 DECREASING THE YOUNG'S MODULUS IN THE CASE OF SLABS.
 WITH $\Delta T = 300^{\circ}C$. (LONG FACE)

DATA:	AL	E	L1	L2	A	t	delT	meth	QSYS	EMSR
	.18E-04	*	.50	.10	.050	.025	300	.6	.35E+08	.06
	'C ⁻¹	N.m ⁻²	m	m	m	m	'C	m	N.m ⁻²	N.m ⁻²



6.2 : SQUARE BILLETS WITHIN THE MOULD

In order to simulate the development of continuously cast structures within the mould, thicknesses of the solidifying shells and temperature differences across them were generated in the computer program of the stress model by means of two logarithmic functions of the solidification time. These functions were established on the basis of typical data found in the literature and are : (see pg 4:62)

$$\text{delt} = 96.93 \quad \text{Log}(0.6 \text{ TIME} + 1) \quad [\text{deg C}] \quad 1$$

and

$$t = 0.00977 \quad \text{Log}(0.15 \text{ TIME} + 1) \quad [\text{m}] \quad 2$$

The solidification time is calculated by the computer program from values of the casting speed, **CS** [m/sec] , and of the metallurgical height, **meth** [m] , which are provided as data to the program:

$$\text{TIME} = \text{meth} / \text{CS} \quad [\text{sec}] \quad 3$$

The length of solidified shell considered rigid in the corner region, **A**, is generated in the program by another logarithmic function established on the basis of the results reported by Krishnamurthy (60),

$$A = t (3.159 - \log(0.1 \text{ TIME} + 1)) \quad 4$$

The quasi-static yield stress at the cooled surface as a function of temperature is generated by the computer program from its value at 1000° C using the equation:-

$$\text{QSYS}(T_c) = \text{QSYS}(1000^\circ \text{C}) (T_s - T_c)/450^\circ \text{C} \quad 5$$

In the first set of results, the behaviour of square billets in a non-tapered mould was analysed for a range of casting speeds varying from 0.01 m.s^{-1} to 0.06 m.s^{-1} in steps of 0.01 m.s^{-1} and a range of metallurgical heights from 0.1 m to 0.6 m with steps of 0.1 m and for section sizes up to 0.5 m square.

The results of this analysis are summarised in figs 12, 13 and 14 on pages 6:39-41 . Each of the Tables 1 to 9 on pages 6:21-38 presents 4 sets of typical examples of the computer print-outs that were obtained, the results presented in the figures summarising the data from some 450 such print-outs.

The 6 graphs in figure 12 (page 6:39), each for a different casting speed, show the detached length of the quarter-section as a function of the total quarter-section length for different parametric values of the metallurgical height*. They demonstrate that a minimum total section length exists for each metallurgical height and casting speed below which the section is totally detached. This minimum total section length increases consistently for any given casting speed as the metallurgical height increases. It also increases consistently for any given metallurgical height as the casting speed decreases.

* NOTE: It must be remembered that the model and the computer program consider, because of double symmetry, only a quarter-section of the real section. In all the computer print-out presented and in the figures the length L referred is related to the quarter-section.

The 6 graphs in figure 12 also show that for a billet of given section cast at a given speed, the detached length always increases as the billet descends down the mould until it is completely detached. If the a billet of small section is cast at a low speed, the billet will be totally detached at an early stage. The metallurgical height at which total detachment first appears for a given section billet at a given casting speed can be extrapolated from the graphs in figure 12.

Figure 13, on page 6:40, shows how the adimensional moment at the corner of the considered section ($-M_3$) varies with the length of the corresponding quarter-section for different casting speeds and metallurgical heights. Negative values of this moment correspond to conditions of tension at the solidification front in the corner region.

Two lines exist for each set of conditions although they coincide below the minimum total quarter-section length identified above, this minimum quarter-section length being indicated by the arrow on each graph. For quarter-section lengths above this minimum, the moment experienced by the total length of section in the absence of any support is always more negative than the moment it experiences when the middle portion is in contact with the mould. Increasing the metallurgical height for any given casting speed causes the moment at the corner to become less negative, and the same trend is seen, at any given metallurgical height as the casting speed decreases.

Figure 14 (pg 6:41) shows the adimensional moment exerted on the considered section at the mid-face position [$M(L_{Section})$]. Once again, each graph shows two lines, one for the supported section and one for the unsupported section. For quarter-section lengths below the minimum total quarter-section length, these lines coincide. Trends similar to those shown by the moment at the corner can be seen in these graphs except that the moment for the supported section shows considerable less variation. In some of the graphs, however, the adimensional moment exerted by the unsupported section exceeds unity, a situation corresponding to the onset of compressive plasticity at the cooled surface.

TABLES 1 A/B: CHARACTERISTIC RESULTS

CASTING SPEED 0.01 m/sec
 METALLURGICAL HEIGHT 0.1 m

DATA: AL E L1 L2 A t delT meth QSYS EMSR
 UNITS: 'C⁻¹ N.m⁻² m m m m 'C m N.m⁻² N.m⁻²

DATA: AL E L1 L2 A t delT meth QSYS EMSR
 dim. .18E-04 .70E+10 .140 .140 .022 .009 188 .100 .272E+08 .0060
 adim. .34E-02 .16E+03 15.6 15.6 2.47 1. YS=.432E+08
 RKstep = .10000 F1 = .50E-02 Q = -.17E-03
 RKerror = .00050 F2 = .50E-02 M3 = -.2200
 ITerror = .00010

X	C	DW/DX	W	M	S0	P	YP	N
2.5	-.001	-.00	-.0*	.28	.16	.86	-.14	.472E+00
3.5	-.001	-.00	-.0*	.30	.18	.85	-.15	.467E+00
4.5	-.001	-.00	-.00	.33	.20	.84	-.16	.463E+00
5.5	-.001	-.00	-.00	.35	.21	.83	-.17	.459E+00
6.5	-.000	-.00	-.01	.37	.23	.82	-.18	.456E+00
7.5	-.000	-.00	-.01	.39	.24	.81	-.19	.453E+00
8.5	.000	-.00	-.01	.40	.25	.80	-.20	.450E+00
9.5	.000	-.00	-.02	.42	.26	.80	-.20	.448E+00
10.5	.000	-.00	-.02	.43	.27	.79	-.21	.446E+00
11.5	.000	-.00	-.02	.44	.28	.79	-.21	.444E+00
12.5	.001	-.00	-.03	.44	.29	.78	-.22	.443E+00
13.5	.001	-.00	-.03	.45	.29	.78	-.22	.442E+00
14.5	.001	-.00	-.03	.45	.29	.78	-.22	.442E+00
15.5	.001	-.00	-.03	.45	.29	.78	-.22	.441E+00
15.6	.001	-.00	-.03	.45	.29	.78	-.22	.441E+00

MINL2(W1) : .140
 SECTION LENGTH : .140
 DETACHED LENGTH : .140

DATA: AL E L1 L2 A t delT meth QSYS EMSR
 dim. .18E-04 .70E+10 .145 .145 .022 .009 188 .100 .272E+08 .0060
 adim. .34E-02 .16E+03 16.2 16.2 2.47 1. YS=.432E+08
 RKstep = .10000 F1 = .52E-02 Q = -.17E-03
 RKerror = .00050 F2 = .52E-02 M3 = -.2063
 ITerror = .00010

X	C	DW/DX	W	M	S0	P	YP	N
2.5	-.001	.00	.0*	.27	.15	.87	-.13	.474E+00
3.5	-.001	-.00	-.0*	.29	.17	.86	-.14	.469E+00
4.5	-.001	-.00	-.00	.32	.19	.84	-.16	.465E+00
5.5	-.001	-.00	-.00	.34	.21	.83	-.17	.461E+00
6.5	-.000	-.00	-.01	.36	.22	.82	-.18	.457E+00
7.5	-.000	-.00	-.01	.38	.24	.81	-.19	.454E+00
8.5	-.000	-.00	-.02	.40	.25	.81	-.19	.451E+00
9.5	.000	-.00	-.02	.41	.26	.80	-.20	.449E+00
10.5	.000	-.00	-.02	.42	.27	.79	-.21	.447E+00
11.5	.000	-.00	-.03	.43	.28	.79	-.21	.445E+00
12.5	.001	-.00	-.03	.44	.29	.78	-.22	.443E+00
13.5	.001	-.00	-.03	.45	.29	.78	-.22	.442E+00
14.5	.001	-.00	-.03	.45	.29	.78	-.22	.441E+00
15.5	.001	-.00	-.03	.46	.30	.78	-.22	.441E+00

MINL2(W1) : .163
 SECTION LENGTH : .163
 DETACHED LENGTH : .145

TABLES 1 C/D: CHARACTERISTIC RESULTS

CASTING SPEED 0.01 m/sec
 METALLURGICAL HEIGHT 0.1 m

DATA: AL E L1 L2 A t delT meth QSYS EMSR
 UNITS: 'C⁻¹ N.m⁻² m m m m 'C m N.m⁻² N.m⁻²

DATA: AL E L1 L2 A t delT meth QSYS EMSR
 dim. .18E-04 .70E+10 .150 .150 .022 .009 188 .100 .272E+08 .0060
 3dim. .34E-02 .16E+03 16.8 16.8 2.47 1. YS=.432E+08
 RKstep = .10000 F1 = .54E-02 Q = -.17E-03
 RKerror = .00050 F2 = .54E-02 M3 = -.1938
 ITerror = .00010

X	C	DW/DX	W	M	S0	F	YP	N
2.5	-.001	-.00	-.0*	.25	.15	.88	-.12	.476E+00
3.5	-.001	-.00	-.0*	.28	.17	.86	-.14	.471E+00
4.5	-.001	-.00	-.00	.31	.18	.85	-.15	.466E+00
5.5	-.001	-.00	-.01	.33	.20	.84	-.16	.462E+00
6.5	-.000	-.00	-.01	.36	.22	.83	-.17	.459E+00
7.5	-.000	-.00	-.01	.38	.23	.82	-.18	.455E+00
8.5	-.000	-.00	-.02	.39	.25	.81	-.19	.452E+00
9.5	.000	-.00	-.02	.41	.26	.80	-.20	.449E+00
10.5	.000	-.00	-.03	.42	.27	.79	-.21	.447E+00
11.5	.000	-.00	-.03	.43	.28	.79	-.21	.445E+00
12.5	.001	-.00	-.03	.44	.29	.78	-.22	.443E+00
13.5	.001	-.00	-.04	.45	.29	.78	-.22	.442E+00
14.5	.001	-.00	-.04	.46	.30	.77	-.23	.441E+00
15.5	.001	-.00	-.04	.46	.30	.77	-.23	.440E+00
16.5	.001	-.00	-.04	.46	.30	.77	-.23	.440E+00
16.7	.001	-.00	-.04	.46	.30	.77	-.23	.440E+00

MINL2(W1) : .191
 SECTION LENGTH : .191
 DETACHED LENGTH : .150

DATA: AL E L1 L2 A t delT meth QSYS EMSR
 dim. .18E-04 .70E+10 .160 .160 .022 .009 188 .100 .272E+08 .0060
 3dim. .34E-02 .16E+03 17.9 17.9 2.47 1. YS=.432E+08
 RKstep = .10000 F1 = .57E-02 Q = -.17E-03
 RKerror = .00050 F2 = .57E-02 M3 = -.1650
 ITerror = .00010

X	C	DW/DX	W	M	S0	F	YP	N
2.5	-.002	.00	.0*	.23	.13	.89	-.11	.481E+00
3.5	-.001	-.00	-.0*	.26	.15	.87	-.13	.476E+00
4.5	-.001	-.00	-.00	.29	.17	.86	-.14	.471E+00
5.5	-.001	-.00	-.01	.32	.19	.85	-.15	.466E+00
6.5	-.001	-.00	-.01	.34	.21	.83	-.17	.462E+00
7.5	-.000	-.01	-.02	.36	.22	.82	-.18	.458E+00
8.5	-.000	-.01	-.02	.38	.24	.81	-.19	.454E+00
9.5	.000	-.01	-.03	.40	.25	.80	-.20	.451E+00
10.5	.000	-.01	-.03	.42	.26	.80	-.20	.448E+00
11.5	.000	-.00	-.04	.43	.28	.79	-.21	.446E+00
12.5	.001	-.00	-.04	.44	.29	.78	-.22	.444E+00
13.5	.001	-.00	-.05	.45	.29	.78	-.22	.442E+00
14.5	.001	-.00	-.05	.46	.30	.77	-.23	.441E+00
15.5	.001	-.00	-.05	.47	.31	.77	-.23	.440E+00
16.5	.001	-.00	-.05	.47	.31	.77	-.23	.439E+00
17.5	.001	-.00	-.05	.47	.31	.77	-.23	.439E+00
17.9	.001	.00	-.05	.47	.31	.77	-.23	.439E+00

MINL2(W1) : .256
 SECTION LENGTH : .256
 DETACHED LENGTH : .160

TABLES 2 A/B: CHARACTERISTIC RESULTS

CASTING SPEED 0.01 m/sec
 METALLURGICAL HEIGHT 0.3 m

DATA: AL E L1 L2 A t delT meth QSYS EMSR
 UNITS: 'C⁻¹ N.m⁻² m m m m 'C m N.m⁻² N.m⁻²

DATA: AL E L1 L2 A t delT meth QSYS EMSR
 dim. .18E-04 .70E+10 .200 .200 .030 .017 285 .300 .412E+08 .0060
 dim. .51E-02 .11E+03 12.0 12.0 1.77 1. YS=.653E+08
 RKstep = .10000 F1 = .74E-02 Q = -.34E-03
 RKerror = .00050 F2 = .74E-02 M3 = -.1973
 ITerror = .00010

X	C	DW/DX	W	M	S0	P	YP	N
1.8	-.002	.00	.0*	.25	.15	.88	-.12	.480E+00
2.8	-.002	-.00	-.0*	.29	.17	.86	-.14	.473E+00
3.8	-.001	-.00	-.00	.33	.20	.84	-.16	.466E+00
4.8	-.001	-.00	-.01	.36	.22	.83	-.17	.461E+00
5.8	-.000	-.00	-.01	.39	.24	.81	-.19	.456E+00
6.8	.000	-.00	-.02	.41	.26	.80	-.20	.452E+00
7.8	.001	-.00	-.02	.43	.27	.79	-.21	.448E+00
8.8	.001	-.00	-.03	.44	.29	.78	-.22	.446E+00
9.8	.001	-.00	-.03	.46	.30	.78	-.22	.444E+00
10.8	.001	-.00	-.03	.46	.30	.77	-.23	.443E+00
11.8	.001	-.00	-.03	.47	.30	.77	-.23	.442E+00

MINL2(W1) : .186
 SECTION LENGTH : .200
 DETACHED LENGTH : .200

DATA: AL E L1 L2 A t delT meth QSYS EMSR
 dim. .18E-04 .70E+10 .205 .205 .030 .017 285 .300 .412E+08 .0060
 dim. .51E-02 .11E+03 12.3 12.3 1.77 1. YS=.653E+08
 RKstep = .10000 F1 = .76E-02 Q = -.34E-03
 RKerror = .00050 F2 = .76E-02 M3 = -.1871
 ITerror = .00010

X	C	DW/DX	W	M	S0	P	YP	N
1.8	-.002	.00	.0*	.24	.14	.88	-.12	.483E+00
2.8	-.002	-.00	-.00	.28	.17	.86	-.14	.475E+00
3.8	-.001	-.00	-.00	.32	.19	.84	-.16	.468E+00
4.8	-.001	-.00	-.01	.35	.22	.83	-.17	.462E+00
5.8	-.000	-.01	-.01	.38	.24	.81	-.19	.457E+00
6.8	.000	-.01	-.02	.41	.26	.80	-.20	.452E+00
7.8	.001	-.00	-.02	.43	.27	.79	-.21	.449E+00
8.8	.001	-.00	-.03	.44	.29	.78	-.22	.446E+00
9.8	.001	-.00	-.03	.46	.30	.78	-.22	.444E+00
10.8	.001	-.00	-.03	.46	.30	.77	-.23	.442E+00
11.8	.001	-.00	-.04	.47	.31	.77	-.23	.442E+00

MINL2(W1) : .209
 SECTION LENGTH : .209
 DETACHED LENGTH : .205

TABLES 2 C/D: CHARACTERISTIC RESULTS

CASTING SPEED 0.01 m/sec
 METALLURGICAL HEIGHT 0.3 m

DATA: AL E L1 L2 A t delT meth QSYS EMSR
 UNITS: 'C⁻¹ N.m⁻² m m m m 'C m N.m⁻² N.m⁻²

DATA: AL E L1 L2 A t delT meth QSYS EMSR
 dim. .18E-04 .70E+10 .215 .215 .030 .017 285 .300 .412E+08 .0060
 dim. .51E-02 .11E+03 12.9 12.9 1.77 1. YS=.653E+08
 RKstep = .10000 F1 = .80E-02 Q = -.34E-03
 RKerror = .00050 F2 = .80E-02 M3 = -.1664
 ITerror = .00010

X	C	DW/DX	W	M	S0	P	YP	N
1.8	-.003	-.00	-.0*	.23	.13	.89	-.11	.487E+00
2.8	-.002	-.00	-.00	.27	.16	.87	-.13	.478E+00
3.8	-.001	-.00	-.00	.31	.18	.85	-.15	.471E+00
4.8	-.001	-.01	-.01	.34	.21	.83	-.17	.464E+00
5.8	-.000	-.01	-.02	.37	.23	.82	-.18	.459E+00
6.8	.000	-.01	-.02	.40	.25	.80	-.20	.454E+00
7.8	.000	-.01	-.03	.42	.27	.79	-.21	.450E+00
8.8	.001	-.01	-.03	.44	.29	.78	-.22	.447E+00
9.8	.001	-.00	-.04	.46	.30	.78	-.22	.444E+00
10.8	.001	-.00	-.04	.47	.31	.77	-.23	.442E+00
11.8	.001	-.00	-.04	.48	.31	.77	-.23	.441E+00
12.8	.002	-.00	-.04	.48	.31	.77	-.23	.440E+00
12.8	.002	-.00	-.04	.48	.31	.77	-.23	.440E+00

MINL2(W1) : .258
 SECTION LENGTH : .258
 DETACHED LENGTH : .215

DATA: AL E L1 L2 A t delT meth QSYS EMSR
 dim. .18E-04 .70E+10 .240 .240 .030 .017 285 .300 .412E+08 .0060
 dim. .51E-02 .11E+03 14.4 14.4 1.77 1. YS=.653E+08
 RKstep = .10000 F1 = .91E-02 Q = -.34E-03
 RKerror = .00050 F2 = .91E-02 M3 = -.1073
 ITerror = .00010

X	C	DW/DX	W	M	S0	P	YP	N
1.8	-.003	-.00	-.0*	.18	.10	.92	-.08	.502E+00
2.8	-.003	-.00	-.00	.22	.13	.89	-.11	.490E+00
3.8	-.002	-.01	-.01	.27	.16	.87	-.13	.480E+00
4.8	-.001	-.01	-.01	.31	.19	.85	-.15	.472E+00
5.8	-.001	-.01	-.02	.35	.21	.83	-.17	.465E+00
6.8	-.000	-.01	-.03	.38	.24	.82	-.18	.459E+00
7.8	.000	-.01	-.04	.41	.26	.80	-.20	.454E+00
8.8	.001	-.01	-.05	.43	.28	.79	-.21	.449E+00
9.8	.001	-.01	-.05	.46	.30	.78	-.22	.446E+00
10.8	.001	-.01	-.06	.47	.31	.77	-.23	.443E+00
11.8	.002	-.00	-.07	.48	.32	.76	-.24	.440E+00
12.8	.002	-.00	-.07	.49	.33	.76	-.24	.439E+00
13.8	.002	-.00	-.07	.50	.33	.76	-.24	.438E+00

MINL2(W1) : .425
 SECTION LENGTH : .425
 DETACHED LENGTH : .240

TABLES 3 A/B: CHARACTERISTIC RESULTS

CASTING SPEED 0.01 m/sec
 METALLURGICAL HEIGHT 0.6 m

DATA: AL E L1 L2 A t delT meth QSYS EMSR
 UNITS: 'C⁻¹ N.m⁻² m m m m 'C m N.m⁻² N.m⁻²

DATA: AL E L1 L2 A t delT meth QSYS EMSR
 dim. .18E-04 .70E+10 .200 .200 .027 .022 350 .600 .506E+08 .0060
 edim. .63E-02 .87E+02 8.9 8.9 1.21 1. YS=.801E+08
 RKstep = .10000 F1 = .87E-02 Q = -.55E-03
 RKerror = .00050 F2 = .87E-02 M3 = -.2297
 ITerror = .00010

X	C	DW/DX	W	M	S0	F	YP	N
1.2	-.003	-.00	-.0*	.27	.16	.87	-.13	.480E+00
2.2	-.002	-.00	-.00	.31	.19	.85	-.15	.471E+00
3.2	-.001	-.00	-.00	.35	.22	.83	-.17	.463E+00
4.2	-.000	-.00	-.01	.39	.24	.81	-.19	.457E+00
5.2	.000	-.00	-.01	.42	.26	.80	-.20	.452E+00
6.2	.001	-.00	-.02	.44	.28	.79	-.21	.448E+00
7.2	.001	-.00	-.02	.45	.29	.78	-.22	.446E+00
8.2	.001	-.00	-.02	.46	.30	.78	-.22	.444E+00
8.8	.001	.00	-.02	.46	.30	.78	-.22	.444E+00

MINL2(W1) : .129
 SECTION LENGTH : .200
 DETACHED LENGTH : .200

DATA: AL E L1 L2 A t delT meth QSYS EMSR
 dim. .18E-04 .70E+10 .225 .225 .027 .022 350 .600 .506E+08 .0060
 edim. .63E-02 .87E+02 10.0 10.0 1.21 1. YS=.801E+08
 RKstep = .10000 F1 = .99E-02 Q = -.55E-03
 RKerror = .00050 F2 = .99E-02 M3 = -.1819
 ITerror = .00010

X	C	DW/DX	W	M	S0	F	YP	N
1.2	-.003	.00	.0*	.22	.13	.89	-.11	.492E+00
2.2	-.002	-.00	-.00	.28	.17	.87	-.13	.480E+00
3.2	-.001	-.00	-.01	.33	.20	.84	-.16	.470E+00
4.2	-.001	-.01	-.01	.37	.23	.82	-.18	.462E+00
5.2	.000	-.01	-.02	.40	.25	.81	-.19	.456E+00
6.2	.001	-.01	-.02	.43	.28	.79	-.21	.451E+00
7.2	.001	-.00	-.03	.45	.29	.78	-.22	.447E+00
8.2	.002	-.00	-.03	.47	.31	.77	-.23	.444E+00
9.2	.002	-.00	-.03	.48	.31	.77	-.23	.442E+00

MINL2(W1) : .221
 SECTION LENGTH : .225
 DETACHED LENGTH : .225

TABLES 3 C/D: CHARACTERISTIC RESULTS

CASTING SPEED 0.01 m/sec
 METALLURGICAL HEIGHT 0.6 m

DATA: AL E L1 L2 A t delT meth QSYS EMSR
 UNITS: 'C⁻¹ N.m⁻² m m m m 'C m N.m⁻² N.m⁻²

DATA: AL E L1 L2 A t delT meth QSYS EMSR
 dim. .18E-04 .70E+10 .230 .230 .027 .022 350 .600 .506E+08 .0060
 edim. .63E-02 .87E+02 10.2 10.2 1.21 1. YS=.801E+08
 RKstep = .10000 F1 = .10E-01 Q = -.55E-03
 RKerror = .00050 F2 = .10E-01 M3 = -.1720
 ITerror = .00010

X	C	DW/DX	W	M	S0	P	YP	N
1.2	-.003	-.00	-.0*	.22	.12	.90	-.10	.495E+00
2.2	-.003	-.00	-.00	.27	.16	.87	-.13	.482E+00
3.2	-.002	-.01	-.01	.32	.19	.85	-.15	.472E+00
4.2	-.001	-.01	-.01	.36	.22	.82	-.18	.463E+00
5.2	.000	-.01	-.02	.40	.25	.81	-.19	.457E+00
6.2	.001	-.01	-.02	.43	.28	.79	-.21	.451E+00
7.2	.001	-.01	-.03	.45	.29	.78	-.22	.447E+00
8.2	.002	-.00	-.03	.47	.31	.77	-.23	.444E+00
9.2	.002	-.00	-.04	.48	.32	.77	-.23	.442E+00
10.2	.002	-.00	-.04	.48	.32	.77	-.23	.442E+00
10.2	.002	-.00	-.04	.48	.32	.77	-.23	.442E+00

MINL2(W1) : .245
 SECTION LENGTH : .245
 DETACHED LENGTH : .230

DATA: AL E L1 L2 A t delT meth QSYS EMSR
 dim. .18E-04 .70E+10 .240 .240 .027 .022 350 .600 .506E+08 .0060
 edim. .63E-02 .87E+02 10.7 10.7 1.21 1. YS=.801E+08
 RKstep = .10000 F1 = .11E-01 Q = -.55E-03
 RKerror = .00050 F2 = .11E-01 M3 = -.1516
 ITerror = .00010

X	C	DW/DX	W	M	S0	P	YP	N
1.2	-.004	-.00	-.0*	.20	.11	.91	-.09	.500E+00
2.2	-.003	-.00	-.00	.26	.15	.88	-.12	.486E+00
3.2	-.002	-.01	-.01	.31	.19	.85	-.15	.475E+00
4.2	-.001	-.01	-.01	.35	.22	.83	-.17	.466E+00
5.2	-.000	-.01	-.02	.39	.25	.81	-.19	.459E+00
6.2	.001	-.01	-.03	.43	.27	.79	-.21	.452E+00
7.2	.001	-.01	-.03	.45	.29	.78	-.22	.448E+00
8.2	.002	-.00	-.04	.47	.31	.77	-.23	.444E+00
9.2	.002	-.00	-.04	.49	.32	.77	-.23	.442E+00
10.2	.002	-.00	-.05	.49	.33	.76	-.24	.441E+00
10.6	.002	-.00	-.05	.49	.33	.76	-.24	.440E+00

MINL2(W1) : .293
 SECTION LENGTH : .293
 DETACHED LENGTH : .240

TABLES 4 A/B: CHARACTERISTIC RESULTS

CASTING SPEED 0.03 m/sec
 METALLURGICAL HEIGHT 0.1 m

DATA: AL E L1 L2 A t delT meth QSYS EMSR
 UNITS: 'C⁻¹ N.m⁻² m m m m 'C m N.m⁻² N.m⁻²

DATA: AL E L1 L2 A t delT meth QSYS EMSR
 dim. .18E-04 .70E+10 .050 .050 .011 .004 106 .100 .154E+08 .0060
 sdim. .19E-02 .29E+03 12.6 12.6 2.87 1. YS=.244E+08
 RKstep = .10000 F1 = .70E-02 Q = -.30E-03
 RKerror = .00050 F2 = .70E-02 M3 = -.1872
 ITerror = .00010

X	C	DW/DX	W	M	S0	P	YP	N
2.9	-.001	.00	.0*	.28	.17	.86	-.14	.474E+00
3.9	-.001	-.00	-.0*	.31	.19	.85	-.15	.468E+00
4.9	-.000	-.00	-.00	.34	.21	.83	-.17	.463E+00
5.9	-.000	-.00	-.00	.37	.23	.82	-.18	.458E+00
6.9	-.000	-.00	-.00	.39	.25	.81	-.19	.454E+00
7.9	.000	-.00	-.01	.41	.26	.80	-.20	.451E+00
8.9	.000	-.00	-.01	.43	.27	.79	-.21	.448E+00
9.9	.000	-.0*	-.01	.44	.28	.79	-.21	.446E+00
10.9	.000	-.0*	-.01	.45	.29	.78	-.22	.445E+00
11.9	.000	-.0*	-.01	.45	.29	.78	-.22	.444E+00

MINL2(W1) : .033
 SECTION LENGTH : .050
 DETACHED LENGTH : .050

DATA: AL E L1 L2 A t delT meth QSYS EMSR
 dim. .18E-04 .70E+10 .060 .060 .011 .004 106 .100 .154E+08 .0060
 sdim. .19E-02 .29E+03 15.1 15.1 2.87 1. YS=.244E+08
 RKstep = .10000 F1 = .85E-02 Q = -.30E-03
 RKerror = .00050 F2 = .85E-02 M3 = -.0957
 ITerror = .00010

X	C	DW/DX	W	M	S0	P	YP	N
2.9	-.001	.00	.0*	.21	.12	.90	-.10	.492E+00
3.9	-.001	-.00	-.0*	.25	.15	.88	-.12	.483E+00
4.9	-.001	-.00	-.00	.29	.17	.86	-.14	.475E+00
5.9	-.000	-.00	-.00	.33	.20	.84	-.16	.468E+00
6.9	-.000	-.00	-.01	.36	.22	.83	-.17	.462E+00
7.9	-.000	-.00	-.01	.39	.24	.81	-.19	.457E+00
8.9	.000	-.00	-.01	.41	.26	.80	-.20	.453E+00
9.9	.000	-.00	-.01	.43	.28	.79	-.21	.449E+00
10.9	.000	-.00	-.02	.45	.29	.78	-.22	.446E+00
11.9	.000	-.00	-.02	.46	.30	.77	-.23	.443E+00
12.9	.001	-.00	-.02	.47	.31	.77	-.23	.442E+00
13.9	.001	-.00	-.02	.48	.32	.77	-.23	.440E+00
14.9	.001	-.00	-.02	.48	.32	.76	-.24	.440E+00

MINL2(W1) : .080
 SECTION LENGTH : .080
 DETACHED LENGTH : .060

TABLES 4 C/D: CHARACTERISTIC RESULTS

CASTING SPEED 0.03 m/sec
 METALLURGICAL HEIGHT 0.1 m

DATA: AL E L1 L2 A t delT meth QSYS EMSR
 UNITS: 'C⁻¹ N.m⁻² m m m m 'C m N.m⁻² N.m⁻²

DATA: AL E L1 L2 A t delT meth QSYS EMSR
 dim. .18E-04 .70E+10 .070 .070 .011 .004 106 .100 .154E+08 .0060
 dim. .19E-02 .29E+03 17.7 17.7 2.87 1. YS=.244E+08
 RKstep = .10000 F1 = .10E-01 Q = -.30E-03
 RKerror = .00050 F2 = .10E-01 M3 = .0139
 IError = .00010

X	C	DW/DX	W	M	S0	P	YP	N
2.9	-.001	.00	.0*	.12	.07	.94	-.06	.524E+00
3.9	-.001	-.00	-.0*	.17	.10	.92	-.08	.505E+00
4.9	-.001	-.00	-.00	.22	.13	.89	-.11	.492E+00
5.9	-.001	-.00	-.01	.27	.16	.87	-.13	.482E+00
6.9	-.001	-.00	-.01	.31	.18	.85	-.15	.474E+00
7.9	-.000	-.00	-.01	.35	.21	.83	-.17	.467E+00
8.9	-.000	-.00	-.02	.38	.24	.82	-.18	.461E+00
9.9	.000	-.00	-.02	.41	.26	.80	-.20	.455E+00
10.9	.000	-.00	-.03	.44	.28	.79	-.21	.450E+00
11.9	.000	-.00	-.03	.46	.30	.78	-.22	.446E+00
12.9	.001	-.00	-.04	.48	.31	.77	-.23	.443E+00
13.9	.001	-.00	-.04	.49	.33	.76	-.24	.440E+00
14.9	.001	-.00	-.04	.51	.34	.75	-.25	.438E+00
15.9	.001	-.00	-.04	.51	.35	.75	-.25	.436E+00
16.9	.001	-.00	-.04	.52	.35	.75	-.25	.435E+00

MINL2(W1) : .165
 SECTION LENGTH : .165
 DETACHED LENGTH : .070

DATA: AL E L1 L2 A t delT meth QSYS EMSR
 dim. .18E-04 .70E+10 .080 .080 .011 .004 106 .100 .154E+08 .0060
 dim. .19E-02 .29E+03 20.2 20.2 2.87 1. YS=.244E+08
 RKstep = .10000 F1 = .12E-01 Q = -.30E-03
 RKerror = .00050 F2 = .12E-01 M3 = .1421
 IError = .00010

X	C	DW/DX	W	M	S0	P	YP	N
2.9	-.002	.00	.0*	.02	.01	1.00	-.00	.854E+00
3.9	-.002	-.00	-.0*	.08	.05	.97	-.03	.565E+00
4.9	-.001	-.00	-.00	.13	.08	.94	-.06	.525E+00
5.9	-.001	-.00	-.01	.19	.11	.91	-.09	.505E+00
6.9	-.001	-.01	-.01	.24	.14	.89	-.11	.492E+00
7.9	-.001	-.01	-.02	.28	.17	.87	-.13	.481E+00
8.9	-.000	-.01	-.03	.33	.20	.84	-.16	.473E+00
9.9	-.000	-.01	-.03	.37	.23	.82	-.18	.465E+00
10.9	.000	-.01	-.04	.40	.25	.81	-.19	.458E+00
11.9	.000	-.01	-.05	.43	.28	.79	-.21	.452E+00
12.9	.000	-.01	-.05	.46	.30	.78	-.22	.447E+00
13.9	.001	-.01	-.06	.49	.32	.76	-.24	.442E+00
14.9	.001	-.01	-.07	.51	.34	.75	-.25	.439E+00
15.9	.001	-.00	-.07	.53	.36	.75	-.25	.435E+00
16.9	.001	-.00	-.08	.54	.37	.74	-.26	.433E+00
17.9	.001	-.00	-.08	.55	.38	.73	-.27	.431E+00
18.9	.001	-.00	-.08	.56	.38	.73	-.27	.430E+00
19.9	.001	-.00	-.08	.56	.39	.73	-.27	.429E+00

MINL2(W1) : .302
 SECTION LENGTH : .302
 DETACHED LENGTH : .080

TABLES 5 A/B: CHARACTERISTIC RESULTS

CASTING SPEED 0.03 m/sec
 METALLURGICAL HEIGHT 0.3 m

DATA: AL E L1 L2 A t delT meth QSYS EMSR
 UNITS: 'C⁻¹ N.m⁻² m m m m 'C m N.m⁻² N.m⁻²

DATA: AL E L1 L2 A t delT meth QSYS EMSR
 dim. .18E-04 .70E+10 .090 .090 .022 .009 188 .300 .272E+08 .0060
 sdim. .34E-02 .16E+03 10.1 10.1 2.47 1. YS=.432E+08
 RKstep = .10000 F1 = .93E-02 Q = -.51E-03
 RKerror = .00050 F2 = .93E-02 M3 = -.1763
 ITerror = .00010

X	C	DW/DX	W	M	S0	P	YP	N
2.5	-.001	.00	.0*	.28	.16	.87	-.13	.479E+00
3.5	-.001	-.00	-.0*	.32	.19	.84	-.16	.470E+00
4.5	-.000	-.00	-.00	.36	.22	.83	-.17	.463E+00
5.5	-.000	-.00	-.00	.39	.24	.81	-.19	.457E+00
6.5	.000	-.00	-.01	.42	.26	.80	-.20	.453E+00
7.5	.000	-.00	-.01	.43	.28	.79	-.21	.449E+00
8.5	.001	-.00	-.01	.45	.29	.78	-.22	.447E+00
9.5	.001	-.00	-.01	.45	.29	.78	-.22	.446E+00

MINL2(W1) : .046
 SECTION LENGTH : .090
 DETACHED LENGTH : .090

DATA: AL E L1 L2 A t delT meth QSYS EMSR
 dim. .18E-04 .70E+10 .105 .105 .022 .009 188 .300 .272E+08 .0060
 sdim. .34E-02 .16E+03 11.7 11.7 2.47 1. YS=.432E+08
 RKstep = .10000 F1 = .11E-01 Q = -.51E-03
 RKerror = .00050 F2 = .11E-01 M3 = -.0975
 ITerror = .00010

X	C	DW/DX	W	M	S0	P	YP	N
2.5	-.002	-.00	-.0*	.22	.13	.90	-.10	.495E+00
3.5	-.001	-.00	-.0*	.27	.16	.87	-.13	.483E+00
4.5	-.001	-.00	-.00	.32	.19	.85	-.15	.473E+00
5.5	-.000	-.00	-.01	.36	.22	.83	-.17	.465E+00
6.5	-.000	-.00	-.01	.40	.25	.81	-.19	.458E+00
7.5	.000	-.00	-.01	.43	.27	.79	-.21	.453E+00
8.5	.001	-.00	-.02	.45	.29	.78	-.22	.448E+00
9.5	.001	-.00	-.02	.47	.31	.77	-.23	.445E+00
10.5	.001	-.00	-.02	.48	.31	.77	-.23	.443E+00
11.5	.001	-.00	-.02	.48	.32	.77	-.23	.443E+00
11.7	.001	-.00	-.02	.48	.32	.77	-.23	.442E+00

MINL2(W1) : .101
 SECTION LENGTH : .105
 DETACHED LENGTH : .105

TABLES 5 C/D: CHARACTERISTIC RESULTS

CASTING SPEED 0.03 m/sec
 METALLURGICAL HEIGHT 0.3 m

DATA: AL E L1 L2 A t delT meth QSYS EMSR
 UNITS: 'C⁻¹ N.m⁻² m m m m 'C m N.m⁻² N.m⁻²

DATA: AL E L1 L2 A t delT meth QSYS EMSR
 dim. .18E-04 .70E+10 .110 .110 .022 .009 188 .300 .272E+08 .0060
 adim. .34E-02 .16E+03 12.3 12.3 2.47 1. YS=.432E+08
 RKstep = .10000 F1 = .12E-01 Q = -.51E-03
 RKerror = .00050 F2 = .12E-01 M3 = -.0675
 ITerror = .00010

X	C	DW/DX	W	M	S0	P	YP	N
2.5	-.002	-.00	-.0*	.20	.11	.91	-.09	.503E+00
3.5	-.002	-.00	-.00	.25	.15	.88	-.12	.488E+00
4.5	-.001	-.00	-.00	.31	.18	.85	-.15	.477E+00
5.5	-.001	-.00	-.01	.35	.21	.83	-.17	.468E+00
6.5	-.000	-.00	-.01	.39	.24	.81	-.19	.461E+00
7.5	.000	-.00	-.02	.42	.27	.80	-.20	.454E+00
8.5	.001	-.00	-.02	.45	.29	.78	-.22	.450E+00
9.5	.001	-.00	-.02	.47	.31	.77	-.23	.446E+00
10.5	.001	-.00	-.03	.48	.32	.77	-.23	.443E+00
11.5	.001	-.00	-.03	.49	.33	.76	-.24	.442E+00
12.3	.001	-.00	-.03	.49	.33	.76	-.24	.441E+00

MINL2(W1) : .129
 SECTION LENGTH : .129
 DETACHED LENGTH : .110

DATA: AL E L1 L2 A t delT meth QSYS EMSR
 dim. .18E-04 .70E+10 .125 .125 .022 .009 188 .300 .272E+08 .0060
 adim. .34E-02 .16E+03 14.0 14.0 2.47 1. YS=.432E+08
 RKstep = .10000 F1 = .13E-01 Q = -.51E-03
 RKerror = .00050 F2 = .13E-01 M3 = .0303
 ITerror = .00010

X	C	DW/DX	W	M	S0	P	YP	N
2.5	-.003	.00	.0*	.12	.07	.95	-.05	.540E+00
3.5	-.002	-.00	-.00	.19	.11	.91	-.09	.510E+00
4.5	-.002	-.00	-.00	.25	.15	.88	-.12	.493E+00
5.5	-.001	-.01	-.01	.30	.18	.86	-.14	.480E+00
6.5	-.001	-.01	-.02	.35	.22	.83	-.17	.470E+00
7.5	-.000	-.01	-.02	.40	.25	.81	-.19	.462E+00
8.5	.000	-.01	-.03	.43	.28	.79	-.21	.455E+00
9.5	.001	-.01	-.03	.46	.30	.78	-.22	.449E+00
10.5	.001	-.00	-.04	.49	.32	.77	-.23	.444E+00
11.5	.001	-.00	-.04	.51	.34	.76	-.24	.441E+00
12.5	.002	-.00	-.05	.52	.35	.75	-.25	.438E+00
13.5	.002	-.00	-.05	.52	.35	.75	-.25	.437E+00
13.9	.002	-.00	-.05	.52	.36	.75	-.25	.437E+00

MINL2(W1) : .230
 SECTION LENGTH : .230
 DETACHED LENGTH : .125

TABLES 6 A/B: CHARACTERISTIC RESULTS

CASTING SPEED 0.03 m/sec
 METALLURGICAL HEIGHT 0.6 m

DATA: AL E L1 L2 A t delT meth QSYS EMSR
 UNITS: 'C⁻¹ N.m⁻² m m m m 'C m N.m⁻² N.m⁻²

DATA: AL E L1 L2 A t delT meth QSYS EMSR
 dim. .18E-04 .70E+10 .100 .100 .028 .014 248 .600 .359E+08 .0060
 adim. .45E-02 .12E+03 7.4 7.4 2.06 1. YS=.569E+08
 RKstep = .10000 F1 = .99E-02 Q = -.78E-03
 RKerror = .00050 F2 = .99E-02 M3 = -.2234
 ITerror = .00010

X	C	DW/DX	W	M	S0	P	YP	N
2.1	-.001	.00	.0*	.31	.19	.85	-.15	.473E+00
3.1	-.001	-.00	-.0*	.36	.22	.83	-.17	.465E+00
4.1	-.000	-.00	-.00	.39	.24	.81	-.19	.458E+00
5.1	.000	-.00	-.00	.42	.27	.80	-.20	.453E+00
6.1	.001	-.00	-.00	.43	.28	.79	-.21	.450E+00
7.1	.001	-.00	-.00	.44	.28	.79	-.21	.449E+00
7.3	.001	.00	-.00	.44	.29	.79	-.21	.449E+00

MINL2(W1) : .025
 SECTION LENGTH : .100
 DETACHED LENGTH : .100

DATA: AL E L1 L2 A t delT meth QSYS EMSR
 dim. .18E-04 .70E+10 .135 .135 .028 .014 248 .600 .359E+08 .0060
 adim. .45E-02 .12E+03 10.0 10.0 2.06 1. YS=.569E+08
 RKstep = .10000 F1 = .14E-01 Q = -.78E-03
 RKerror = .00050 F2 = .14E-01 M3 = -.0773
 ITerror = .00010

X	C	DW/DX	W	M	S0	P	YP	N
2.1	-.003	-.00	-.0*	.20	.12	.91	-.09	.507E+00
3.1	-.002	-.00	-.00	.27	.16	.87	-.13	.489E+00
4.1	-.001	-.00	-.00	.33	.20	.84	-.16	.475E+00
5.1	-.000	-.00	-.01	.38	.24	.82	-.18	.465E+00
6.1	.000	-.00	-.01	.42	.27	.80	-.20	.457E+00
7.1	.001	-.00	-.02	.45	.29	.78	-.22	.451E+00
8.1	.001	-.00	-.02	.48	.31	.77	-.23	.447E+00
9.1	.001	-.00	-.02	.49	.32	.77	-.23	.444E+00
9.9	.002	-.00	-.02	.49	.33	.76	-.24	.444E+00

MINL2(W1) : .122
 SECTION LENGTH : .135
 DETACHED LENGTH : .135

TABLES 6 C/D: CHARACTERISTIC RESULTS

CASTING SPEED 0.03 m/sec
 METALLURGICAL HEIGHT 0.6 m

DATA: AL E L1 L2 A t delT meth QSYS EMSR
 UNITS: 'C⁻¹ N.m⁻² m m m m 'C m N.m⁻² N.m⁻²

DATA: AL E L1 L2 A t delT meth QSYS EMSR
 dim. .18E-04 .70E+10 .140 .140 .028 .014 248 .600 .359E+08 .0060
 3dim. .45E-02 .12E+03 10.3 10.3 2.06 1. YS=.569E+08
 RKstep = .10000 F1 = .14E-01 Q = -.78E-03
 RKerror = .00050 F2 = .14E-01 M3 = -.0530
 ITerror = .00010

X	C	DW/DX	W	M	S0	P	YP	N
2.1	-.003	-.00	-.0*	.18	.11	.92	-.08	.515E+00
3.1	-.002	-.00	-.00	.26	.15	.88	-.12	.494E+00
4.1	-.001	-.00	-.00	.32	.19	.85	-.15	.479E+00
5.1	-.000	-.00	-.01	.37	.23	.82	-.18	.468E+00
6.1	.000	-.00	-.01	.42	.27	.80	-.20	.459E+00
7.1	.001	-.00	-.02	.45	.29	.78	-.22	.452E+00
8.1	.001	-.00	-.02	.48	.31	.77	-.23	.447E+00
9.1	.002	-.00	-.03	.49	.33	.76	-.24	.444E+00
10.1	.002	-.00	-.03	.50	.33	.76	-.24	.443E+00
10.3	.002	-.00	-.03	.50	.34	.76	-.24	.443E+00

MINL2(W1) : .145
 SECTION LENGTH : .145
 DETACHED LENGTH : .140

DATA: AL E L1 L2 A t delT meth QSYS EMSR
 dim. .18E-04 .70E+10 .160 .160 .028 .014 248 .600 .359E+08 .0060
 3dim. .45E-02 .12E+03 11.8 11.8 2.06 1. YS=.569E+08
 RKstep = .10000 F1 = .17E-01 Q = -.78E-03
 RKerror = .00050 F2 = .17E-01 M3 = .0567
 ITerror = .00010

X	C	DW/DX	W	M	S0	P	YP	N
2.1	-.004	-.00	-.0*	.10	.06	.96	-.04	.576E+00
3.1	-.003	-.00	-.00	.18	.11	.92	-.08	.522E+00
4.1	-.002	-.01	-.01	.26	.15	.88	-.12	.497E+00
5.1	-.001	-.01	-.01	.33	.20	.85	-.15	.481E+00
6.1	-.000	-.01	-.02	.38	.24	.82	-.18	.468E+00
7.1	.000	-.01	-.03	.43	.28	.80	-.20	.458E+00
8.1	.001	-.01	-.04	.47	.31	.78	-.22	.451E+00
9.1	.002	-.01	-.04	.50	.34	.76	-.24	.445E+00
10.1	.002	-.00	-.05	.52	.35	.75	-.25	.441E+00
11.1	.002	-.00	-.05	.53	.36	.75	-.25	.439E+00
11.7	.002	-.00	-.05	.54	.37	.74	-.26	.438E+00

MINL2(W1) : .270
 SECTION LENGTH : .270
 DETACHED LENGTH : .160

TABLES 7 A/B: CHARACTERISTIC RESULTS

CASTING SPEED 0.06 m/sec
 METALLURGICAL HEIGHT 0.1 m

DATA: AL E L1 L2 A t delT meth QSYS EMSR
 UNITS: 'C⁻¹ N.m⁻² m m m m 'C m N.m⁻² N.m⁻²

DATA: AL E L1 L2 A t delT meth QSYS EMSR
 dim. .18E-04 .70E+10 .025 .025 .007 .002 67 .100 .970E+07 .0060
 adim. .12E-02 .46E+03 11.5 11.5 3.00 1. YS=.154E+08
 RKstep = .10000 F1 = .10E-01 Q = -.48E-03
 RKerror = .00050 F2 = .10E-01 M3 = -.1200
 ITerror = .00010

X	C	DW/DX	H	M	S0	P	YP	N
3.0	-.001	.00	.0*	.26	.15	.88	-.12	.484E+00
4.0	-.000	-.0*	-.0*	.30	.18	.85	-.15	.475E+00
5.0	-.000	-.0*	-.0*	.34	.21	.83	-.17	.467E+00
6.0	-.000	-.0*	-.00	.38	.24	.82	-.18	.461E+00
7.0	.000	-.0*	-.00	.41	.26	.80	-.20	.455E+00
8.0	.000	-.0*	-.00	.43	.28	.79	-.21	.451E+00
9.0	.000	-.0*	-.00	.45	.29	.78	-.22	.448E+00
10.0	.000	-.0*	-.00	.46	.30	.78	-.22	.446E+00
11.0	.000	-.0*	-.00	.46	.30	.78	-.22	.445E+00
11.4	.000	.0*	-.00	.46	.30	.78	-.22	.445E+00

MINL2(W1) : .015
 SECTION LENGTH : .025
 DETACHED LENGTH : .025

DATA: AL E L1 L2 A t delT meth QSYS EMSR
 dim. .18E-04 .70E+10 .030 .030 .007 .002 67 .100 .970E+07 .0060
 adim. .12E-02 .46E+03 13.8 13.8 3.00 1. YS=.154E+08
 RKstep = .10000 F1 = .12E-01 Q = -.48E-03
 RKerror = .00050 F2 = .12E-01 M3 = -.0002
 ITerror = .00010

X	C	DW/DX	H	M	S0	P	YP	N
3.0	-.001	-.00	-.0*	.17	.10	.92	-.08	.512E+00
4.0	-.001	-.00	-.0*	.23	.13	.89	-.11	.495E+00
5.0	-.000	-.00	-.00	.28	.17	.87	-.13	.483E+00
6.0	-.000	-.00	-.00	.33	.20	.84	-.16	.473E+00
7.0	-.000	-.00	-.00	.37	.23	.82	-.18	.465E+00
8.0	.000	-.00	-.01	.41	.26	.80	-.20	.458E+00
9.0	.000	-.00	-.01	.44	.28	.79	-.21	.452E+00
10.0	.000	-.00	-.01	.46	.30	.78	-.22	.447E+00
11.0	.000	-.00	-.01	.48	.32	.77	-.23	.444E+00
12.0	.000	-.0*	-.01	.50	.33	.76	-.24	.442E+00
13.0	.000	-.0*	-.01	.50	.34	.76	-.24	.440E+00
13.7	.000	-.0*	-.01	.50	.34	.76	-.24	.440E+00

MINL2(W1) : .041
 SECTION LENGTH : .041
 DETACHED LENGTH : .030

TABLES 7 C/D: CHARACTERISTIC RESULTS

CASTING SPEED 0.06 m/sec
 METALLURGICAL HEIGHT 0.1 m

DATA: AL E L1 L2 A t delT meth QSYS EMSR
 UNITS: 'C⁻¹ N.m⁻² m m m m 'C m N.m⁻² N.m⁻²

DATA: AL E L1 L2 A t delT meth QSYS EMSR
 dim. .18E-04 .70E+10 .040 .040 .007 .002 67 .100 .970E+07 .0060
 #dim. .12E-02 .46E+03 18.3 18.3 3.00 1. YS=.154E+08
 FKstep = .10000 F1 = .17E-01 Q = -.48E-03
 RKerror = .00050 F2 = .17E-01 M3 = .3172
 ITerror = .00010

X	C	DW/DX	W	M	S0	P	YF	N
3.0	-.001	.00	.0*	-.08	-.03	.95	.05	.390E+00
4.0	-.001	-.00	-.0*	.01	.01	.99	.01	.196E+01
5.0	-.001	-.00	-.00	.09	.05	.97	-.03	.586E+00
6.0	-.001	-.00	-.01	.16	.09	.93	-.07	.531E+00
7.0	-.001	-.00	-.01	.23	.13	.90	-.10	.506E+00
8.0	-.000	-.00	-.01	.29	.17	.87	-.13	.489E+00
9.0	-.000	-.00	-.02	.35	.21	.84	-.16	.476E+00
10.0	-.000	-.00	-.02	.40	.25	.81	-.19	.466E+00
11.0	.000	-.00	-.03	.44	.29	.79	-.21	.457E+00
12.0	.000	-.00	-.03	.48	.32	.77	-.23	.449E+00
13.0	.001	-.00	-.04	.51	.35	.76	-.24	.442E+00
14.0	.001	-.00	-.04	.54	.37	.74	-.26	.437E+00
15.0	.001	-.00	-.04	.56	.39	.73	-.27	.433E+00
16.0	.001	-.00	-.05	.58	.41	.72	-.28	.430E+00
17.0	.001	-.00	-.05	.59	.42	.72	-.28	.428E+00
18.0	.001	-.00	-.05	.60	.42	.72	-.28	.427E+00
18.3	.001	.00	-.05	.60	.42	.72	-.28	.427E+00

MINL2(W1) : .155
 SECTION LENGTH : .155
 DETACHED LENGTH : .040

DATA: AL E L1 L2 A t delT meth QSYS EMSR
 dim. .18E-04 .70E+10 .045 .045 .007 .002 67 .100 .970E+07 .0060
 #dim. .12E-02 .46E+03 20.6 20.6 3.00 1. YS=.154E+08
 RKstep = .10000 F1 = .19E-01 Q = -.48E-03
 RKerror = .00050 F2 = .19E-01 M3 = .5133
 ITerror = .00010

X	C	DW/DX	W	M	S0	P	YF	N
3.0	-.002	.00	.0*	-.24	-.13	.87	.13	.431E+00
4.0	-.002	-.00	-.0*	-.14	-.07	.92	.08	.420E+00
5.0	-.001	-.00	-.00	-.05	-.02	.96	.04	.319E+00
6.0	-.001	-.00	-.01	.04	.03	.99	-.01	.764E+00
7.0	-.001	-.01	-.01	.12	.07	.95	-.05	.565E+00
8.0	-.001	-.01	-.02	.19	.11	.92	-.08	.523E+00
9.0	-.001	-.01	-.02	.26	.16	.88	-.12	.500E+00
10.0	-.000	-.01	-.03	.33	.20	.85	-.15	.484E+00
11.0	-.000	-.01	-.04	.38	.24	.82	-.18	.471E+00
12.0	.000	-.01	-.05	.44	.28	.80	-.20	.460E+00
13.0	.000	-.01	-.05	.48	.32	.77	-.23	.451E+00
14.0	.001	-.01	-.06	.52	.35	.75	-.25	.443E+00
15.0	.001	-.01	-.07	.56	.39	.73	-.27	.436E+00
16.0	.001	-.01	-.07	.59	.41	.72	-.28	.430E+00
17.0	.001	-.00	-.08	.61	.44	.71	-.29	.426E+00
18.0	.001	-.00	-.08	.63	.46	.70	-.30	.422E+00
19.0	.001	-.00	-.08	.64	.47	.69	-.31	.420E+00
20.0	.001	-.00	-.09	.65	.47	.69	-.31	.418E+00
20.6	.001	-.00	-.09	.65	.48	.69	-.31	.418E+00

MINL2(W1) : .267
 SECTION LENGTH : .267
 DETACHED LENGTH : .045

TABLES 8 A/B: CHARACTERISTIC RESULTS

CASTING SPEED 0.06 m/sec
 METALLURGICAL HEIGHT 0.3 m

DATA: AL E L1 L2 A t delT meth QSYS EMSR
 UNITS: 'C⁻¹ N.m⁻² m m m m 'C m N.m⁻² N.m⁻²

DATA: AL E L1 L2 A t delT meth QSYS EMSR
 dim. .18E-04 .70E+10 .060 .060 .015 .005 134 .300 .194E+08 .0060
 edim. .24E-02 .23E+03 11.0 11.0 2.75 1. YS=.308E+08
 RKstep = .10000 F1 = .14E-01 Q = -.72E-03
 RKerror = .00050 F2 = .14E-01 M3 = -.0216
 ITerror = .00010

X	C	DW/DX	W	M	S0	P	YP	N
2.8	-.001	.00	.0*	.20	.12	.91	-.09	.508E+00
3.8	-.001	-.00	-.0*	.27	.16	.87	-.13	.490E+00
4.8	-.001	-.00	-.00	.33	.20	.85	-.15	.477E+00
5.8	-.000	-.00	-.00	.38	.23	.82	-.18	.467E+00
6.8	.000	-.00	-.01	.42	.26	.80	-.20	.459E+00
7.8	.000	-.00	-.01	.45	.29	.79	-.21	.453E+00
8.8	.001	-.00	-.01	.47	.31	.77	-.23	.448E+00
9.8	.001	-.00	-.01	.49	.32	.77	-.23	.445E+00
10.8	.001	-.00	-.01	.49	.33	.76	-.24	.444E+00
11.0	.001	-.00	-.01	.49	.33	.76	-.24	.444E+00

MINL2(W1) : .053
 SECTION LENGTH : .060
 DETACHED LENGTH : .060

DATA: AL E L1 L2 A t delT meth QSYS EMSR
 dim. .18E-04 .70E+10 .065 .065 .015 .005 134 .300 .194E+08 .0060
 edim. .24E-02 .23E+03 11.9 11.9 2.75 1. YS=.308E+08
 RKstep = .10000 F1 = .16E-01 Q = -.72E-03
 RKerror = .00050 F2 = .16E-01 M3 = .0430
 ITerror = .00010

X	C	DW/DX	W	M	S0	P	YP	N
2.8	-.002	-.00	-.0*	.16	.09	.93	-.07	.530E+00
3.8	-.001	-.00	-.0*	.23	.14	.89	-.11	.503E+00
4.8	-.001	-.00	-.00	.30	.18	.86	-.14	.486E+00
5.8	-.000	-.00	-.01	.35	.22	.83	-.17	.473E+00
6.8	-.000	-.00	-.01	.40	.25	.81	-.19	.463E+00
7.8	.000	-.00	-.01	.44	.28	.79	-.21	.456E+00
8.8	.001	-.00	-.02	.47	.31	.78	-.22	.450E+00
9.8	.001	-.00	-.02	.49	.33	.76	-.24	.445E+00
10.8	.001	-.00	-.02	.51	.34	.76	-.24	.442E+00
11.8	.001	-.00	-.02	.51	.35	.75	-.25	.441E+00
11.8	.001	-.00	-.02	.51	.35	.75	-.25	.441E+00

MINL2(W1) : .080
 SECTION LENGTH : .080
 DETACHED LENGTH : .065

TABLES 8 C/D: CHARACTERISTIC RESULTS

CASTING SPEED 0.06 m/sec
 METALLURGICAL HEIGHT 0.3 m

DATA: AL E L1 L2 A t delT meth QSYS EMSR
 UNITS: 'C⁻¹ N.m⁻² m m m m 'C m N.m⁻² N.m⁻²

DATA: AL E L1 L2 A t delT meth QSYS EMSR
 dim. .18E-04 .70E+10 .085 .085 .015 .005 134 .300 .194E+08 .0060
 edim. .24E-02 .23E+03 15.5 15.5 2.75 1. YS=.308E+08
 RKstep = .10000 F1 = .21E-01 Q = -.72E-03
 RKerror = .00050 F2 = .21E-01 M3 = .3680
 ITerror = .00010

X	C	DW/DX	W	M	S0	P	YP	N
2.8	-.003	.00	.0*	-.10	-.04	.94	.06	.387E+00
3.8	-.002	-.00	-.00	.01	.01	.99	.01	.208E+01
4.8	-.002	-.00	-.01	.10	.06	.96	-.04	.587E+00
5.8	-.001	-.01	-.01	.19	.11	.92	-.08	.528E+00
6.8	-.001	-.01	-.02	.27	.16	.88	-.12	.501E+00
7.8	-.000	-.01	-.03	.34	.21	.84	-.16	.483E+00
8.8	.000	-.01	-.03	.41	.26	.81	-.19	.469E+00
9.8	.000	-.01	-.04	.46	.30	.78	-.22	.457E+00
10.8	.001	-.01	-.05	.51	.34	.76	-.24	.448E+00
11.8	.001	-.01	-.06	.54	.37	.74	-.26	.441E+00
12.8	.002	-.01	-.06	.57	.40	.73	-.27	.435E+00
13.8	.002	-.00	-.07	.59	.42	.72	-.28	.431E+00
14.8	.002	-.00	-.07	.60	.43	.72	-.28	.429E+00

MINL2(W1) : .286
 SECTION LENGTH : .286
 DETACHED LENGTH : .085

DATA: AL E L1 L2 A t delT meth QSYS EMSR
 dim. .18E-04 .70E+10 .100 .100 .015 .005 134 .300 .194E+08 .0060
 edim. .24E-02 .23E+03 18.3 18.3 2.75 1. YS=.308E+08
 RKstep = .10000 F1 = .25E-01 Q = -.72E-03
 RKerror = .00050 F2 = .25E-01 M3 = .6719
 ITerror = .00010

X	C	DW/DX	W	M	S0	P	YP	N
2.8	-.005	-.00	-.0*	-.35	-.21	.81	.19	.419E+00
3.8	-.004	-.00	-.00	-.22	-.12	.87	.13	.418E+00
4.8	-.003	-.01	-.01	-.10	-.04	.94	.06	.370E+00
5.8	-.002	-.01	-.02	.01	.02	.99	.01	.149E+01
6.8	-.002	-.01	-.03	.12	.07	.96	-.04	.592E+00
7.8	-.001	-.01	-.04	.21	.13	.91	-.09	.530E+00
8.8	-.001	-.01	-.06	.30	.18	.87	-.13	.501E+00
9.8	-.000	-.02	-.07	.38	.24	.83	-.17	.481E+00
10.8	.000	-.02	-.09	.44	.29	.80	-.20	.465E+00
11.8	.001	-.01	-.10	.51	.34	.77	-.23	.452E+00
12.8	.001	-.01	-.12	.56	.38	.74	-.26	.442E+00
13.8	.002	-.01	-.13	.60	.43	.72	-.28	.433E+00
14.8	.002	-.01	-.14	.64	.46	.70	-.30	.426E+00
15.8	.003	-.01	-.15	.66	.49	.69	-.31	.421E+00
16.8	.003	-.00	-.15	.68	.51	.68	-.32	.417E+00
17.8	.003	-.00	-.16	.69	.51	.68	-.32	.415E+00

MINL2(W1) : .610
 SECTION LENGTH : .610
 DETACHED LENGTH : .100

TABLES 9 A/B: CHARACTERISTIC RESULTS

CASTING SPEED 0.06 m/sec
 METALLURGICAL HEIGHT 0.6 m

DATA: AL E L1 L2 A t delT meth QSYS EMSR
 UNITS: 'C⁻¹ N.m⁻² m m m m 'C m N.m⁻² N.m⁻²

DATA: AL E L1 L2 A t delT meth QSYS EMSR
 dim. .18E-04 .70E+10 .090 .090 .022 .009 188 .600 .272E+08 .0060
 edim. .34E-02 .16E+03 10.1 10.1 2.47 1. YS=.432E+08
 RKstep = .10000 F1 = .19E-01 Q = -.10E-02
 RKerror = .00050 F2 = .19E-01 M3 = .0453
 ITerror = .00010

X	C	DW/DX	W	M	S0	P	YP	N
2.5	-.002	-.00	-.0*	.16	.09	.93	-.07	.537E+00
3.5	-.002	-.00	-.00	.25	.15	.89	-.11	.504E+00
4.5	-.001	-.00	-.00	.32	.20	.85	-.15	.485E+00
5.5	-.000	-.00	-.01	.38	.24	.82	-.18	.471E+00
6.5	.000	-.00	-.01	.43	.28	.80	-.20	.460E+00
7.5	.001	-.00	-.01	.47	.31	.78	-.22	.453E+00
8.5	.001	-.00	-.02	.50	.33	.76	-.24	.448E+00
9.5	.001	-.00	-.02	.51	.34	.76	-.24	.445E+00

MINL2(W1) : .090
 SECTION LENGTH : .090
 DETACHED LENGTH : .090

DATA: AL E L1 L2 A t delT meth QSYS EMSR
 dim. .18E-04 .70E+10 .095 .095 .022 .009 188 .600 .272E+08 .0060
 edim. .34E-02 .16E+03 10.6 10.6 2.47 1. YS=.432E+08
 RKstep = .10000 F1 = .20E-01 Q = -.10E-02
 RKerror = .00050 F2 = .20E-01 M3 = .0957
 ITerror = .00010

X	C	DW/DX	W	M	S0	P	YP	N
2.5	-.003	-.00	-.0*	.12	.07	.95	-.05	.564E+00
3.5	-.002	-.00	-.00	.22	.13	.90	-.10	.516E+00
4.5	-.001	-.00	-.00	.30	.18	.86	-.14	.492E+00
5.5	-.000	-.00	-.01	.37	.23	.83	-.17	.476E+00
6.5	.000	-.00	-.01	.42	.27	.80	-.20	.463E+00
7.5	.001	-.00	-.02	.47	.31	.78	-.22	.454E+00
8.5	.001	-.00	-.02	.50	.34	.76	-.24	.448E+00
9.5	.002	-.00	-.02	.52	.35	.75	-.25	.444E+00
10.5	.002	-.00	-.02	.53	.36	.75	-.25	.442E+00
10.5	.002	.00	-.02	.53	.36	.75	-.25	.442E+00

MINL2(W1) : .116
 SECTION LENGTH : .116
 DETACHED LENGTH : .095

TABLES 9 C/D: CHARACTERISTIC RESULTS

CASTING SPEED 0.06 m/sec
 METALLURGICAL HEIGHT 0.6 m

DATA: AL E L1 L2 A t delT meth QSYS EMSR
 UNITS: 'C⁻¹ N.m⁻² m m m m 'C m N.m⁻² N.m⁻²

DATA: AL E L1 L2 A t delT meth QSYS EMSR
 dim. .18E-04 .70E+10 .100 .100 .022 .009 188 .600 .272E+08 .0060
 sdim. .34E-02 .16E+03 11.2 11.2 2.47 1. YS=.432E+08
 RKstep = .10000 F1 = .21E-01 Q = -.10E-02
 RKerror = .00050 F2 = .21E-01 M3 = .1516
 ITerror = .00010

X	C	DW/DX	W	M	S0	F	YP	N
2.5	-.003	-.00	-.0*	.08	.05	.97	-.03	.619E+00
3.5	-.002	-.00	-.00	.18	.11	.92	-.08	.533E+00
4.5	-.001	-.00	-.01	.27	.16	.88	-.12	.502E+00
5.5	-.001	-.01	-.01	.35	.21	.84	-.16	.482E+00
6.5	.000	-.01	-.02	.41	.26	.81	-.19	.468E+00
7.5	.001	-.01	-.02	.46	.30	.78	-.22	.457E+00
8.5	.001	-.00	-.03	.50	.33	.77	-.23	.449E+00
9.5	.002	-.00	-.03	.53	.36	.75	-.25	.444E+00
10.5	.002	-.00	-.03	.54	.37	.74	-.26	.441E+00

MINL2(W1) : .152
 SECTION LENGTH : .152
 DETACHED LENGTH : .100

DATA: AL E L1 L2 A t delT meth QSYS EMSR
 dim. .18E-04 .70E+10 .140 .140 .022 .009 188 .600 .272E+08 .0060
 sdim. .34E-02 .16E+03 15.6 15.6 2.47 1. YS=.432E+08
 RKstep = .10000 F1 = .30E-01 Q = -.10E-02
 RKerror = .00050 F2 = .30E-01 M3 = .7029
 ITerror = .00010

X	C	DW/DX	W	M	S0	F	YP	N
2.5	-.007	-.00	-.0*	-.36	-.22	.80	.20	.412E+00
3.5	-.005	-.01	-.00	-.21	-.11	.88	.12	.406E+00
4.5	-.004	-.01	-.01	-.06	-.02	.95	.05	.275E+00
5.5	-.003	-.01	-.02	.07	.05	.98	-.02	.720E+00
6.5	-.002	-.02	-.04	.18	.11	.92	-.08	.557E+00
7.5	-.001	-.02	-.06	.29	.18	.87	-.13	.512E+00
8.5	-.000	-.02	-.07	.39	.24	.83	-.17	.485E+00
9.5	.001	-.02	-.09	.47	.31	.79	-.21	.466E+00
10.5	.002	-.02	-.11	.54	.37	.75	-.25	.451E+00
11.5	.002	-.02	-.13	.59	.42	.73	-.27	.439E+00
12.5	.003	-.01	-.14	.64	.46	.70	-.30	.430E+00
13.5	.004	-.01	-.15	.67	.50	.69	-.31	.423E+00
14.5	.004	-.00	-.16	.69	.52	.68	-.32	.419E+00
15.5	.004	-.00	-.16	.70	.53	.67	-.33	.417E+00
15.6	.004	-.00	-.16	.70	.53	.67	-.33	.417E+00

MINL2(W1) : .725
 SECTION LENGTH : .725
 DETACHED LENGTH : .140

FIG.12 DETACHED LENGTH vs. BILLET QUARTER-SECTION LENGTH

AS A FUNCTION OF CASTING SPEED AND METALLURGICAL HEIGHT

NOTE THAT THE QUARTER-SECTION LENGTH USED IS HALF THE BILLET'S SECTION LENGTH

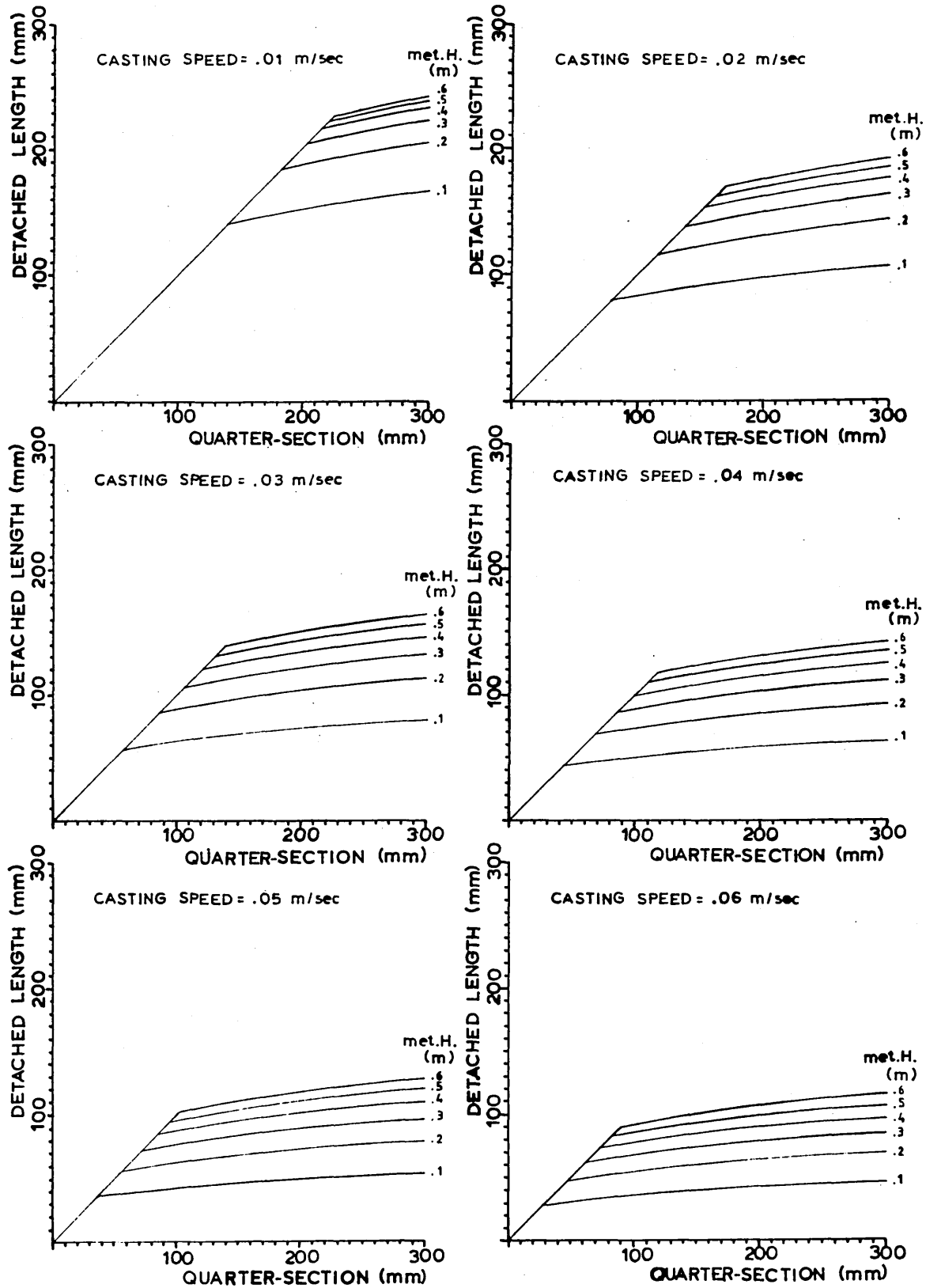


FIG.13 ADIMENSIONAL MOMENT AT THE CORNER VS. QUARTER-SECTION LENGTH AS A FUNCTION OF CASTING SPEED AND METALLURGICAL HEIGHT

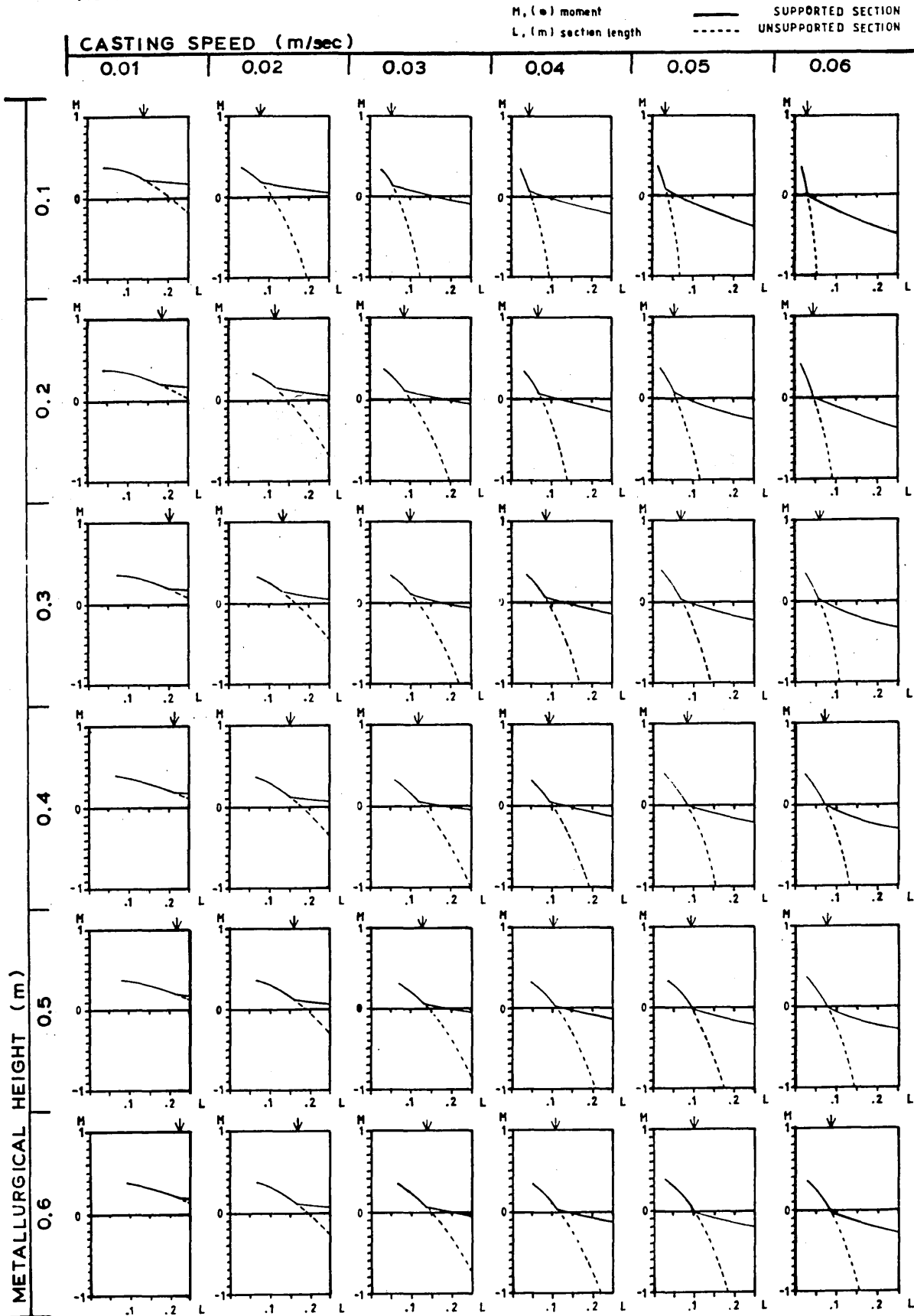
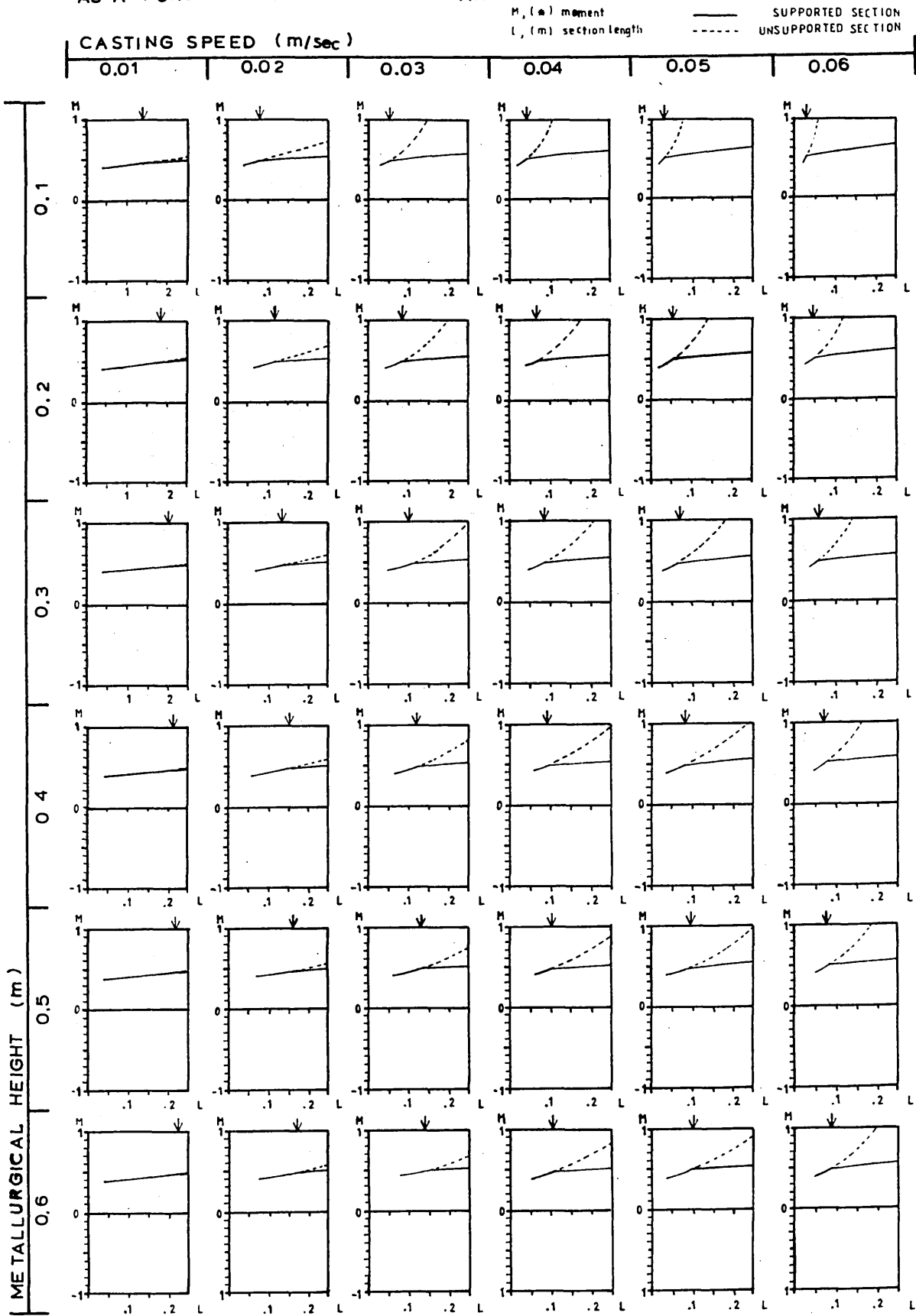


FIG. 14 ADIMENSIONAL MOMENT AT MID-FACE vs. QUARTER-SECTION LENGTH AS A FUNCTION OF CASTING SPEED AND METALLURGICAL HEIGHT



6.3 : EFFECT OF HALVING THE LENGTH OF CORNER ASSUMED RIGID ON THE RESULTS PREDICTED FOR BILLETS WITHIN THE MOULD

The previous investigation was repeated for a casting speed of 0.06 m/sec, and metallurgical heights of 0.1 m, 0.3 m and 0.6 m, using half the corner length predicted by Krishnamurthy.

For this purpose, the relevant equation used in the computer program (eq.4 in this chapter) was modified accordingly,

$$A = t (3.159 - \log(0.1 \text{ TIME} + 1)) / 2 \quad 6$$

The results of this analysis are summarised in figs 15 and 16 on page 6:51 . The corresponding results of the previous investigation are also included in these figures to facilitate comparison. Each of the Tables 10 to 12 on pages 6:45-49 present 4 sets of typical examples of the computer print-outs that were obtained, the results presented in the figures summarising the data from some 50 such print-outs corresponding to the present investigation apart from those corresponding to the previous investigation.

The second column of three graphs in figure 15, shows how the adimensional moment at the corner of the considered section varies with the length of the corresponding quarter-section at different metallurgical heights for the casting speed considered (0.06 m/sec) assuming the rigid corner length to be half that predicted by Krishnamurthy. The first column shows the corresponding results obtained in the previous investigation using Krishnamurthy's corner length.

Halving the rigid corner length has increased the value of the moment at the corner considerably; the minimum quarter-section length leading to a negative moment at the corner for each metallurgical height has thus doubled.

The fourth column of three graphs in figure 15 shows the adimensional moment at the rigid corner length as a function of the billet's quarter-section length at different metallurgical heights for the casting speed considered but assuming half Krishnamurthy's corner length as the rigid corner length. The third column shows the corresponding results obtained when the whole of Krishnamurthy's corner length was assumed to be rigid. The moments obtained are extremely similar although this had not been the case for the moment at the corner. This is because the change in the rigid corner length changes the moment at the corner, this change then being added to moment values all along the beam. The third and fourth columns in figure 15 compare moments at different lengths, and the change in corner moment compensates more or less completely for the change in position.

Figure 16, for a casting speed of 0.06 m/sec, compares the results obtained in the two investigations for the detached length of the quarter-section as a function of the total quarter-section length for different parametric values of the metallurgical height. The dotted lines correspond to the results obtained using half Krishnamurthy's corner length as rigid.

The drop observed in the curves represents a significant reduction in the detached length for any given section length. The minimum total section length below which the section is totally detached at each of the metallurgical heights considered has been reduced sufficiently to explain why it is the corner moment for the supported beams that changes significantly when the rigid length is reduced (see figure 15).

TABLES 10 A/B: RESULTS USING HALF KRISHNAMURTHY'S CORNER LENGTH
 CASTING SPEED 0.06 m/sec
 METALLURGICAL HEIGHT 0.1 m

DATA: AL E L1 L2 A t delT meth QSYS EMSR
 UNITS: 'C⁻¹ N.m⁻² m m m m 'C m N.m⁻² N.m⁻²

DATA: AL E L1 L2 A t delT meth QSYS EMSR
 dim. .18E-04 .70E+10 .022 .022 .003 .002 67 .100 .970E+07 .0060
 edim. .12E-02 .46E+03 10.1 10.1 1.50 1. YS=.154E+08
 RKstep = .10000 F1 = .87E-02 Q = -.48E-03
 RKerror = .00050 F2 = .87E-02 M3 = -.2031
 ITerror = .00010
 LONG BEAM :

X	C	DW/DX	W	M	S0	F	YF	N
1.5	-.001	-.00	-.0*	.25	.15	.88	-.12	.483E+00
2.5	-.000	-.0*	-.0*	.30	.18	.86	-.14	.473E+00
3.5	-.000	-.0*	-.0*	.34	.21	.83	-.17	.466E+00
4.5	-.000	-.0*	-.00	.38	.23	.82	-.18	.459E+00
5.5	.000	-.0*	-.00	.41	.26	.80	-.20	.454E+00
6.5	.000	-.0*	-.00	.43	.27	.79	-.21	.450E+00
7.5	.000	-.0*	-.00	.45	.29	.78	-.22	.447E+00
8.5	.000	-.0*	-.01	.46	.30	.78	-.22	.444E+00
9.5	.000	-.0*	-.01	.47	.30	.77	-.23	.443E+00

MINL2(W1) : .018
 SECTION LENGTH : .022
 DETACHED LENGTH : .022

DATA: AL E L1 L2 A t delT meth QSYS EMSR
 dim. .18E-04 .70E+10 .030 .030 .003 .002 67 .100 .970E+07 .0060
 edim. .12E-02 .46E+03 13.8 13.8 1.50 1. YS=.154E+08
 RKstep = .10000 F1 = .12E-01 Q = -.48E-03
 RKerror = .00050 F2 = .12E-01 M3 = -.0273
 ITerror = .00010
 LONG BEAM :

X	C	DW/DX	W	M	S0	F	YF	N
1.5	-.001	.00	.0*	.10	.06	.96	-.04	.548E+00
2.5	-.001	-.00	-.0*	.17	.10	.92	-.08	.514E+00
3.5	-.001	-.00	-.00	.23	.13	.89	-.11	.496E+00
4.5	-.000	-.00	-.00	.29	.17	.87	-.13	.482E+00
5.5	-.000	-.00	-.01	.34	.20	.84	-.16	.472E+00
6.5	-.000	-.00	-.01	.38	.24	.82	-.18	.463E+00
7.5	.000	-.00	-.01	.42	.27	.80	-.20	.456E+00
8.5	.000	-.00	-.01	.45	.29	.78	-.22	.450E+00
9.5	.000	-.00	-.02	.48	.32	.77	-.23	.445E+00
10.5	.000	-.00	-.02	.50	.33	.76	-.24	.441E+00
11.5	.001	-.00	-.02	.52	.35	.75	-.25	.438E+00
12.5	.001	-.00	-.02	.53	.36	.75	-.25	.436E+00
13.5	.001	-.00	-.02	.53	.36	.74	-.26	.435E+00
13.7	.001	-.00	-.02	.53	.36	.74	-.26	.435E+00

MINL2(W1) : .067
 SECTION LENGTH : .067
 DETACHED LENGTH : .030

TABLES 10 C/D: RESULTS USING HALF KRISHNAMURTHY'S CORNER LENGTH
 CASTING SPEED 0.06 m/sec
 METALLURGICAL HEIGHT 0.1 m

DATA: AL E L1 L2 A t delT meth QSYS EMSR
 UNITS: 'C⁻¹ N.m⁻² m m m m 'C m N.m⁻² N.m⁻²

DATA: AL E L1 L2 A t delT meth QSYS EMSR
 dim. .18E-04 .70E+10 .042 .042 .003 .002 67 .100 .970E+07 .0060
 edim. .12E-02 .46E+03 19.3 19.3 1.50 1. YS=.154E+08
 RKstep = .10000 F1 = .17E-01 Q = -.48E-03
 RKerror = .00050 F2 = .17E-01 M3 = .3578
 ITerror = .00010

LONG BEAM :

X	C	DW/DX	W	M	S0	F	YP	N
1.5	-.002	-.00	-.0*	-.25	-.14	.86	.14	.434E+00
2.5	-.002	-.00	-.0*	-.15	-.08	.91	.09	.426E+00
3.5	-.001	-.00	-.00	-.06	-.02	.96	.04	.355E+00
4.5	-.001	-.00	-.01	.03	.02	1.00	-.00	.829E+00
5.5	-.001	-.01	-.01	.11	.07	.96	-.04	.566E+00
6.5	-.001	-.01	-.02	.18	.11	.92	-.08	.523E+00
7.5	-.001	-.01	-.03	.25	.15	.88	-.12	.500E+00
8.5	-.000	-.01	-.03	.32	.19	.85	-.15	.483E+00
9.5	-.000	-.01	-.04	.38	.24	.82	-.18	.470E+00
10.5	.000	-.01	-.05	.43	.28	.80	-.20	.459E+00
11.5	.000	-.01	-.06	.48	.32	.77	-.23	.450E+00
12.5	.001	-.01	-.06	.52	.35	.75	-.25	.442E+00
13.5	.001	-.01	-.07	.56	.38	.74	-.26	.435E+00
14.5	.001	-.01	-.08	.59	.41	.72	-.28	.429E+00
15.5	.001	-.00	-.08	.61	.44	.71	-.29	.425E+00
16.5	.001	-.00	-.08	.63	.46	.70	-.30	.421E+00
17.5	.001	-.00	-.09	.64	.47	.69	-.31	.418E+00
18.5	.001	-.00	-.09	.65	.48	.69	-.31	.417E+00

MINL2(W1) : .277

SECTION LENGTH : .277

DETACHED LENGTH : .042

DATA: AL E L1 L2 A t delT meth QSYS EMSR
 dim. .18E-04 .70E+10 .034 .034 .003 .002 67 .100 .970E+07 .0060
 edim. .12E-02 .46E+03 15.6 15.6 1.50 1. YS=.154E+08
 RKstep = .10000 F1 = .14E-01 Q = -.48E-03
 RKerror = .00050 F2 = .14E-01 M3 = .0852
 ITerror = .00010

LONG BEAM :

X	C	DW/DX	W	M	S0	F	YP	N
1.5	-.001	.00	.0*	-.00	.01	.99	.01	-.281E+01
2.5	-.001	-.00	-.0*	.08	.05	.97	-.03	.582E+00
3.5	-.001	-.00	-.00	.15	.09	.93	-.07	.527E+00
4.5	-.001	-.00	-.00	.21	.13	.90	-.10	.503E+00
5.5	-.000	-.00	-.01	.28	.16	.87	-.13	.488E+00
6.5	-.000	-.00	-.01	.33	.20	.84	-.16	.475E+00
7.5	-.000	-.00	-.02	.38	.24	.82	-.18	.465E+00
8.5	.000	-.00	-.02	.42	.27	.80	-.20	.457E+00
9.5	.000	-.00	-.02	.46	.30	.78	-.22	.450E+00
10.5	.000	-.00	-.03	.49	.33	.76	-.24	.444E+00
11.5	.001	-.00	-.03	.52	.35	.75	-.25	.439E+00
12.5	.001	-.00	-.03	.54	.37	.74	-.26	.435E+00
13.5	.001	-.00	-.03	.56	.38	.73	-.27	.432E+00
14.5	.001	-.00	-.04	.56	.39	.73	-.27	.430E+00
15.5	.001	-.00	-.04	.57	.40	.73	-.27	.430E+00
15.5	.001	.00	-.04	.57	.40	.73	-.27	.430E+00

MINL2(W1) : .113

SECTION LENGTH : .113

DETACHED LENGTH : .034

TABLES 11 A/B: RESULTS USING HALF KRISHNAMURTHY'S CORNER LENGTH
 CASTING SPEED 0.06 m/sec
 METALLURGICAL HEIGHT 0.3 m

DATA: AL E L1 L2 A t delT meth QSYS EMSR
 UNITS: 'C⁻¹ N.m⁻² m m m m 'C m N.m⁻² N.m⁻²

DATA: AL E L1 L2 A t delT meth QSYS EMSR
 dim. .18E-04 .70E+10 .050 .050 .008 .005 134 .300 .194E+08 .0060
 bdim. .24E-02 .23E+03 9.1 9.1 1.38 1. YS=.308E+08

RKstep = .10000 F1 = .12E-01 Q = -.72E-03
 RKerror = .00050 F2 = .12E-01 M3 = -.1609
 IError = .00010

LONG BEAM :

X	C	DW/DX	W	M	S0	P	YP	N
1.4	-.001	.00	-.0*	.22	.13	.90	-.10	.496E+00
2.4	-.001	-.00	-.0*	.28	.17	.87	-.13	.482E+00
3.4	-.000	-.00	-.00	.34	.21	.84	-.16	.471E+00
4.4	-.000	-.00	-.00	.38	.24	.82	-.18	.462E+00
5.4	.000	-.00	-.01	.42	.27	.80	-.20	.455E+00
6.4	.000	-.00	-.01	.45	.29	.78	-.22	.450E+00
7.4	.001	-.00	-.01	.47	.31	.77	-.23	.446E+00
8.4	.001	-.00	-.01	.48	.32	.77	-.23	.444E+00

MINL2(W1) : .042

SECTION LENGTH : .050

DETACHED LENGTH : .050

DATA: AL E L1 L2 A t delT meth QSYS EMSR
 dim. .18E-04 .70E+10 .054 .054 .008 .005 134 .300 .194E+08 .0060
 bdim. .24E-02 .23E+03 9.9 9.9 1.38 1. YS=.308E+08

RKstep = .10000 F1 = .13E-01 Q = -.72E-03
 RKerror = .00050 F2 = .13E-01 M3 = -.1211
 IError = .00010

LONG BEAM :

X	C	DW/DX	W	M	S0	P	YP	N
1.4	-.001	-.00	-.0*	.19	.11	.91	-.09	.509E+00
2.4	-.001	-.00	-.0*	.26	.15	.88	-.12	.490E+00
3.4	-.001	-.00	-.00	.32	.19	.85	-.15	.477E+00
4.4	-.000	-.00	-.00	.37	.23	.82	-.18	.466E+00
5.4	.000	-.00	-.01	.41	.26	.80	-.20	.458E+00
6.4	.000	-.00	-.01	.45	.29	.79	-.21	.451E+00
7.4	.001	-.00	-.01	.47	.31	.77	-.23	.447E+00
8.4	.001	-.00	-.01	.49	.32	.76	-.24	.443E+00
9.4	.001	-.00	-.01	.50	.33	.76	-.24	.442E+00
9.8	.001	-.00	-.01	.50	.33	.76	-.24	.442E+00

MINL2(W1) : .061

SECTION LENGTH : .061

DETACHED LENGTH : .054

TABLES 11 C/D: RESULTS USING HALF KRISHNAMURTHY'S CORNER LENGTH
 CASTING SPEED 0.06 m/sec
 METALLURGICAL HEIGHT 0.3 m

DATA: AL E L1 L2 A t delT meth QSYS EMSR
 UNITS: 'C⁻¹ N.m⁻² m m m m 'C m N.m⁻² N.m⁻²

DATA: AL E L1 L2 A t delT meth QSYS EMSR
 dim. .18E-04 .70E+10 .076 .076 .008 .005 134 .300 .194E+08 .0060
 edim. .24E-02 .23E+03 13.9 13.9 1.38 1. YS=.308E+08
 RKstep = .10000 F1 = .19E-01 Q = -.72E-03
 RKerror = .00050 F2 = .19E-01 M3 = .1742
 ITerror = .00010

LONG BEAM :

X	C	DW/DX	W	M	S0	P	YP	N
1.4	-.003	.00	.0*	-.08	-.03	.95	.05	.376E+00
2.4	-.002	-.00	-.00	.03	.02	1.00	-.00	.855E+00
3.4	-.002	-.00	-.00	.12	.07	.95	-.05	.561E+00
4.4	-.001	-.01	-.01	.21	.12	.91	-.09	.517E+00
5.4	-.001	-.01	-.02	.28	.17	.87	-.13	.493E+00
6.4	-.000	-.01	-.02	.35	.22	.84	-.16	.477E+00
7.4	.000	-.01	-.03	.41	.26	.81	-.19	.464E+00
8.4	.001	-.01	-.04	.47	.31	.78	-.22	.454E+00
9.4	.001	-.01	-.05	.51	.34	.76	-.24	.445E+00
10.4	.001	-.01	-.05	.54	.37	.74	-.26	.438E+00
11.4	.002	-.00	-.06	.57	.40	.73	-.27	.433E+00
12.4	.002	-.00	-.06	.59	.41	.72	-.28	.430E+00
13.4	.002	-.00	-.07	.60	.42	.72	-.28	.428E+00
13.8	.002	.00	-.07	.60	.42	.72	-.28	.428E+00

MINL2(W1) : .260
 SECTION LENGTH : .260
 DETACHED LENGTH : .076

DATA: AL E L1 L2 A t delT meth QSYS EMSR
 dim. .18E-04 .70E+10 .080 .080 .008 .005 134 .300 .194E+08 .0060
 edim. .24E-02 .23E+03 14.6 14.6 1.38 1. YS=.308E+08
 RKstep = .10000 F1 = .20E-01 Q = -.72E-03
 RKerror = .00050 F2 = .20E-01 M3 = .2398
 ITerror = .00010

LONG BEAM :

X	C	DW/DX	W	M	S0	P	YP	N
1.4	-.003	-.00	-.0*	-.14	-.07	.92	.08	.415E+00
2.4	-.003	-.00	-.00	-.03	-.00	.98	.02	.159E+00
3.4	-.002	-.01	-.01	.07	.05	.97	-.03	.624E+00
4.4	-.002	-.01	-.01	.17	.10	.93	-.07	.537E+00
5.4	-.001	-.01	-.02	.25	.15	.89	-.11	.505E+00
6.4	-.001	-.01	-.03	.33	.20	.85	-.15	.485E+00
7.4	-.000	-.01	-.04	.39	.25	.82	-.18	.470E+00
8.4	.000	-.01	-.05	.45	.29	.79	-.21	.458E+00
9.4	.001	-.01	-.06	.50	.33	.76	-.24	.448E+00
10.4	.001	-.01	-.07	.54	.37	.74	-.26	.440E+00
11.4	.002	-.01	-.07	.57	.40	.73	-.27	.434E+00
12.4	.002	-.00	-.08	.60	.42	.72	-.28	.429E+00
13.4	.002	-.00	-.08	.61	.44	.71	-.29	.426E+00
14.4	.002	-.00	-.08	.62	.44	.71	-.29	.425E+00
14.6	.002	-.00	-.08	.62	.44	.71	-.29	.425E+00

MINL2(W1) : .326
 SECTION LENGTH : .326
 DETACHED LENGTH : .080

TABLES 12 A/B: RESULTS USING HALF KRISHNAMURTHY'S CORNER LENGTH
 CASTING SPEED 0.06 m/sec
 METALLURGICAL HEIGHT 0.6 m

DATA: AL E L1 L2 A t delT meth QSYS EMSR
 UNITS: 'C⁻¹ N.m⁻² m m m m 'C m N.m⁻² N.m⁻²

DATA: AL E L1 L2 A t delT meth QSYS EMSR
 dim. .18E-04 .70E+10 .076 .076 .011 .009 188 .600 .272E+08 .0060
 edim. .34E-02 .16E+03 8.5 8.5 1.23 1. YS=.432E+08
 RKstep = .10000 F1 = .15E-01 Q = -.10E-02
 RKerror = .00050 F2 = .15E-01 M3 = -.1129
 ITerror = .00010

LONG BEAM :

X	C	DW/DX	W	M	S0	F	YP	N
1.2	-.002	.00	.0*	.18	.10	.92	-.08	.518E+00
2.2	-.001	-.00	-.0*	.26	.16	.88	-.12	.493E+00
3.2	-.001	-.00	-.00	.33	.20	.84	-.16	.477E+00
4.2	-.000	-.00	-.01	.39	.25	.81	-.19	.465E+00
5.2	.000	-.00	-.01	.44	.28	.79	-.21	.456E+00
6.2	.001	-.00	-.01	.47	.31	.78	-.22	.449E+00
7.2	.001	-.00	-.01	.49	.33	.76	-.24	.445E+00
8.2	.001	-.00	-.02	.50	.34	.76	-.24	.443E+00
8.4	.001	.00	-.02	.50	.34	.76	-.24	.443E+00

MINL2(W1) : .073
 SECTION LENGTH : .076
 DETACHED LENGTH : .076

DATA: AL E L1 L2 A t delT meth QSYS EMSR
 dim. .18E-04 .70E+10 .080 .080 .011 .009 188 .600 .272E+08 .0060
 edim. .34E-02 .16E+03 8.9 8.9 1.23 1. YS=.432E+08
 RKstep = .10000 F1 = .16E-01 Q = -.10E-02
 RKerror = .00050 F2 = .16E-01 M3 = -.0801
 ITerror = .00010

LONG BEAM :

X	C	DW/DX	W	M	S0	F	YP	N
1.2	-.002	.00	.0*	.15	.09	.93	-.07	.533E+00
2.2	-.002	-.00	-.00	.24	.14	.89	-.11	.501E+00
3.2	-.001	-.00	-.00	.32	.19	.85	-.15	.482E+00
4.2	-.000	-.00	-.01	.38	.24	.82	-.18	.469E+00
5.2	.000	-.00	-.01	.43	.28	.80	-.20	.458E+00
6.2	.001	-.00	-.01	.47	.31	.78	-.22	.450E+00
7.2	.001	-.00	-.02	.50	.33	.76	-.24	.445E+00
8.2	.001	-.00	-.02	.51	.34	.76	-.24	.442E+00
8.9	.001	.00	-.02	.51	.35	.75	-.25	.442E+00

MINL2(W1) : .093
 SECTION LENGTH : .093
 DETACHED LENGTH : .080

TABLES 12 C/D: RESULTS USING HALF KRISHNAMURTHY'S CORNER LENGTH
 CASTING SPEED 0.06 m/sec
 METALLURGICAL HEIGHT 0.6 m

DATA: AL E L1 L2 A t delT meth QSYS EMSR
 UNITS: 'C⁻¹ N.m⁻² m m m m 'C m N.m⁻² N.m⁻²

DATA: AL E L1 L2 A t delT meth QSYS EMSR
 dim. .18E-04 .70E+10 .100 .100 .011 .009 188 .600 .272E+08 .0060
 adim. .34E-02 .16E+03 11.2 11.2 1.23 1. YS=.432E+08
 RKstep = .10000 F1 = .21E-01 Q = -.10E-02
 RKerror = .00050 F2 = .21E-01 M3 = .1156
 ITerror = .00010

LONG BEAM :

X	C	DW/DX	W	M	S0	P	YF	N
1.2	-.004	-.00	-.0*	-.02	-.00	.98	.02	.922E-01
2.2	-.003	-.00	-.00	.09	.06	.97	-.03	.603E+00
3.2	-.002	-.01	-.01	.19	.12	.91	-.09	.527E+00
4.2	-.001	-.01	-.01	.29	.17	.87	-.13	.497E+00
5.2	-.000	-.01	-.02	.36	.23	.83	-.17	.478E+00
6.2	.000	-.01	-.03	.43	.28	.80	-.20	.463E+00
7.2	.001	-.01	-.04	.49	.32	.77	-.23	.452E+00
8.2	.002	-.01	-.04	.53	.36	.75	-.25	.444E+00
9.2	.002	-.00	-.05	.56	.39	.74	-.26	.438E+00
10.2	.002	-.00	-.05	.58	.40	.73	-.27	.434E+00
11.2	.002	.00	-.05	.58	.41	.73	-.27	.433E+00

MINL2(W1) ; .248

SECTION LENGTH ; .248

DETACHED LENGTH ; .100

DATA: AL E L1 L2 A t delT meth QSYS EMSR
 dim. .18E-04 .70E+10 .105 .105 .011 .009 188 .600 .272E+08 .0060
 adim. .34E-02 .16E+03 11.7 11.7 1.23 1. YS=.432E+08
 RKstep = .10000 F1 = .22E-01 Q = -.10E-02
 RKerror = .00050 F2 = .22E-01 M3 = .1719
 ITerror = .00010

LONG BEAM :

X	C	DW/DX	W	M	S0	P	YF	N
1.2	-.004	.00	.0*	-.08	-.03	.95	.05	.353E+00
2.2	-.003	-.00	-.00	.05	.03	.99	-.01	.730E+00
3.2	-.002	-.01	-.01	.16	.09	.93	-.07	.549E+00
4.2	-.002	-.01	-.01	.26	.15	.89	-.11	.508E+00
5.2	-.001	-.01	-.02	.34	.21	.84	-.16	.485E+00
6.2	.000	-.01	-.03	.41	.26	.81	-.19	.468E+00
7.2	.001	-.01	-.04	.48	.31	.78	-.22	.455E+00
8.2	.002	-.01	-.05	.52	.36	.75	-.25	.446E+00
9.2	.002	-.01	-.06	.56	.39	.74	-.26	.438E+00
10.2	.002	-.00	-.06	.59	.41	.72	-.28	.433E+00
11.2	.003	-.00	-.06	.60	.42	.72	-.28	.431E+00
11.7	.003	.00	-.06	.60	.42	.72	-.28	.431E+00

MINL2(W1) ; .300

SECTION LENGTH ; .300

DETACHED LENGTH ; .105

FIG.15 EFFECT OF HALVING THE RIGID CORNER LENGTH ON THE MOMENT AT THE CORNER AND AT THE RIGID BOUNDARY
 A_k IS THE CORNER LENGTH PREDICTED BY KRISHNAMURTHY
 CASTING SPEED = 0.06 m/sec

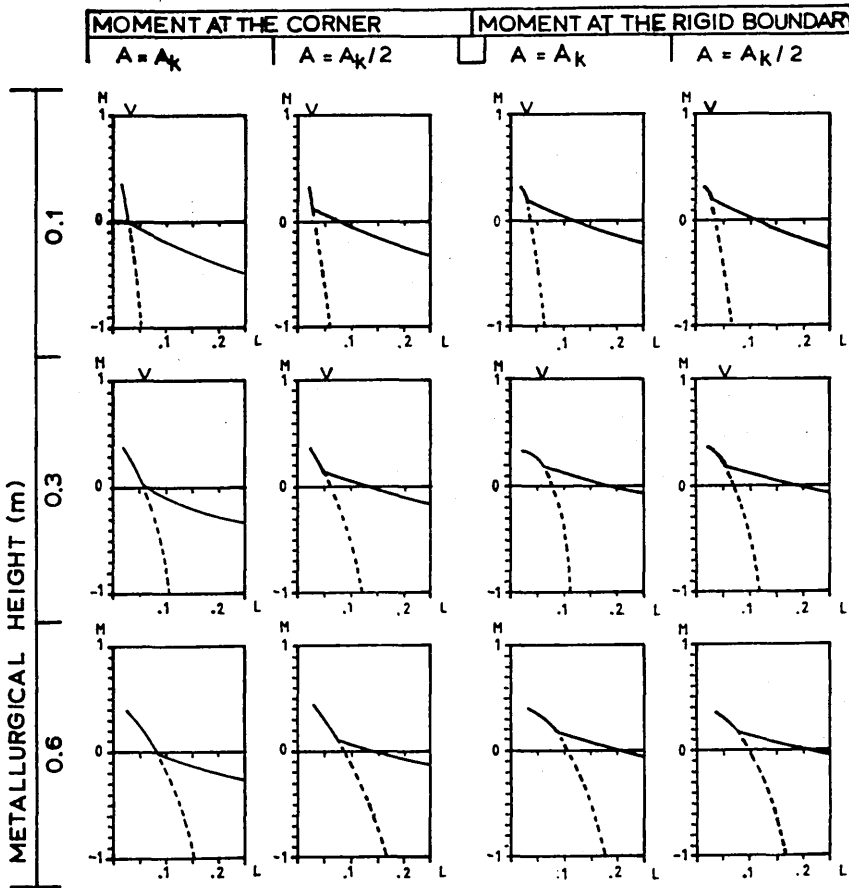
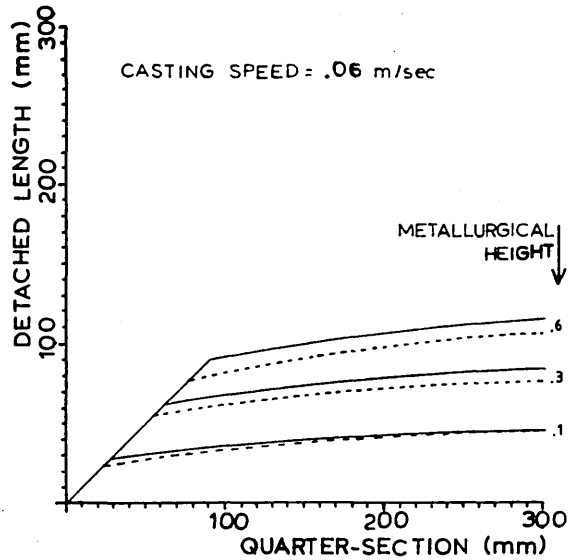


FIG.16 EFFECT OF HALVING THE CORNER LENGTH ON THE DETACHED LENGTH vs. SECTION

— $A = A_k$
 - - - $A = A_k/2$



6.4 : EFFECT OF REDUCING THE ASSUMED VALUE OF THE QUASI-STATIC YIELD STRESS AT 1000°C ON THE RESULTS PREDICTED FOR BILLETS WITHIN THE MOULD

The value of the quasi-static yield stress at 1000°C was changed from $6.5 \times 10^7 \text{ N.m}^{-2}$ to 4.0 N.m^{-2} . Because of the form of equation 5 (page 6:17), this change changes the value of the quasi-static yield stress at all points across the section.

The effect of this reduction is shown in figure 17 (page 6:59), and typical results are presented on tables 13 to 15 (pages 6:53-58). The arrows on top of the graphs point to the quarter-section length at which supported and unsupported moments diverge, the change (a slight reduction) is not very significant. The adimensional moment at the corner, however, is magnified and becomes negative at shorter section lengths. The most important consequence is the reduction in the total section length at which the moments at the corner and at the rigid boundary become negative, while the moment at the middle of the face has actually become more positive.

TABLES 13 A/B: RESULTS FOR A LOW YIELD STRESS STEEL
 CASTING SPEED 0.06 m/sec
 METALLURGICAL HEIGHT 0.1 m

DATA: AL E L1 L2 A t delT meth QSYS EMSR
 UNITS: 'C⁻¹ N.m⁻² m m m m 'C m N.m⁻² N.m⁻²

DATA: AL E L1 L2 A t delT meth QSYS EMSR
 dim. .18E-04 .70E+10 .025 .025 .007 .002 67 .100 .597E+07 .0060
 adim. .12E-02 .74E+03 11.5 11.5 3.00 1. YS=.947E+07
 RKstep = .10000 F1 = .16E-01 Q = -.78E-03
 RKerror = .00050 F2 = .16E-01 M3 = -.1031
 ITerror = .00010

X	C	DW/DX	W	M	S0	P	YP	N
3.0	-.001	.00	.0*	.33	.20	.85	-.15	.479E+00
4.0	-.000	-.0*	-.0*	.40	.26	.81	-.19	.464E+00
5.0	-.000	-.0*	-.00	.47	.31	.78	-.22	.451E+00
6.0	-.000	-.00	-.00	.52	.35	.75	-.25	.440E+00
7.0	.000	-.00	-.00	.57	.40	.73	-.27	.431E+00
8.0	.000	-.00	-.00	.61	.43	.71	-.29	.424E+00
9.0	.000	-.0*	-.01	.63	.46	.70	-.30	.419E+00
10.0	.000	-.0*	-.01	.65	.48	.69	-.31	.416E+00
11.0	.000	-.0*	-.01	.66	.49	.68	-.32	.414E+00
11.4	.000	-.0*	-.01	.66	.49	.68	-.32	.414E+00

MINL2(W1) : .020
 SECTION LENGTH : .025
 DETACHED LENGTH : .025

DATA: AL E L1 L2 A t delT meth QSYS EMSR
 dim. .18E-04 .70E+10 .030 .030 .007 .002 67 .100 .597E+07 .0060
 adim. .12E-02 .74E+03 13.8 13.8 3.00 1. YS=.947E+07
 RKstep = .10000 F1 = .20E-01 Q = -.78E-03
 RKerror = .00050 F2 = .20E-01 M3 = .0975
 ITerror = .00010

X	C	DW/DX	W	M	S0	P	YP	N
3.0	-.001	-.00	-.0*	.18	.11	.92	-.08	.530E+00
4.0	-.001	-.00	-.0*	.28	.17	.87	-.13	.498E+00
5.0	-.001	-.00	-.00	.36	.23	.83	-.17	.477E+00
6.0	-.000	-.00	-.00	.44	.29	.79	-.21	.460E+00
7.0	-.000	-.00	-.01	.51	.34	.76	-.24	.447E+00
8.0	.000	-.00	-.01	.57	.39	.73	-.27	.435E+00
9.0	.000	-.00	-.01	.62	.44	.71	-.29	.426E+00
10.0	.000	-.00	-.01	.66	.48	.69	-.31	.418E+00
11.0	.000	-.00	-.01	.69	.51	.67	-.33	.412E+00
12.0	.001	-.00	-.02	.71	.54	.66	-.34	.408E+00
13.0	.001	-.00	-.02	.72	.55	.66	-.34	.405E+00
13.7	.001	-.00	-.02	.72	.55	.66	-.34	.405E+00

MINL2(W1) : .050
 SECTION LENGTH : .050
 DETACHED LENGTH : .030

TABLES 13 C/D: RESULTS FOR A LOW YIELD STRESS STEEL
 CASTING SPEED 0.06 m/sec
 METALLURGICAL HEIGHT 0.1 m

DATA: AL E L1 L2 A t delT meth QSYS EMSR
 UNITS: 'C⁻¹ N.m⁻² m m m m 'C m N.m⁻² N.m⁻²

DATA: AL E L1 L2 A t delT meth QSYS EMSR
 dim. .18E-04 .70E+10 .035 .035 .007 .002 67 .100 .597E+07 .0060
 adim. .12E-02 .74E+03 16.1 16.1 3.00 1. YS=.947E+07
 RKstep = .10000 F1 = .23E-01 Q = -.78E-03
 RKerror = .00050 F2 = .23E-01 M3 = .3449
 IError = .00010

X	C	DW/DX	W	M	S0	P	YP	N
3.0	-.001	.00	.0*	-.01	.01	.98	.02	-.410E+00
4.0	-.001	-.00	-.0*	.10	.07	.96	-.04	.598E+00
5.0	-.001	-.00	-.00	.21	.13	.91	-.09	.526E+00
6.0	-.001	-.00	-.00	.31	.19	.86	-.14	.495E+00
7.0	-.000	-.00	-.01	.40	.25	.82	-.18	.473E+00
8.0	-.000	-.00	-.01	.48	.32	.78	-.22	.456E+00
9.0	-.000	-.00	-.02	.55	.38	.74	-.26	.442E+00
10.0	.000	-.00	-.02	.61	.44	.71	-.29	.430E+00
11.0	.000	-.00	-.02	.66	.49	.69	-.31	.419E+00
12.0	.001	-.00	-.03	.71	.53	.67	-.33	.411E+00
13.0	.001	-.00	-.03	.74	.57	.65	-.35	.404E+00
14.0	.001	-.00	-.03	.76	.60	.64	-.36	.399E+00
15.0	.001	-.00	-.03	.78	.62	.63	-.37	.396E+00
16.0	.001	-.00	-.03	.78	.63	.63	-.37	.395E+00
16.0	.001	.00	-.03	.78	.63	.63	-.37	.395E+00

MINL2(W1) : .100
 SECTION LENGTH : .100
 DETACHED LENGTH : .035

DATA: AL E L1 L2 A t delT meth QSYS EMSR
 dim. .18E-04 .70E+10 .040 .040 .007 .002 67 .100 .597E+07 .0060
 adim. .12E-02 .74E+03 18.3 18.3 3.00 1. YS=.947E+07
 RKstep = .10000 F1 = .27E-01 Q = -.78E-03
 RKerror = .00050 F2 = .27E-01 M3 = .6328
 IError = .00010

X	C	DW/DX	W	M	S0	P	YP	N
3.0	-.002	-.00	-.0*	-.25	-.13	.86	.14	.417E+00
4.0	-.001	-.00	-.0*	-.11	-.05	.93	.07	.369E+00
5.0	-.001	-.00	-.00	.02	.02	1.00	.00	.114E+01
6.0	-.001	-.00	-.01	.14	.09	.94	-.06	.577E+00
7.0	-.001	-.00	-.01	.25	.15	.89	-.11	.520E+00
8.0	-.001	-.01	-.02	.35	.22	.84	-.16	.490E+00
9.0	-.000	-.01	-.02	.44	.29	.80	-.20	.468E+00
10.0	-.000	-.01	-.03	.53	.36	.76	-.24	.450E+00
11.0	.000	-.01	-.03	.60	.42	.72	-.28	.435E+00
12.0	.000	-.01	-.04	.66	.49	.69	-.31	.422E+00
13.0	.001	-.01	-.05	.72	.55	.66	-.34	.411E+00
14.0	.001	-.00	-.05	.76	.60	.64	-.36	.402E+00
15.0	.001	-.00	-.06	.80	.65	.62	-.38	.394E+00
16.0	.001	-.00	-.06	.83	.68	.61	-.39	.389E+00
17.0	.001	-.00	-.06	.84	.70	.60	-.40	.385E+00
18.0	.001	-.00	-.06	.85	.71	.60	-.40	.384E+00
18.3	.001	-.00	-.06	.85	.72	.60	-.40	.384E+00

MINL2(W1) : .182
 SECTION LENGTH : .182
 DETACHED LENGTH : .040

TABLES 14 A/B: RESULTS FOR A LOW YIELD STRESS STEEL
 CASTING SPEED 0.06 m/sec
 METALLURGICAL HEIGHT 0.3 m

DATA: AL E L1 L2 A t delT meth QSYS EMSR
 UNITS: 'C⁻¹ N.m⁻² m m m m 'C m N.m⁻² N.m⁻²

DATA: AL E L1 L2 A t delT meth QSYS EMSR
 dim. .18E-04 .70E+10 .055 .055 .015 .005 134 .300 .119E+08 .0060
 adim. .24E-02 .37E+03 10.1 10.1 2.75 1. YS=.189E+08
 RKstep = .10000 F1 = .21E-01 Q = -.12E-02
 RKerror = .00050 F2 = .21E-01 M3 = -.0396
 ITerror = .00010

X	C	DW/DX	W	M	S0	P	YP	N
2.8	-.001	-.00	-.0*	.30	.19	.86	-.14	.493E+00
3.8	-.001	-.00	-.0*	.40	.25	.82	-.18	.471E+00
4.8	-.001	-.00	-.00	.48	.32	.78	-.22	.454E+00
5.8	-.000	-.00	-.00	.55	.38	.74	-.26	.440E+00
6.8	.000	-.00	-.01	.60	.43	.72	-.28	.430E+00
7.8	.001	-.00	-.01	.64	.46	.70	-.30	.422E+00
8.8	.001	-.00	-.01	.67	.49	.68	-.32	.417E+00
9.8	.001	-.00	-.01	.68	.50	.68	-.32	.415E+00

MINL2(W1) : .042
 SECTION LENGTH : .055
 DETACHED LENGTH : .055

DATA: AL E L1 L2 A t delT meth QSYS EMSR
 dim. .18E-04 .70E+10 .060 .060 .015 .005 134 .300 .119E+08 .0060
 adim. .24E-02 .37E+03 11.0 11.0 2.75 1. YS=.189E+08
 RKstep = .10000 F1 = .23E-01 Q = -.12E-02
 RKerror = .00050 F2 = .23E-01 M3 = .0594
 ITerror = .00010

X	C	DW/DX	W	M	S0	P	YP	N
2.8	-.002	-.00	-.0*	.23	.14	.90	-.10	.518E+00
3.8	-.001	-.00	-.0*	.34	.21	.84	-.16	.487E+00
4.8	-.001	-.00	-.00	.44	.28	.80	-.20	.465E+00
5.8	-.000	-.00	-.01	.52	.35	.76	-.24	.449E+00
6.8	.000	-.00	-.01	.58	.41	.73	-.27	.435E+00
7.8	.000	-.00	-.01	.63	.46	.70	-.30	.425E+00
8.8	.001	-.00	-.01	.67	.50	.68	-.32	.417E+00
9.8	.001	-.00	-.02	.70	.52	.67	-.33	.413E+00
10.8	.001	-.00	-.02	.71	.54	.67	-.33	.411E+00
11.0	.001	-.00	-.02	.71	.54	.67	-.33	.411E+00

MINL2(W1) : .066
 SECTION LENGTH : .066
 DETACHED LENGTH : .060

TABLES 14 C/D: RESULTS FOR A LOW YIELD STRESS STEEL
 CASTING SPEED 0.06 m/sec
 METALLURGICAL HEIGHT 0.3 m

DATA: AL E L1 L2 A t delT meth QSYS EMSR
 UNITS: 'C⁻¹ N.m⁻² m m m m 'C m N.m⁻² N.m⁻²

DATA: AL E L1 L2 A t delT meth QSYS EMSR
 dim. .18E-04 .70E+10 .080 .080 .015 .005 134 .300 .119E+08 .0060
 adim. .24E-02 .37E+03 14.6 14.6 2.75 1. YS=.189E+08
 RKstep = .10000 F1 = .32E-01 Q = -.12E-02
 RKerror = .00050 F2 = .32E-01 M3 = .5641
 ITerror = .00010

X	C	DW/DX	W	M	S0	P	YP	N
2.8	-.003	-.00	-.0*	-.16	-.07	.90	.10	.385E+00
3.8	-.002	-.00	-.00	.00	.02	.99	.01	.659E+01
4.8	-.002	-.00	-.01	.15	.09	.94	-.06	.588E+00
5.8	-.002	-.01	-.01	.28	.17	.88	-.12	.519E+00
6.8	-.001	-.01	-.02	.40	.25	.82	-.18	.485E+00
7.8	-.000	-.01	-.03	.50	.33	.77	-.23	.461E+00
8.8	.000	-.01	-.04	.59	.41	.73	-.27	.442E+00
9.8	.001	-.01	-.04	.66	.49	.69	-.31	.426E+00
10.8	.001	-.01	-.05	.73	.55	.66	-.34	.413E+00
11.8	.002	-.01	-.06	.77	.61	.64	-.36	.403E+00
12.8	.002	-.00	-.06	.81	.65	.62	-.38	.396E+00
13.8	.002	-.00	-.07	.83	.68	.62	-.38	.392E+00
14.6	.002	-.00	-.07	.83	.68	.61	-.39	.391E+00

MINL2(W1) : .253
 SECTION LENGTH : .253
 DETACHED LENGTH : .080

DATA: AL E L1 L2 A t delT meth QSYS EMSR
 dim. .18E-04 .70E+10 .085 .085 .015 .005 134 .300 .119E+08 .0060
 adim. .24E-02 .37E+03 15.5 15.5 2.75 1. YS=.189E+08
 RKstep = .10000 F1 = .34E-01 Q = -.12E-02
 RKerror = .00050 F2 = .34E-01 M3 = .7166
 ITerror = .00010

X	C	DW/DX	W	M	S0	P	YP	N
2.8	-.003	.00	.0*	-.28	-.15	.84	.16	.407E+00
3.8	-.003	-.00	-.00	-.11	-.04	.93	.07	.340E+00
4.8	-.002	-.01	-.01	.05	.04	.99	-.01	.835E+00
5.8	-.002	-.01	-.01	.19	.12	.92	-.08	.562E+00
6.8	-.001	-.01	-.02	.32	.20	.86	-.14	.508E+00
7.8	-.001	-.01	-.03	.44	.29	.80	-.20	.477E+00
8.8	-.000	-.01	-.04	.54	.37	.75	-.25	.454E+00
9.8	.000	-.01	-.05	.63	.45	.71	-.29	.435E+00
10.8	.001	-.01	-.06	.70	.53	.68	-.32	.419E+00
11.8	.002	-.01	-.07	.76	.60	.65	-.35	.407E+00
12.8	.002	-.01	-.08	.81	.66	.62	-.38	.397E+00
13.8	.002	-.00	-.09	.84	.70	.61	-.39	.390E+00
14.8	.003	-.00	-.09	.86	.72	.60	-.40	.386E+00

MINL2(W1) : .331
 SECTION LENGTH : .331
 DETACHED LENGTH : .085

TABLES 15 A/B: RESULTS FOR A LOW YIELD STRESS STEEL
 CASTING SPEED 0.06 m/sec
 METALLURGICAL HEIGHT 0.6 m

DATA: AL E L1 L2 A t delT meth QSYS EMSR
 UNITS: 'C⁻¹ N.m⁻² m m m m 'C m N.m⁻² N.m⁻²

DATA: AL E L1 L2 A t delT meth QSYS EMSR
 dim. .18E-04 .70E+10 .085 .085 .022 .009 188 .600 .168E+08 .0060
 adim. .34E-02 .26E+03 9.5 9.5 2.47 1. YS=.266E+08
 RKstep = .10000 F1 = .28E-01 Q = -.17E-02
 RKerror = .00050 F2 = .28E-01 M3 = .0898
 ITerror = .00010

X	C	DW/DX	W	M	S0	P	YP	N
2.5	-.002	.00	.0*	.22	.13	.91	-.09	.534E+00
3.5	-.002	-.00	-.0*	.35	.22	.84	-.16	.492E+00
4.5	-.001	-.00	-.00	.46	.30	.79	-.21	.465E+00
5.5	-.000	-.00	-.01	.55	.38	.75	-.25	.446E+00
6.5	.001	-.00	-.01	.62	.45	.71	-.29	.432E+00
7.5	.001	-.00	-.01	.67	.50	.69	-.31	.421E+00
8.5	.001	-.00	-.02	.70	.53	.67	-.33	.415E+00
9.5	.002	-.00	-.02	.71	.54	.67	-.33	.413E+00
9.5	.002	.00	-.02	.71	.54	.67	-.33	.413E+00

MINL2(W1) : .079
 SECTION LENGTH : .085
 DETACHED LENGTH : .085

DATA: AL E L1 L2 A t delT meth QSYS EMSR
 dim. .18E-04 .70E+10 .090 .090 .022 .009 188 .600 .168E+08 .0060
 adim. .34E-02 .26E+03 10.1 10.1 2.47 1. YS=.266E+08
 RKstep = .10000 F1 = .30E-01 Q = -.17E-02
 RKerror = .00050 F2 = .30E-01 M3 = .1709
 ITerror = .00010

X	C	DW/DX	W	M	S0	P	YP	N
2.5	-.003	.00	.0*	.16	.10	.94	-.06	.572E+00
3.5	-.002	-.00	-.00	.30	.19	.87	-.13	.508E+00
4.5	-.001	-.00	-.00	.42	.27	.81	-.19	.476E+00
5.5	-.000	-.00	-.01	.53	.36	.76	-.24	.453E+00
6.5	.000	-.00	-.01	.61	.43	.72	-.28	.436E+00
7.5	.001	-.00	-.02	.67	.49	.69	-.31	.423E+00
8.5	.002	-.00	-.02	.71	.54	.67	-.33	.415E+00
9.5	.002	-.00	-.02	.73	.56	.66	-.34	.410E+00

MINL2(W1) : .107
 SECTION LENGTH : .107
 DETACHED LENGTH : .090

TABLES 15 C/D: RESULTS FOR A LOW YIELD STRESS STEEL
 CASTING SPEED 0.06 m/sec
 METALLURGICAL HEIGHT 0.6 m

DATA: AL E L1 L2 A t delT meth QSYS EMSR
 UNITS: 'C⁻¹ N.m⁻² m m m m 'C m N.m⁻² N.m⁻²

DATA: AL E L1 L2 A t delT meth QSYS EMSR
 dim. .18E-04 .70E+10 .100 .100 .022 .009 188 .600 .168E+08 .0060
 edim. .34E-02 .26E+03 11.2 11.2 2.47 1. YS=.266E+08
 RKstep = .10000 F1 = .34E-01 Q = -.17E-02
 RKerror = .00050 F2 = .34E-01 M3 = .3504
 ITerror = .00010

X	C	DW/DX	W	M	S0	F	YP	N
2.5	-.003	.00	.0*	.03	.03	1.00	.00	.113E+01
3.5	-.003	-.00	-.00	.19	.12	.92	-.08	.564E+00
4.5	-.002	-.01	-.01	.33	.21	.85	-.15	.505E+00
5.5	-.001	-.01	-.01	.46	.30	.80	-.20	.473E+00
6.5	-.000	-.01	-.02	.56	.39	.74	-.26	.449E+00
7.5	.001	-.01	-.03	.64	.47	.70	-.30	.432E+00
8.5	.001	-.01	-.03	.71	.53	.67	-.33	.418E+00
9.5	.002	-.00	-.04	.75	.58	.65	-.35	.409E+00
10.5	.002	-.00	-.04	.78	.61	.64	-.36	.404E+00

MINL2(W1) : .177
 SECTION LENGTH : .177
 DETACHED LENGTH : .100

DATA: AL E L1 L2 A t delT meth QSYS EMSR
 dim. .18E-04 .70E+10 .110 .110 .022 .009 188 .600 .168E+08 .0060
 edim. .34E-02 .26E+03 12.3 12.3 2.47 1. YS=.266E+08
 RKstep = .10000 F1 = .37E-01 Q = -.17E-02
 RKerror = .00050 F2 = .37E-01 M3 = .5516
 ITerror = .00010

X	C	DW/DX	W	M	S0	F	YP	N
2.5	-.004	-.00	-.0*	-.13	-.05	.91	.09	.351E+00
3.5	-.003	-.00	-.00	.06	.05	.99	-.01	.839E+00
4.5	-.002	-.01	-.01	.22	.14	.91	-.09	.556E+00
5.5	-.002	-.01	-.01	.37	.23	.84	-.16	.501E+00
6.5	-.001	-.01	-.02	.49	.33	.78	-.22	.468E+00
7.5	.000	-.01	-.03	.60	.42	.73	-.27	.445E+00
8.5	.001	-.01	-.04	.68	.51	.69	-.31	.426E+00
9.5	.002	-.01	-.05	.75	.58	.66	-.34	.412E+00
10.5	.003	-.01	-.06	.80	.64	.63	-.37	.402E+00
11.5	.003	-.00	-.06	.82	.67	.62	-.38	.397E+00
12.3	.003	-.00	-.06	.83	.68	.62	-.38	.395E+00

MINL2(W1) : .276
 SECTION LENGTH : .276
 DETACHED LENGTH : .110

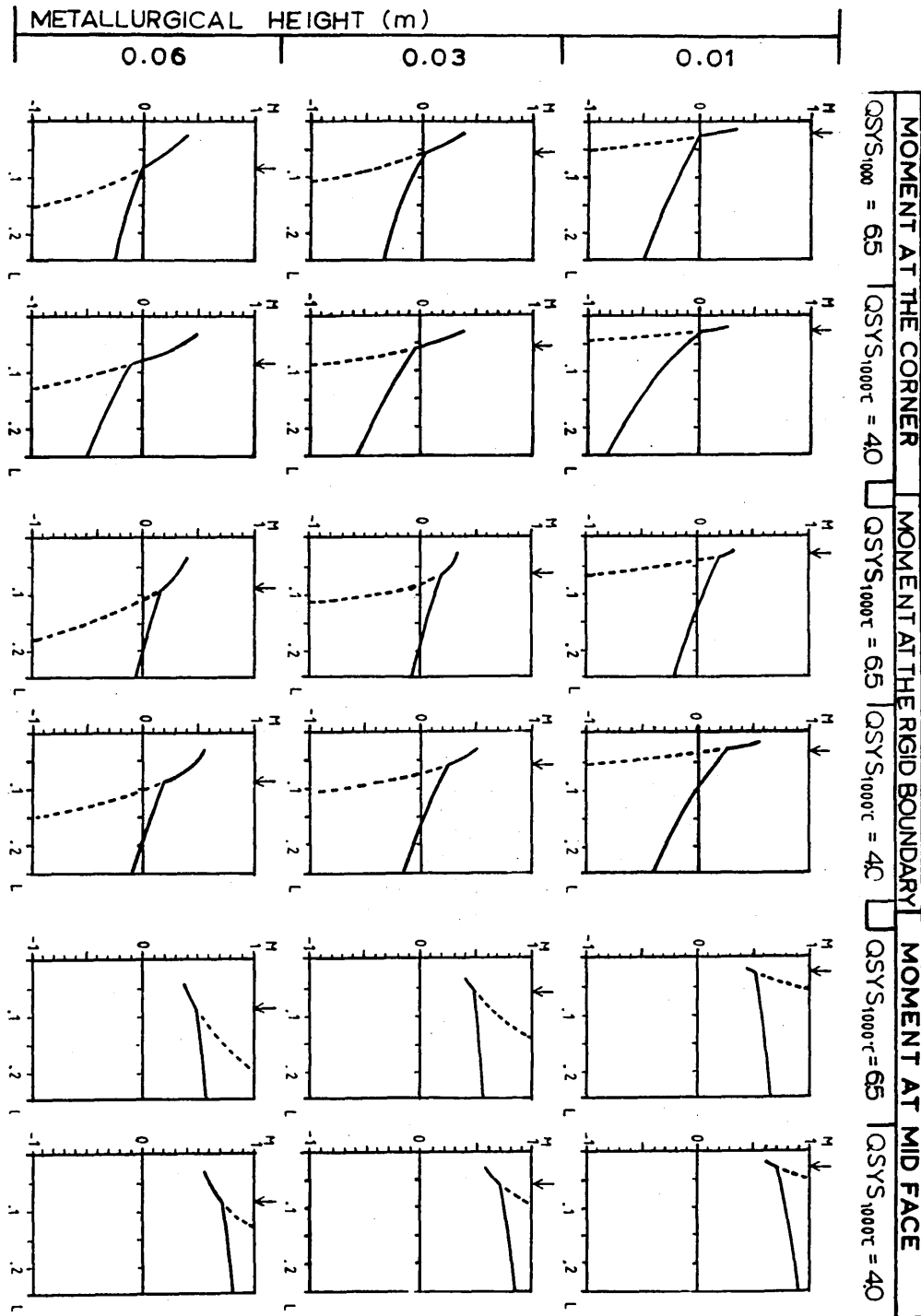
FIG.17 EFFECT OF REDUCING THE YIELD STRESS ON THE MOMENT

QSYS_{1000°C}: QUASI STATIC YIELD STRESS AT 1000 °C, ($\times 10^7$ N/m²)

M: MOMENT (ADIMENSIONAL)
L: HALF BILLET SECTION (m)

— SUPPORTED SECTION
- - - UNSUPPORTED SECTION

CASTING SPEED = 0.06 m/sec



MOMENT AT THE CORNER
 QSYS_{1000°C} = 65 | QSYS_{1000°C} = 40
MOMENT AT THE RIGID BOUNDARY
 QSYS_{1000°C} = 65 | QSYS_{1000°C} = 40
MOMENT AT MID FACE
 QSYS_{1000°C} = 65 | QSYS_{1000°C} = 40

6.5 : THE EFFECT OF DOUBLING THE YOUNG'S MODULUS ON THE RESULTS PREDICTED FOR BILLETS WITHIN THE MOULD

The value of the Young's modulus was changed from 7×10^9 to 15×10^9 N.m⁻². The effect of this change is shown in figure 18 (page 6:67), typical results are presented on tables 16 to 18 (pages 6:61-66). The moments at any point along the shell become more positive. There is also an increase in the minimum section length at which the unsupported and supported moments diverge, although this increase does not compensate for the increase in the values of the unsupported moment. The minimum section lengths at which the unsupported and supported moments are negative have both increased.

TABLES 16 A/B: RESULTS USING A HIGHER YOUNG'S MODULUS
 CASTING SPEED 0.06 m/sec
 METALLURGICAL HEIGHT 0.1 m

DATA: AL E L1 L2 A t delT meth QSYS EMSR
 UNITS: 'C⁻¹ N.m⁻² m m m m 'C m N.m⁻² N.m⁻²

DATA: AL E L1 L2 A t delT meth QSYS EMSR
 dim. .18E-04 .15E+11 .030 .030 .007 .002 67 .100 .970E+07 .0060
 edim. .12E-02 .98E+03 13.8 13.8 3.00 1. YS=.154E+08
 RKstep = .10000 F1 = .12E-01 Q = -.48E-03
 RKerror = .00050 F2 = .12E-01 M3 = -.2539
 ITerror = .00010

X	C	DW/DX	W	M	S0	P	YF	N
3.0	-.001	.00	.0*	.43	.27	.80	-.20	.454E+00
4.0	-.000	-.0*	-.0*	.48	.32	.77	-.23	.444E+00
5.0	-.000	-.0*	-.0*	.54	.37	.74	-.26	.434E+00
6.0	-.000	-.00	-.00	.59	.41	.72	-.28	.425E+00
7.0	-.000	-.00	-.00	.63	.45	.70	-.30	.417E+00
8.0	.000	-.00	-.00	.66	.49	.68	-.32	.410E+00
9.0	.000	-.00	-.01	.69	.52	.66	-.34	.405E+00
10.0	.000	-.00	-.01	.72	.55	.65	-.35	.400E+00
11.0	.000	-.0*	-.01	.74	.58	.64	-.36	.396E+00
12.0	.000	-.0*	-.01	.75	.59	.64	-.36	.394E+00
13.0	.000	-.0*	-.01	.76	.60	.63	-.37	.392E+00
13.7	.000	.0*	-.01	.76	.60	.63	-.37	.392E+00

MINL2(W1) : .028
 SECTION LENGTH : .030
 DETACHED LENGTH : .030

DATA: AL E L1 L2 A t delT meth QSYS EMSR
 dim. .18E-04 .15E+11 .040 .040 .007 .002 67 .100 .970E+07 .0060
 edim. .12E-02 .98E+03 18.3 18.3 3.00 1. YS=.154E+08
 RKstep = .10000 F1 = .17E-01 Q = -.48E-03
 RKerror = .00050 F2 = .17E-01 M3 = .0633
 ITerror = .00010

X	C	DW/DX	W	M	S0	P	YF	N
3.0	-.001	-.00	-.0*	.17	.10	.92	-.08	.524E+00
4.0	-.001	-.00	-.0*	.26	.15	.88	-.12	.497E+00
5.0	-.001	-.00	-.00	.34	.21	.84	-.16	.478E+00
6.0	-.001	-.00	-.00	.41	.26	.81	-.19	.462E+00
7.0	-.000	-.00	-.01	.48	.32	.77	-.23	.449E+00
8.0	-.000	-.00	-.01	.54	.37	.74	-.26	.437E+00
9.0	-.000	-.00	-.01	.60	.43	.71	-.29	.426E+00
10.0	-.000	-.00	-.02	.65	.48	.69	-.31	.416E+00
11.0	.000	-.00	-.02	.70	.53	.67	-.33	.408E+00
12.0	.000	-.00	-.03	.73	.57	.65	-.35	.400E+00
13.0	.000	-.00	-.03	.77	.61	.63	-.37	.393E+00
14.0	.001	-.00	-.03	.80	.65	.62	-.38	.388E+00
15.0	.001	-.00	-.03	.82	.68	.61	-.39	.383E+00
16.0	.001	-.00	-.04	.83	.70	.60	-.40	.380E+00
17.0	.001	-.00	-.04	.84	.72	.59	-.41	.378E+00
18.0	.001	-.00	-.04	.85	.72	.59	-.41	.377E+00
18.3	.001	-.00	-.04	.85	.72	.59	-.41	.377E+00

MINL2(W1) : .111
 SECTION LENGTH : .111
 DETACHED LENGTH : .040

TABLES 16 C/D: RESULTS USING A HIGHER YOUNG'S MODULUS

CASTING SPEED 0.06 m/sec

METALLURGICAL HEIGHT 0.1 m

DATA: AL E L1 L2 A t delT meth QSYS EMSR
 UNITS: 'C⁻¹ N.m⁻² m m m m 'C m N.m⁻² N.m⁻²

DATA: AL E L1 L2 A t delT meth QSYS EMSR
 dim. .18E-04 .15E+11 .050 .050 .007 .002 67 .100 .970E+07 .0060
 edim. .12E-02 .98E+03 22.9 22.9 3.00 1. YS=.154E+08
 RKstep = .10000 F1 = .21E-01 Q = -.48E-03
 RKerror = .00050 F2 = .21E-01 M3 = .4949
 ITerror = .00010

X	C	DW/DX	W	M	S0	P	YF	N
3.0	-.001	-.00	-.0*	-.19	-.10	.89	.11	.423E+00
4.0	-.001	-.00	-.0*	-.08	-.03	.95	.05	.364E+00
5.0	-.001	-.00	-.00	.03	.02	1.00	-.00	.902E+00
6.0	-.001	-.00	-.01	.13	.08	.95	-.05	.567E+00
7.0	-.001	-.00	-.01	.22	.13	.90	-.10	.518E+00
8.0	-.001	-.01	-.02	.31	.19	.86	-.14	.491E+00
9.0	-.001	-.01	-.02	.39	.25	.82	-.18	.472E+00
10.0	-.001	-.01	-.03	.47	.31	.78	-.22	.456E+00
11.0	-.000	-.01	-.04	.54	.37	.75	-.25	.442E+00
12.0	-.000	-.01	-.04	.61	.43	.71	-.29	.429E+00
13.0	.000	-.01	-.05	.67	.49	.68	-.32	.417E+00
14.0	.000	-.01	-.06	.72	.55	.66	-.34	.406E+00
15.0	.000	-.01	-.07	.77	.61	.63	-.37	.396E+00
16.0	.001	-.01	-.07	.81	.66	.61	-.39	.388E+00
17.0	.001	-.01	-.08	.85	.72	.60	-.40	.380E+00
18.0	.001	-.01	-.09	.88	.76	.58	-.42	.374E+00
19.0	.001	-.00	-.09	.90	.80	.57	-.43	.368E+00
20.0	.001	-.00	-.10	.92	.83	.56	-.44	.364E+00
21.0	.001	-.00	-.10	.94	.85	.55	-.45	.361E+00
22.0	.001	-.00	-.10	.95	.87	.55	-.45	.359E+00
22.9	.001	-.00	-.10	.95	.87	.55	-.45	.359E+00

MINL2(W1) : .283
 SECTION LENGTH : .283
 DETACHED LENGTH : .050

TABLES 17 A/B: RESULTS USING A HIGHER YOUNG'S MODULUS
 CASTING SPEED 0.06 m/sec
 METALLURGICAL HEIGHT 0.3 m

DATA: AL E L1 L2 A t delT meth QSYS EMSR
 UNITS: 'C⁻¹ N.m⁻² m m m m 'C m N.m⁻² N.m⁻²

DATA: AL E L1 L2 A t delT meth QSYS EMSR
 dim. .18E-04 .15E+11 .065 .065 .015 .005 134 .300 .194E+08 .0060
 adim. .24E-02 .49E+03 11.9 11.9 2.75 1. YS=.308E+08
 RKstep = .10000 F1 = .16E-01 Q = -.72E-03
 RKerror = .00050 F2 = .16E-01 M3 = -.2122
 ITerror = .00010

X	C	DW/DX	W	M	S0	F	YP	N
2.8	-.001	-.00	-.0*	.41	.26	.81	-.19	.462E+00
3.8	-.001	-.00	-.0*	.48	.32	.77	-.23	.447E+00
4.8	-.001	-.00	-.00	.55	.38	.74	-.26	.435E+00
5.8	-.000	-.00	-.00	.61	.43	.71	-.29	.424E+00
6.8	-.000	-.00	-.01	.66	.48	.68	-.32	.414E+00
7.8	.000	-.00	-.01	.70	.53	.67	-.33	.407E+00
8.8	.000	-.00	-.01	.73	.56	.65	-.35	.401E+00
9.8	.001	-.00	-.01	.75	.59	.64	-.36	.396E+00
10.8	.001	-.00	-.01	.76	.61	.63	-.37	.393E+00
11.8	.001	-.00	-.02	.77	.61	.63	-.37	.392E+00
11.8	.001	.00	-.02	.77	.61	.63	-.37	.392E+00

MINL2(W1) : .056
 SECTION LENGTH : .065
 DETACHED LENGTH : .065

DATA: AL E L1 L2 A t delT meth QSYS EMSR
 dim. .18E-04 .15E+11 .070 .070 .015 .005 134 .300 .194E+08 .0060
 adim. .24E-02 .49E+03 12.8 12.8 2.75 1. YS=.308E+08
 RKstep = .10000 F1 = .17E-01 Q = -.72E-03
 RKerror = .00050 F2 = .17E-01 M3 = -.1393
 ITerror = .00010

X	C	DW/DX	W	M	S0	F	YP	N
2.8	-.001	.00	.0*	.35	.22	.83	-.17	.475E+00
3.8	-.001	-.00	-.0*	.44	.28	.79	-.21	.458E+00
4.8	-.001	-.00	-.00	.51	.34	.76	-.24	.443E+00
5.8	-.001	-.00	-.01	.58	.40	.73	-.27	.431E+00
6.8	-.000	-.00	-.01	.63	.46	.70	-.30	.420E+00
7.8	.000	-.00	-.01	.68	.51	.67	-.33	.411E+00
8.8	.000	-.00	-.01	.72	.55	.65	-.35	.403E+00
9.8	.001	-.00	-.02	.75	.59	.64	-.36	.397E+00
10.8	.001	-.00	-.02	.77	.62	.63	-.37	.393E+00
11.8	.001	-.00	-.02	.78	.63	.62	-.38	.390E+00
12.8	.001	-.00	-.02	.79	.64	.62	-.38	.389E+00
12.8	.001	.00	-.02	.79	.64	.62	-.38	.389E+00

MINL2(W1) : .080
 SECTION LENGTH : .080
 DETACHED LENGTH : .070

TABLES 17 C/D: RESULTS USING A HIGHER YOUNG'S MODULUS
 CASTING SPEED 0.06 m/sec
 METALLURGICAL HEIGHT 0.3 m

DATA: AL E L1 L2 A t delT meth QSYS EMSR
 UNITS: 'C⁻¹ N.m⁻² m m m m 'C m N.m⁻² N.m⁻²

DATA: AL E L1 L2 A t delT meth QSYS EMSR
 dim. .18E-04 .15E+11 .085 .085 .015 .005 134 .300 .194E+08 .0060
 edim. .24E-02 .49E+03 15.5 15.5 2.75 1. YS=.308E+08
 RKstep = .10000 F1 = .21E-01 Q = -.72E-03
 RKerror = .00050 F2 = .21E-01 M3 = .1147
 ITerror = .00010

X	C	DW/DX	W	M	S0	P	YF	N
2.8	-.002	.00	.0*	.15	.09	.93	-.07	.547E+00
3.8	-.002	-.00	-.0*	.26	.16	.88	-.12	.505E+00
4.8	-.001	-.00	-.00	.36	.22	.84	-.16	.480E+00
5.8	-.001	-.00	-.01	.45	.29	.79	-.21	.460E+00
6.8	-.001	-.01	-.01	.53	.36	.75	-.25	.444E+00
7.8	-.000	-.01	-.02	.60	.42	.72	-.28	.430E+00
8.8	-.000	-.01	-.03	.66	.49	.69	-.31	.418E+00
9.8	.000	-.01	-.03	.71	.55	.66	-.34	.407E+00
10.8	.001	-.01	-.04	.76	.60	.64	-.36	.398E+00
11.8	.001	-.01	-.04	.80	.65	.62	-.38	.391E+00
12.8	.001	-.00	-.05	.82	.68	.61	-.39	.385E+00
13.8	.001	-.00	-.05	.84	.71	.60	-.40	.381E+00
14.8	.002	-.00	-.05	.86	.73	.59	-.41	.378E+00

MINL2(W1) : .199
 SECTION LENGTH : .199
 DETACHED LENGTH : .085

DATA: AL E L1 L2 A t delT meth QSYS EMSR
 dim. .18E-04 .15E+11 .090 .090 .015 .005 134 .300 .194E+08 .0060
 edim. .24E-02 .49E+03 16.5 16.5 2.75 1. YS=.308E+08
 RKstep = .10000 F1 = .22E-01 Q = -.72E-03
 RKerror = .00050 F2 = .22E-01 M3 = .2123
 ITerror = .00010

X	C	DW/DX	W	M	S0	P	YF	N
2.8	-.002	-.00	-.0*	.07	.05	.97	-.03	.641E+00
3.8	-.002	-.00	-.00	.19	.11	.92	-.08	.534E+00
4.8	-.002	-.00	-.00	.29	.18	.87	-.13	.498E+00
5.8	-.001	-.01	-.01	.39	.25	.82	-.18	.474E+00
6.8	-.001	-.01	-.02	.48	.32	.78	-.22	.455E+00
7.8	-.001	-.01	-.02	.56	.38	.74	-.26	.439E+00
8.8	-.000	-.01	-.03	.63	.45	.70	-.30	.425E+00
9.8	.000	-.01	-.04	.69	.52	.67	-.33	.413E+00
10.8	.001	-.01	-.05	.74	.58	.65	-.35	.402E+00
11.8	.001	-.01	-.05	.79	.63	.63	-.37	.393E+00
12.8	.001	-.01	-.06	.82	.68	.61	-.39	.386E+00
13.8	.001	-.00	-.06	.85	.72	.59	-.41	.380E+00
14.8	.002	-.00	-.07	.87	.75	.59	-.41	.376E+00
15.8	.002	-.00	-.07	.88	.76	.58	-.42	.374E+00

MINL2(W1) : .257
 SECTION LENGTH : .257
 DETACHED LENGTH : .090

TABLES 18 A/B: RESULTS USING A HIGHER YOUNG'S MODULUS
 CASTING SPEED 0.06 m/sec
 METALLURGICAL HEIGHT 0.6 m

DATA: AL E L1 L2 A t delT meth QSYS EMSR
 UNITS: 'C⁻¹ N.m⁻² m m m m 'C m N.m⁻² N.m⁻²

DATA: AL E L1 L2 A t delT meth QSYS EMSR
 dim. .18E-04 .15E+11 .095 .095 .022 .009 188 .600 .272E+08 .0060
 bdim. .34E-02 .35E+03 10.6 10.6 2.47 1. YS=.432E+08
 RKstep = .10000 F1 = .20E-01 Q = -.10E-02
 RKerror = .00050 F2 = .20E-01 M3 = -.1604
 ITerror = .00010

X	C	DW/DX	W	M	S0	P	YF	N
2.5	-.002	.00	.0*	.38	.24	.82	-.18	.473E+00
3.5	-.001	-.00	-.0*	.47	.31	.78	-.22	.454E+00
4.5	-.001	-.00	-.00	.55	.38	.74	-.26	.438E+00
5.5	-.000	-.00	-.01	.62	.45	.70	-.30	.424E+00
6.5	.000	-.00	-.01	.68	.51	.68	-.32	.413E+00
7.5	.001	-.00	-.01	.73	.56	.65	-.35	.404E+00
8.5	.001	-.00	-.02	.76	.60	.64	-.36	.398E+00
9.5	.001	-.00	-.02	.78	.62	.63	-.37	.393E+00
10.5	.001	-.00	-.02	.79	.63	.62	-.38	.392E+00
10.5	.001	.00	-.02	.79	.63	.62	-.38	.392E+00

MINL2(W1) : .080
 SECTION LENGTH : .095
 DETACHED LENGTH : .095

DATA: AL E L1 L2 A t delT meth QSYS EMSR
 dim. .18E-04 .15E+11 .100 .100 .022 .009 188 .600 .272E+08 .0060
 bdim. .34E-02 .35E+03 11.2 11.2 2.47 1. YS=.432E+08
 RKstep = .10000 F1 = .21E-01 Q = -.10E-02
 RKerror = .00050 F2 = .21E-01 M3 = -.1041
 ITerror = .00010

X	C	DW/DX	W	M	S0	P	YF	N
2.5	-.002	.00	.0*	.34	.21	.85	-.15	.484E+00
3.5	-.002	-.00	-.0*	.44	.28	.80	-.20	.462E+00
4.5	-.001	-.00	-.00	.53	.36	.75	-.25	.444E+00
5.5	-.001	-.00	-.01	.60	.43	.72	-.28	.429E+00
6.5	-.000	-.00	-.01	.67	.49	.68	-.32	.417E+00
7.5	.000	-.00	-.02	.72	.55	.66	-.34	.407E+00
8.5	.001	-.00	-.02	.76	.60	.64	-.36	.399E+00
9.5	.001	-.00	-.02	.78	.63	.63	-.37	.393E+00
10.5	.001	-.00	-.02	.80	.65	.62	-.38	.390E+00

MINL2(W1) : .105
 SECTION LENGTH : .105
 DETACHED LENGTH : .100

TABLES 18 C/D: RESULTS USING A HIGHER YOUNG'S MODULUS
 CASTING SPEED 0.06 m/sec
 METALLURGICAL HEIGHT 0.6 m

DATA: AL E L1 L2 A t delT meth QSYS EMSR
 UNITS: 'C⁻¹ N.m⁻² m m m m 'C m N.m⁻² N.m⁻²

DATA: AL E L1 L2 A t delT meth QSYS EMSR
 dim. .18E-04 .15E+11 .115 .115 .022 .009 188 .600 .272E+08 .0060
 edim. .34E-02 .35E+03 12.8 12.8 2.47 1. YS=.432E+08
 RKstep = .10000 F1 = .24E-01 Q = -.10E-02
 RKerror = .00050 F2 = .24E-01 M3 = .0787
 ITerror = .00010

X	C	DW/DX	W	M	S0	P	YP	N
2.5	-.003	-.00	-.0*	.19	.12	.92	-.08	.537E+00
3.5	-.002	-.00	-.00	.31	.19	.86	-.14	.495E+00
4.5	-.002	-.00	-.01	.42	.27	.80	-.20	.469E+00
5.5	-.001	-.01	-.01	.52	.35	.76	-.24	.449E+00
6.5	-.001	-.01	-.02	.60	.43	.72	-.28	.432E+00
7.5	.000	-.01	-.02	.68	.50	.68	-.32	.417E+00
8.5	.001	-.01	-.03	.74	.57	.65	-.35	.405E+00
9.5	.001	-.01	-.04	.78	.63	.63	-.37	.395E+00
10.5	.002	-.00	-.04	.82	.67	.61	-.39	.388E+00
11.5	.002	-.00	-.05	.84	.71	.60	-.40	.383E+00
12.5	.002	-.00	-.05	.85	.72	.60	-.40	.381E+00
12.8	.002	.00	-.05	.85	.72	.59	-.41	.381E+00

MINL2(W1) : .202
 SECTION LENGTH : .202
 DETACHED LENGTH : .115

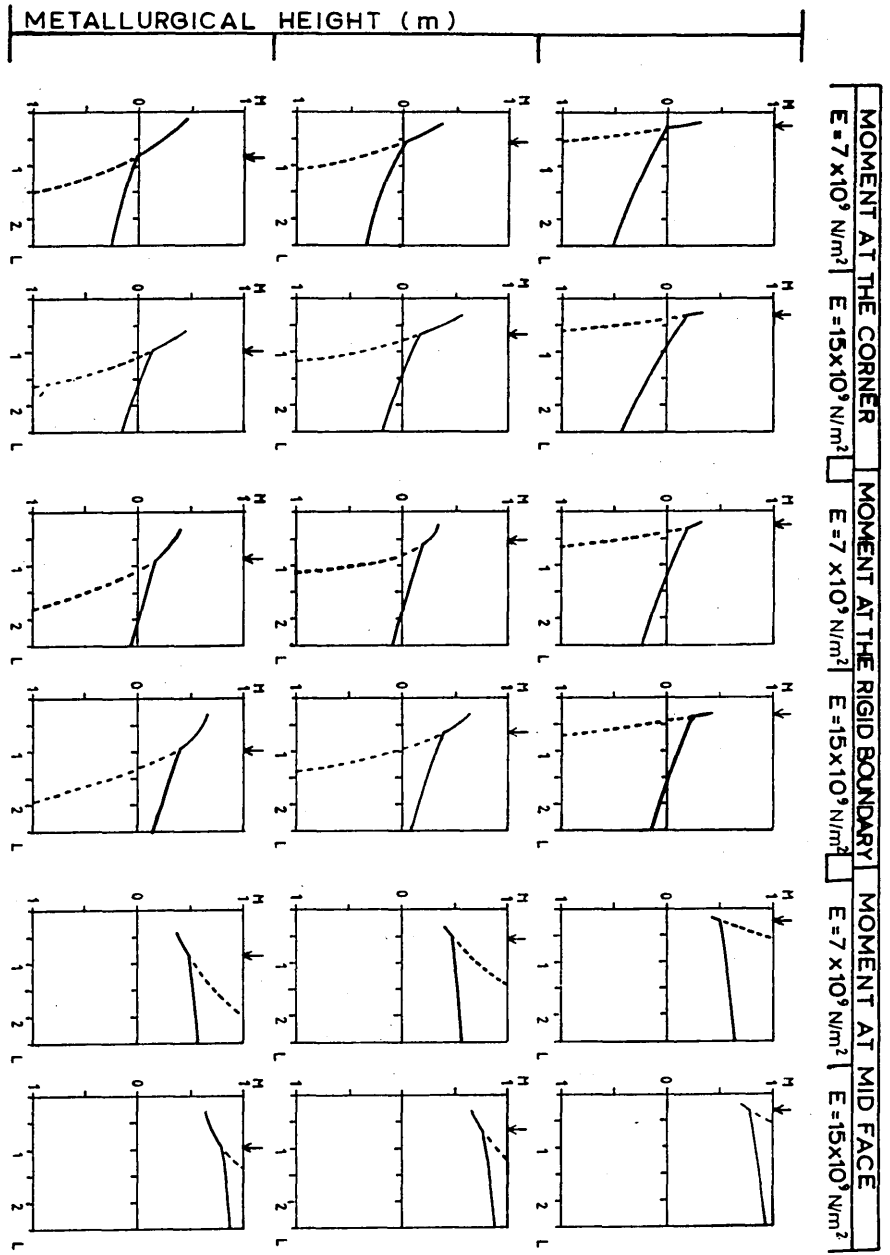
DATA: AL E L1 L2 A t delT meth QSYS EMSR
 dim. .18E-04 .15E+11 .120 .120 .022 .009 188 .600 .272E+08 .0060
 edim. .34E-02 .35E+03 13.4 13.4 2.47 1. YS=.432E+08
 RKstep = .10000 F1 = .25E-01 Q = -.10E-02
 RKerror = .00050 F2 = .25E-01 M3 = .1499
 ITerror = .00010

X	C	DW/DX	W	M	S0	P	YP	N
2.5	-.003	.00	.0*	.14	.08	.95	-.05	.576E+00
3.5	-.003	-.00	-.00	.26	.16	.88	-.12	.512E+00
4.5	-.002	-.00	-.01	.38	.24	.83	-.17	.481E+00
5.5	-.001	-.01	-.01	.48	.32	.78	-.22	.458E+00
6.5	-.001	-.01	-.02	.57	.40	.73	-.27	.439E+00
7.5	-.000	-.01	-.03	.65	.48	.69	-.31	.423E+00
8.5	.000	-.01	-.03	.72	.55	.66	-.34	.409E+00
9.5	.001	-.01	-.04	.77	.62	.63	-.37	.398E+00
10.5	.002	-.01	-.05	.82	.67	.61	-.39	.390E+00
11.5	.002	-.00	-.05	.85	.71	.60	-.40	.383E+00
12.5	.002	-.00	-.06	.86	.74	.59	-.41	.380E+00
13.4	.002	-.00	-.06	.87	.74	.59	-.41	.379E+00

MINL2(W1) : .246
 SECTION LENGTH : .246
 DETACHED LENGTH : .120

FIG.18 EFFECT OF DOUBLING THE YOUNG'S MODULUS ON THE MOMENT

E : YOUNG'S MODULUS ($\times 10^9$ N/m²) M : MOMENT (ADIMENSIONAL) — SUPPORTED SECTION
 L : HALF BILLET SECTION (m) - - - UNSUPPORTED SECTION



6.6 ANALYSIS OF OFF CORNER CRACKING IN A SLAB

Fig 19 (Page 6:71) shows the deflected corner section of a 1300 mm x 300 mm slab cast at a high speed of 0.03 m.s^{-1} at a metallurgical height of 0.1 m, that is high in the mould. The numerical results obtained from the computer for this case and the data used are presented as a table within the figure. All the distances in the figure are adimensional, representing fractions of the actual solid metal thickness. Three different scales have been used, however. Distances along the section have been drawn to a scale that is half that used for the thickness and deflections of the section away from the mould wall have been drawn to a scale that is five times the thickness scale.

Only the detached length of the solidifying shell are presented. Of the 650 mm to the middle of the long face, only 78 mm has become detached from the mould wall in the vicinity of the corner. The short face, measuring only 150 mm up to the axis of symmetry, is slightly more detached than the long face - 81 mm. It can be seen that the gap between the short face of the section and the mould wall is greater in the corner than the gap between the long face and the mould wall. This is due to the greater magnitude of the contraction experienced by the long face by virtue of its greater length. That this greater gap does not result in a much larger difference between the detached lengths of the two sides is due to the rotation of the corner. It can be seen that the corner rotates towards the short face of the mould, this

rotation shortening the detached length of the short face and lengthening that of the long face. The corner rotates in an attempt to equalise the detached lengths along the two faces.

The dotted area represents plasticity. The distance between the surface of the slab and the elasto-plastic boundary is given by p . Note that the plastic region diminishes on approaching the corner along both shells until it reaches a point where $p = t$. Data in the table show that the stress in this plastic region is compressive (Y_P is the yield stress at the plastic limit, negative in compression). Between the point where $p = t$ and the corner itself, however, the plastic stress is tensile. The point where $p = t$ is thus a point of inflection for the moment, although it does not coincide with the point of inflection for the curvature. This latter point is also indicated in the figure.

Figure 19 shows tensile plasticity at the solidification front in the corner region. This is a necessary condition for the formation of internal cracks.

Figure 20, on page 6:72 shows the effect of reducing the casting speed. The figure has been drawn for conditions that are identical to those for which Figure 19 was drawn, except for the casting speed which has been reduced from 0.03 m.s^{-1} to 0.02 m.s^{-1} . In particular, it is worth noting that the figures has been drawn for the same metallurgical height.

Figure 20 shows that the effect of the reduction in casting speed has been to 'move' the point of moment inflection into

the corner so that the entire section is in compression at the solidification front. Thus the conditions necessary for the generation of internal cracks in the off corner region are removed.

The computer results from which this graph has been drawn are shown in the table that is on the accompanying page, Page 6:73, as are the values used to obtain the results.

The numerical results show that a second effect of reducing the casting speed has been to reduce the magnitude of the adimensional moment at the corner by a factor greater than 2 and to reduce the moment at all points along the length, although by a factor that diminishes with distance from the corner.

The data also shows that the detached lengths have both been increased by some 26% as the section is thicker and stronger. The gap between the short face and the mould has been more or less unaffected by the speed change reduction, whereas the gap between the long face and the mould has been increased marginally - from 0.8 mm to 0.9 mm. This increase is due to the greater contraction of the long face at this lower casting speed due to its lower average temperature.

FIG. 19 1300mm x 300mm
SLAB
CAST AT HIGH SPEED
(CS=0.03m/sec)
HIGH IN THE MOULD
(met.Height=0.1m)

DATA: M. E L1 L2 A t delT meth OSYS EMSF
dim. .18E-04 .70E+10 .078 .081 .011 .004 106 .100 .710E+07 .0060
dim. .19E-02 .62E+03 19.7 20.4 2.87 1. YS=.113E+08
RKstep = .10000 F1 = .25E-01 D = -.65E-03
Ferror = .00050 F2 = .24E-01 M3 = .5475
ITerror = .00010

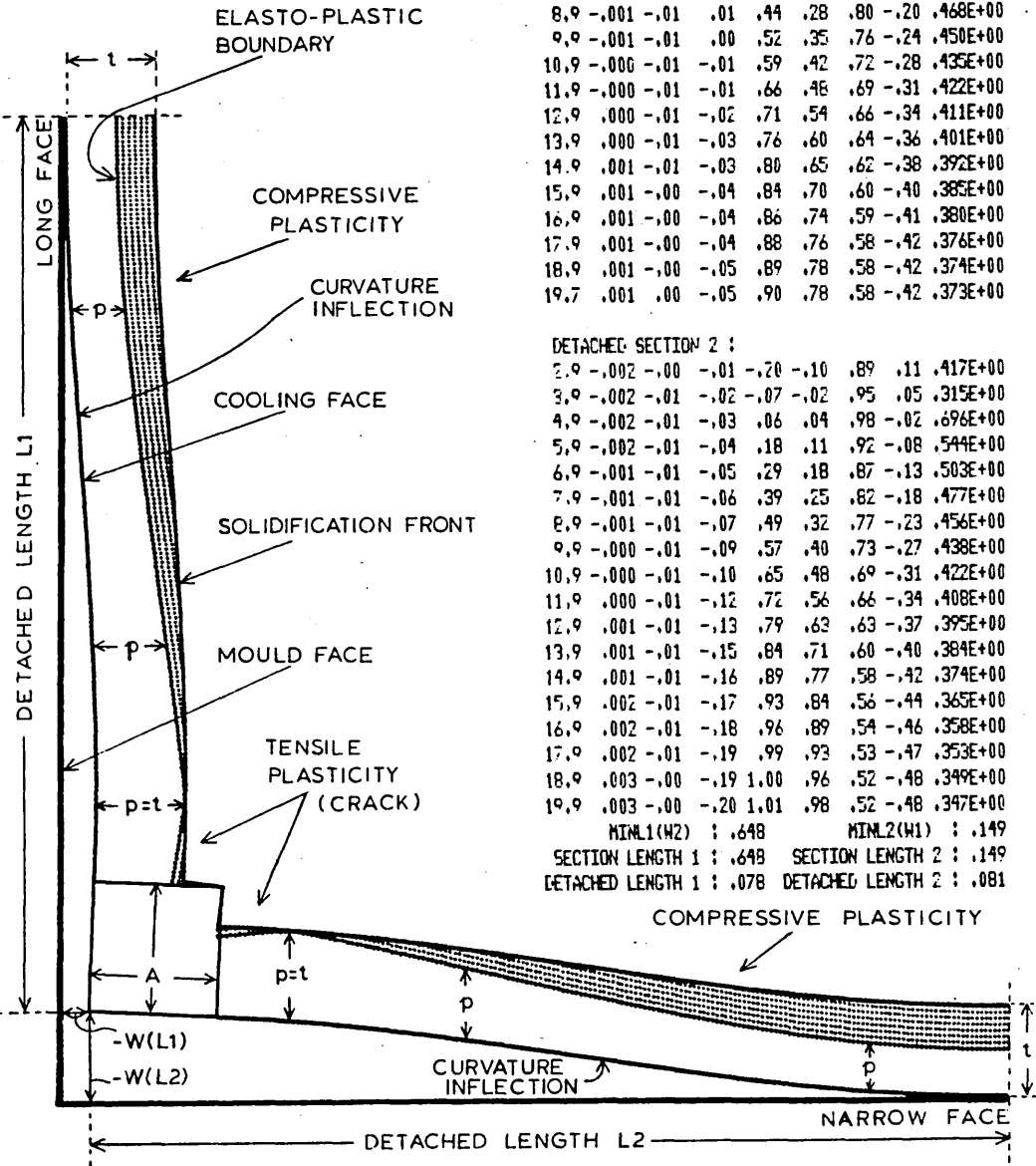
Scale:

- 0.8 mm
- 4.0 mm
- 8.0 mm

W(X)

t, p

L₁, L₂, A, X



DETACHED SECTION 1 :

X	C	DW/DX	W	H	SO	P	YP	N
2.9	-.002	.00	.01	-.21	-.11	.88	.12	.416E+00
3.9	-.002	.00	.02	-.09	-.03	.94	.06	.349E+00
4.9	-.002	.00	.02	.03	.03	1.00	-.00	.867E+00
5.9	-.002	-.00	.02	.15	.09	.94	-.06	.567E+00
6.9	-.001	-.00	.02	.25	.15	.89	-.11	.516E+00
7.9	-.001	-.00	.01	.35	.22	.84	-.16	.488E+00
8.9	-.001	-.01	.01	.44	.28	.80	-.20	.468E+00
9.9	-.001	-.01	.00	.52	.35	.76	-.24	.450E+00
10.9	-.000	-.01	-.01	.59	.42	.72	-.28	.435E+00
11.9	-.000	-.01	-.01	.66	.48	.69	-.31	.422E+00
12.9	-.000	-.01	-.02	.71	.54	.66	-.34	.411E+00
13.9	.000	-.01	-.03	.76	.60	.64	-.36	.401E+00
14.9	.001	-.01	-.03	.80	.65	.62	-.38	.392E+00
15.9	.001	-.00	-.04	.84	.70	.60	-.40	.385E+00
16.9	.001	-.00	-.04	.86	.74	.59	-.41	.380E+00
17.9	.001	-.00	-.04	.88	.76	.58	-.42	.376E+00
18.9	.001	-.00	-.05	.89	.78	.58	-.42	.374E+00
19.7	.001	.00	-.05	.90	.78	.58	-.42	.373E+00

DETACHED SECTION 2 :

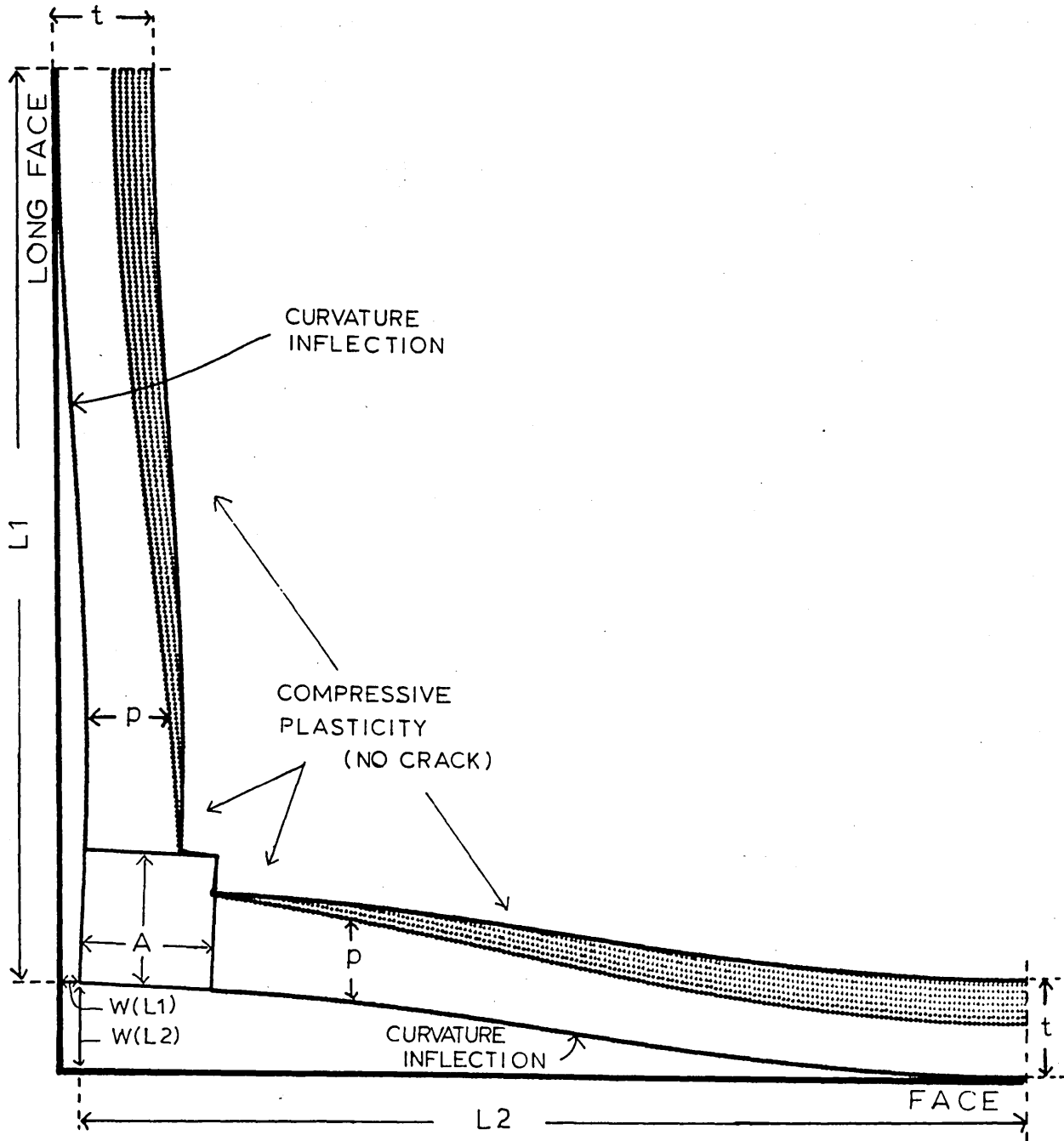
2.9	-.002	-.00	-.01	-.70	-.10	.89	.11	.417E+00
3.9	-.002	-.01	-.02	-.07	-.02	.95	.05	.315E+00
4.9	-.002	-.01	-.03	.06	.04	.98	-.02	.696E+00
5.9	-.002	-.01	-.04	.18	.11	.92	-.08	.544E+00
6.9	-.001	-.01	-.05	.29	.18	.87	-.13	.503E+00
7.9	-.001	-.01	-.06	.39	.25	.82	-.18	.477E+00
8.9	-.001	-.01	-.07	.49	.32	.77	-.23	.456E+00
9.9	-.000	-.01	-.09	.57	.40	.73	-.27	.438E+00
10.9	-.000	-.01	-.10	.65	.48	.69	-.31	.422E+00
11.9	.000	-.01	-.12	.72	.56	.66	-.34	.408E+00
12.9	.001	-.01	-.13	.79	.63	.63	-.37	.395E+00
13.9	.001	-.01	-.15	.84	.71	.60	-.40	.384E+00
14.9	.001	-.01	-.16	.89	.77	.58	-.42	.374E+00
15.9	.002	-.01	-.17	.93	.84	.56	-.44	.365E+00
16.9	.002	-.01	-.18	.96	.89	.54	-.46	.358E+00
17.9	.002	-.01	-.19	.99	.93	.53	-.47	.353E+00
18.9	.003	-.00	-.19	1.00	.96	.52	-.48	.349E+00
19.9	.003	-.00	-.20	1.01	.98	.52	-.48	.347E+00

MIN1(W2) : .648 MIN2(W1) : .149
SECTION LENGTH 1 : .648 SECTION LENGTH 2 : .149
DETACHED LENGTH 1 : .078 DETACHED LENGTH 2 : .081

FIG. 20 1300mmx 300mm
 SLAB
 CAST AT INTERMEDIATE
 SPEED (CS = 0.02 m/sec)
 METALLURGICAL
 HEIGHT = 0.1 m

DATA AND RESULTS TABLE
 ON NEXT PAGE

- 1mm $W(X)$
- 5mm t, p
- 10mm L_1, L_2, A, X



DATA AND RESULTS TABLE FOR FIGURE 20

DATA: AL E L1 L2 A t delT meth QSYS EMSR
 dim. .18E-04 .70E+10 .1034 .1079 .015 .005 134 .100 .896E+07 .0060
 adim. .24E-02 .49E+03 18.91 19.73 2.75 1. YS=.142E+08
 RKstep = .10000 F1 = .19E-01 Q = -.52E-03
 RKerror = .00050 F2 = .19E-01 M3 = .2103
 ITerror = .00010

DETACHED SECTION 1 :

X	C	DW/DX	W	M	S0	P	YP	N
2.8	-.002	.00	.01	.03	.03	.99	-.01	.810E+00
3.8	-.002	.00	.02	.13	.08	.95	-.05	.559E+00
4.8	-.002	.00	.02	.22	.13	.90	-.10	.514E+00
5.8	-.002	-.00	.02	.30	.19	.86	-.14	.490E+00
6.8	-.001	-.00	.01	.38	.24	.82	-.18	.472E+00
7.8	-.001	-.00	.01	.46	.30	.79	-.21	.457E+00
8.8	-.001	-.01	.00	.52	.35	.75	-.25	.444E+00
9.8	-.001	-.01	-.00	.58	.41	.72	-.28	.432E+00
10.8	-.000	-.01	-.01	.64	.46	.70	-.30	.421E+00
11.8	.000	-.01	-.01	.68	.51	.67	-.33	.412E+00
12.8	.000	-.01	-.02	.72	.56	.65	-.35	.404E+00
13.8	.001	-.01	-.03	.76	.60	.64	-.36	.397E+00
14.8	.001	-.00	-.03	.79	.64	.62	-.38	.391E+00
15.8	.001	-.00	-.04	.81	.67	.61	-.39	.386E+00
16.8	.001	-.00	-.04	.83	.69	.60	-.40	.383E+00
17.8	.001	-.00	-.04	.84	.70	.60	-.40	.381E+00
18.8	.001	-.00	-.04	.84	.71	.60	-.40	.380E+00
18.8	.001	.00	-.04	.84	.71	.60	-.40	.380E+00

DETACHED SECTION 2 :

2.8	-.002	-.00	-.01	.04	.03	.99	-.01	.714E+00
3.8	-.002	-.01	-.02	.15	.09	.94	-.06	.545E+00
4.8	-.002	-.01	-.03	.24	.14	.89	-.11	.506E+00
5.8	-.002	-.01	-.03	.33	.20	.85	-.15	.482E+00
6.8	-.001	-.01	-.05	.42	.26	.81	-.19	.464E+00
7.8	-.001	-.01	-.06	.49	.33	.77	-.23	.449E+00
8.8	-.001	-.01	-.07	.56	.39	.73	-.27	.435E+00
9.8	-.000	-.01	-.09	.63	.45	.70	-.30	.422E+00
10.8	.000	-.01	-.10	.69	.52	.67	-.33	.410E+00
11.8	.001	-.01	-.11	.74	.58	.65	-.35	.400E+00
12.8	.001	-.01	-.13	.79	.64	.62	-.38	.391E+00
13.8	.001	-.01	-.14	.83	.69	.60	-.40	.383E+00
14.8	.002	-.01	-.15	.86	.74	.59	-.41	.375E+00
15.8	.002	-.01	-.16	.89	.78	.57	-.43	.370E+00
16.8	.002	-.01	-.17	.91	.81	.56	-.44	.365E+00
17.8	.002	-.00	-.17	.93	.84	.55	-.45	.362E+00
18.8	.002	-.00	-.18	.94	.85	.55	-.45	.360E+00
19.7	.002	.00	-.18	.94	.86	.55	-.45	.359E+00

MINL1(W2) : .650 MINL2(W1) : .149
 SECTION LENGTH 1: .650 SECTION LENGTH 2: .149
 DETACHED LENGTH 1: .10340 DETACHED LENGTH 2: .10790

6.7 ANALYSIS OF CRACK PROGRESSION WITHIN THE MOULD DURING THE CASTING OF SQUARE BILLETS

In a final analysis, the progression within the mould of off corner cracks in square billets was investigated.

The results presented in figure 12 (page 6:39) were used to determine the relationship between casting speed, metallurgical height, total section length and detached length. Table 19 below summarises a typical set of results from that analysis for a casting speed of 0.01 m.s^{-1} .

Table 19: Relationship between section length, detached length and metallurgical height for a casting speed of 0.01 m.s^{-1}

Section length/mm	Metallurgical Height/mm					
	0.1	0.2	0.3	0.4	0.5	0.6
140	140					
183	150	183				
203	153	187	203			
216	154	190	206	216		
220	155	191	207	216	220	
225	156	192	208	217	222	225
250	152	184	200	200	200	200
300	160	197	213	223	228	231

It shows for example, that for a square billet with a half side of 220 mm and cast at 0.01 m.s^{-1} the length detached from the mould at a metallurgical height of 0.3 m is 207 mm. It then shows that, at this casting speed, the entire section has sufficient strength to become completely detached from the mould at a metallurgical height of 0.5 m.

The data in this and similar tables was used to develop a series of figures showing the distortion in the corner of the section and the regions of plasticity developing there.

Figures 21 to 23 on pages 6:79-81 are drawn for a billet 200 mm square and cast at 0.06 m.s^{-1} . Figure 21 shows the detached sections in the corner at a metallurgical height of 0.1 m, these detached sections being 36 mm long. At this casting speed, there is no tensile plasticity in the off corner region so that these casting conditions would appear perfectly secure.

Figures 22 and 23 show the billet at the same casting speed lower down the mould at metallurgical heights of 0.3 and 0.6 m respectively. The detached lengths along the two faces have increased to 68 mm and 92 mm respectively. This is not obvious from the figures which suggest that the detached lengths have decreased not increased. It must be remembered, however, that the thickness of the solid metal is the basis of the scales used in drawing the figures. The solidified thickness used in drawing figures 21, 22 and 23 are 0.002m, 0.005m and 0.009m respectively so that scales to which the detached lengths have been drawn are in the ratios of these thicknesses.

This change in the scale to which these figures are drawn also obscures the growth that takes place in the thickness of the gap as the billet moves down the mould. The tables of computer results included with each figure show that the width of the gap at the corner is 0.06 mm when the metallurgical

height is 0.1 m, 0.10 mm when the height is 0.3 m and 0.18 mm when the height is 0.6 m.

Figures 22 and 23 show an increase in compressive plasticity in the off corner region as the billet moves down the mould so that there would appear to be no tendency for off corner cracks to form for this sized billet cast at the indicated speed.

The next set of figures on pages 6:82-85 also show an increase in the degree of compressive plasticity as the billet moves down the mould. This set of figures relates to a billet 250 mm square cast at the same speed and shows the distortion of its corner region at the same three values of the metallurgical height.

In this case Figure 24 on page 6:82 shows that tensile plasticity can be seen in the corner region high in the mould at the metallurgical height of 0.001 m which suggest the formation of cracks there. However, the general increase in the degree of compressive plasticity on movement down the mould can be seen in figures 25 and 26 to have removed the region of tensile plasticity suggesting that the crack, once formed, would not grow further while the billet remained in the mould.

The crack could, however, grow immediately the billet emerges from the mould. Figure 27 on page 6:85 has been drawn at the same metallurgical height as figure 26 except that the restraining influence of the mould has been taken away. Since

the thickness of solidified metal is the same in both cases, the scales are the same so that the greater distorted length shown in figure 27 truly represents a greater degree of distortion. Within the mould, figure 26 shows the detached length of the half section to be 96.5 mm and at this length that is unsupported in the mould. Outside the mould, the entire 125 mm of the half section is unsupported so that it immediately bows out to a far greater extent. A high degree of tensile plasticity immediately appears in the off corner region and it is apparent that cracks would now restart to grow in this region.

Figures 28 to 30 on pages 6:86-87 show the effect of decreasing the quasi-static yield stress from $6.5 \times 10^7 \text{ N.m}^{-2}$ to $2.4 \times 10^7 \text{ N.m}^{-2}$. The casting speed has not been reduced, but in order to be able to avoid the development of tensile cracks in the off corner region, it has been necessary to reduce the section size to 166 mm square. As it is, figure 28 shows that a small degree of tensile plasticity forms in the corner regions high in the mould, but this tensile plasticity disappears as the billet moves down the mould (Figures 29 and 30).

The formation and subsequent behaviour of cracks is further analysed in fig 31 on page 6:88 in terms of stress distribution diagrams at the rigid boundary, at the point of curvature inflection and at the mid point of the face (point of attachment).

The top row of diagrams shows the stress distribution across the section at the rigid boundary. This distribution indicates the existence of tensile plasticity at the rigid boundary when the metallurgical height is 0.1 m because the stress distribution line meets the yield stress line on the right of the diagram. The stress distribution at this boundary rotates anti-clockwise as the billet moves down the mould stopping the further growth of the region of tensile plasticity and giving rise to compressive plasticity at the solidification front.

The middle row of stress distribution diagrams show the development of stresses at the point of curvature inflection. Very little change in the stress takes place as the billet moves down the mould and the stresses nowhere approach critical values.

This cannot be said for the stress distributions for the middle of the face shown in the bottom row of diagrams. The left hand diagram shows that the stress at the cooled surface at a point high in the mould (metallurgical height 0.1 m) reaches the elastic limit. This would suggest the formation of a mid-face crack except for the further figures on the bottom row which show that the stress distribution now rotates clockwise with passage down the mould. Thus the region of tensile plasticity at the cooled surface that existed high in the mould will disappear.

Fig 21: DETACHED CORNER SECTION FOR 200 mm SQUARE BILLET AT A METALLURGICAL HEIGHT OF 0.1 m, CAST AT 0.06 m.s⁻¹ : INITIAL PREDICTION.

DATA AL E L1 L2 A t delT meth QSYS EMSR
 'C-1 N.m⁻² m m m m 'C m N.m⁻² N.m⁻²

FIG. 21

DATA: AL E L1 L2 A t delT meth QSYS EMSR
 dim. .18E-04 .70E+10 .0362 .0362 .007 .002 67 .100 .970E+07 .0060
 adim. .12E-02 .46E+03 16.60 16.60 3.00 1. YS=.154E+08
 RKstep = .10000 F1 = .15E-01 Q = -.48E-03
 RKerror = .00050 F2 = .15E-01 M3 = .1844
 IError = .00001

DETACHED SECTION 1 :

X	C	DW/DX	W	M	S0	F	YF	N
3.0	-.001	.00	.0*	.03	.02	.99	-.01	.762E+00
4.0	-.001	-.00	-.0*	.10	.06	.96	-.04	.558E+00
5.0	-.001	-.00	-.00	.17	.10	.92	-.08	.520E+00
6.0	-.001	-.00	-.00	.24	.14	.89	-.11	.499E+00
7.0	-.000	-.00	-.01	.29	.18	.86	-.14	.485E+00
8.0	-.000	-.00	-.01	.35	.21	.84	-.16	.474E+00
9.0	-.000	-.00	-.01	.39	.25	.81	-.19	.464E+00
10.0	.000	-.00	-.02	.43	.28	.79	-.21	.456E+00
11.0	.000	-.00	-.02	.47	.31	.78	-.22	.449E+00
12.0	.000	-.00	-.02	.50	.33	.76	-.24	.444E+00
13.0	.001	-.00	-.03	.52	.35	.75	-.25	.439E+00
14.0	.001	-.00	-.03	.54	.37	.74	-.26	.436E+00
15.0	.001	-.00	-.03	.55	.38	.74	-.26	.434E+00
16.0	.001	-.00	-.03	.56	.38	.73	-.27	.433E+00
16.6	.001	-.00	-.03	.56	.39	.73	-.27	.432E+00

Scale:
 1.4 mm W(X)
 7 mm t, p
 14mm L1, L2, A, X

DETACHED SECTION 2 :

X	C	DW/DX	W	M	S0	F	YF	N
3.0	-.001	-.00	-.0*	.03	.02	.99	-.01	.762E+00
4.0	-.001	-.00	-.0*	.10	.06	.96	-.04	.558E+00
5.0	-.001	-.00	-.00	.17	.10	.92	-.08	.520E+00
6.0	-.001	-.00	-.00	.24	.14	.89	-.11	.499E+00
7.0	-.000	-.00	-.01	.29	.18	.86	-.14	.485E+00
8.0	-.000	-.00	-.01	.35	.21	.84	-.16	.474E+00
9.0	-.000	-.00	-.01	.39	.25	.81	-.19	.464E+00
10.0	.000	-.00	-.02	.43	.28	.79	-.21	.456E+00
11.0	.000	-.00	-.02	.47	.31	.78	-.22	.449E+00
12.0	.000	-.00	-.02	.50	.33	.76	-.24	.444E+00
13.0	.001	-.00	-.03	.52	.35	.75	-.25	.439E+00
14.0	.001	-.00	-.03	.54	.37	.74	-.26	.436E+00
15.0	.001	-.00	-.03	.55	.38	.74	-.26	.434E+00
16.0	.001	-.00	-.03	.56	.38	.73	-.27	.433E+00
16.6	.001	-.00	-.03	.56	.39	.73	-.27	.432E+00

MINL1(W2) : .100 MINL2(W1) : .100
 SECTION LENGTH 1: .100 SECTION LENGTH 2: .100
 DETACHED LENGTH 1: .03618 DETACHED LENGTH 2: .03618

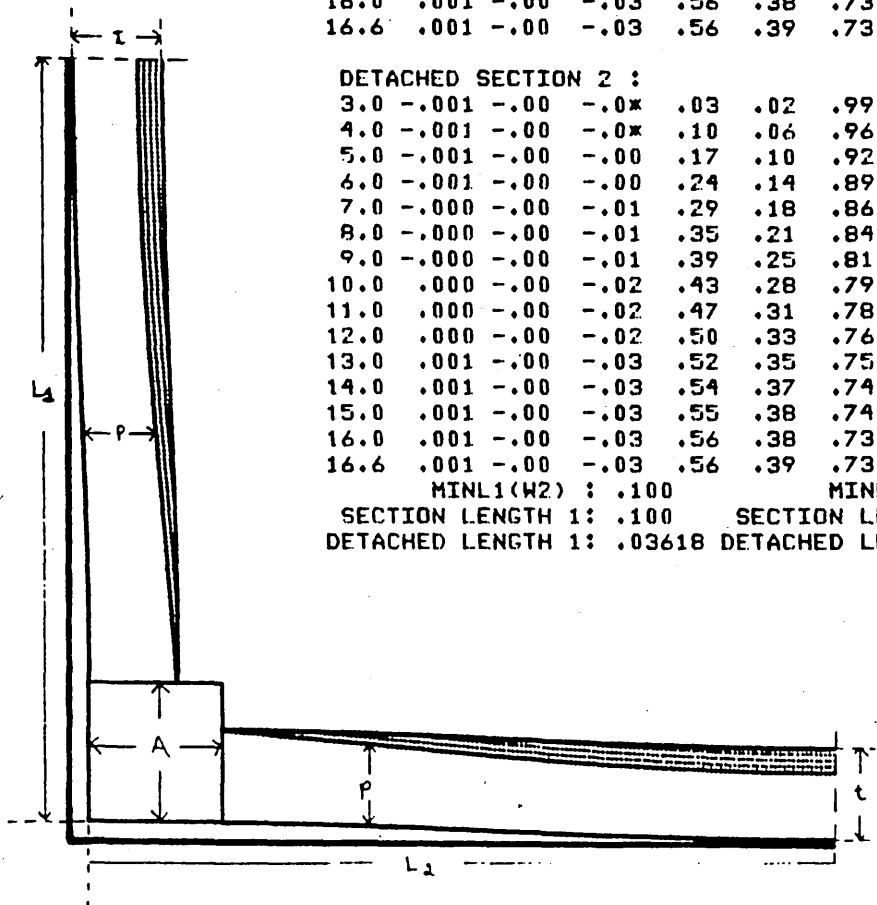


Fig 22: DETACHED CORNER SECTION FOR 200 mm SQUARE BILLET AT A METALLURGICAL HEIGHT OF 0.3 m, CAST AT 0.06 m s⁻¹ : INITIAL PREDICTION

DATA AL E L1 L2 A t delT meth QSYS EMSR
 'C⁻¹ N.m⁻² m m m m 'C m N.m⁻² N.m⁻²

FIG.22

DATA: AL E L1 L2 A t delT meth QSYS EMSR
 dim. .18E-04 .70E+10 .0680 .0680 .015 .005 134 .300 .194E+08 .0060
 edim. .24E-02 .23E+03 12.44 12.44 2.75 1. YS=.308E+08
 RKstep = .10000 F1 = .16E-01 Q = -.72E-03
 RKerror = .00050 F2 = .16E-01 M3 = .0867
 ITerror = .00002

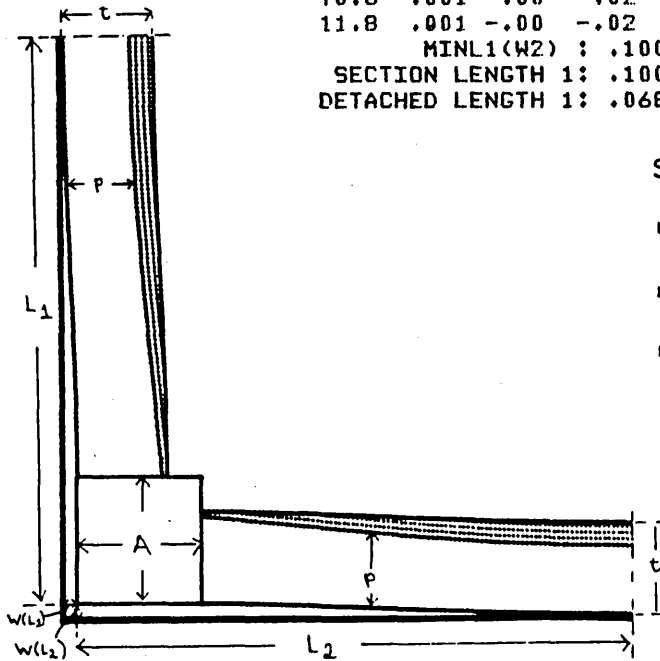
DETACHED SECTION 1 :

X	C	DW/DX	W	M	S0	P	YF	N
2.8	-.002	.00	.0*	.12	.07	.95	-.05	.551E+00
3.8	-.001	-.00	-.0*	.20	.12	.91	-.09	.514E+00
4.8	-.001	-.00	-.00	.27	.16	.87	-.13	.493E+00
5.8	-.001	-.00	-.01	.33	.20	.84	-.16	.479E+00
6.8	-.000	-.00	-.01	.39	.24	.82	-.18	.467E+00
7.8	.000	-.00	-.01	.43	.28	.80	-.20	.458E+00
8.8	.001	-.00	-.02	.47	.31	.78	-.22	.451E+00
9.8	.001	-.00	-.02	.49	.33	.76	-.24	.446E+00
10.8	.001	-.00	-.02	.51	.35	.76	-.24	.442E+00
11.8	.001	-.00	-.02	.52	.35	.75	-.25	.440E+00

DETACHED SECTION 2 :

2.8	-.002	-.00	-.0*	.12	.07	.95	-.05	.551E+00
3.8	-.001	-.00	-.0*	.20	.12	.91	-.09	.514E+00
4.8	-.001	-.00	-.00	.27	.16	.87	-.13	.493E+00
5.8	-.001	-.00	-.01	.33	.20	.84	-.16	.479E+00
6.8	-.000	-.00	-.01	.39	.24	.82	-.18	.467E+00
7.8	.000	-.00	-.01	.43	.28	.80	-.20	.458E+00
8.8	.001	-.00	-.02	.47	.31	.78	-.22	.451E+00
9.8	.001	-.00	-.02	.49	.33	.76	-.24	.446E+00
10.8	.001	-.00	-.02	.51	.35	.76	-.24	.442E+00
11.8	.001	-.00	-.02	.52	.35	.75	-.25	.440E+00

MINL1(W2) : .100 MINL2(W1) : .100
 SECTION LENGTH 1 : .100 SECTION LENGTH 2 : .100
 DETACHED LENGTH 1 : .06800 DETACHED LENGTH 2 : .06800



Scale:
 1 mm W(X)
 5 mm t, p
 10 mm L₁, L₂, A, X

Fig 23: DETACHED CORNER SECTION FOR 200 mm SQUARE BILLET AT A METALLURGICAL HEIGHT OF 0.6 m. CAST AT 0.06 m.s⁻¹ : INITIAL PREDICTION.

DATA: AL E L1 L2 A t delT meth QSYS EMSR
 'C-1 N.m⁻² m m m m 'C m N.m⁻² N.m⁻²

FIG. 23

DATA: AL E L1 L2 A t delT meth QSYS EMSR
 dim. .18E-04 .70E+10 .0920 .0920 .022 .009 188 .600 .272E+08 .0060
 adim. .34E-02 .16E+03 10.28 10.28 2.47 1. YS=.432E+08
 RKstep = .10000 F1 = .19E-01 Q = -.10E-02
 RKerror = .00050 F2 = .19E-01 M3 = .0657
 ITerror = .00002

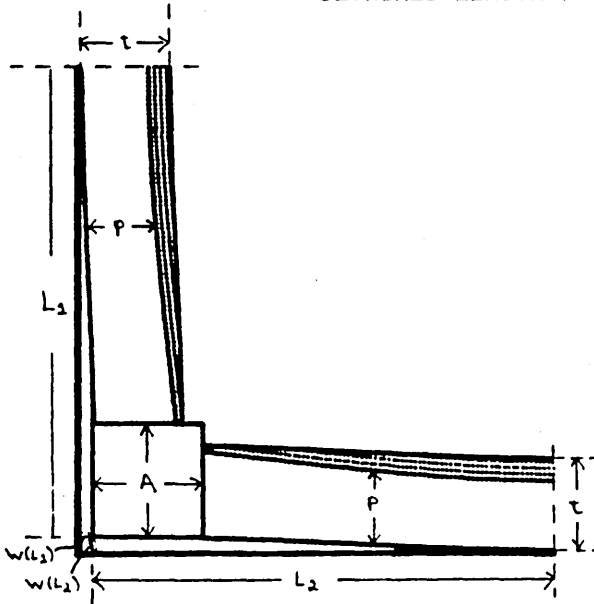
DETACHED SECTION 1 :

X	C	DW/DX	W	M	S0	P	YF	N
2.5	-.002	-.00	-.0*	.14	.09	.94	-.06	.546E+00
3.5	-.002	-.00	-.00	.23	.14	.89	-.11	.509E+00
4.5	-.001	-.00	-.00	.31	.19	.86	-.14	.488E+00
5.5	-.000	-.00	-.01	.38	.24	.82	-.18	.473E+00
6.5	.000	-.00	-.01	.43	.28	.80	-.20	.462E+00
7.5	.001	-.00	-.02	.47	.31	.78	-.22	.453E+00
8.5	.001	-.00	-.02	.50	.33	.76	-.24	.448E+00
9.5	.001	-.00	-.02	.51	.35	.76	-.24	.445E+00
10.3	.001	-.00	-.02	.52	.35	.75	-.25	.444E+00

DETACHED SECTION 2 :

X	C	DW/DX	W	M	S0	P	YF	N
2.5	-.002	.00	.0*	.14	.09	.94	-.06	.546E+00
3.5	-.002	-.00	-.00	.23	.14	.89	-.11	.509E+00
4.5	-.001	-.00	-.00	.31	.19	.86	-.14	.488E+00
5.5	-.000	-.00	-.01	.38	.24	.82	-.18	.473E+00
6.5	.000	-.00	-.01	.43	.28	.80	-.20	.462E+00
7.5	.001	-.00	-.02	.47	.31	.78	-.22	.453E+00
8.5	.001	-.00	-.02	.50	.33	.76	-.24	.448E+00
9.5	.001	-.00	-.02	.51	.35	.76	-.24	.445E+00
10.3	.001	.00	-.02	.52	.35	.75	-.25	.444E+00

MINL1(W2) : .100 MINL2(W1) : .100
 SECTION LENGTH 1: .100 SECTION LENGTH 2: .100
 DETACHED LENGTH 1: .09200 DETACHED LENGTH 2: .09200



Scale:

1.8 mm W(X)

9 mm t, p

18 mm L1, L2, A, X

Fig 24: DETACHED CORNER SECTION FOR 250 mm SQUARE BILLET AT A METALLURGICAL HEIGHT OF 0.1 m, CAST AT 0.06 m.s⁻¹ : INITIAL PREDICTION.

DATA: AL E L1 L2 A t delT meth QSYS EMSR
 'C-1 N.m⁻² m m m m 'C m N.m⁻² N.m⁻²

FIG. 24

DATA: AL E L1 L2 A t delT meth QSYS EMSR
 dim. .18E-04 .70E+10 .0380 .0380 .007 .002 67 .100 .970E+07 .0060
 adim. .12E-02 .46E+03 17.43 17.43 3.00 1. YS=.154E+08
 RKstep = .10000 F1 = .16E-01 Q = -.48E-03
 RKerror = .00050 F2 = .16E-01 M3 = .2455
 ITerror = .00001

DETACHED SECTION 1 :

X	C	DW/DX	W	M	S0	F	YF	N
3.0	-.001	-.00	-.0*	-.02	-.00	.98	.02	.134E+00
4.0	-.001	-.00	-.0*	.06	.04	.98	-.02	.626E+00
5.0	-.001	-.00	-.00	.13	.08	.94	-.06	.541E+00
6.0	-.001	-.00	-.00	.20	.12	.91	-.09	.512E+00
7.0	-.001	-.00	-.01	.26	.16	.88	-.12	.494E+00
8.0	-.000	-.00	-.01	.32	.20	.85	-.15	.480E+00
9.0	-.000	-.00	-.02	.37	.23	.82	-.18	.469E+00
10.0	.000	-.00	-.02	.42	.27	.80	-.20	.460E+00
11.0	.000	-.00	-.02	.46	.30	.78	-.22	.452E+00
12.0	.000	-.00	-.03	.49	.33	.77	-.23	.446E+00
13.0	.001	-.00	-.03	.52	.35	.75	-.25	.440E+00
14.0	.001	-.00	-.03	.54	.37	.74	-.26	.436E+00
15.0	.001	-.00	-.04	.56	.39	.73	-.27	.433E+00
16.0	.001	-.00	-.04	.57	.40	.73	-.27	.431E+00
17.0	.001	-.00	-.04	.58	.40	.72	-.28	.430E+00
17.4	.001	.00	-.04	.58	.40	.72	-.28	.430E+00

Scale:

0.4 mm W(X)

2 mm t, p

4 mm L₁, L₂, A, X

DETACHED SECTION 2 :

3.0	-.001	.00	.0*	-.02	-.00	.98	.02	.134E+00
4.0	-.001	-.00	-.0*	.06	.04	.98	-.02	.626E+00
5.0	-.001	-.00	-.00	.13	.08	.94	-.06	.541E+00
6.0	-.001	-.00	-.00	.20	.12	.91	-.09	.512E+00
7.0	-.001	-.00	-.01	.26	.16	.88	-.12	.494E+00
8.0	-.000	-.00	-.01	.32	.20	.85	-.15	.480E+00
9.0	-.000	-.00	-.02	.37	.23	.82	-.18	.469E+00
10.0	.000	-.00	-.02	.42	.27	.80	-.20	.460E+00
11.0	.000	-.00	-.02	.46	.30	.78	-.22	.452E+00
12.0	.000	-.00	-.03	.49	.33	.77	-.23	.446E+00
13.0	.001	-.00	-.03	.52	.35	.75	-.25	.440E+00
14.0	.001	-.00	-.03	.54	.37	.74	-.26	.436E+00
15.0	.001	-.00	-.04	.56	.39	.73	-.27	.433E+00
16.0	.001	-.00	-.04	.57	.40	.73	-.27	.431E+00
17.0	.001	-.00	-.04	.58	.40	.72	-.28	.430E+00
17.4	.001	.00	-.04	.58	.40	.72	-.28	.430E+00

MINL1(W2) : .125

MINL2(W1) : .125

SECTION LENGTH 1 : .125

SECTION LENGTH 2 : .125

DETACHED LENGTH 1 : .03800

DETACHED LENGTH 2 : .03800

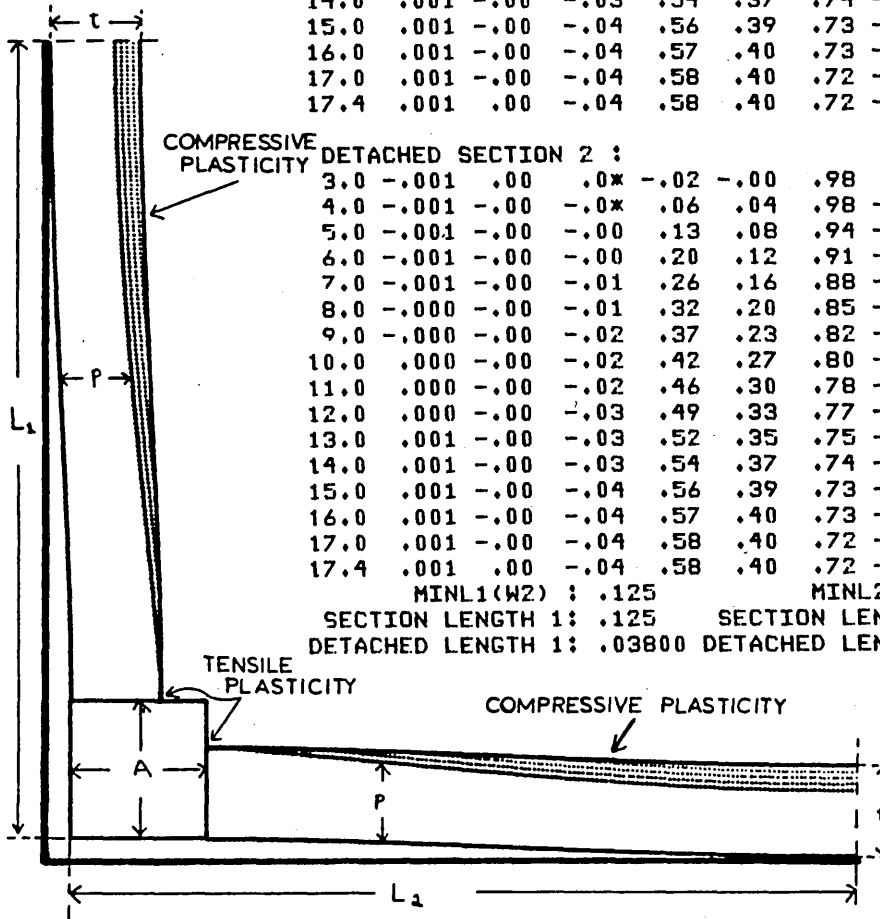


Fig 25: DETACHED CORNER SECTION FOR 250 mm SQUARE BILLET AT A METALLURGICAL HEIGHT OF 0.3 m, CAST AT 0.06 m.s⁻¹ : INITIAL PREDICTION.

DATA: AL 'C-1 E N.m⁻² L1 m L2 m A m t m delT 'C meth m QSYS N.m⁻² EMSR N.m⁻²

FIG. 25

DATA: AL dim. .18E-04 E .70E+10 L1 .0711 L2 .0711 A .015 t .005 delT 134 meth .300 QSYS .194E+08 EMSR .0060
 adim. .24E-02 .23E+03 13.01 13.01 2.75 1. YS=.308E+08
 RKstep = .10000 F1 = .17E-01 G = -.72E-03
 RKerror = .00050 F2 = .17E-01 M3 = .1335
 ITerror = .00001

DETACHED SECTION 1 :

X	C	DW/DX	W	M	S0	P	YF	N
2.8	-.002	.00	.0*	.09	.05	.97	-.03	.589E+00
3.8	-.002	-.00	-.0*	.17	.10	.92	-.08	.528E+00
4.8	-.001	-.00	-.00	.25	.15	.89	-.11	.502E+00
5.8	-.001	-.00	-.01	.31	.19	.85	-.15	.485E+00
6.8	-.000	-.00	-.01	.37	.23	.83	-.17	.472E+00
7.8	.000	-.00	-.02	.42	.27	.80	-.20	.461E+00
8.8	.001	-.00	-.02	.46	.30	.78	-.22	.453E+00
9.8	.001	-.00	-.02	.49	.33	.77	-.23	.447E+00
10.8	.001	-.00	-.03	.52	.35	.75	-.25	.442E+00
11.8	.001	-.00	-.03	.53	.36	.75	-.25	.439E+00
12.8	.001	-.00	-.03	.54	.37	.74	-.26	.438E+00

Scale:

1mm W(X)

5mm t p

10mm L₁, L₂, A, X

DETACHED SECTION 2 :

X	C	DW/DX	W	M	S0	P	YF	N
2.8	-.002	-.00	-.0*	.09	.05	.97	-.03	.589E+00
3.8	-.002	-.00	-.0*	.17	.10	.92	-.08	.528E+00
4.8	-.001	-.00	-.00	.25	.15	.89	-.11	.502E+00
5.8	-.001	-.00	-.01	.31	.19	.85	-.15	.485E+00
6.8	-.000	-.00	-.01	.37	.23	.83	-.17	.472E+00
7.8	.000	-.00	-.02	.42	.27	.80	-.20	.461E+00
8.8	.001	-.00	-.02	.46	.30	.78	-.22	.453E+00
9.8	.001	-.00	-.02	.49	.33	.77	-.23	.447E+00
10.8	.001	-.00	-.03	.52	.35	.75	-.25	.442E+00
11.8	.001	-.00	-.03	.53	.36	.75	-.25	.439E+00
12.8	.001	-.00	-.03	.54	.37	.74	-.26	.438E+00

MINL1(W2) : .125 MINL2(W1) : .125
 SECTION LENGTH 1 : .125 SECTION LENGTH 2 : .125
 DETACHED LENGTH 1 : .07115 DETACHED LENGTH 2 : .07115

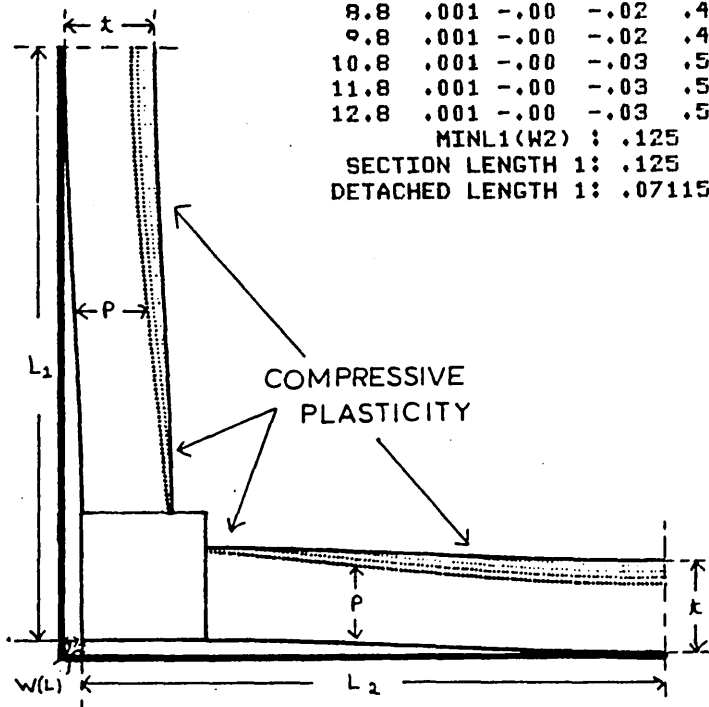


Fig 26: DETACHED CORNER SECTION FOR 250 mm SQUARE BILLET AT A METALLURGICAL HEIGHT OF 0.6 m CAST AT 0.06 m.s⁻¹ : INITIAL PREDICTION.

DATA: AL E L1 L2 A t delT meth QSYS EMSR
 'C⁻¹ N.m⁻² m m m m 'C m N.m⁻² N.m⁻²

FIG.26

DATA: AL E L1 L2 A t delT meth QSYS EMSR
 dim. .18E-04 .70E+10 .0965 .0965 .022 .009 188 .600 .272E+08 .0060
 adm. .34E-02 .16E+03 10.78 10.78 2.47 1. YS=.432E+08
 RKstep = .10000 F1 = .20E-01 R = -.10E-02
 RKerror = .00050 F2 = .20E-01 M3 = .1123
 ITerror = .00001

DETACHED SECTION 1 :										
X	C	DW/DX	W	M	S0	F	YF	N		
2.5	-.003	-.00	-.0*	.11	.07	.96	-.04	.576E+00		
3.5	-.002	-.00	-.00	.21	.12	.91	-.09	.521E+00		
4.5	-.001	-.00	-.00	.29	.18	.87	-.13	.495E+00		
5.5	-.000	-.00	-.01	.36	.22	.83	-.17	.478E+00		
6.5	.000	-.00	-.01	.42	.27	.80	-.20	.465E+00		
7.5	.001	-.00	-.02	.47	.31	.78	-.22	.455E+00		
8.5	.001	-.00	-.02	.50	.33	.76	-.24	.448E+00		
9.5	.002	-.00	-.03	.52	.35	.75	-.25	.444E+00		
10.5	.002	-.00	-.03	.53	.36	.75	-.25	.442E+00		
10.7	.002	.00	-.03	.53	.36	.75	-.25	.442E+00		

DETACHED SECTION 2 :										
X	C	DW/DX	W	M	S0	F	YF	N		
2.5	-.003	.00	.0*	.11	.07	.96	-.04	.576E+00		
3.5	-.002	-.00	-.00	.21	.12	.91	-.09	.521E+00		
4.5	-.001	-.00	-.00	.29	.18	.87	-.13	.495E+00		
5.5	-.000	-.00	-.01	.36	.22	.83	-.17	.478E+00		
6.5	.000	-.00	-.01	.42	.27	.80	-.20	.465E+00		
7.5	.001	-.00	-.02	.47	.31	.78	-.22	.455E+00		
8.5	.001	-.00	-.02	.50	.33	.76	-.24	.448E+00		
9.5	.002	-.00	-.03	.52	.35	.75	-.25	.444E+00		
10.5	.002	-.00	-.03	.53	.36	.75	-.25	.442E+00		
10.7	.002	.00	-.03	.53	.36	.75	-.25	.442E+00		

MINL1(W2) : .125 MINL2(W1) : .125
 SECTION LENGTH 1 : .125 SECTION LENGTH 2 : .125
 DETACHED LENGTH 1 : .09650 DETACHED LENGTH 2 : .09650

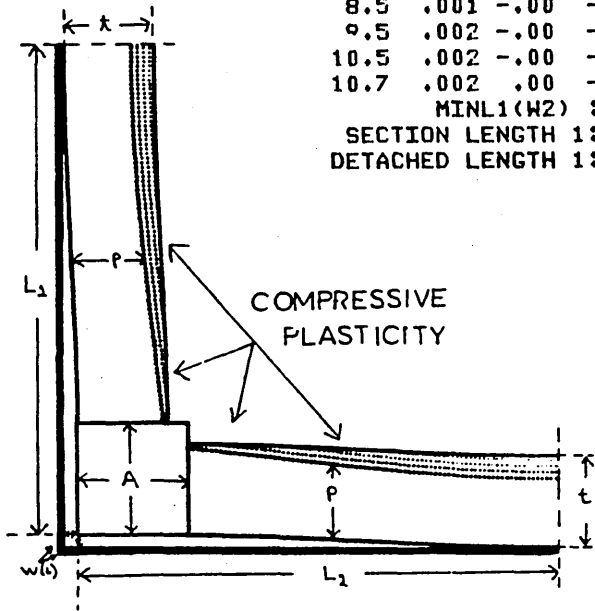


Fig 27: DETACHED CORNER SECTION FOR 250 mm SQUARE BILLET AT A METALLURGICAL HEIGHT OF 0.6 m BUT OUT OF THE MOULD CAST AT 0.06 m.s⁻¹ : INITIAL PREDICTION.

DATA: AL 'C-1 E N.m⁻² L1 m L2 m A m t m delT meth 'C m QSYS N.m⁻² EMSR N.m⁻²

FIG.27

DATA: AL E L1 L2 A t delT meth QSYS EMSR
 dim. .18E-04 .70E+10 .1250 .1250 .022 .009 188 .600 .272E+08 .0060
 adim. .34E-02 .16E+03 13.96 13.96 2.47 1. YS=.432E+08
 RKstep = .10000 F1 = .26E-01 G = -.10E-02
 RKerror = .00050 F2 = .26E-01 M3 = .4740
 ITerror = .00001

DETACHED SECTION 1 :

X	C	DW/DX	W	H	S0	P	YF	N
2.5	-.005	-.00	-.0*	-.17	-.09	.90	.10	.406E+00
3.5	-.004	-.00	-.00	-.04	-.01	.97	.03	.180E+00
4.5	-.003	-.01	-.01	.08	.06	.97	-.03	.651E+00
5.5	-.002	-.01	-.02	.19	.12	.92	-.08	.543E+00
6.5	-.001	-.01	-.03	.29	.18	.87	-.13	.506E+00
7.5	-.000	-.01	-.04	.38	.24	.83	-.17	.483E+00
8.5	.000	-.01	-.05	.45	.29	.79	-.21	.466E+00
9.5	.001	-.01	-.06	.51	.34	.76	-.24	.453E+00
10.5	.002	-.01	-.07	.56	.39	.74	-.26	.443E+00
11.5	.003	-.01	-.08	.60	.42	.72	-.28	.435E+00
12.5	.003	-.00	-.09	.62	.45	.71	-.29	.430E+00
13.5	.003	-.00	-.09	.63	.46	.70	-.30	.428E+00
13.9	.003	.00	-.09	.64	.46	.70	-.30	.427E+00

Scale:

1.8 mm

W(X)

9 mm

t, p

18. mm

L₁, L₂, A, X

DETACHED SECTION 2 :

2.5	-.005	.00	.0*	-.17	-.09	.90	.10	.406E+00
3.5	-.004	-.00	-.00	-.04	-.01	.97	.03	.180E+00
4.5	-.003	-.01	-.01	.08	.06	.97	-.03	.651E+00
5.5	-.002	-.01	-.02	.19	.12	.92	-.08	.543E+00
6.5	-.001	-.01	-.03	.29	.18	.87	-.13	.506E+00
7.5	-.000	-.01	-.04	.38	.24	.83	-.17	.483E+00
8.5	.000	-.01	-.05	.45	.29	.79	-.21	.466E+00
9.5	.001	-.01	-.06	.51	.34	.76	-.24	.453E+00
10.5	.002	-.01	-.07	.56	.39	.74	-.26	.443E+00
11.5	.003	-.01	-.08	.60	.42	.72	-.28	.435E+00
12.5	.003	-.00	-.09	.62	.45	.71	-.29	.430E+00
13.5	.003	-.00	-.09	.63	.46	.70	-.30	.428E+00
13.9	.003	.00	-.09	.64	.46	.70	-.30	.427E+00

MINL2(W1)

DETACHED LENGTH 1: .125
OUT OF THE MOULD

DETACHED LENGTH 2: .12500
OUT OF THE MOULD

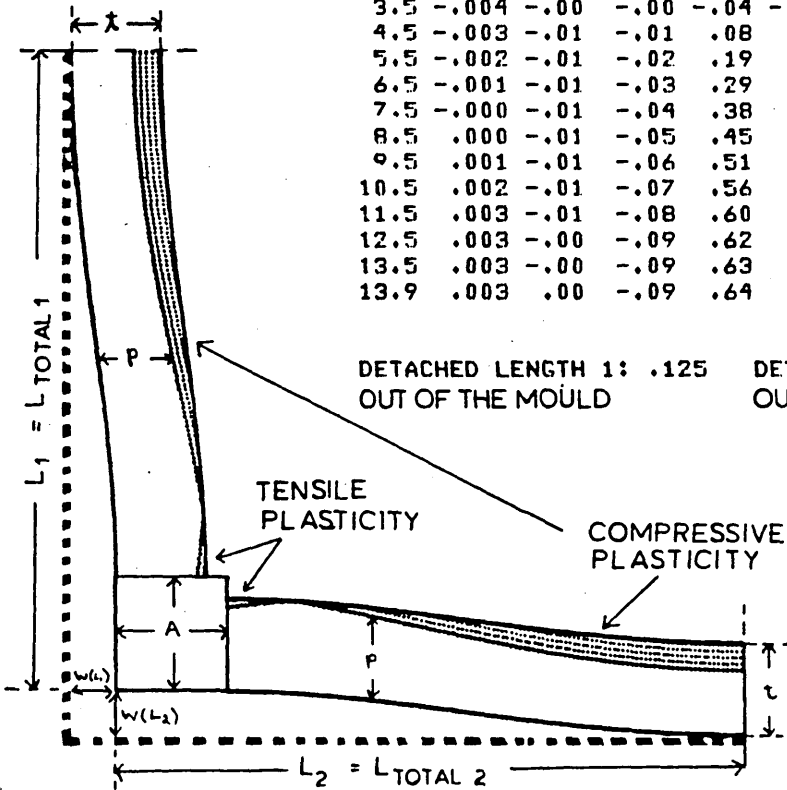


Fig 28/29

DETACHED CORNER SECTION FOR 166 mm SQUARE BILLET
 AT METALLURGICAL HEIGHTS OF 0.1 AND 0.3 m,
 CAST AT 0.06 m.s⁻¹ : INITIAL PREDICTION.

DATA AL E L1 L2 A t delT meth QSYS EMSR
 'C⁻¹ N.m⁻² m m m m 'C m N.m⁻² N.m⁻²

FIG. 29
 DATA: AL E L1 L2 A t delT meth QSYS EMSR
 dia. .18E-04 .70E+10 .060 .060 .015 .005 134 .300 .717E+07 .0060
 adia. .24E-02 .62E+03 11.0 11.0 2.75 1. YS=.114E+08
 PKstep = .10000 F1 = .39E-01 Q = -.19E-02
 PKerror = .00050 F2 = .39E-01 N3 = .2975
 ITerror = .00001

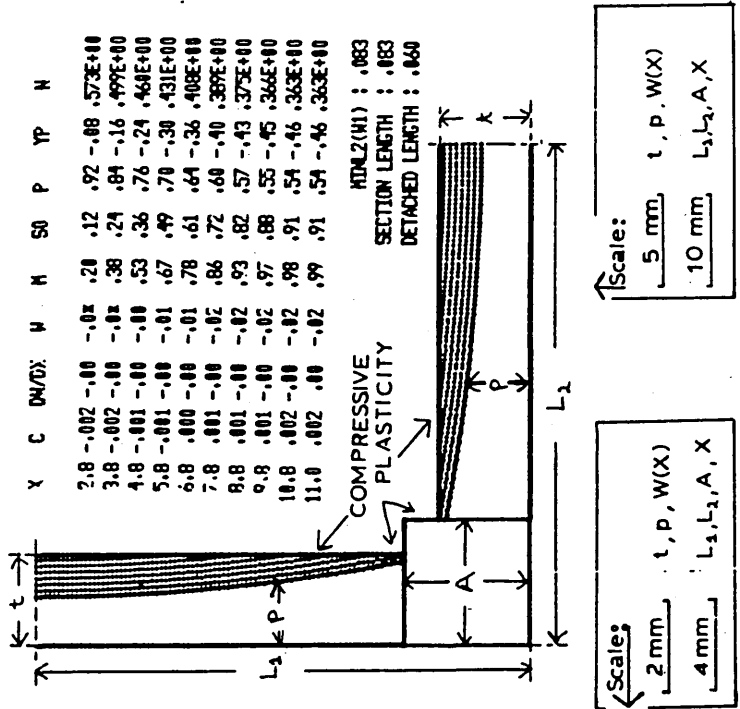


FIG. 28
 DATA: AL E L1 L2 A t delT meth QSYS EMSR
 dia. .18E-04 .70E+10 .032 .032 .007 .002 67 .100 .358E+07 .0060
 adia. .12E-02 .12E+04 14.7 14.7 3.00 1. YS=.548E+07
 PKstep = .10000 F1 = .35E-01 Q = -.13E-02
 PKerror = .00050 F2 = .35E-01 N3 = .5240
 ITerror = .00001

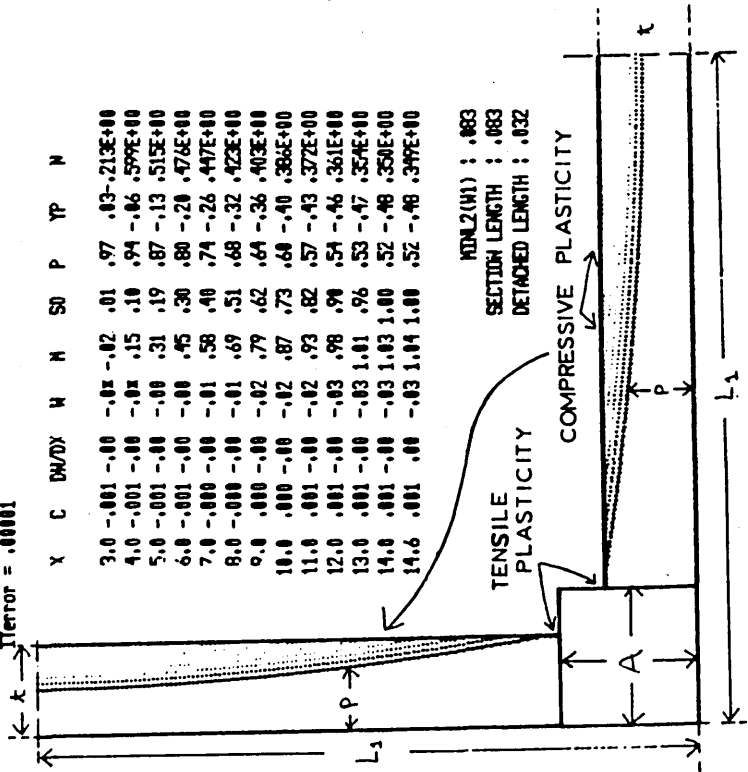


Fig 30: DETACHED CORNER SECTION FOR 166 mm SQUARE BILLET AT A METALLURGICAL HEIGHT OF 0.6 m. CAST AT 0.06 m.s⁻¹ : SECOND PREDICTION

DATA AL E L1 L2 A t delT meth QSYS EMSR
 'C⁻¹ N.m⁻² m m m m 'C m N.m⁻² N.m⁻²

FIG. 30

DATA: AL E L1 L2 A t delT meth QSYS EMSR
 dim. .18E-04 .70E+10 .0814 .0814 .022 .009 188 .600 .101E+08 .0060
 adim. .34E-02 .44E+03 9.09 9.09 2.47 1. YS=.159E+08
 RKstep = .10000 F1 = .45E-01 Q = -.28E-02
 RKerror = .00050 F2 = .45E-01 M3 = .2431
 ITerror = .00001

DETACHED SECTION 1 :

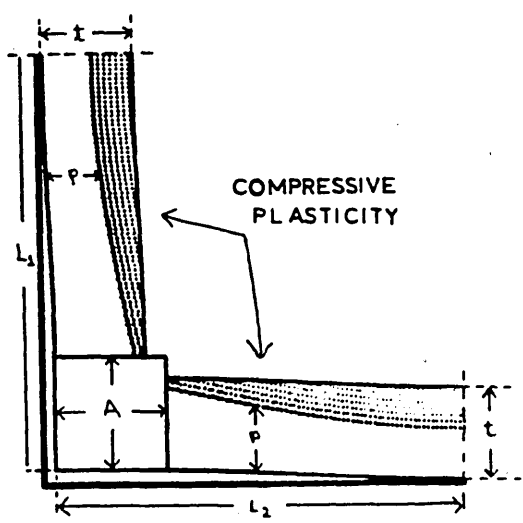
X	C	DW/DX	W	M	S0	P	YF	N
2.5	-.003	-.00	-.0*	.25	.16	.90	-.10	.557E+00
3.5	-.002	-.00	-.00	.45	.30	.80	-.20	.486E+00
4.5	-.001	-.00	-.00	.62	.44	.72	-.28	.446E+00
5.5	-.000	-.00	-.01	.76	.59	.66	-.34	.416E+00
6.5	.001	-.00	-.01	.86	.72	.61	-.39	.393E+00
7.5	.002	-.00	-.02	.93	.82	.57	-.43	.378E+00
8.5	.002	-.00	-.02	.97	.88	.56	-.44	.369E+00

DETACHED SECTION 2 :

2.5	-.003	.00	.0*	.25	.16	.90	-.10	.557E+00
3.5	-.002	-.00	-.00	.45	.30	.80	-.20	.486E+00
4.5	-.001	-.00	-.00	.62	.44	.72	-.28	.446E+00
5.5	-.000	-.00	-.01	.76	.59	.66	-.34	.416E+00
6.5	.001	-.00	-.01	.86	.72	.61	-.39	.393E+00
7.5	.002	-.00	-.02	.93	.82	.57	-.43	.378E+00
8.5	.002	-.00	-.02	.97	.88	.56	-.44	.369E+00

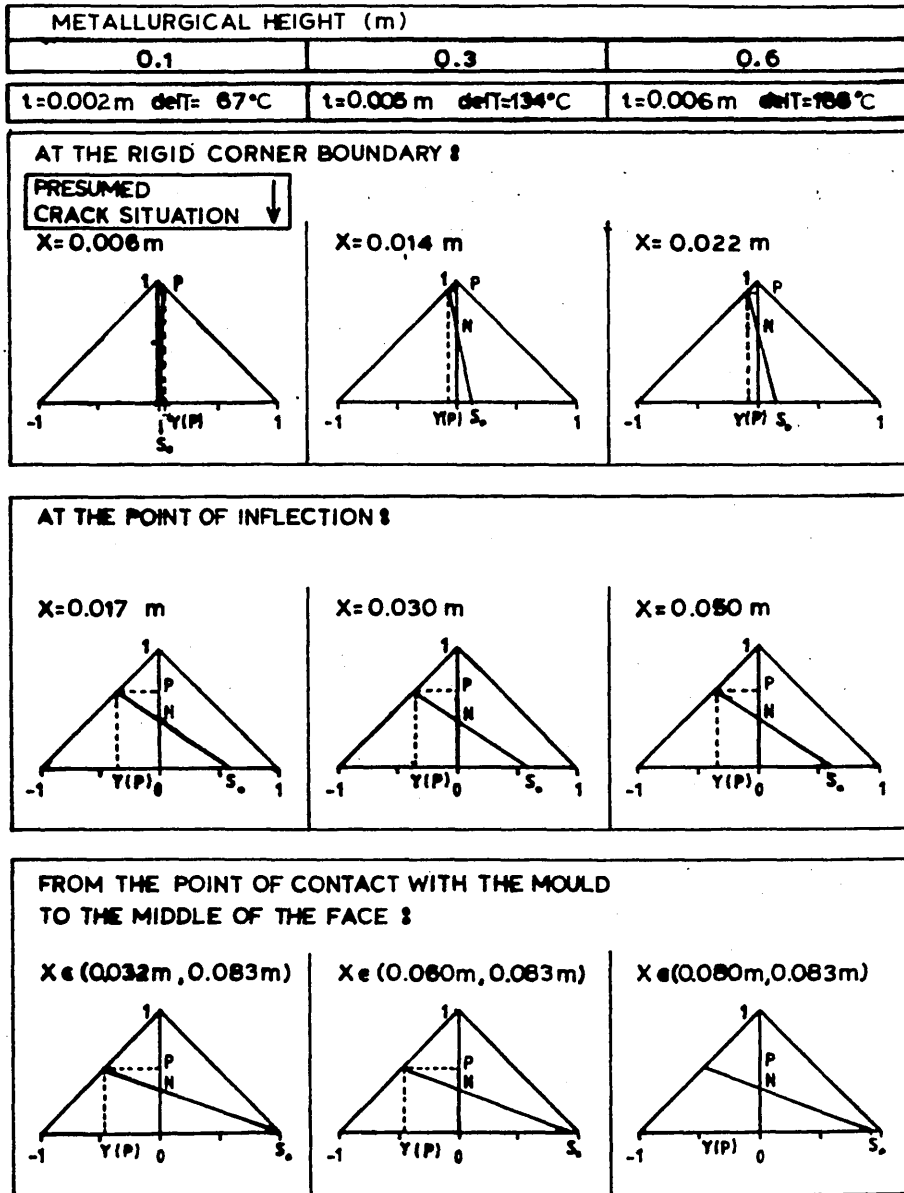
MINL1(W2) : .083 MINL2(W1) : .083

SECTION LENGTH 1 : .083 SECTION LENGTH 2 : .083
 DETACHED LENGTH 1 : .08140 DETACHED LENGTH 2 : .08140



Scale:
 1.8 mm W(x)
 9 mm p, t
 18 mm L1, L2, A, X

FIG. 31 CROSS-SECTION STRESS DISTRIBUTION:
 THE FORMATION OF AN OFF-CORNER CRACK
 IN A 16.6cmx16.6cm BILLET
 CAST AT HIGH SPEED $Q_{SYS} = 2.4 \times 10^7 \text{ N.m}^{-2}$



ESTIMATED CASTING SPEED = 0.06 m/sec

**CHAPTER 7 :
DISCUSSION**

The model developed in this research follows on from the work of previous authors who have considered the behaviour of the thin shells solidifying within the continuously casting mould in terms of beam theory but differs from their work by incorporating the assumption of rigid corners.

The previous models based on beam theory assumed that beams representing the solidifying shells along each side of a continuously cast billet or slab were either fixed or simply supported at both ends. The assumption that these thin shells behave as beams effectively describes their flexible mechanical behaviour but the support assumptions neglect mechanical interactions between the shells along adjacent sides.

The assumption made in this work, that the corner acts effectively as a rigid hinge, allows the solidifying shell at a given metallurgical height to be considered as a flexible rectangular structure.

In common with previous workers, it is assumed in this work that a transversal section of the billet or slab at a certain metallurgical height within the mould can be considered independently of the material above and below it. This means that its history is adequately specified by the thickness of the solidifying shell and the temperature distribution across

it and that -within the mould- the mechanical interaction between successive sections is negligible. That this is the usual assumption for both thermal models and stress models for the early stages of solidification in the continuous casting process is justified because the second derivatives of temperature and stress as functions of solidification time can be considered to be negligible.

As well as models based on beam theory, a number of authors have used the finite element method. The model used here differs from models based on the finite element method in that it is closer to an analytical solution. It also accounts adequately for the bending phenomena, which, as is pointed out in the literature survey, the finite element method does not yet appear to have done.

However complicated it might prove to be in practice, the expression derived in chapter four for the curvature of the shells (eq. 6.7.2, page 4:46) can be integrated analytically as it is a rational function which can be decomposed into partial fractions. The use of a standard Runge-Kutta algorithm to integrate this expression for the curvature, and the subsequent necessary iteration, does not limit the flexibility of the model to any significant extent.

This is an important distinction from the finite element method as the current limited understanding of mechanical behaviour of metals during the early stages of their rapid solidification in the continuous casting process and the

uncertainty of the data available on the mechanical properties of steel at high temperature dictate generality and flexibility to be essential criteria for the design of a model which is to advance our understanding of the continuous casting process.

Nor do finite element methods overcome the need to introduce simplifying assumptions concerning the mechanical behaviour of steel. Although it has proven to be extremely useful in the analysis of elastic structures, application of the finite element method to structures in which significant plastic deformation occurs is restricted by the need to introduce a number of simplifying assumptions in order to formulate the stiffness matrices used. The amount of computation required to deal with structures which depart significantly from elastic behaviour, as is the case of the one considered in this research, further limits the contribution that finite element techniques can make to our understanding of basic trends.

7.1 DISTORTION AND STRESS DISTRIBUTION

Figure 1 (page 7:5), shows the shape and extent of the entire quarter section of the solidified shells of a 1300 mm x 300 mm slab cast at high speed (0.03 m/sec) as it is predicted by this model at a metallurgical height of 0.1 m.

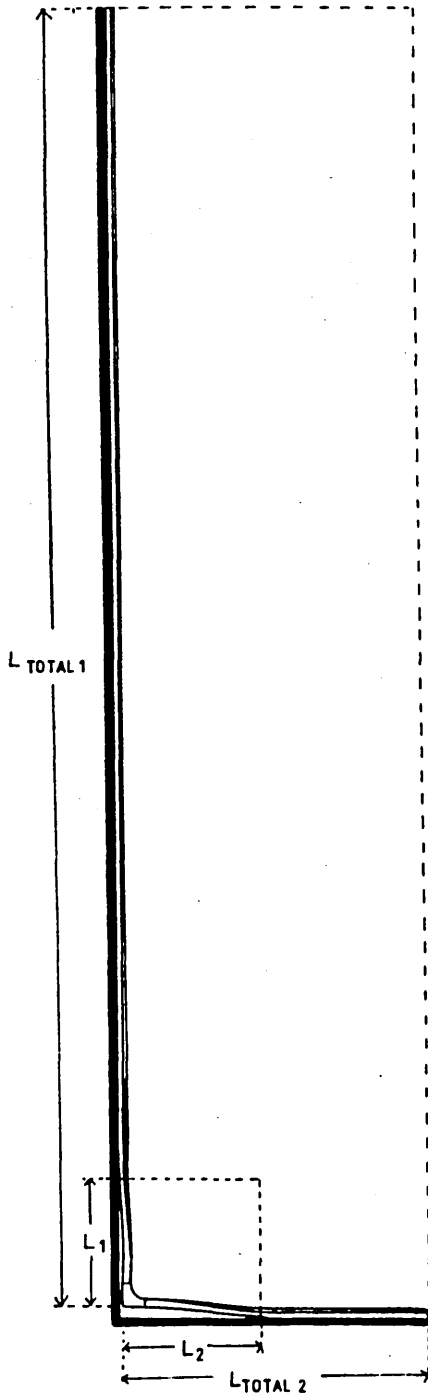
This figure corresponds to the same situation and the same computer results as figure 6.19 (page 6:71), but has been drawn so that the thickness and section lengths are represented by the same scale, the deflections by a scale ten times greater and the corner region has been drawn more realistically as a quarter circle. The figure shows the extent of the air gap at the corner and places it in perspective with the rest of the solidified structure. The figure also shows the assumption made in this work that the thickness and stress distribution are constant along the entire portion of the shell that is in contact with the mould wall and that this stress distribution is identical to that at the point of attachment.

Figure 2 on page 7:6 shows the deflected corner region drawn in the same way except that the scales have all been drawn to a greater magnification.

Plotted in this way the figure illustrates some of the basic ideas and results of the model. It shows how the extent of plasticity varies along the shell and how this variation is related to the curvature of the shell, It shows, also, that

Figure 1 : 1300 mm x 300 mm SLAB CAST AT 0.03 m.s^{-1} AT A METALLURGICAL HEIGHT OF 0.1 m, THICKNESSES AND LENGTHS DRAWN TO THE SAME SCALE - ENTIRE QUARTER SECTION

DATA:	AL	E	L1	L2	A	t	delT	meth	QSYS	EMSR
UNITS	'C ⁻¹	N.m ⁻²	m	m	m	m	'C	m	N.m ⁻²	N.m ⁻²



the corner rotates in the case of a slab due to the different extents of contraction on the long and short faces - no other previous model having been able to account for this rotation. Finally, the figure shows that local regions of tensile plasticity can exist in the corner region because of the behaviour of the rigid corner.

Such regions of local plasticity occur when the position of the elasto-plastic boundary coincides with the thickness of the shell, $p=t$, at a position x from the corner. The stress at the elasto-plastic boundary changes sign at this point from positive values near the corner to negative values further away.

Thus the current model predicts the existence of local regions of tensile plasticity adjacent to the solidification front near the corner and regions of compressive plasticity at the solidification front further towards the point of contact with the mould and the middle of the face. Tensile plasticity at the solidification front is a necessary condition for the formation of the internal cracks that are frequently observed in the off-corner region in both billets and slabs cast at high speed. Experimental investigations have established that these internal diagonal cracks originate within the mould (56,65).

Reducing the casting speed reduces the magnitude of the stresses along the whole structure and reduces the extent of this off-corner region of tensile plasticity adjacent to the

solidification front. This latter reduction can produce a situation in which the plastic region is compressive all along the solidification front as illustrated in figure 6.20 .

The basic effect of reducing the casting speed is to make the structure thicker and stronger at all metallurgical heights so that it can better withstand the applied metallostatic pressure. A reduction in casting speed also produces lower temperatures at any given metallurgical height resulting in slightly bigger deflections and longer detached lengths. The results obtained, however, demonstrate that the gain in strength more than compensates for the increase in the net force that the detached lengths must withstand.

The presence of an off-corner internal region of tensile plasticity is directly related to the behaviour of the corner as a rigid hinge. If this condition had been relaxed in the model, the corner would have distorted under the action of the ferrostatic pressure so as to relieve the tension at the solidification front in the off-corner region. Without the rigid corner assumption, tensile plasticity at the solidification front could only have been predicted over the whole shell and not just locally within the off-corner region.

This is the case of results predicted by models based on the finite element method when they do not introduce a specific corner condition (38,37,48). Grill et al. (39) must have introduced a corner condition to their gap formation model because of the peculiar way in which the stresses they report

at the cooled surface jump from maximum tensile values to maximum compressive values from one node to the next. The only condition which could explain such behaviour is a total restriction from movement coupled with an external load assumptions which does not correspond to reality. Even then their finite element based model does not appear to predict local regions of tensile plasticity at the solidification front.

The finite element based results presented by Zetterlund and Kristiansson (48) are consistent in that they do not show violent swings from compressive to tensile stresses between adjacent nodes but show a continuous variation of stress. They can only obtain conditions of tensile plasticity at the solidification front, however, if such conditions exist along the whole structure and if they are generated by a slower cooling rate at the cooled surface than at the solidification front, such a slower cooling rate placing the entire solidification front in tension. This tension arises from the differential contraction of the solidified metal and not from moments imposed by the metallostatic pressure. Zetterlund and Kristiansson contrive to obtain the maximum tensile stress in the off corner region because they assume the solid metal thickness to be least there, thus maximising the value of the differential contraction gradient at the off-corner point.

The assumption of a rigid corner made in this research follows on from the work developed by K V Krishnamurthy (60) which assumed that the solidification process is only affected by

the two dimensional heat flow within a finite region close to the corner edge. Outside the corner region the isothermal surfaces including the solidification front are planes parallel to the sides of the billets. Krishnamurthy's model showed good agreement with experimental results related to the solidification of lead in the form of a simulated square billet edge.

In the case of continuously cast billets and slabs, the variation of heat transfer resulting from the formation of an air gap in the vicinity of the corner appears to produce a departure from this basic idea as illustrated by shells examined after break-out which are thicker towards the middle of the face than near the corner (28). Such break-out shells tend, however, to confirm the validity of Krishnamurthy's approach since the solidification front profile in the near vicinity of the corner corresponds in shape to the predictions of his research. The corner itself is much thicker than the shells in its immediate vicinity, and it is this difference, together with the lower temperature at the corner, that determine the corner as a rigid hinge.

The values predicted by Krishnamurthy (60) for the extent of the corner region are related to the shape he adopted for the iso-thermal surfaces. These values have been used in the present work as the rigid corner length in the analysis of the behaviour of billets and slabs within the mould. The values probably represent an over estimation, but as figure 1 in this chapter illustrates, not a serious overestimation.

The region of tensile plasticity adjacent to the solidification front is likely to advance further towards the corner as the characteristics of the shell will not, in reality, undergo a step change at the assumed boundary of rigidity. However, the thickness and the temperature do, in fact, vary rapidly within the corner region and this has a significant effect on the relative rigidity of the shell. Moreover, if the positions of internal off corner cracks that have been reported (58) can be taken as an indication of the region of maximum tensile plasticity, they can be seen to lie fairly close to the rigid boundary predicted from Krishnamurthy's work.

These internal corner cracks have been observed in slabs of similar sections cast at speeds lower than the 0.02 m.s^{-1} for which figure 1 in this chapter has been predicted. It is a characteristic of the model at its current stage of development that it over-estimates casting speeds for crack free casting. The reasons for this over-estimation are discussed in section 7.4

7.2 THE FORMATION AND PROPAGATION OF LONGITUDINAL OFF-CORNER CRACKS

The formation of longitudinal off-corner cracks is a major problem in both slabs and billets. From a quality control point of view they have been classified into surface longitudinal corner cracks and internal off-corner cracks as they raise different quality problems. Empirical evidence, however, relates both internal and external off-corner cracks to the same influencing factors

- High casting speed.
- Gap formation and distortion within the mould.
- Distortion within the secondary cooling zone.
- High pouring temperature.

These factors correspond to those listed by Brimacombe and Sorimachi (65) with the exception of high casting speed related to the formation of internal off-corner (diagonal) cracks in billets. Such cracks they relate to small billet sizes. The results of this research, however, suggest that even in this case, it is the high casting speed that is the significant factor since these smaller billet sizes are cast at very high speeds. Thus high casting speed would appear to be the cause of internal off-corner cracks both in in slabs, as suggested by Brimacombe and Sorimachi, and in small billets

Indeed, this work suggests that the effect of reducing billet size for any given casting speed is to reduce crack formation.

Such a trend is in agreement with work of Jauch (68), who relates the formation of longitudinal cracks in continuously cast billets and blooms directly to high casting speed.

Longitudinal cracks are said to originate both within the mould and within the secondary cooling zone (56-70). Wyckaert (70) argued that, since surface longitudinal cracks are observed in slabs at the exit of the mould before they propagate towards the center of the slab in the secondary cooling zone, they must be triggered in the mould. Contrary to the other authors cited here, however, he suggests that internal longitudinal cracks are always triggered at the top of the secondary cooling zone.

The model developed here suggest that internal cracks initiated at the solidification front high in the mould can propagate either towards the surface or towards the center, depending on the the evolution of the stress distribution within the solidifying shell. This is in agreement with Wyckaert's observation that longitudinal cracks originate in the mould and with Fujii et al(61) who concluded that internal cracks grow discontinuously.

Figures 21-23 on pages 6:79-81 in chapter 6 illustrates the deformation of the detached corner section of a 200 mm square billet at different metallurgical heights within the mould. It is followed by a second similar set of figures, 24-26 on pages 6:82-84, which apply to a 250 mm square billet under identical conditions.

In both cases the casting speed used in the calculations is 0.06 m.s^{-1} , although the phenomena illustrated by the figures is thought in fact to correspond to a lower casting speed for reasons that will be discussed in section 7.4.

The plastic region at the solidification front of the 200 mm billet is always in compression as the billet descends down the mould from metallurgical heights of 0.1 m to 0.6 m. During the descent, however, the region of compressive plasticity appears to move towards the corner, increasing the extent of the plastic zone at the rigid boundary. This apparent movement, which as we shall see always occurs within the mould is due to the changing balance between deformation of the shells due to thermal effects and deformation due to the mechanical load and to the strengthening of the shell, this strengthening reducing the contrast in rigidity between the corner region and the shells.

In the case of the 250 mm billet, shown within the mould on pages 6:82 to 6:84, a region of tensile plasticity can be observed at the solidification front in the off corner region at a metallurgical height of 0.1 m. As before, however, the region of compressive plasticity moves towards the corner as the billet moves down the mould, causing the region of tensile plasticity in the off-corner region to disappear.

It is clear that as these billets descend down the mould, they move away from the condition of tensile plasticity adjacent to

the solidification front, a condition that has been identified previously as necessary for the formation of an internal crack. It is possible, however, that the existence of tensile plasticity adjacent to the solidification front near the corner of the billet at a metallurgical height of 0.1m may have been enough to trigger the formation of a crack. The question to be considered is what then happened to that crack as the billet moves down the mould.

In order to better illustrate what could happen in such a case, the original series of figures related to the 250 mm billet was completed with two additional figures presented in this chapter for the intermediate metallurgical heights of 0.12 m and 0.20 m (Fig. 3 & 4 on pages 7:16-17). The results shown in these figures allow figure 5 to be drawn (page 7.18) which illustrates how the stress distribution at the rigid boundary where a crack has possibly been triggered develops as the billet descends from 0.1 m to 0.3 m. The stress distribution is illustrated by means of triangles similar to those introduced in chapter four

Although the stresses involved are relatively small, they are enough to involve tensile plasticity near the solidification front (towards the tip of the triangle) at a metallurgical height of 0.1 m. The corresponding adimensional stress, S_0 , is negative at the surface of the billet - the cooled surface is in compression. The distance between the neutral axis and the surface of the billet is 0.134 times the thickness of the shell - $0.134 \times 2.8\text{mm} = 0.375\text{mm}$. If a crack were to form under

FIG 3: DETACHED CORNER SECTION FOR 250 mm SQUARE BILLET AT A METALLURGICAL HEIGHT OF 0.12 m AT 0.06 m.s⁻¹ : INITIAL PREDICTION.

DATA: AL E L1 L2 A t delT meth QSYS EMSR
 UNITS 'C⁻¹ N.m⁻² m m m m 'C m N.m⁻² N.m⁻²

DATA: Al E L1 L2 A t delT meth QSYS EMSR
 dim. .18E-04 .70E+10 .0426 .0426 .008 .003 76 .120 .110E+08 .0060
 *dim. .14E-02 .40E+03 16.60 16.60 2.98 1, YS=.175E+08
 PKstep = .10000 F1 = .16E-01 Q = -.50E-03
 RKerror = .00050 F2 = .16E-01 M3 = .2172
 ITerror = .00001

DETACHED SECTION 1 :

X	C	DW/DX	W	H	S0	F	YF	N
3.0	-.001	-.00	-.0x	.00	.01	.99	.01	.213E+01
4.0	-.001	-.00	-.0x	.08	.05	.97	-.03	.582E+00
5.0	-.001	-.00	-.00	.16	.09	.93	-.07	.529E+00
6.0	-.001	-.00	-.01	.23	.13	.90	-.10	.504E+00
7.0	-.000	-.00	-.01	.29	.17	.87	-.13	.488E+00
8.0	-.000	-.00	-.01	.34	.21	.84	-.16	.476E+00
9.0	-.000	-.00	-.02	.39	.25	.82	-.18	.466E+00
10.0	.000	-.00	-.02	.43	.28	.79	-.21	.457E+00
11.0	.000	-.00	-.03	.47	.31	.78	-.22	.450E+00
12.0	.001	-.00	-.03	.50	.34	.76	-.24	.444E+00
13.0	.001	-.00	-.03	.53	.36	.75	-.25	.439E+00
14.0	.001	-.00	-.04	.55	.37	.74	-.26	.435E+00
15.0	.001	-.00	-.04	.56	.39	.73	-.27	.433E+00
16.0	.001	-.00	-.04	.57	.39	.73	-.27	.432E+00

DETACHED SECTION 2 :

X	C	DW/DX	W	H	S0	F	YF	N
3.0	-.001	.00	.0x	.00	.01	.99	.01	.213E+01
4.0	-.001	-.00	-.0x	.08	.05	.97	-.03	.582E+00
5.0	-.001	-.00	-.00	.16	.09	.93	-.07	.529E+00
6.0	-.001	-.00	-.01	.23	.13	.90	-.10	.504E+00
7.0	-.000	-.00	-.01	.29	.17	.87	-.13	.488E+00
8.0	-.000	-.00	-.01	.34	.21	.84	-.16	.476E+00
9.0	-.000	-.00	-.02	.39	.25	.82	-.18	.466E+00
10.0	.000	-.00	-.02	.43	.28	.79	-.21	.457E+00
11.0	.000	-.00	-.03	.47	.31	.78	-.22	.450E+00
12.0	.001	-.00	-.03	.50	.34	.76	-.24	.444E+00
13.0	.001	-.00	-.03	.53	.36	.75	-.25	.439E+00
14.0	.001	-.00	-.03	.55	.37	.74	-.26	.435E+00
15.0	.001	-.00	-.04	.56	.39	.73	-.27	.433E+00
16.0	.001	-.00	-.04	.57	.39	.73	-.27	.432E+00

MINL1(W2) : .125 MINL2(W1) : .125
 SECTION LENGTH 1 : .125 SECTION LENGTH 2 : .125
 DETACHED LENGTH 1 : .04256 DETACHED LENGTH 2 : .04256

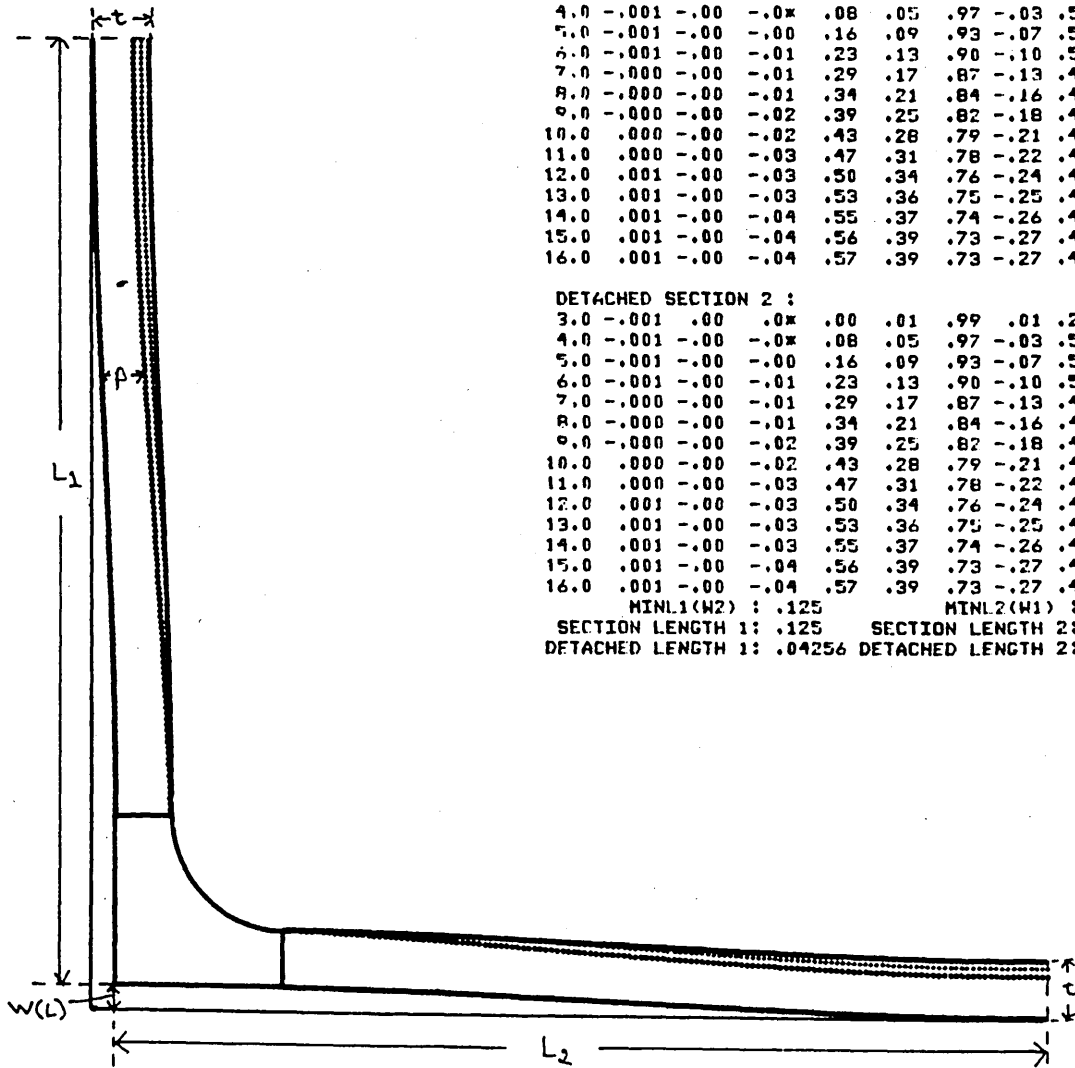


FIG 4 DETACHED CORNER SECTION FOR 250 mm SQUARE BILLET AT A METALLURGICAL HEIGHT OF 0.2 m AT 0.06 m.s⁻¹ : INITIAL PREDICTION

DATA: AL E L1 L2 A t delT meth QSYS EMSR
 UNITS 'C⁻¹ N.m⁻² m m m m 'C m N.m⁻² N.m⁻²

DATA: AL E L1 L2 A t delT meth QSYS EMSR
 dim. .18E-04 .70E+10 .0575 .0575 .011 .004 106 .200 .154E+08 .0060
 adim. .19E-02 .29E+03 14.52 14.52 2.87 1. YS=.244E+08
 RKstep = .10000 F1 = .16E-01 Q = -.60E-03
 RKerror = .00050 F2 = .16E-01 M3 = .1613
 ITerror = .00001

DETACHED SECTION 1 :

X	C	DW/DX	W	M	S0	P	YP	N
2.9	-.002	-.00	-.0x	.06	.04	.98	-.02	.634E+00
3.9	-.001	-.00	-.0x	.14	.08	.94	-.06	.540E+00
4.9	-.001	-.00	-.00	.21	.12	.90	-.10	.510E+00
5.9	-.001	-.00	-.01	.28	.17	.87	-.13	.491E+00
6.9	-.000	-.00	-.01	.34	.21	.84	-.16	.478E+00
7.9	-.000	-.00	-.01	.39	.24	.82	-.18	.467E+00
8.9	.000	-.00	-.02	.43	.28	.79	-.21	.458E+00
9.9	.000	-.00	-.02	.47	.31	.78	-.22	.450E+00
10.9	.001	-.00	-.03	.50	.33	.76	-.24	.445E+00
11.9	.001	-.00	-.03	.52	.35	.75	-.25	.440E+00
12.9	.001	-.00	-.03	.54	.37	.74	-.26	.437E+00
13.9	.001	-.00	-.03	.55	.38	.74	-.26	.436E+00

DETACHED SECTION 2 :

2.9	-.002	.00	.0x	.06	.04	.98	-.02	.634E+00
3.9	-.001	-.00	-.0x	.14	.08	.94	-.06	.540E+00
4.9	-.001	-.00	-.00	.21	.12	.90	-.10	.510E+00
5.9	-.001	-.00	-.01	.28	.17	.87	-.13	.491E+00
6.9	-.000	-.00	-.01	.34	.21	.84	-.16	.478E+00
7.9	-.000	-.00	-.01	.39	.24	.82	-.18	.467E+00
8.9	.000	-.00	-.02	.43	.28	.79	-.21	.458E+00
9.9	.000	-.00	-.02	.47	.31	.78	-.22	.450E+00
10.9	.001	-.00	-.03	.50	.33	.76	-.24	.445E+00
11.9	.001	-.00	-.03	.52	.35	.75	-.25	.440E+00
12.9	.001	-.00	-.03	.54	.37	.74	-.26	.437E+00
13.9	.001	-.00	-.03	.55	.38	.74	-.26	.436E+00

MINL1(W2) : .125 MINL2(W1) : .125
 SECTION LENGTH 1 : .125 SECTION LENGTH 2 : .125
 DETACHED LENGTH 1 : .05750 DETACHED LENGTH 2 : .05750

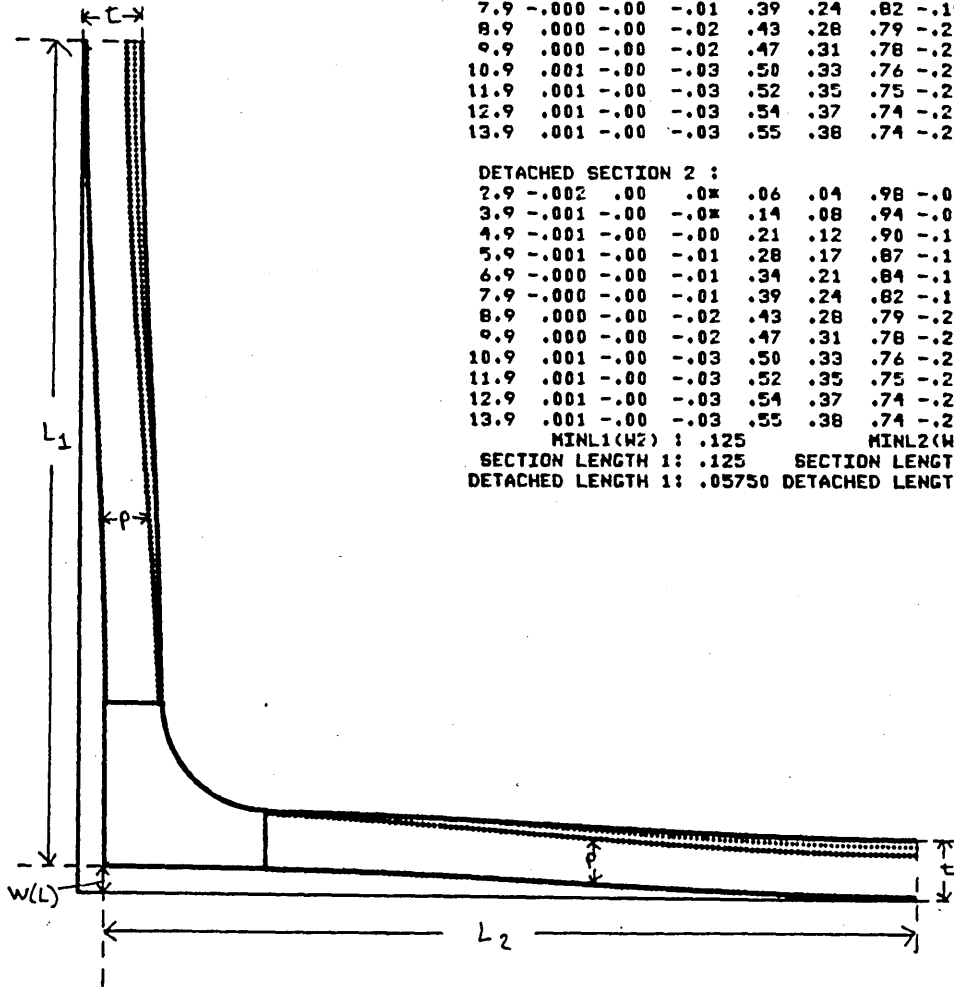
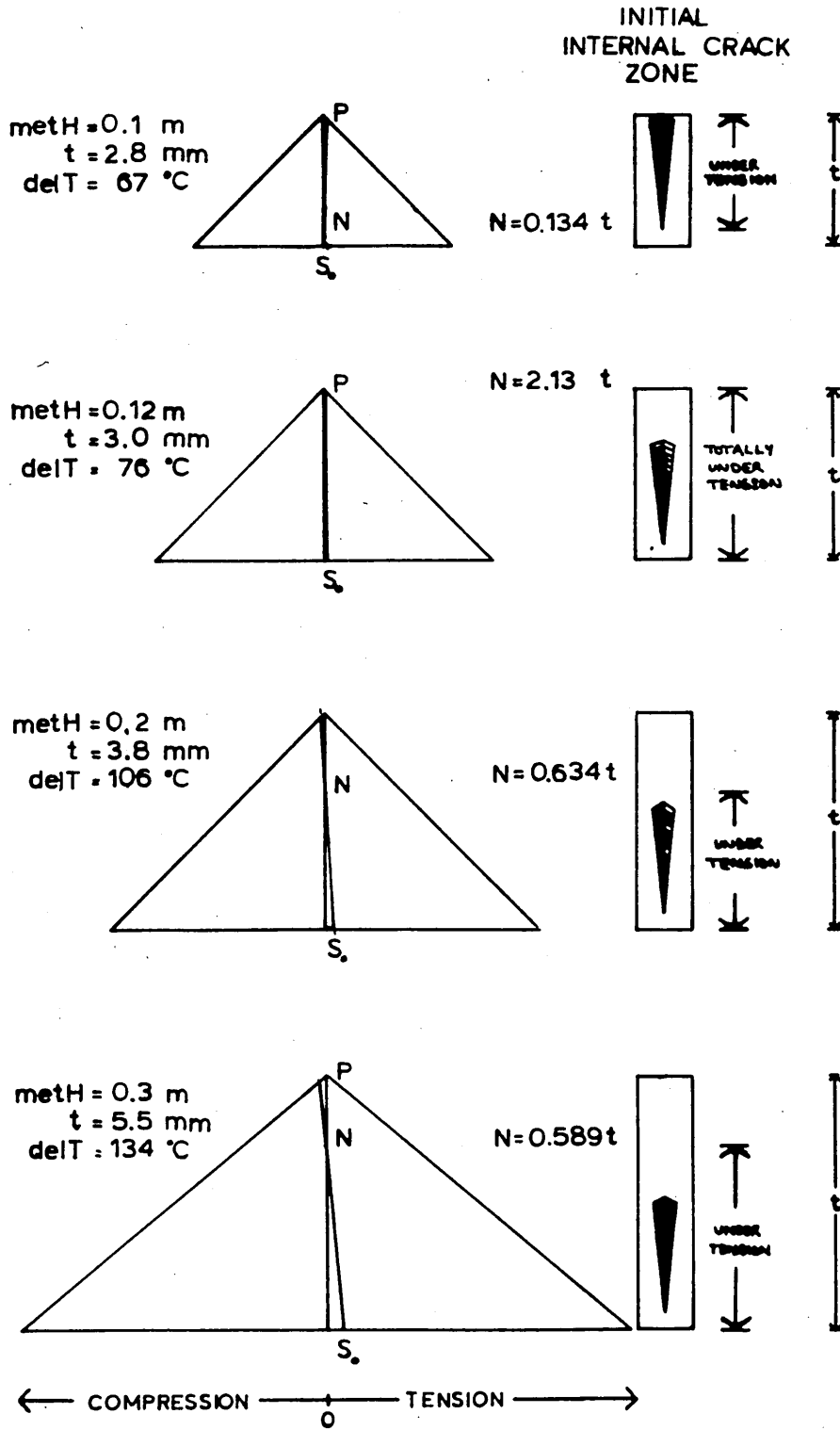


FIG 5: EVOLUTION OF AN INTERNAL CRACK IN A 250 mm SQUARE BILLET CAST AT $0.06 \text{ m}\cdot\text{s}^{-1}$.



these conditions it could run approximately from the solidification front to the neutral axis that is from 2.8mm from the surface to 0.375mm from the surface. It would not be able to run beyond the neutral axis because the metal there would be under compression. This initial potential crack zone is represented next to the triangle in the figure.

The following triangles show that this initial crack zone remains contained within the solidifying shell whilst the stress distribution rotates as the billet moves down the mould, the neutral axis moving out of the cooled surface and returning through the solidification front beyond the crack zone. Once this has happened, the crack zone is placed in a region of tensile stress. At a metallurgical height of 0.3 m for example, the region of tensile stress runs from the cooled surface to the neutral axis which is $0.589 \times 5.5\text{mm}$, or 3.24 mm, into the solidified shell so that the crack zone is completely contained in this tensile region.

Whether or not the crack would propagate towards the surface depends on a number of other factors such as the the magnitude of the tensile stresses involved, the degree of porosity in the crack zone and its stress raising characteristics. It is worth noting, however, that the level of tensile stress involved increases towards the billet surface. Once a crack started to grow towards this surface, then, its growth rate would tend to accelerate.

THE OCCURANCE OF BREAKOUTS AT THE MOULD EXIT.

At its current state of development the model is not equipped to predict the deformation and stress distributions that arise where the billet emerges from the mould and the mould's restraining influence is suddenly removed. For this to be done, the model would have to take into account shear forces acting between successive layers of the strand where the strand bulges suddenly at the mould exit. The model can, however, indicate the magnitude of the deformations and stresses to which the solidified shell would be suddenly subject.

As the billet shell emerges from the mould, the support of the mould is removed and the deformation of the structure will tend towards that of totally unsupported shells. Shear stress exerted by the solidified shell in the mould will limit the degree of deformation that can occur, but the behaviour of a totally unsupported structure at the mould exit indicates the form of the deformation to which the structure will tend as it leaves the mould.

Figure 27 in Chapter 6. page 6:85, illustrates such a hypothetical situation for the 250 mm square billet at a metallurgical height of 0.6 m and is to be compared with figure 26 which is drawn for the same billet at the same metallurgical height but within the mould. Comparison between these two figures shows the extent of the sudden deformation to which the solidified shells would tend. Such comparison is made easier because both diagrams are drawn to the same scale there being no change in solidified metal thickness.

Regions of tensile plasticity can now again be seen at the solidification front in the off-corner region.

Figure 6 on page 7:22 shows the stress distribution triangles at the rigid mould boundary corresponding to the supported and unsupported situations. It also shows an intermediate situation in which the cross-section is totally under tension, the neutral axis being at infinity.

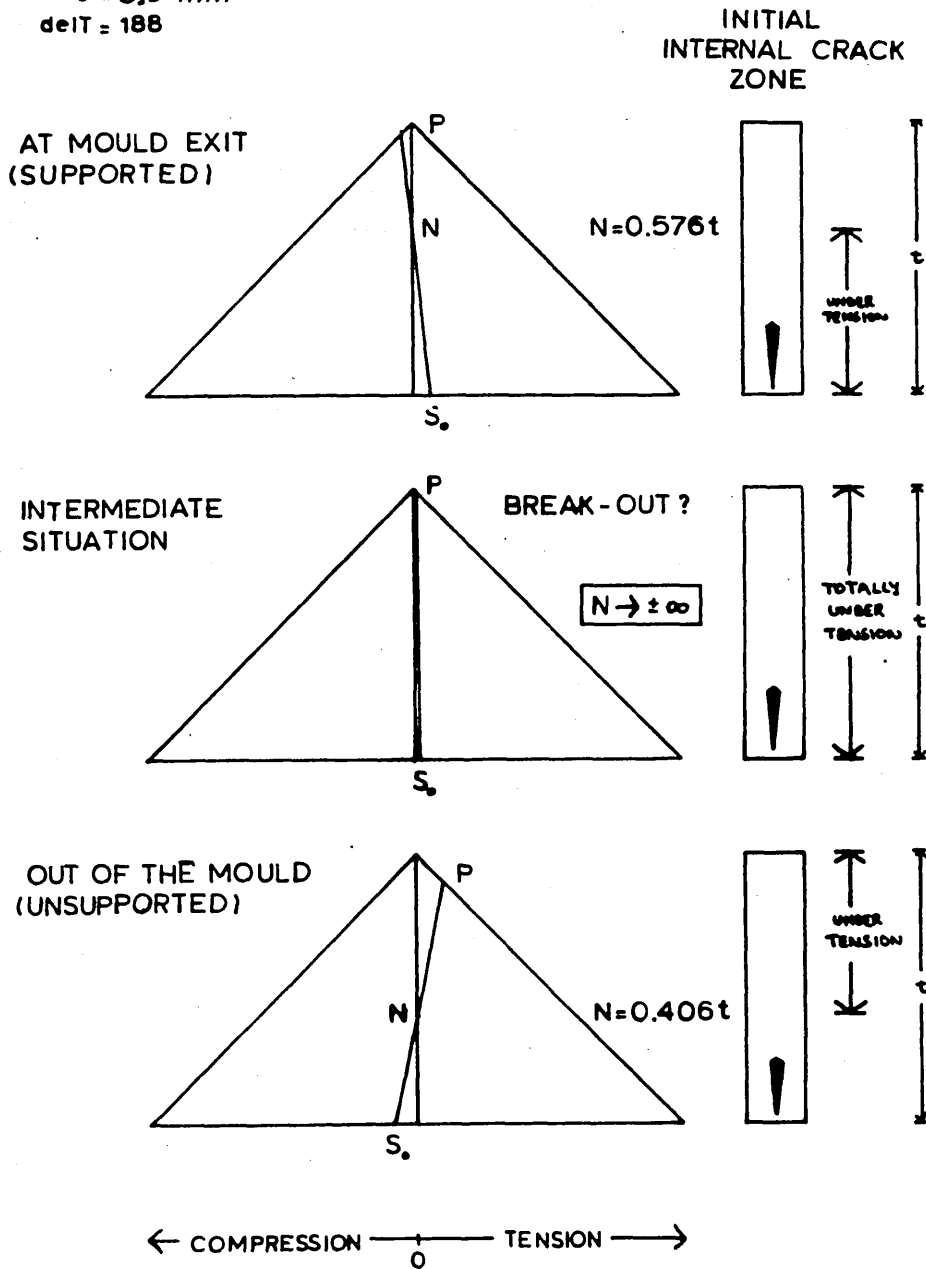
The behaviour of the crack under these conditions is difficult to predict. Were it to be of sufficient extent and the metal sufficiently weak, the crack could propagate during the period of total tension in both directions, ie. towards the surface and towards the centre. Such behaviour would result in break-out.

Alternatively, the establishment of compressive stress once again on the outside of the shell and tensile stresses towards the solidification front could drive the crack towards the inside of the billet - starting a diagonal off-corner crack. This situation is, in fact, the most likely since, during the period of total tension, the crack is more likely to run inwards - towards the weaker material at the higher temperatures.

The relationship between casting speed and section size is critical in this respect. The rotation of the stress distribution line at the rigid boundary when the 200 mm square billet emerges from the mould, for example, would not involve a change in the sign of the moment. It would not, therefore

FIG 6: EVOLUTION OF AN INTERNAL CRACK AT THE MOULD EXIT IN A 250 mm SQUARE BILLET CAST AT 0.06 m.s⁻¹.

metH=0.6 m
 t = 8,9 mm
 delT = 188



involve a period of total tension across the shell; the solidification front would remain in compression.

That this is so is best illustrated by fig 15 in Chapter 6, page 6:51. which shows how the moments at the corner and at the rigid boundary vary with section length for both supported and unsupported conditions, the unsupported conditions being shown by dotted lines. The third figure in the bottom row relates to the casting of billets at 0.06 m.s^{-1} and shows that the unsupported moment corresponding to a half section length of 0.125 m is negative whereas the supported moment is positive - hence the rotation of the stress distribution line. For a half-section length of 0.1 m, however, both moments are positive and not very far apart. The stress distribution line will rotate very little and the tension/compression environment of the crack will not change. Within the limitations of the model in its current state of development, the model would appear to indicate that 200 mm square billets could be safely cast at 0.06 m.s^{-1} but 250 mm square billets cast at the same speed would be prone either to break-out or, more likely, to diagonal off corner cracking. As stated previously, the model over-estimates the casting speeds at which casting can be carried out successfully, the important thing is that model indicates how critical is the relationship between section size and casting speed.

7.3 CHARACTERISTIC BEHAVIOUR OF THE MODEL

As demonstrated in Section 7.2, the model developed in this thesis is able to reproduce behaviour very similar to that shown by industrial continuous casting plants. The significance of this, however, is limited by the uncertainty over the mechanical properties of steels at high temperatures and our present limited understanding of the mechanical behaviour of steels solidifying in the mould of a continuous casting machine.

This limitation is true of all other models for which agreement has been reported between numerical predictions and some industrial observations made under restricted conditions. Such agreements normally result from adjustments made to the empirical parameters incorporated in the model. The fact that these adjustments result in agreement between the model and the industrial performance does not, necessarily, prove the capacity of the model to predict behaviour. There is a fundamental difference between reproducing known results and predicting unknown behaviour.

However, the lack of adequate data on the high temperature mechanical behaviour of recently solidified metals means that some form of adjustment must be allowed for. For such an adjustment to be meaningful, however, it has to be related to a diversity of industrial observations made under a wide range of different conditions.

Before a given model can be justified, therefore, it must demonstrate the ability to predict overall results and trends and not merely to reproduce individual situations. The behaviour demonstrated by the model must be examined and compared with observed behaviour.

Such an examination is a major task, even for the model developed in this work which is considered to be far more flexible than previous models based on the finite element method and more realistic than the previous models based on beam theory. The examination of the behaviour predicted by the model for square billets in the mould, reported in sections 6.2 to 6.5 and 6.7, is considered to be an initial stage in the comprehensive examination that is required.

Figures such as figure 6.12 on page 6:39 demonstrate that, for any given metallurgical height and casting speed, there is a maximum section length that is totally detached from the mould. Since continuous casting moulds tend to be of the same height, this means that a one to one relationship exists between the section size and the casting speed that will result in that section being totally self-supporting when it leaves the mould. The existence of such a relationship is demonstrated in practice by observation of how the bulging of the billet faces at the exit of the mould is determined by the casting speed (68). This is an important confirmation that the qualitative behaviour of the model is in accord with industrial practice.

Graphs such as those of figures 6.13 to 6.16 on pages 6:39-41 show that increasing the casting speed for any given size of cross section will result, at any given metallurgical height, in the development of negative moments both at the corner and at the boundary between the corner region considered rigid and the remainder of the structure. These negative moments can exist easily for the unsupported shell but also, at higher speeds, for the shell still partly supported in the mould.

The elastic stress distribution lines, one of the fundamental concepts involved in the model, have been drawn repeatedly, see for example Figures 6.1 to 6.11 on pages 6:6-16. In those figures, a negative moment can be seen to be associated with tensile plasticity close to the solidification front.

Figures 6.13 , 6.15, 6.17 and 6.18 on pages 6:40/51/59/67 demonstrate that for any given steel solidifying in the mould a one to one relationship exists, at any metallurgical height, between the section size and the casting speed that will result in tensile plasticity close to the solidification front in the off-corner regions of the billet - That is, there is a one to one relationship between the section size and the casting speed that will result in conditions propitious to the generation of internal diagonal cracks.

Small billets are more likely to have cracks not because they are small, but because they are too big for the casting speeds at which they are cast.

The model is verified also in this respect by industrial experience (68,71,72).

The model does not contradict Ushijima's empirical observation that it is possible, for a given section billet, to increase the casting speed -within a limited range- without reaching a cracking situation (58), but it certainly contradicts Ushijima's concluding remark that small size and not casting speed is to blame for the formation of diagonal cracks in billets, a conclusion which was carried on in later articles (65). The existence of a casting speed limit below which no cracking should occur, illustrated for instance by figure 6.13, explains why Ushijima was misled in his conclusion. The model also contradicts the conclusion drawn by Ushijima (58) that unevenness of cooling is the only possible explanation for the formation of internal cracks. The model's present behaviour under the assumption of even cooling suggests that the **usually small** unevenness of cooling in industrial continuous casting moulds has only a secondary effect on the formation of diagonal cracks in billets.

Although the qualitative behaviour demonstrated by the model is now in accord with industrial experience, its numerical predictions do not correspond with industrial practice.

Whatever the reasons why billets of any given section are cast at the speed that they are cast, the formation of internal cracks has been reported to be a problem at values lower than those indicated by the model.

Figure 7, on page 7:34, illustrates the numerical discrepancy between the model's predictions and reported industrial practice.

The figure includes two curves which are representative of the initial predictions of the model.

One curve represents, as a function of the casting speed, the minimum section length which a billet is predicted to require in order for the moment at the assumed rigid boundary to be negative at a metallurgical height of 0.1 m. This curve, therefore corresponds to the minimum section lengths for which tensile plasticity is predicted to occur at 10cm from the meniscus.

The second predicted curve shown represents, also as a function of the casting speed and at the same metallurgical height, the minimum section lengths required for the moment at the corner of the billet to be negative. This second curve is representative of the first curve within a more realistic range of section sizes and casting speeds.

Figure 7 compares these two curves with industrial data (23,37,38,48,58,64,68). Most of the specific billet casting information reported in the literature corresponds to industrial trials under non standard conditions. Jauch (68), however, summarizes data which corresponds to industrial practice in the German Federal Republic - Although Jauch only refers specifically the range of speeds at which billets of

extreme section sizes are cast, the dotted lines in figure 7 are representative of the relationship between section size and casting speed he describes.

Figure 7 shows that a similar relationship is displayed by each series of industrial trials reported although they appear to have been undertaken at relatively slower casting speeds. It is interesting to note that the three trials reported by Ushijima (58) as having resulted in no cracking involved billets of 130mm section cast at speeds below 0.024 m.s^{-1} , nearly half as slow as the speeds reported in more recent articles for similar sections.

The numerical discrepancy between the initial predictions and the reported values of section size and casting speed is thought to be determined to a great extent by two factors : the use of thicknesses related to the liquidus temperature and the use of values of the yield stress which are too high.

The use of values of shell thickness corresponding to liquidus temperature represents an overestimation of the thickness of the solidifying shell under stress, as the contribution of the mushy zone to the build-up of stresses can be considered to be significantly smaller than that of the portion of the shell which is effectively solid. Reducing the thickness to **0.6 of its "liquidus" value** results in a significant reduction of the minimum section length required for a negative moment at the rigid boundary to occur. At a casting speed of 0.06 m.s^{-1} ,

and a metallurgical height of 0.1 m, this minimum section length is reduced in this way from 250 mm to 150mm, as illustrated in figure 7. The corresponding computer print-out is presented in figure 8 on page 7:35. Although this is a rough first approximation of an adjustment of the model which requires further refinement, it demonstrates the importance of making such an adjustment.

The values of the yield stress used for the initial predictions correspond to the highest values reported by Kitaoka (52). Reducing the value of the quasi-static yield stress at 1000 degC, used to derive yield stress values at higher temperatures, from $6.5 \times 10^{-7} \text{ N.m}^{-2}$ to $3.0 \times 10^{-7} \text{ N.m}^{-2}$ reduces further the critical minimum section length considered from 150 mm to about 120 mm. This latter prediction can be seen in figure 7 to have a much better correspondance with industrial practice values of section size and casting speed. The complete results for this new set of data are presented in figure 9 on page 7:40.

The examples referred illustrate how sensitive the model is to further adjustments. Although it is necessary to consider their specific effect for other casting speeds and at other metallurgical heights. the minimum section length curves must follow the displacement described for one particular casting speed. This downwards displacement of the curves will also involve some change in their slopes, but these slopes will clearly remain negative at all points. The curves

corresponding to other metallurgical height will respond with similar displacements to the adjustments made.

Therefore, the qualitative behaviour of the model described previously will not be affected and its validity is not impaired.

However, the adjustments introduced have important qualitative implications. Notice, in figures 8 and 9, that the reduction of the yield stress has involved an increase of the adimensional moment along the solidifying shell. At the points of contact with the mould, in particular, the adimensional moment given in the table of figure 9 ($M(15.6) = 0.94$) approaches unity, and the stress at the cooling surface of the billet is approaching its yield value. The change does not affect all moments along the beam in the same proportion because a new overall equilibrium has to be established for the lower yield stress values used. This response to a necessary decrease of the yield stress values used is described in Section 6.4, and is illustrated in figure 6.17 on page 6:59, for a more comprehensive set of results. These results imply that compressive plasticity at the surface of the billets is going to be predicted for lower values of the yield stress.

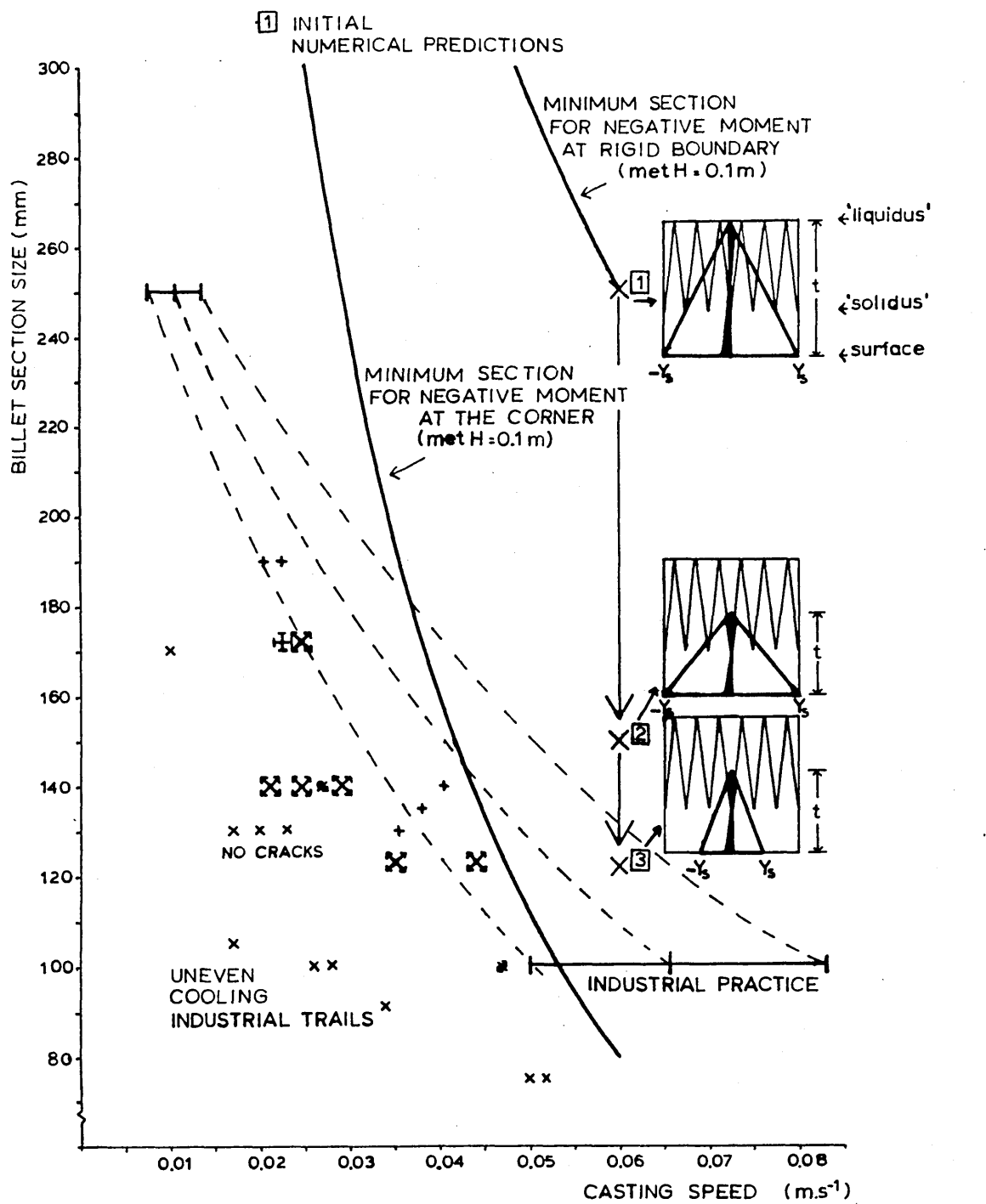
The fact that the plasticity at the surface of the billets is compressive and that the steel is at lower temperatures than in the internal regions of tensile plasticity, confirms the

prediction of a predominant tendency for cracks to be originated internally. However, it is a limitation of the model at this stage that its application is restricted to conditions which preclude plasticity at the surface of the solidifying shell. Although this does not invalidate the predictions made, it limits its capacity to make more accurate predictions. Figures 6.17 & 6.18, show that in order to reduce any further the values of the yield stress used, or in order to increase the values of the Young's modulus used, it is necessary to consider plasticity at the surface of the billet.

An essential characteristic of the behaviour of the model is yet to be put in evidence. The predictions made up to this point have failed to show that for any given section billet, cast at any given speed, maximum negative moments are reached at a metallurgical height which is not equal to zero. However, the preliminary results presented in Section 6.1 show that very high in the mould, where the temperature gradient across the shell is important but the metallostatic pressure is negligible, the moment at the corner is **positive**. The numerical adjustment of the model has thus important qualitative significance in providing further understanding on how and at what height maximum negative moments are reached as this is significant to explaining why cracks occur at different metallurgical heights in the mould.

The model also does not, at present, account for the observation that surface cracks tend to be closer to the edge

of the corner in billets than in slabs (64,68). This is a consequence of the need for further refinement of the assumption of a rigid corner. Figure 6.15, on page 6:51, illustrates the effect of reducing the length of rigid corner. The moment at the rigid boundary does not change significantly although the rigid boundary has been displaced. This is interesting in that it shows that the basic prediction of tensile plasticity near the corner is not affected although the distance at which it occurs can be adjusted further. This adjustment is limited, however, by the restriction that the length of the corner could not be considered, within the present form of the model, to be actually smaller than the thickness. It follows from previous considerations that in an initial stage of solidification **positive** moments at the corner would be predicted. In addition, empirical observations (58 have shown that the radius of curvature surface of the corner (determined by the shape of industrial moulds) is important in determining the formation of internal or external cracks. It would, therefore, be expected that further refinement of the rigid corner assumption would contribute significantly to our understanding - Although much is to be learned yet from the simple rigid corner assumption made.



- ☒ Fredriksson (23)
- ⊕ Grill (37)
- ☒ Sorimachi (38)
- ⊗ Zetterlund (48)
- × Ushijima (58)
- + Van Drunen (64)
- Jauch (68)

Figure 7 REPORTED VALUES OF BILLET SIZE IN RELATION TO CASTING SPEED AND INITIAL NUMERICAL PREDICTIONS.

Figure 8 : RESULTS WITH A THICKNESS REDUCED TO 0.6 IT'S
LIQUIDUS TEMPERATURE PREDICTED VALUE,

QSYS 1000 degC 6.5 x 10⁷ N.m⁻²
CASTING SPEED 0.06 m.s⁻¹
METALLURGICAL HEIGHT 0.1 m

DATA: AL E L1 L2 A t delT meth QSYS EMSR
UNITS: 'C⁻¹ N.m⁻² m m m m 'C m N.m⁻² N.m⁻²

DATA: AL E L1 L2 A t delT meth QSYS EMSR
dim. .18E-04 .70E+10 .0230 .0230 .004 .001 67 .100 .970E+07 .0060
dim. .12E-02 .46E+03 17.58 17.58 3.00 1. YS=.154E+08
RKstep = .10000 F1 = .16E-01 Q = -.48E-03
RKerror = .00050 F2 = .16E-01 M3 = .2556
ITerror = .00010

DETACHED SECTION 1 :

X	C	DW/DX	W	M	S0	F	YF	N
3.0	-.001	-.00	-.0*	-.03	-.01	.98	.02	.230E+00
4.0	-.001	-.00	-.0*	.05	.03	.98	-.02	.647E+00
5.0	-.001	-.00	-.00	.13	.07	.95	-.05	.546E+00
6.0	-.001	-.00	-.01	.20	.11	.91	-.09	.514E+00
7.0	-.001	-.00	-.01	.26	.15	.88	-.12	.495E+00
8.0	-.000	-.00	-.01	.32	.19	.85	-.15	.481E+00
9.0	-.000	-.00	-.02	.37	.23	.83	-.17	.470E+00
10.0	.000	-.00	-.02	.42	.27	.80	-.20	.461E+00
11.0	.000	-.00	-.03	.46	.30	.78	-.22	.453E+00
12.0	.000	-.00	-.03	.49	.33	.77	-.23	.446E+00
13.0	.001	-.00	-.03	.52	.35	.75	-.25	.440E+00
14.0	.001	-.00	-.04	.54	.37	.74	-.26	.436E+00
15.0	.001	-.00	-.04	.56	.39	.73	-.27	.433E+00
16.0	.001	-.00	-.04	.57	.40	.73	-.27	.430E+00
17.0	.001	-.00	-.04	.58	.41	.72	-.28	.429E+00
17.5	.001	-.00	-.04	.58	.41	.72	-.28	.429E+00

DETACHED SECTION 2 :

X	C	DW/DX	W	M	S0	F	YF	N
3.0	-.001	.00	.0*	-.03	-.01	.98	.02	.230E+00
4.0	-.001	-.00	-.0*	.05	.03	.98	-.02	.647E+00
5.0	-.001	-.00	-.00	.13	.07	.95	-.05	.546E+00
6.0	-.001	-.00	-.00	.20	.11	.91	-.09	.514E+00
7.0	-.001	-.00	-.01	.26	.15	.88	-.12	.495E+00
8.0	-.000	-.00	-.01	.32	.19	.85	-.15	.481E+00
9.0	-.000	-.00	-.02	.37	.23	.83	-.17	.470E+00
10.0	.000	-.00	-.02	.42	.27	.80	-.20	.461E+00
11.0	.000	-.00	-.02	.46	.30	.78	-.22	.453E+00
12.0	.000	-.00	-.03	.49	.33	.77	-.23	.446E+00
13.0	.001	-.00	-.03	.52	.35	.75	-.25	.440E+00
14.0	.001	-.00	-.03	.54	.37	.74	-.26	.436E+00
15.0	.001	-.00	-.04	.56	.39	.73	-.27	.433E+00
16.0	.001	-.00	-.04	.57	.40	.73	-.27	.430E+00
17.0	.001	-.00	-.04	.58	.41	.72	-.28	.429E+00
17.5	.001	.00	-.04	.58	.41	.72	-.28	.429E+00

MINL1(W2) : .075 MINL2(W1) : .078
SECTION LENGTH 1 : .075 SECTION LENGTH 2 : .078
DETACHED LENGTH 1 : .02300 DETACHED LENGTH 2 : .02300

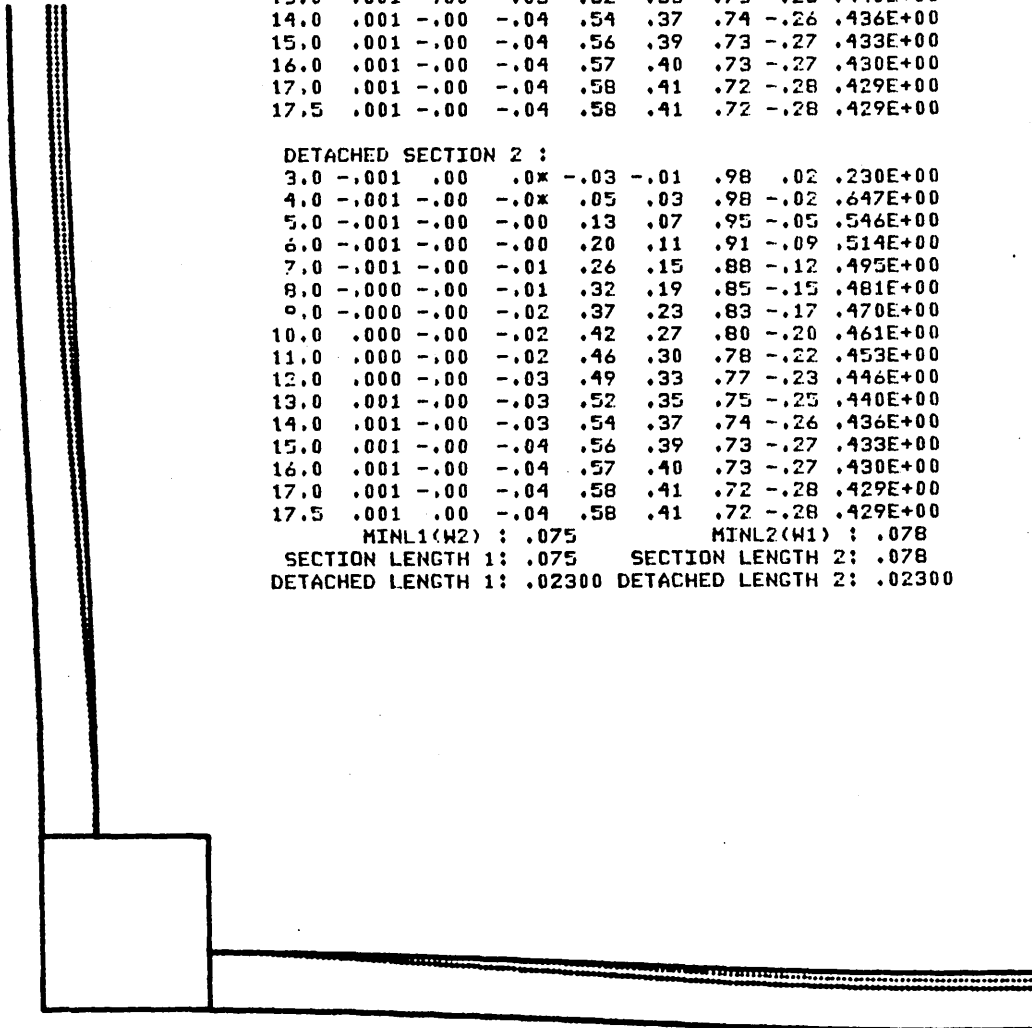


Figure 9 : RESULTS WITH A THICKNESS REDUCED TO 0.6 IT'S LIQUIDUS TEMPERATURE PREDICTED VALUE AND LOWER YIELD STRESSES.

QSYS 1000 degC 3.0 x 10⁷ N.m⁻²
 CASTING SPEED 0.06 m.s⁻¹
 METALLURGICAL HEIGHT 0.1 m

DATA: AL E L1 L2 A t delT meth QSYS EMSR
 UNITS: 'C⁻¹ N.m⁻² m m m m 'C m N.m⁻² N.m⁻²

DATA: AL E L1 L2 A t delT meth QSYS EMSR
 dia. .18E-04 .70E+10 .0205 .0205 .004 .001 67 .100 .448E+07 .0060
 +dia. .12E-02 .99E+03 15.67 15.67 3.00 1. YS=.710E+07
 RKstep = .10000 F1 = .30E-01 Q = -.10E-02
 RKerror = .00050 F2 = .30E-01 M3 = .4941
 ITerror = .00001

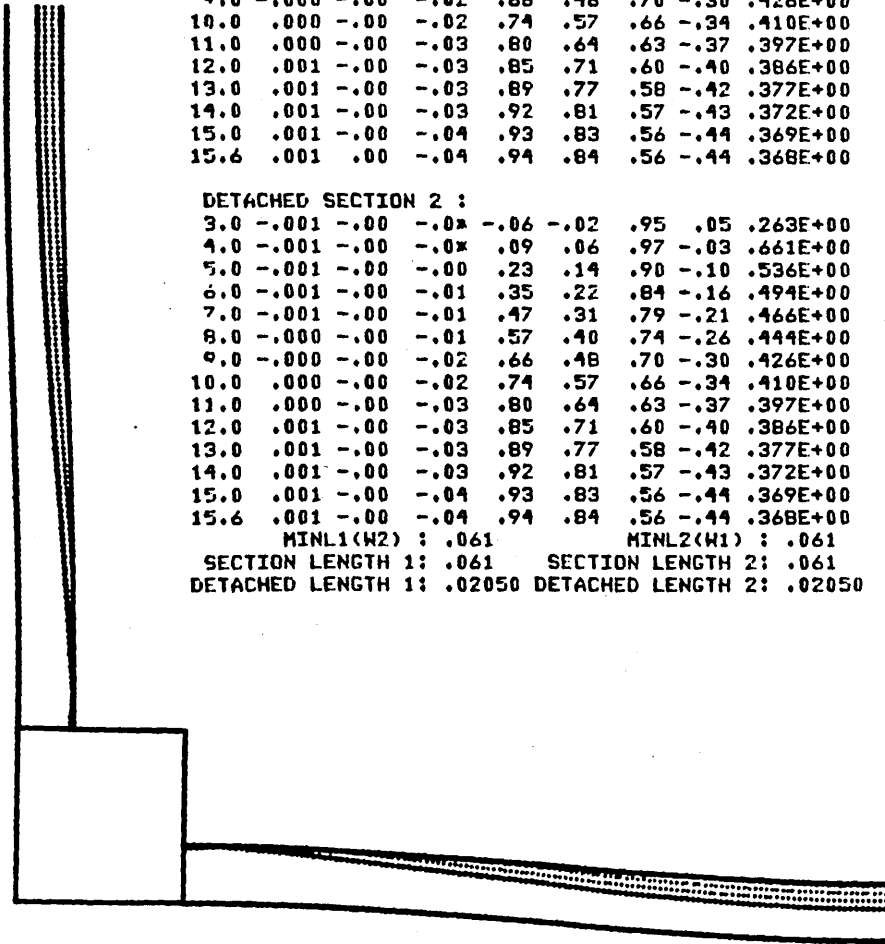
DETACHED SECTION 1 :

X	C	DW/DX	W	M	S0	P	YF	N
3.0	-.001	.00	.0x	-.06	-.02	.95	.05	.263E+00
4.0	-.001	-.00	-.0x	.09	.06	.97	-.03	.661E+00
5.0	-.001	-.00	-.00	.23	.14	.90	-.10	.536E+00
6.0	-.001	-.00	-.01	.35	.22	.84	-.16	.494E+00
7.0	-.001	-.00	-.01	.47	.31	.79	-.21	.466E+00
8.0	-.000	-.00	-.01	.57	.40	.74	-.26	.444E+00
9.0	-.000	-.00	-.02	.66	.48	.70	-.30	.426E+00
10.0	.000	-.00	-.02	.74	.57	.66	-.34	.410E+00
11.0	.000	-.00	-.03	.80	.64	.63	-.37	.397E+00
12.0	.001	-.00	-.03	.85	.71	.60	-.40	.386E+00
13.0	.001	-.00	-.03	.89	.77	.58	-.42	.377E+00
14.0	.001	-.00	-.03	.92	.81	.57	-.43	.372E+00
15.0	.001	-.00	-.04	.93	.83	.56	-.44	.369E+00
15.6	.001	.00	-.04	.94	.84	.56	-.44	.368E+00

DETACHED SECTION 2 :

X	C	DW/DX	W	M	S0	P	YF	N
3.0	-.001	-.00	-.0x	-.06	-.02	.95	.05	.263E+00
4.0	-.001	-.00	-.0x	.09	.06	.97	-.03	.661E+00
5.0	-.001	-.00	-.00	.23	.14	.90	-.10	.536E+00
6.0	-.001	-.00	-.01	.35	.22	.84	-.16	.494E+00
7.0	-.001	-.00	-.01	.47	.31	.79	-.21	.466E+00
8.0	-.000	-.00	-.01	.57	.40	.74	-.26	.444E+00
9.0	-.000	-.00	-.02	.66	.48	.70	-.30	.426E+00
10.0	.000	-.00	-.02	.74	.57	.66	-.34	.410E+00
11.0	.000	-.00	-.03	.80	.64	.63	-.37	.397E+00
12.0	.001	-.00	-.03	.85	.71	.60	-.40	.386E+00
13.0	.001	-.00	-.03	.89	.77	.58	-.42	.377E+00
14.0	.001	-.00	-.03	.92	.81	.57	-.43	.372E+00
15.0	.001	-.00	-.04	.93	.83	.56	-.44	.369E+00
15.6	.001	-.00	-.04	.94	.84	.56	-.44	.368E+00

MINL1(W2) : .061 MINL2(W1) : .061
 SECTION LENGTH 1 : .061 SECTION LENGTH 2 : .061
 DETACHED LENGTH 1 : .02050 DETACHED LENGTH 2 : .02050



7.4 BASIC ASSUMPTIONS

This work has formulated a theoretical model for the mechanical behaviour of the solidifying shell in the mould of a continuous casting machine. Some of the assumptions as to the physical phenomena upon which the model is based are common to other models that have been proposed. Some are unique to this model. The accord with industrial practice demonstrated by the model confirms the validity of these assumptions as a basis to gain understanding.

Independence of the structure at each metallurgical height.

The model assumes that the behaviour of the solidifying shell is fully determined at any one height by parameters that can be defined at that height. These parameters could include the instantaneous average strain rate, the rate of change of overall strain with metallurgical height, the temperature distribution, the metallostatic pressure etc. However, the fact that internal filaments in the shell at a certain height were formed by solidification higher up the mould when the shell had a different shape is not assumed to influence the shell's mechanical behaviour. In effect, the shell at any height with a specified thickness and a specified temperature distribution is assumed to forget how these values came about. This assumption is similar to that made when considering high temperature deformation processes such as hot rolling where the rates at which dynamic softening processes will occur are

assumed to preclude any strain hardening effects (53).

In addition to this forgetfulness effect, the shell at any one height is assumed not to interact mechanically with the shell above it and below it. This assumption is made by all the authors who have analysed mechanical behaviour in the mould. It is justified because the mould limits the strain variations that can occur with changing metallurgical height. The net mechanical force exerted on the shell at any height, through the influence of a shear modulus in the shell, will be vanishingly small because the second differential of the strain with metallurgical height is small. Immediately below the mould where this constraint is removed, however, this assumption would no longer be valid. The metal would bulge out until constrained by the system of support rolls. Between these rolls, also, the assumption would not be valid and this has given rise to a range of models analysing inter-roll bulging.

Double symmetry of the cross-section.

The double symmetry of the cross-section of industrial moulds allows to restrict the analysis to a quarter section. The effect of occasional perturbations which can affect the symmetrical conditions is neglected. The surface of the billet or slab is thus assumed to be parallel to the mould surface at the axis of symmetry.

Beam behaviour:

- .- Cross-section of the solidifying shell/beams originally perpendicular to the cooling wall remain plane and perpendicular to the cooling wall during bending of beam.
- .- Vertical and lateral stresses are neglected, no Poisson's ratio effect.
- .- Distances along the deflected beam are approximated by their projection along the corresponding axis

These are standard assumptions of beam theory which are considered to be appropriate to describe the behaviour of the shell in the mould. At this early stage of solidification the thickness is small compared with the length of even the short faces, and as the mould limits the distortion deflections are also small relative to this length. Both vertical and lateral stresses are negligible relative to stresses along the shell but for the corner region which is assumed rigid.

Constant thickness and constant temperature distribution along the shell

The thickness of the shell and the temperature distribution across it, are assumed to be constant all along the shell at a given metallurgical height.

A significant variation of thickness such as that illustrated by some breakout shells (66) would aggravate the stresses in the thin portion of the shell. Tensile plasticity close to the solidification front in the off-corner portion of the shell, in particular, would be significantly aggravated by a reduction in thickness.

However, the main cause of the variation in thickness illustrated by break-out shells has been shown to result from erosion due to badly placed bifurcated nozzles (72). The correction of this misplacement minimizes variations in thickness in all but the corner portion of the shell.

The variation of heat transfer along the faces due to the gap formation also affects the thickness and temperature distribution, but to a lesser extent. To account properly for this variation the stress model developed would have to be coupled to an adequate heat transfer model but there is no mathematical obstacle in considering varying conditions along the beam. The numerical integration of the curvature, which relates the equilibrium of the cross-section of the shell to the overall equilibrium of the structure, does not require conditions to be constant along the shell

**Linear temperature distribution
across the thickness of the shell.**

The temperature is assumed to be linearly distributed across the thickness of the shell. Although a departure from linearity is associated with the liberation of latent heat, it will tend to be localised towards the solidification front. The effect of neglecting this departure from linearity is small and is more than compensated by the simplification gained.

Rigid corner

By assuming the corner to be effectively rigid, the model has been able to demonstrate the fundamental role that the relative rigidity of the corner plays in the distortion of the shell and the development of local regions of tensile plasticity off the corner. The accord achieved with empirical observation shows this assumption to be the basis for further refinement.

Elasto-perfectly plastic behaviour

The validity of the elasto-perfectly plastic assumption is clearly illustrated by the stress/strain curves reported by Kitaoka et al (52) for steels at high temperature presented in figures 2.16 and 2.17 on page 2:31.

Yield stress linearly dependent upon the temperature

The yield stress is taken as a linear function of the local temperature which is zero at the solidification front. Again, this corresponds to the results reported by Kitaoka (52).

Constant Young's modulus

This simplifying assumption which is also made by Weiner & Boley (28) is reasonable given the uncertainty of the experimental measurements reported. Kitaoka's stress/strain curves (52) suggest the Young's modulus to be constant.

The physical analogue contributed to the research in providing a basis for understanding which was instrumental in the development of the theoretical model.

When the construction of this analogue was finally completed, the theoretical tools for the prediction of the distortion of the bimetallic structure had been developed to satisfaction. The computer program presented in appendix 2 had demonstrated it's capacity to predict the deflection of the bimetallic structure in various experiments reported in chapter 3.

The shape distortion of the bimetallic structure is analogous to that of the solidifying shell, and the role of the rigid corner is clearly illustrated. The analogy, however, ends here as the stress build-up which determines the formation of cracks in continuous casting billets and slabs is fundamentally different to the stress build-up within the bimetallic strips. Subjecting the bimetallic strips structure to extreme conditions would lead to failure at the bond between the two metals which form each strip before any significant plasticity could originate within the metals.

8.1 CONCLUSIONS

A theoretical model has been formulated which relates the stresses within the thin shells of steel solidifying in the mould of a continuous casting machine to shape distortion and gap formation. This model, in accord with industrial practice, demonstrates :

- 1.- A monotonously increasing relationship between metallurgical height down the mould and the extent of the gap for any billet section and casting speed.
- 2.- A one to one relationship between casting speed and the maximum section length which is totally detached from the mould at any metallurgical height.
- 3.- A one to one relationship between casting speed and the maximum section length which does not present tensile plasticity close to the solidification front near the corner.
- 4.- A monotonously^{ically} increasing relationship between casting speed and bulging at the exit of the mould.

A mechanism of crack propagation has been demonstrated which provides explanation for both internal and external cracks.

On the basis of this mechanism, the model demonstrates how an internal crack originated high in the mould can propagate to the surface of the billet or slab before mould exit. Thus, the predictions of the theoretical model show that external cracks observed at mould exit could in certain circumstances be originated internally.

8.2 FURTHER WORK

The work has shown that plasticity tends to occur at the outer surface as well as at the solidification front, it is therefore prioritary to extend the elastic and plastic stress distribution equations and the cross-section moment and force equilibrium equations for this case. This will improve the flexibility of the model and allow for better numerical predictions to be made.

The criteria used to define the thickness of the shell under stress should be refined further. It seems convenient to define an effective thickness in relation to both the liquidus and solidus temperatures. This would involve the testing of various hypotheses in relation with practical observations.

A comparative analysis of the behaviour of different steels related to their propensity to crack formation can be undertaken with data available in the literature. The results reported by Kitaoka (52) for different steels provide a good initial basis for further investigation.

The behaviour of the model could now be investigated as far up the mould as necessary in order to identify the metallurgical height giving the maximum tensile plasticity close to the solidification front. This would allow the prediction of the maximum section sizes which could be cast at any given speed without tensile plasticity close to the solidification front.

REFERENCES

- 1.- Matuscha, B.; Arch.Eisenhuttenwes 2 (1928/29) pgs.405/13.
- 2.- Mikura, E.T.; Report SM/97/48 (1948) BISRA.
- 3.- Diener, A. , Drastik, A. & Haumann, W.; Arch.Eisenhuttenwes 43 (1972) pgs. 523/33.
- 4.- Mackenzie, ^{I.M.} A. & Donald, A.; ^{Journal} ~~Trans.~~ Iron Steel Inst. 166 (1950) pgs. 19/28.
- 5.- Behrens, K.F. & Weingart, F.; Stahl and Eisen 89 (1969) pgs. 1457/67.
- 6.- Behrens, K.F. & Weingart, F.; Thyssenforch 2 (1970) pgs. 55/65.
- 7.- Bishop, M.F. , Brandt, F.A. & Pellini, W.S.; Trans.American Inst.Min.Met. 194 (1952) pgs. 44/48.
- 8.- Druzhinin, V.P. & Mazun, A.I.; Stahl in English 5 (1961) pgs. 328/9.
- 9.- Veinik, A.I.; Thermodynamics for the foundryman (1960) MacLaren New York.
- 10.- Martinez-Fueyo, F.; M.Phil Thesis (1978) Sheffield City Polytechnic.
- 11.- Tezuka, M. , Tatukawa, M. , Wakimoto, H. & Shimada, M.; Tetsu-to-Hagane 60 n4 (1974), SIOI.
- 12.- Rudoi, L.S.; I Gornorudn Prom 15 n2 (1974) pgs. 15/6.
- 13.- Roztkov, V.P. , Martynov, O.V. & Sherbakov, L.M.; Izv.VUZ Chernaya Metall. 5 (1974) pgs.53/4.
- 14.- Akimenko, A.D. & Skortsov, A.A.; Izv.VUZ Chernaya Metall. 12 (1958) pgs. 45/50.
- 15.- Jacobi, H. ; Archiv.Eisenhuttenwes 47 n7 (1976) pgs.441/6.
- 16.- Klipov, A.D., Kolpakov, A.I., Chigrinov, M.G. & Ballard, E.R.; Stahl in English 2 (1971) pgs. 107/11.
- 17.- Takeuchi, H., Mori, H., Nishida, T., Yanai, T. & Mukunashi, k.; Trans ISIJ 19 (1979) pgs.274/82.
- 18.- Hills, A.W.D. ; Msc advanced lectures on continuous casting. Sheffield City Polythecnic, 1979.

- 19 - Volk G. & Wunnemberg, K. Kleipzig Fachber 80 (1972) pgs. 491/9.
- 20.- Ul'yanov, V.A., Kitaev, E.M. & Skvortsov, A.A. : Izv VUZ Chernaya Metall. 11 (1978) pgs. 34/8.
- 21.- Taylor, C.R.: "CC up to date" special lecture Metall. Trans. 6B (1975) pgs. 359/75
- 22.- Singh, S.N & Blazek, K.E Journal of Metals Oct. (1974) pgs. 17/27
- 23.- Fredriksson, H. & Thegerstrom, M ; Scand. Journal Metall. 8 (1979) pgs. 232-240.
- 24.- Akimenko, A.D., Skvortsov, A.A., Stoyanov, A.Yu., Dvoretiskii L N. Pokrovskii, V.A. & Zhuravlev, P.Ya. Steel in the USSR Feb. (1979) pgs. 95/7
- 25.- Dyudkin, D.A., Onopchenco, V.M., Taub, L.A., Kovalenko, V.S. & Kondratyuk, A.M ; Steel in the USSR Sep. (1979) pgs 450/1
- 26.- Savage, J.; J. Iron Steel Inst. 198 (1962) pgs. 41/7.
- 27 - Tien R.H. & Koump V.; J. Appl. Mech. 36 Dec. (1969) pgs. 763/7
- 28.- Weiner, J.H. & Boley, B.A.; J. Mech. Phys. Solids 11 (1963) pgs 145/54.
- 29.- Richmond, O. & Tien, R.H.; J. Mech. Phys. Solids 19 (1971) pgs 273/84
- 30.- Oeters, F. & Saderman, K.; Archiv. fur das Eisenhuttewesen 45 nll (1974) pg. 737 (translation 17pgs).
- 31.- Adenis, J.P., Coats, K.M. Ragone, D.V.; J. Inst. of Metals 91 (1963) pgs. 395/403
- 32.- Hills, A.W.D.; JISI Jan. (1965) pgs. 18/26.
- 33 - Hills A.W D ; Trans AIME 239 Jul (1969) pgs. 1481/92.
- 34.- Bamberger, M., Nadin, S., Barry, G.B.; Iron and Steel Int. Feb (1977) pgs. 43/8
- 35.- Brimacombe, J.K., Weinberg, F.; JISI Jan (1973) pgs. 24/33.
- 36 - Brimacombe J K. Lait J E., Weinberg F.; Iron Making Steel-Making n2 (1974) pgs. 90/7.
- 37 - Gill, A. Brimacombe J K. & Weinberg F Iron Making Steel-Making n1 (1976) pgs. 38/47.

- 38 - Sorimachi K. & Brimacombe J K.; IronMaking SteelMaking n4 (1977) pgs. 240/5.
- 39.- Grill,A.,Sorimachi,K.,Brimacombe,J.K.;Metall.Trans. 7b Jun (1976) pgs. 177/89
- 40.- Irving,W.R.; JISI Mar.(1967) pgs. 271/7.
- 41 - Irving,W.R. & Perkins.A. Math.Process Models in Iron & Steel Making, chap.IV The Metals Society (1975).
- 42 - Mizikar E.A.; Trans AIME 239 Nov (1967) pgs. 1747/53.
- 43.- Pehlke,R.D.; Metals Eng.Quarterly May (1964) pgs. 42/7.
- 44 - Szekely.J. & Yadaya R.T.; Math Process Models in Iron & Steel Making, chap.IV The Metals Society (1975).
- 45 - Rubinstein L I.; "The Stefan Problem" Translation of Mathematical Monographs AMS, vol.27 (1971).
- 46 - Williams J.R.,Lewis R.W.,Morgan K..Int.J Num.Methods in Eng. 14 (1979) pgs 1/9.
- 47 - Kristiansson.J O.;J.of Thermal Stresses 5 (1982) pgs.315/330.
- 48.- Zetterlund,E.H.,Kristiansson,J.O.;Scand.Journal Metall. 12 (1982) pgs. 211/216
- 49.- Yamada,Y.,Yoshimura,N.;Int.J.Mech.Sc. 10 (1968) pgs.1189/1196
- 50.- Knothe,K.,Muller,W.; Int.J.Mech. 22 (1980) pgs 167/172.
- 51 - Wray,P.J. & Holmes,M.F.; Metall.Trans. 6A (1975) pgs.1189/96.
- 52.- Kitaoka,H.,Kinoshita,K.& Emi,T.; Kawasaki Seitetsu Giho n3 12 (1980) pgs 93/101
- 53.- Jonas,J.J.,Sellars,C.M.,Tegart,W.J.McG.;Int.Metal. Reviews 14 (1969) pgs. 1/24.
- 54.- Sellars,C.M.,Tegart,W.J.McG.;Int.Metal.Reviews 17 (1972) pgs. 1/23
- 55.- Cristescu,N.; "Dynamic Plasticity" North-Holland Publishing Company, Amsterdam (1967).
- 56.- Irving,W.R.,Perkins,A.,Gray,R.; IronMaking SteelMaking n3 (1984) pgs. 146/151.
- 57.- Irving,W.R. & Perkins,A. ; IronMaking SteelMaking n3 (1984) pgs. 152/162

- 58.- Usuijima K.; ISIJ April (1965) pgs.529/539
- 59.- Delmont,A., "Modelos Matematicos de Transferencia de Calor en el Proceso de Colada Continua" Maths-Degree Thesis, Universidad Central de Venezuela. (1978).
- 60 - Krishnamurthy K.V.; "Studies on solidification of metals with two dimensional heat flow". PhD Thesis. Imperial College (1969)
- 61.- Fujii,H., Ohashi,T., Hiromoto,T. ; Trans ISIJ vol 18 (1978) pgs. 510/518
- 62.- Nakato,H., Ozawa,M., Kinoshita,K., Habu,Y., Emi,T.; Trans ISIJ vol 24 (1984) pgs.957/965
- 63.- Miyasaki,J., Takasuke,M., Narita,K.; 2d Process Technology Conference AIME Chicago (1981) pgs 35/43.
- 64.- Van Drunen,G., Brimacombe,J.K., Weinberg,F. IronMaking SteelMaking n2 (1975) pgs 125/133
- 65.- Brimacombe,J.K., Sorimachi, K IronMaking SteelMaking n2 (1975) pgs 489/505
- 66.- Schmidt,L. & Fredriksson,H.; IronMaking SteelMaking n1 (1975) pgs 61/67.
- 67.- Kojima,S., Matsukawa,T., Kodama,M. ; 2d Process Technology Conference AIME Chicago (1981) pgs 255/262
- 68.- Jauch,R. . Stahl Eisen 1978. 98 (6) March(1978) pgs. 244/254
- 69.- Nemoto,H. ; Transactions ISIJ 16 (1978) pgs. 51/65.
- 70.- Weinberg F. ; Metall Trans, 10b dec(1979) pgs 513/522.
- 71.- Stiebitz,J. & Doljesi,Z. ; Hutn.Listy 32 (1977) pgs 794/805.
- 72.- Wyckaert,A. ; SEASI Quarterly oct(1975) pgs 60/71.
- 73 - Samarasekera I.V. & Brimacombe J.K. Int.Metals Reviews n6 (1978) pgs. 286/300

Al 1 CHARACTERISTICS AND THERMAL BEHAVIOUR OF BIMETALLIC STRIPS

The bimetallic strips used in the physical model are strips of composite metal comprising two layers with different thermal expansion coefficients: a high expansion (H.E.) layer and a low expansion (L.E.) layer, rigidly bonded at their interface.

When uniformly heated the bimetallic strip bends into the arc of a circle, as the H.E. layer will tend to expand more than the L.E. layer and the rigid bond forces a compromise between the expansions. The bond leads to the bending and it also leads to a build up of moments within the strip which do not disappear with the bending but reach an equilibrium distribution.

In analysing the behaviour of bimetallic strips, the width of the strip is assumed to be much smaller than its length and the Bernoulli-Euler assumption is made, that is, sections which are plane and perpendicular to the axis of the strip (or beam) before thermal or mechanical loading remain so after loading and the effect of lateral contraction is negligible (Poisson's ratio is taken as equal to zero).

Within the range of temperatures and loads used in this work, the bimetallic strips behave elastically so that Hooke's Law stands.

For the sake of simplicity an initially flat bimetallic beam is considered in the analysis; this is not a restriction though as it is assumed that the equations of equilibrium are

linear relations between the forces and couples involved both in the thermal and in the mechanical behaviour of the beams.

Let us now assume that the strip is heated uniformly through a temperature change $T - T_0$,

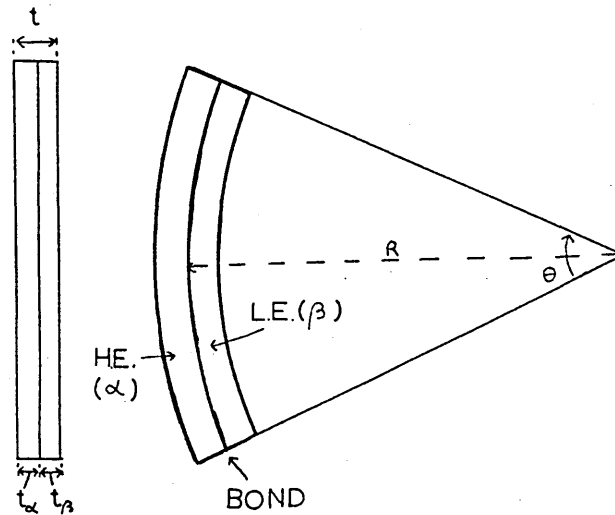


FIGURE 1 : DEFLECTION OF BIMETALLIC STRIP

t_α : thickness of H.E. layer.

t_β : thickness of L.E. layer.

L_0 : initial length of the beam.

L_α : length of the H.E. layer neutral plane.

L_β : length of the L.E. layer neutral plane.

d_α : distance from the H.E. layer neutral plane to the bond.

d_β : distance from the L.E. layer neutral plane to the bond.

R : the radius of curvature of the bond.

α : coefficient of thermal expansion of H.E. layer.

β : coefficient of thermal expansion of L.E. layer.

θ : angle subtended at the centre of curvature.

E_α : Young's modulus of elasticity of H.E. layer.

E_β : Young's modulus of elasticity of L.E. layer.

We then have,

$$L_{\alpha} > R \theta \quad ; \quad L_{\alpha} = (R + d_{\alpha}) \theta \quad \text{where } d_{\alpha} > 0 \quad 1$$

$$L_{\beta} > R \theta \quad ; \quad L_{\beta} = (R - d_{\beta}) \theta \quad \text{where } d_{\beta} > 0 \quad 2$$

and,

$$L_{\alpha} - L_{\beta} = (d_{\alpha} + d_{\beta}) \theta > 0 \quad 3$$

Now, the length of each Normal plane is the length that each layer would reach if unrestrained by the other, that is,

$$L_{\alpha} = L_0 [1 + \alpha (T - T_0)] \quad 4$$

$$L_{\beta} = L_0 [1 + \beta (T - T_0)] \quad 5$$

and,

$$L_{\alpha} - L_{\beta} = L_0 (\alpha - \beta) (T - T_0) \quad 6$$

We then have,

$$(d_{\alpha} + d_{\beta}) \theta = L_0 (\alpha - \beta) (T - T_0) \quad 7$$

that is,

$$\theta = L_0 (\alpha - \beta) (T - T_0) / (d_{\alpha} + d_{\beta}) \quad 8$$

We need to find equations for "d" and "d" in terms of the basic characteristics of the strip.

The stress and strain vary with the distance from the bond.

Lets consider a small filament of thickness "x" and at a distance "x" from the bond. On any cross section of this filament we have,

$$\sigma(x) = E_{\alpha} \xi(x) \quad \forall x \quad (0, t_{\alpha}) \quad (\text{H.E. layer}) \quad 9$$

$$\sigma(x) = E_{\beta} \xi(x) \quad \forall x \quad (-t_{\beta}, 0) \quad (\text{L.E. layer}) \quad 10$$

where " $\sigma(x)$ " is the stress acting upon the cross section and " $\xi(x)$ " is the strain in the direction perpendicular to the cross section.

The strain is given by,

$$\xi(x) = \frac{L_\alpha - (R+x) \Theta}{L_\alpha} \quad \forall x \quad (0, t_\alpha) \quad (\text{H.E. layer}) \quad 11$$

$$\xi(x) = - \frac{L_\beta - (R+x) \Theta}{L_\beta} \quad \forall x \quad (-t_\beta, 0) \quad (\text{L.E. layer}) \quad 12$$

Then, the stress is given by Hooke's Law,

$$\sigma(x) = E_\alpha \frac{L_\alpha - (R+x) \Theta}{L} \quad , \quad \forall x \quad (0, t_\alpha) \quad (\text{H.E. layer}) \quad 13$$

$$\sigma(x) = - E_\beta \frac{L_\beta - (R+x) \Theta}{L} \quad , \quad \forall x \quad (-t_\beta, 0) \quad (\text{L.E. layer}) \quad 14$$

from equations (1) and (2),

$$\sigma(x) = (E_\alpha \Theta / L) (d - x) \quad , \quad \forall x \quad (0, t_\alpha) \quad (\text{H.E. layer}) \quad 15$$

$$\sigma(x) = (E_\beta \Theta / L) (d + x) \quad , \quad \forall x \quad (-t_\beta, 0) \quad (\text{L.E. layer}) \quad 16$$

The force on the cross section considered in each layer is,

$$F_\alpha(x) = E_\alpha W \Theta / L_\alpha (d_\alpha - x) x \quad , \quad \forall x \quad (0, t_\alpha) \quad (\text{H.E. layer}) \quad 17$$

$$F_\beta(x) = E_\beta W \Theta / L_\beta (d_\beta + x) x \quad , \quad \forall x \quad (-t_\beta, 0) \quad (\text{L.E. layer}) \quad 18$$

and the moments of these forces about the bond are,

$$M_\alpha(x) = E_\alpha W \Theta / L_\alpha (d_\alpha x - x) x \quad , \quad \forall x \quad (0, t_\alpha) \quad (\text{H.E. layer}) \quad 19$$

$$M_\beta(x) = E_\beta W \Theta / L_\beta (d_\beta x + x) x \quad , \quad \forall x \quad (-t_\beta, 0) \quad (\text{H.E. layer}) \quad 20$$

Integrating the forces within each layer,

$$F_\alpha = \int_0^{t_\alpha} \frac{E W \Theta}{L} (d_\alpha - x) dx \quad (\text{H.E. layer}) \quad 21$$

$$F_\beta = \int_{-t_\beta}^0 \frac{E W \Theta}{L} (d_\beta + x) dx \quad (\text{L.E. layer}) \quad 22$$

that is,

$$F_{\alpha} = \frac{E_{\alpha} W \Theta}{L_{\alpha}} (2 d_{\alpha} t_{\alpha} - t_{\alpha}^2) \quad (\text{H.E. layer}) \quad 23$$

$$F_{\beta} = - \frac{E_{\beta} W \Theta}{L_{\beta}} (2 d_{\beta} t_{\beta} - t_{\beta}^2) \quad (\text{L.E. layer}) \quad 24$$

Integrating the moments within each layer,

$$M = \int_0^{t_{\alpha}} \frac{E_{\alpha} W \Theta}{L_{\alpha}} (d_{\alpha} x - x^2) dx \quad (\text{H.E. layer}) \quad 25$$

$$M = \int_{t_{\beta}}^0 \frac{E_{\beta} W \Theta}{L_{\beta}} (d_{\beta} x + x^2) dx \quad (\text{L.E. layer}) \quad 26$$

that is,

$$M_{\alpha} = \frac{E_{\alpha} W \Theta}{L_{\alpha}} (3 d_{\alpha} t_{\alpha}^2 - 2 t_{\alpha}^3) \quad (\text{H.E. layer}) \quad 27$$

$$M_{\beta} = - \frac{E_{\beta} W \Theta}{L_{\beta}} (3 d_{\beta} t_{\beta}^2 - 2 t_{\beta}^3) \quad (\text{L.E. layer}) \quad 28$$

For equilibrium,

$$F_{\alpha} + F_{\beta} = 0 \quad 29$$

$$M_{\alpha} + M_{\beta} = 0 \quad 30$$

We then have from (29), (23) and (24),

$$E_{\alpha} (2 d_{\alpha} t_{\alpha} - t_{\alpha}^2) - E_{\beta} (2 d_{\beta} t_{\beta} - t_{\beta}^2) = 0 \quad 31$$

and from (30), (27) and (28),

$$E_{\alpha} (3 d_{\alpha} t_{\alpha}^2 - 2 t_{\alpha}^3) + E_{\beta} (3 d_{\beta} t_{\beta}^2 - 2 t_{\beta}^3) = 0 \quad 32$$

Let,

$$n = E_{\alpha} / E_{\beta} \quad ; \quad m = t_{\alpha} / t_{\beta} \quad 33$$

we then have,

$$2 n m d_{\alpha} - 2 d_{\beta} + (t_{\beta} - n m t_{\alpha}) = 0 \quad 34$$

$$3 n m^2 d_{\alpha} + 3 d_{\beta} - (2 t_{\beta} + 2 n m^2 t_{\alpha}) = 0 \quad 35$$

that is,

$$d_{\alpha} = \frac{t_{\alpha} (1 + 3 n m^2 + 4 n m^3)}{6 n m (1 + m)} \quad 36$$

$$d_{\beta} = \frac{t_{\beta} (4 + 3 m + n m^3)}{6 (1 + m)} \quad 37$$

We can now express equation (8) in term of the basic characteristics of the strip using (36) and (37),

$$\Theta = \frac{6 (\alpha - \beta) (T - T_0) n m^2 (1 + m) L_0}{(1 + 4 n m^3 + 3 n m^2) t_{\alpha} + (4 n m^2 + 3 n m^3 + n^2 m^5) t_{\beta}} \quad 38$$

That is, in term of $t = t_{\alpha} + t_{\beta}$,

$$\Theta = \frac{6 L_0 (\alpha - \beta) (1 + m)^2 (T - T_0)}{t [3 (1 + m)^2 + (1 + n m) (1/n m + m^2)]} \quad 39$$

Since the radius of curvature R can be assumed to be very much greater than the thickness of the bimetallic strip, the following approximation can be made,

$$L_0 = R \theta$$

and, from equation 39, we have,

$$\frac{l}{R} = \frac{6 (\alpha - \beta) (1 + m)^2 (T - T_0)}{t [3 (1 + m)^2 + (1 + n m) (1/n m + m^2)]} \quad 40$$

The majority of commercial bimetals, and in particular the one used (TELCON 200), are made with components of equal thickness and so that the moduli of elasticity are similar. Equation 40 can therefore be simplified by putting $m = n = 1$,

$$\frac{l}{R} = \frac{3}{2 t} (\alpha - \beta) (T - T_0) \quad 41$$

Al.2 THE EFFECT OF THERMAL STRESS UPON THE STRUCTURE

Equation Al.1.41 gives the change of curvature of an unrestrained bimetallic strip as temperature changes from T_0 to T . As part of the structure it will interact with the other bimetallic strip considered. An equilibrium configuration is reached and as the corner is considered rigid we know that the moments which the strips apply upon each other at the corner are equal and opposite. As the strips are fixed at right angles their deflections at the rigid-elastic boundaries are equal and opposite. So are the slopes of these deflections.

Not taking into account the mechanical load for the time being, the deflection of each strip results from the combined effects of its own thermal bending and of the moment to which it is subjected at the corner. Under the assumption of elasticity the principle of superposition states that the resulting deflection is the sum of the deflections corresponding to both factors. One way of splitting the situation considered in two is to consider separately two situations with the corner pinned. In one situation the strips bend freely subjected to the temperature change. In the other they bend subjected to a moment at the corner. The principle of superposition implies that the resulting deflection is simply the sum of the deflections obtained in these situations. This principle also applies to the angle of rotation at the corner.

Figure 2 illustrates the superposition adopted in the analysis,

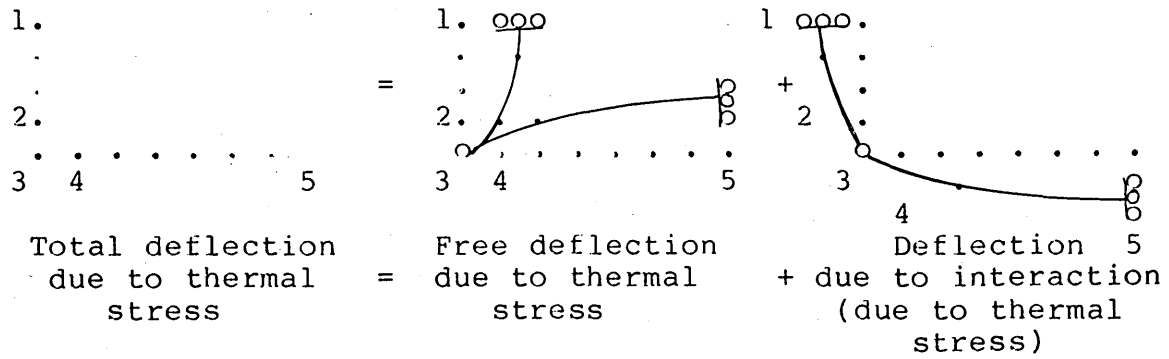


FIGURE 2 : SUPERPOSITION OF FREE DEFLECTION DUE TO TEMPERATURE VARIATION AND DEFLECTION DUE TO INTERACTION.

Both the node notation and an x,y reference system with the corner as the origin are used in the analysis. The x axis corresponds to the short beam (or strip) in the flat position while the y axis corresponds to the long beam in its flat position.

we thus have, using the principle of superposition,

$$u = u^f + u^i$$

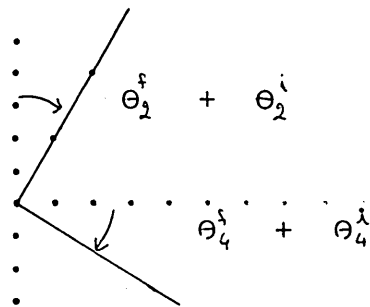
$$\theta = \theta^f + \theta^i$$

the presence of a rigid right-angle corner implies,

$$\theta_2^f = \theta_4^f$$

that is,

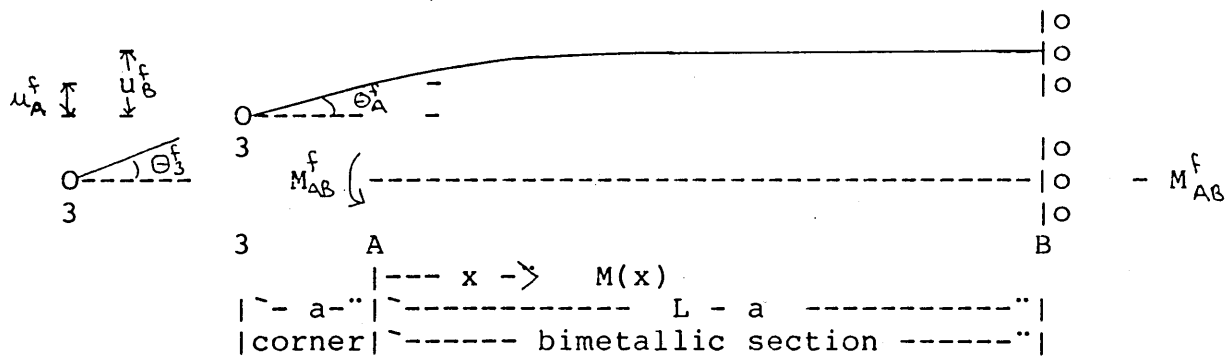
$$\theta_2^f + \theta_2^i = \theta_4^f + \theta_4^i$$



this equation will ensure the compatibility of our partial solutions.

FREE DEFLECTION DUE TO TEMPERATURE VARIATION

BIMETALLIC SECTIONS, ON NODES REFERENCE SYSTEM



$$\frac{1}{R} = \frac{d^2 u^f}{dx^2} = - \frac{3}{2t} (\alpha - \beta) (T - T_0) \tag{1}$$

$$\frac{du^f}{dx} = - \frac{3}{2t} (\alpha - \beta) (T - T_0) x + C_1 \tag{2}$$

$$u^f = - \frac{3}{2t} (\alpha - \beta) (T - T_0) \frac{1}{2} x^2 + C_1 x + C_2 \tag{3}$$

boundary conditions:

$$u^f = a \frac{du^f}{dx} \quad \text{at } x = 0 \tag{4}$$

$$\frac{du^f}{dx} = 0 \quad \text{at } x = L - a \tag{5}$$

we have, by definition, $\left. \frac{du^f}{dx} \right|_{x=0} = \theta_A^f$; $u^f|_{x=0} = u_A^f$ 6

then,

$$C_1 = \theta_A^f = \frac{3}{2t} (\alpha - \beta) (T - T_0) (L - a) \tag{7}$$

$$C_2 = u_A^f = a \theta_A^f \tag{8}$$

and we have,

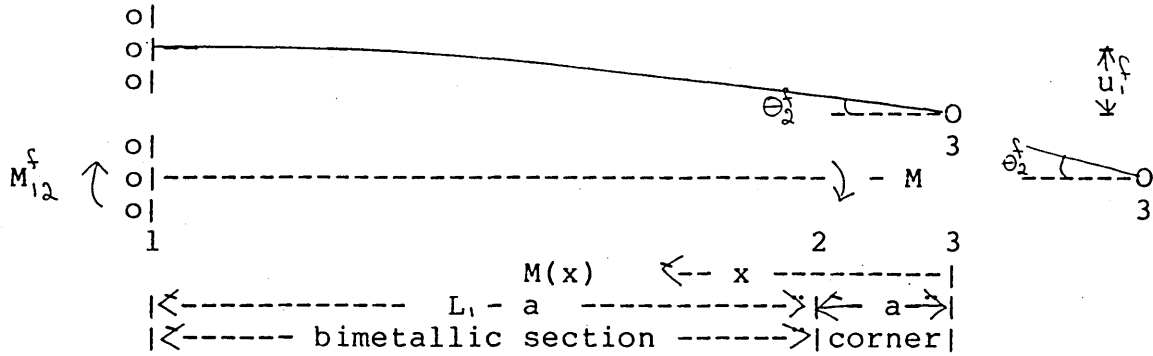
$$\frac{du^f}{dx} = \theta_A^f \left(1 - \frac{x}{L-a} \right) \tag{9}$$

and,

$$u^f = \theta_A^f \left(a + x - \frac{1}{2} \frac{x^2}{L-a} \right) \tag{9}$$

BIMETALLIC SECTIONS, ON x-y REFERENCE SYSTEM
(FREE DEFLECTION DUE TO TEMPERATURE VARIATION)

BIMETALLIC SECTION x ,

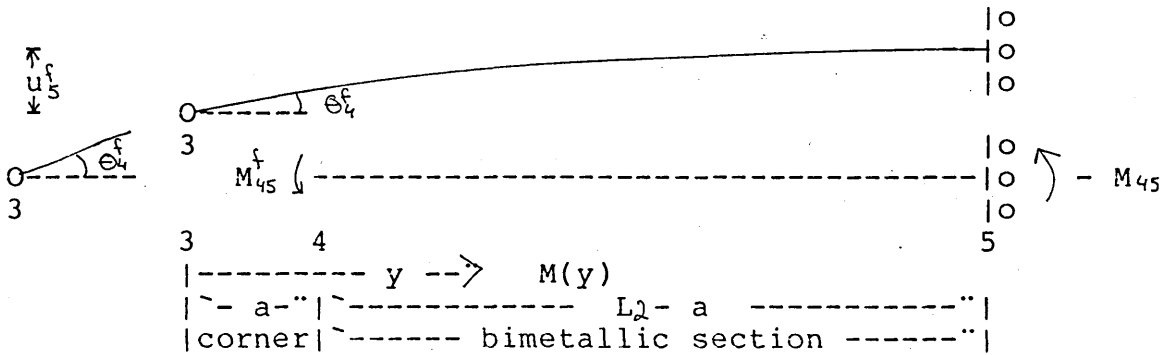


$$\theta_2^f = -\frac{3}{2t} (\alpha - \beta) (T - T_0) (L_1 - a) \quad 10$$

$$\frac{du^f}{dx} = -\theta_2^f \left(1 - \frac{x - a}{L_1 - a} \right) \quad \forall x \in (a, L_1) \quad 11$$

$$u^f = -\theta_2^f \left(x - \frac{1}{2} \frac{(x - a)}{L_1 - a} \right) \quad \forall x \in (a, L_1) \quad 12$$

BIMETALLIC SECTION y ,

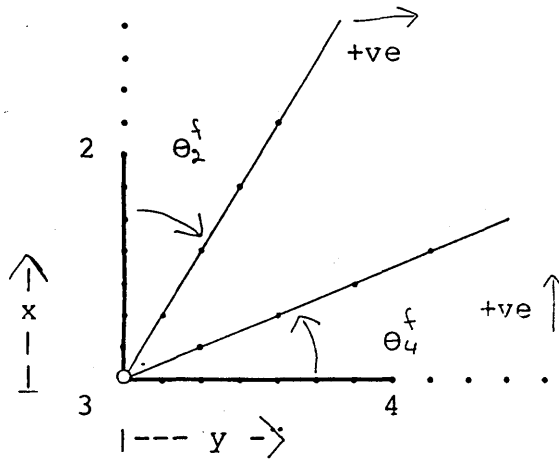


$$\theta_4^f = \frac{3}{2t} (\alpha - \beta) (T - T_0) (L_2 - a) \quad 13$$

$$\frac{du^f}{dy} = \theta_4^f \left(1 - \frac{y - a}{L_2 - a} \right) \quad \forall y \in (a, L_2) \quad 14$$

$$u^f = \theta_4^f \left(y - \frac{1}{2} \frac{(y - a)}{L_2 - a} \right) \quad \forall y \in (a, L_2) \quad 15$$

CORNER SECTIONS, ON x-y REFERENCE SYSTEM
(FREE DEFLECTION DUE TO TEMPERATURE VARIATION)



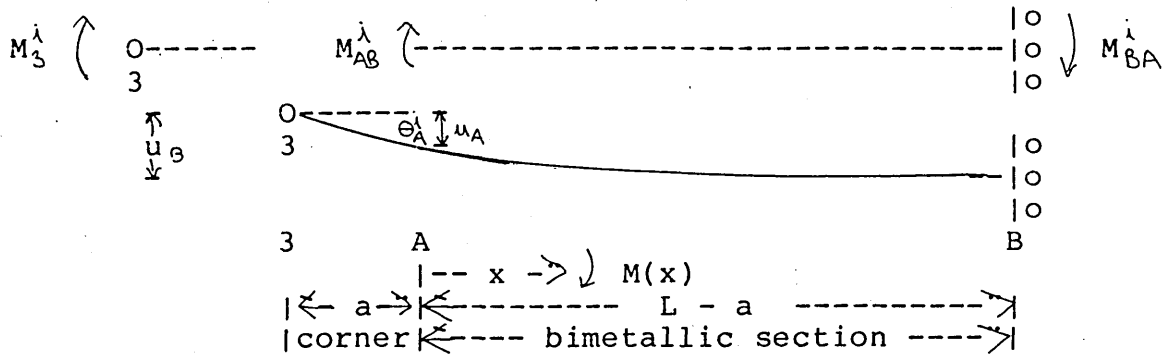
```

*****
*
*   u^f(x) = - x theta_2^f           \forall x \in (0,a)           *   16
*
*
*   u^f(y) =   y theta_4^f           \forall y \in (0,a)           *   17
*
*****

```

DEFLECTION DUE TO INTERACTION (DUE TO T VARIATION)

BIMETALLIC SECTIONS, ON NODES REFERENCE SYSTEM



$$M_{AB}^i = M_3^i \quad ; \quad M(x) = -M_3^i \quad 18$$

$$E I \frac{d^2 u^i}{dx^2} = -M_3^i \quad 19$$

$$E I \frac{du^i}{dx} = -M_3^i x + C_1 \quad 20$$

$$E I u^i = -1/2 M_3^i x^2 + C_1 x + C_2 \quad 21$$

boundary conditions:

$$u^i = a \frac{du^i}{dx} \quad \text{at } x = 0 \quad 22$$

$$\frac{du^i}{dx} = 0 \quad \text{at } x = L-a \quad 23$$

we have, by definition, $\frac{du^i}{dx} \Big|_{x=0} = \theta_A^i \quad ; \quad u^i \Big|_{x=0} = u_A \quad 24$

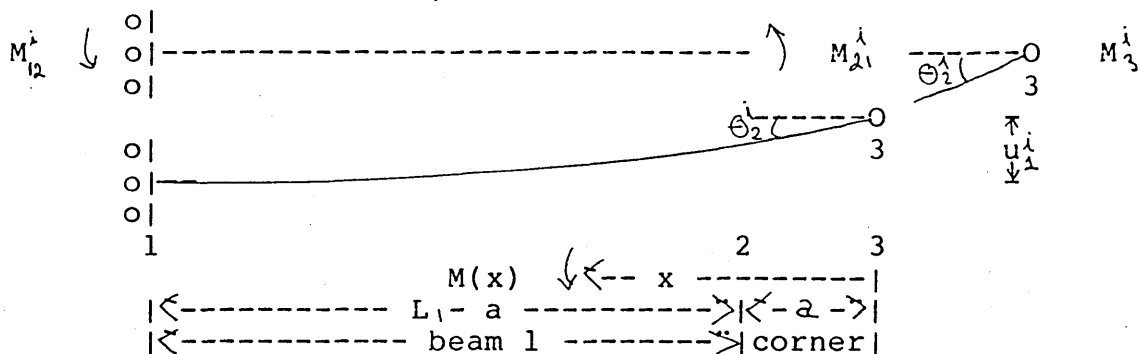
then,
$$C_1 = \theta_A^i = -M_3^i \frac{(L-a)}{E I} \quad 25$$

$$C_2 = u^i = -a \theta_A^i E I \quad 26$$

and we have,
$$\frac{du^i}{dx} = -\theta_A^i \left(1 - \frac{x}{L-a} \right) \quad \text{and,} \quad u^i = -\theta_A^i \left(a + x - \frac{1}{2} \frac{x^2}{L-a} \right) \quad 27$$

BIMETALLIC SECTIONS, ON x-y REFERENCE SYSTEM
(DEFLECTION DUE TO INTERACTION (DUE TO T VARIATION))

BIMETALLIC SECTION x ,

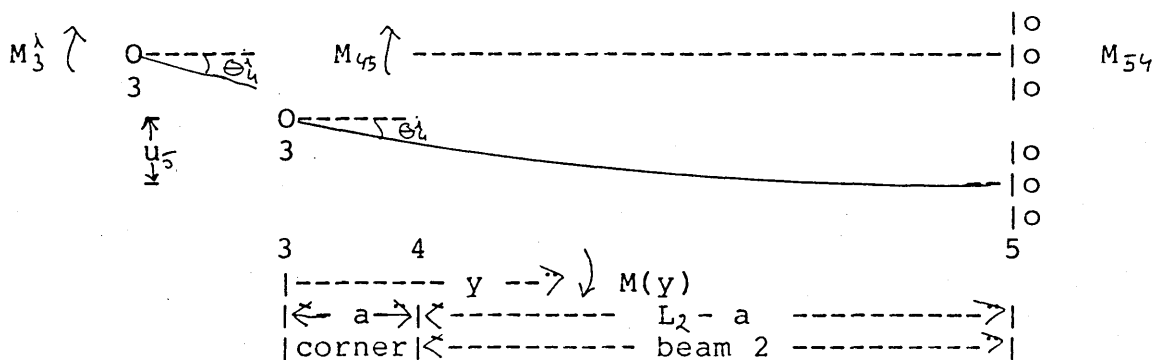


$$\theta_2^\lambda = - M_3^\lambda \frac{L_1 - a}{E_1 I_1} \quad 28$$

$$\frac{du^\lambda}{dx} = - \theta_2^\lambda \left(1 - \frac{x - a}{L - a} \right) \quad \forall x \in (a, L_1) \quad 29$$

$$u^\lambda = - \theta_2^\lambda \left(x - 1/2 \frac{(x-a)}{L - a} \right) \quad \forall x \in (a, L_1) \quad 30$$

BIMETALLIC SECTION y ,

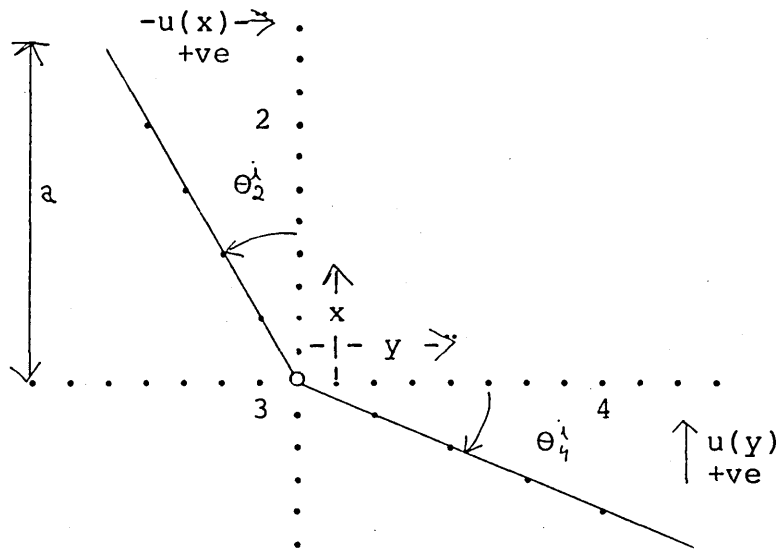


$$\theta_4^\lambda = M_3^\lambda \frac{L_2 - a}{E_2 I_2} \quad 31$$

$$\frac{du^\lambda}{dy} = \theta_4^\lambda \left(1 - \frac{y - a}{L - a} \right) \quad \forall y \in (a, L_2) \quad 32$$

$$u^\lambda = \theta_4^\lambda \left(y - 1/2 \frac{(y-a)}{L - a} \right) \quad \forall y \in (a, L_2) \quad 33$$

CORNER SECTIONS, ON x-y REFERENCE SYSTEM
 (DEFLECTION DUE TO INTERACTION (DUE TO T VARIATION))



```

*****
*
*   u^i(x) = - x  theta_2^i          forall x in (0,a)          *   34
*
*
*   u^lambda(y) = y  theta_4^i          forall y in (0,a)          *   35
*
*****
    
```

DEFLECTION DUE TO TEMPERATURE VARIATION,

As a rigid, right angle, corner has been assumed, compatibility requires,

$$\theta^T = \theta_2^f + \theta_2^l = \theta_4^f + \theta_4^l \quad 36$$

That is, using equations 10, 13, 28 and 31,

$$\begin{aligned} -\frac{3}{2t} (\alpha - \beta) (T - T_0) (L_1 - a) - M_3^l \frac{(L_1 - a)}{E_1 I_1} &= \\ &= \frac{3}{2t} (\alpha - \beta) (T - T_0) (L_2 - a) + M_3^l \frac{(L_2 - a)}{E_2 I_2} \end{aligned} \quad 37$$

Then,

$$M_3^l = - \left[\frac{L_1 - a}{E_1 I_1} + \frac{L_2 - a}{E_2 I_2} \right] \frac{3}{2} (\alpha - \beta) (T - T_0) \left[\frac{L_1 - a}{t_1} - \frac{L_2 - a}{t_2} \right] \quad 38$$

substituting M in eq. 36, i.e. in any member of eq. 37,

$$\theta^T = - \frac{3}{2} (\alpha - \beta) (T - T_0) \left[\frac{E_1 I_1}{L_1 - a} + \frac{E_2 I_2}{L_2 - a} \right] \left[\frac{E_1 I_1}{t_1} - \frac{E_2 I_2}{t_2} \right] \quad 39$$

the deflection is then given by superposition,

$$v^T = u^f + u^l \quad 40$$

DEFLECTION DUE TO TEMPERATURE VARIATION:

$$\forall x \in (0, a) \quad , \quad v^T = - \theta^T x \quad 41$$

$$\forall x \in (a, L) \quad , \quad v^T = - \theta^T \left(x - \frac{1}{2} \frac{x - a}{L_1 - a} \right) \quad 42$$

$$\forall y \in (0, a) \quad , \quad v^T = \theta^T y \quad 43$$

$$\forall y \in (a, L) \quad , \quad v^T = \theta^T \left(y - \frac{1}{2} \frac{y - a}{L_2 - a} \right) \quad 44$$

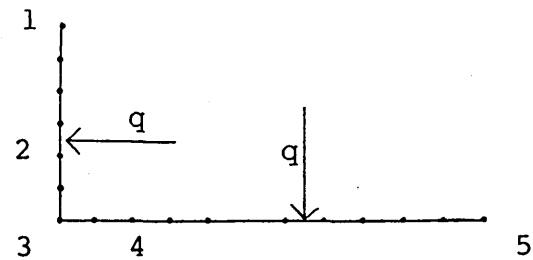
A1.3 THE EFFECT OF THE LOAD UPON THE STRUCTURE

Two cases are considered.

- 1 - Uniformly distributed load, udl.
- 2.- Discretely distributed load, ddl.

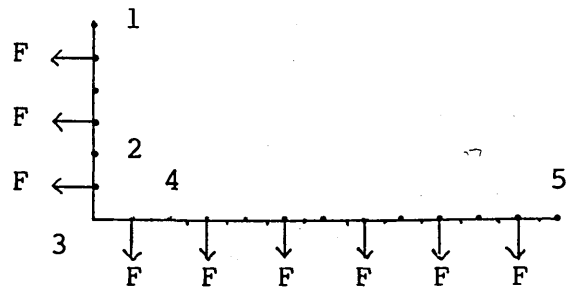
In both cases, the load is applied to the beams (bimetallic and corner sections) perpendicularly towards the outside of the structure.

The udl case, corresponds to the actual distribution of load in the continuous casting cross section being modelled, where the load is

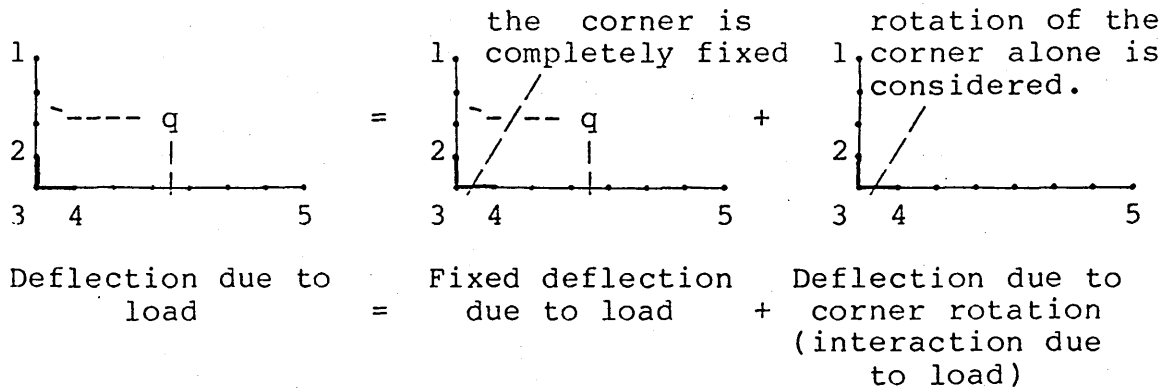


the ferrostatic pressure acting upon the solidified skin.

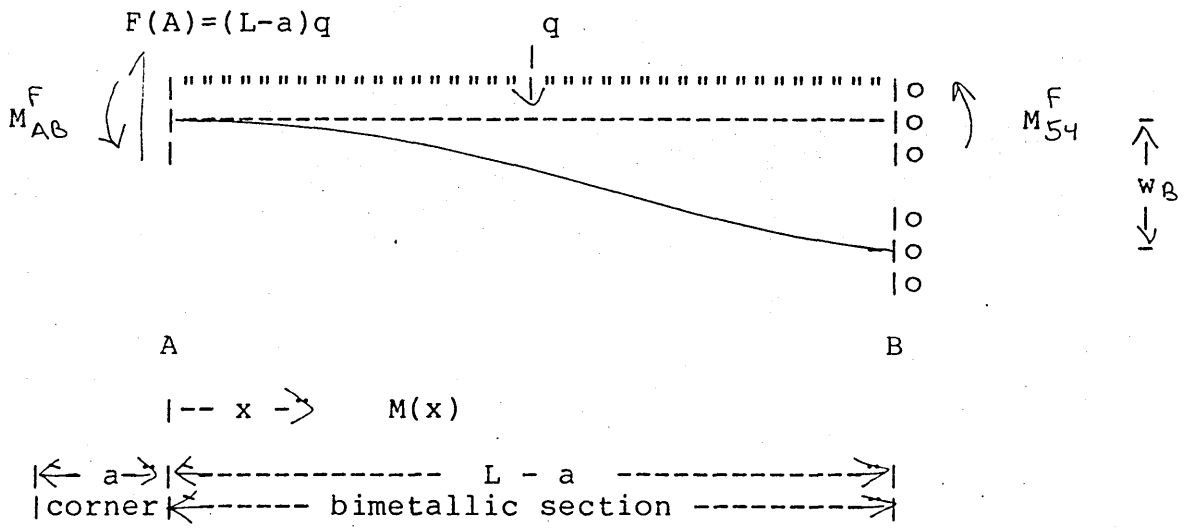
The ddl case, corresponds to the physical analogue, a discrete number of equal forces is applied to the beams in order to simulate the udl of the real process.



The situation under analysis can be splitted in two, first the deflection due to the load is considered with the corner completely fixed and then the effect of the rotation of the corner is considered. The principle of superposition and the condition of right angle rigid corner are used in a similar way than in the case of the thermal bending to obtain the resulting deflection.



FIXED-CORNER DEFLECTION OF THE BIMETALLIC SECTIONS DUE TO A UNIFORMLY DISTRIBUTED LOAD (udl)



The effect of the load alone is considered. It is assumed that there is no rotation and no displacement at node *3*. Hence, as the corner is assumed to be perfectly rigid, there is no rotation and no displacement at node *A*. It is also assumed that there is no rotation at node *B*.

Taking moments about a cut in x we have the equilibrium equation,

$$M(x) + M_{AB}^F - (L-a) q x + 1/2 q x^2 = 0 \quad 1$$

$$M(x) = - M_{AB}^F + (L-a) q x - 1/2 q x^2 \quad 2$$

$$E I \frac{d^2 w^F}{dx^2} = M(x) \quad 3$$

$$E I \frac{dw^F}{dx} = - M_{AB}^F x + 1/2 (L-a) q x^2 - 1/6 q x^3 + C \quad 4$$

$$E I w = -1/2 M_{AB}^F x^2 + 1/6 (L-a) q x^3 - 1/24 q x^4 + C_1 x + C_2 \quad 5$$

boundary conditions:

$$\frac{dw^F}{dx^F} = w^F = 0 \quad \text{at } x = 0 \quad 6$$

$$\frac{dw}{dx} = 0 \quad \text{at } x = L-a \quad 7$$

then, $C_1 = 0$ 8

$$C_2 = 0 \quad 9$$

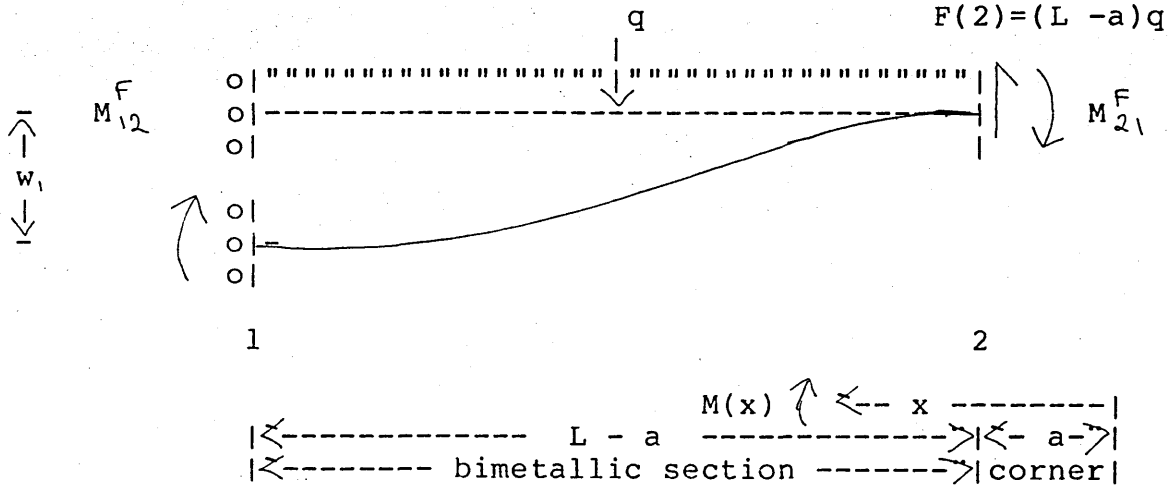
and we have,

```
*****
*
*  $M_{AB}^F = -1/2 (L-a)q (L-a) + 1/6 q (L-a)^2$  * 10
*
* and  $\forall x \in (a, L)$ , *
*
*  $E I \frac{dw^F}{dx} = 1/3 q(L-a)^2 x - 1/2 q(L-a) x^2 + 1/6 q x^3$  * 11
*
*  $E I w = 1/6 q(L-a)^2 x^2 - 1/6 q(L-a) x^3 + 1/24 q x^4$  * 12
*
*****
```

then, using the x-y reference system defined, we have,

FIXED-CORNER DEFLECTION DUE TO udl

BIMETALLIC SECTION x,

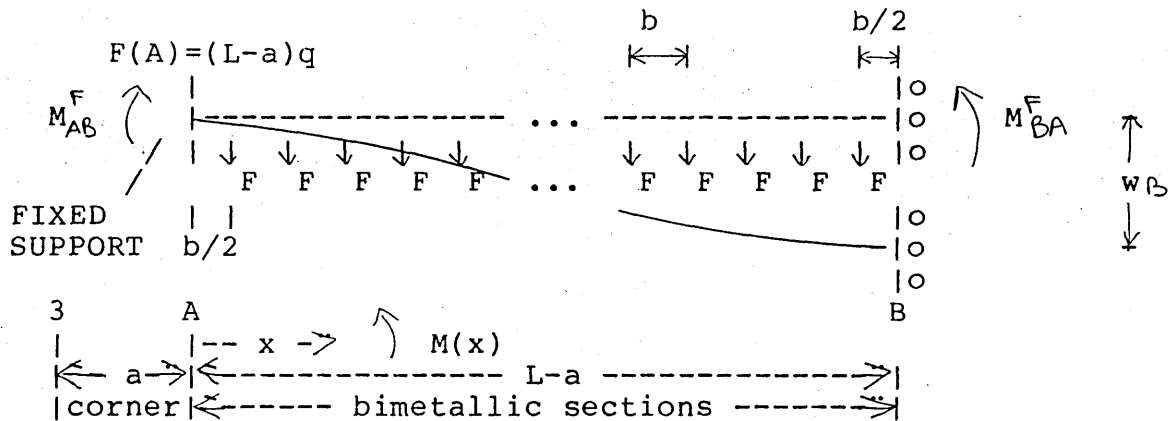


```

*****
*
*      M12F = - 1/3 q (L1-a)
*
*      and V x (a,L ),
*
*      dw
*      E1 I1 ---= 1/3 q(L1-a)2 (x-a) -1/2 q(L1-a)(x-a)2 +1/6 q(x-a)3
*      dx
*
*      E1 I1 w = 1/6 q(L1-a)2 (x-a) -1/6 q(L1-a)(x-a)2 +1/24 q(x-a)3
*
*****
    
```

11
12
13

FIXED-CORNER DEFLECTION OF THE BIMETALLIC SECTIONS DUE TO A DISCRETELY DISTRIBUTED LOAD (ddl)



The effect of the loads alone is considered. It is assumed that there is no rotation and no displacement at node *3*. Hence, as the corner is assumed to be perfectly rigid, there is no rotation and no displacement at node *A*. It is also assumed that there is no rotation at node *B*.

K loads of equal magnitude F are distributed along the beam at an equal distance b , of each other, and at a distance $b/2$ of the nodes,

$$K \in \mathbb{N} \quad ; \quad b = \frac{L-a}{K} \quad ; \quad F = \frac{q(L-a)}{K} \quad 19$$

Let $k(x)$ be defined, $\forall x \in [0, L-a] = [*A*, *B*]$, by,

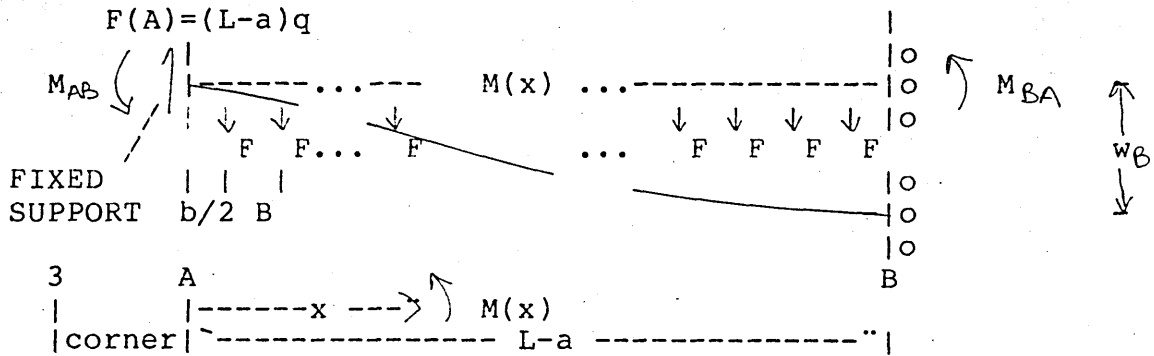
$$\begin{aligned} \forall x \in [0, b/2) & : & k(x) &= 0 \\ \forall x \in [b/2, L-a] & : & k(x) &= [x/b + 1/2] \end{aligned} \quad 20$$

where $[x/b + 1/2]$ is the natural part of $(x/b + 1/2)$.

Let $P([*A*, *B*])$ be a partition of $[*A*, *B*]$ (the closed interval determined by the nodes $*A*$ and $*B*$), defined by,

$$P([*A*, *B*]) = \left\{ [0, b/2) ; [(1-1/2)b, (1+1/2)b) ; \dots ; [(m-1/2)b, (m+1/2)b) ; \dots ; [(K-1-1/2)b, (K-1+1/2)b) ; [(K-1/2)b, L-a] \right\} \quad 21$$

where $m \in [2, K-2] \subset \mathbb{N}$



If we take moments about a cut at x $[*A*, *B*]$, we have,

$$M(x) = -M_{AB}^F + q(L-a)x - k(x) \frac{q(L-a)}{K} \left[\frac{1}{2} (k(x)-1) b + x - (k(x)-1/2) b \right] \quad 22$$

from the definition of b , reordering,

$$M(x) = -M_{AB}^F + \left[x \left(1 - k(x)/K \right) + \frac{1}{2} \left(\frac{k(x)}{K} \right)^2 (L-a) \right] q(L-a) \quad 23$$

We have,

$$E I \frac{d^2 w^F}{dx^2} = M(x) \quad 24$$

and we can integrate within each interval of $P([*A*, *B*])$,

$$E I \frac{dw^F}{dx} = -M_{AB}^F x + \left[\frac{1}{2} \left(1 - k(x)/K \right) x^2 + \frac{1}{2} \left(\frac{k(x)}{K} \right)^2 (L-a)x \right] q(L-a) + C [K(x)] \quad 25$$

$$E I w^F = -\frac{1}{2} M_{AB}^F x^2 + \left[\frac{1}{6} \left(1 - k(x)/K \right) x^3 + \frac{1}{4} \left(\frac{k(x)}{K} \right)^2 (L-a) x^2 \right] q(L-a) + C_1 [k(x)] x + C_2 [k(x)] \quad 26$$

boundary conditions:

$$\frac{dw^F}{dx} = w_A^F = 0 \quad \text{at } x = 0 \quad 27$$

$$\frac{dw^F}{dx} = 0 \quad \text{at } x = L-a \quad 28$$

Also, the deflection and its derivative are continuous functions, so at the boundary between each pair of intervals of $P([*A*,*B*])$ we have,

$$\lim_{x \rightarrow x_0}^+ w^F = \lim_{x \rightarrow x_0}^- w^F \quad \forall x_0 = (k(x) - 1/2) b, \quad k(x) \in (1, K) \quad 29$$

$$\lim_{x \rightarrow x_0}^+ \frac{dw^F}{dx} = \lim_{x \rightarrow x_0}^- \frac{dw^F}{dx} \quad \forall x_0 = (k(x) - 1/2) b, \quad k(x) \in (1, K) \quad 30$$

then,

$$C_1 [0] = 0 \quad 31$$

$$C_2 [0] = 0 \quad 32$$

$$C_1 [K] = (L-a) (M_{AB}^F - 1/2 q(L-a)^2) \quad 33$$

And at the boundary between each pair of intervals of the partition $P([*A*,*B*])$, that is, at $x = (k(x) - 1/2)(L-a)/K$ for any $k(x) \in (1, K)$, we have, according to the boundary condition equation 30,

$$- M_{AB}^F x + 1/2 [(1 - (k(x)-1)/K) x_0^2 + (k(x)-1)^2 / K^2 (L-a) x_0] q(L-a) + C_1 [k(x)-1] \quad 34$$

$$= - M_{AB}^F x + 1/2 [(1 - k(x)/K) x_0^2 + k(x)^2 / K^2 (L-a) x_0] q(L-a) + C_1 [k(x)] \quad 35$$

then,

$$C_1[k(x)] = C_1[k(x)-1] - 1/2 q \frac{(L-a)^3}{K^3} (k(x)-1/2)^2 \quad 36$$

$$C_1[k(x)] = C_1[0] - \sum_{i=1}^{k(x)} 1/2 q \frac{(L-a)^3}{K^3} (k(x)-1/2)^2 \quad 37$$

We then have,

```
*****
*
*          (L-a)^3
*   C [k(x)] = - 1/2 q ----- (1/3 k^3(x) - 1/12 k(x))
*          K^3
*
*****
```

38

hence,

$$C_1[K] = - 1/2 q \frac{(L-a)^3}{K^3} (1/3 K^3 - 1/12 K) \quad 39$$

$$C_1[K] = - 1/2 q (L-a)^3 (1/3 - 1/12 K^2) \quad 40$$

and from our boundary condition $\frac{dw^F}{dx} = 0$ at $x = L-a$, (28)

$$C[K] = (L-a) [M_{AB}^F - 1/2 q (L-a)^2] \quad 41$$

then,

$$M_{AB}^F = - 1/2 q (L-a)^2 (1/3 - 1/12 K^2) + 1/2 q (L-a)^2 \quad 42$$

```
*****
*
*   M_{AB}^F = 1/3 q (L-a)^2 (1 - 1/8 K )
*
*****
```

43

At the boundary between each pair of intervals of the partition $P([*A*,*B*])$, that is, at $x = (k(x) - 1/2)(L-a)/K$ for any $k(x) \in (1, K)$, we have, according to the boundary condition on the derivative, equation 30,

$$\begin{aligned}
 & -1/2 M_{AB}^F x_0^2 + [1/6(1 - \frac{k(x)-1}{K})x_0^3 + 1/4 \frac{(k(x)-1)^2}{K^2} (L-a)x_0^2] q (L-a) \\
 & + C_1 [k(x)-1] x_0 + C_2 [k(x)-1] = \\
 & - 1/2 M_{AB}^F x_0^2 + [1/6(1 - \frac{k(x)}{K})x_0^3 + 1/4 \frac{k^2(x)}{K^2} (L-a)x_0^2] q (L-a) \\
 & + C_1 [k(x)] x_0 + C_2 [k(x)]
 \end{aligned} \tag{44}$$

then,

$$\begin{aligned}
 C_2 [k(x)] &= C_2 [k(x)-1] - (C_1 [k(x)] - C_1 [k(x)-1]) x_0 \\
 &+ [1/6 K x_0^3 - 1/2 \frac{k(x)}{K^2} (L-a) x_0^2] q (L-a)
 \end{aligned} \tag{45}$$

$$\begin{aligned}
 C_2 [k(x)] &= C_2 [k(x)-1] + 1/2 q \frac{(k(x)-1/2)^3}{K^4} (L-a)^4 + \\
 &+ 1/6 q \frac{(k(x)-1/2)^3}{K^4} (L-a)^3 - 1/2 q \frac{(k(x)-1/2)^3}{K^4} (L-a)^3
 \end{aligned} \tag{46}$$

$$C_2 [k(x)] = C_2 [k(x)-1] + 1/6 q \frac{(k(x)-1/2)^3}{K^4} (L-a)^3 \tag{47}$$

$$C_2 [k(x)] = C_2 [0] + \sum_{i=1}^{k(x)} 1/6 q \frac{(i-1/2)^3}{K^4} (L-a)^3 \tag{48}$$

$$\begin{aligned}
 & \text{*****} \\
 & * \\
 & * \quad C_2 [k(x)] = 1/6 q \frac{(L-a)^4}{K^4} (1/4 k^4(x) - 1/8 k^2(x)) \quad * \\
 & * \\
 & \text{*****}
 \end{aligned} \tag{49}$$

then,

$$\begin{aligned}
 E \quad I \quad \frac{dw^F}{dx} = & - 1/3 (1 - 1/8 K^2) x \quad q (L-a)^2 \\
 & + [1/2(1 - \frac{k(x)}{K}) x^2 + 1/2 \frac{k^2(x)}{K^2} (L-a) x] q (L-a) \\
 & - 1/2 (1/3 k^3(x) - 1/12 k(x)) q \frac{(L-a)^3}{K^3}
 \end{aligned}$$

50

$$\begin{aligned}
 E \quad I \quad \frac{dw^F}{dx} = & 1/2 (1 - \frac{k(x)}{K}) x^2 q (L-a) \\
 & - 1/3 (1 - \frac{1}{8K^2} - 3/2 \frac{k^2(x)}{K^2}) x q (L-a)^2 \\
 & - 1/3 (1/2 k^3(x) - 1/8 k(x)) K^{-3} q (L-a)^3
 \end{aligned}$$

51

and,

$$\begin{aligned}
 E \quad I \quad w^F = & - 1/6 (1 - \frac{1}{8K^2}) q (L-a)^2 \\
 & + [1/6(1 - \frac{k(x)}{K}) x^3 + 1/4 \frac{k^2(x)}{K^2} (L-a) x^2] q (L-a) \\
 & - 1/2 (1/3 k^3(x) - 1/12 k(x)) x q \frac{(L-a)^3}{K^3} \\
 & + 1/6 (1/4 k^4(x) - 1/8 k^2(x)) q \frac{(L-a)^4}{K^4}
 \end{aligned}$$

52

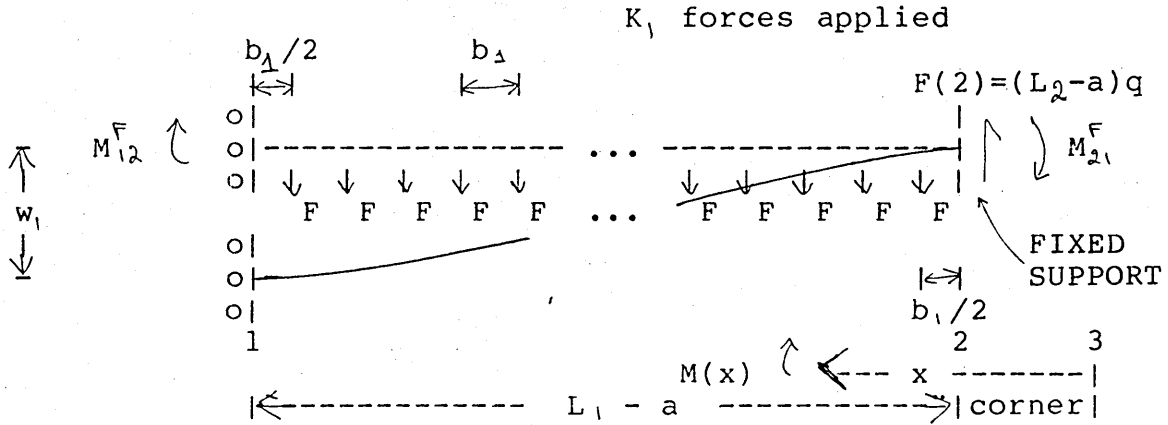
$$\begin{aligned}
 E \quad I \quad w^F = & 1/6 (1 - \frac{k(x)}{K}) x^3 q (L-a) \\
 & - 1/6 (1 - 3/2 \frac{k^2(x)}{K^2} - \frac{1}{8K^2}) q (L-a)^2 \\
 & - 1/6 (k^3(x) - 1/4 k(x)) K^{-3} x q (L-a)^3 \\
 & + 1/24 (k^4(x) - 1/2 k^2(x)) K^{-4} q (L-a)^4
 \end{aligned}$$

53

Using the x-y reference system defined we have,

FIXED CORNER DEFLECTION DUE TO ddl

BIMETALLIC SECTION x ,



$$M_{21}^F = - \frac{1}{3} q (L_1 - a)^2 \left(1 - \frac{1}{8K_1^2} \right) \quad 54$$

and $\forall x \in (a, L_1)$,

$$\begin{aligned} \frac{E_1 I_1}{q} \frac{dw^F}{dx} = & - \frac{1}{2} (L_1 - a) \left(1 - \frac{k(x)}{K_1} \right) (x-a)^2 \\ & + \frac{1}{3} (L_1 - a)^2 \left(1 - \frac{1}{8K_1^2} - \frac{3k(x)}{2K_1^2} \right) (x-a) \\ & + \frac{1}{3} (L_1 - a)^3 \left(\frac{1}{2} k^3(x) - \frac{1}{8} k(x) \right) K^3 \end{aligned} \quad 55$$

$$\begin{aligned} \frac{E I}{q} w^F = & - \frac{1}{6} (L_1 - a) \left(1 - \frac{k(x)}{K_1} \right) (x-a)^3 \\ & + \frac{1}{6} (L_1 - a)^2 \left(1 - \frac{1}{8K_1^2} - \frac{3k(x)}{2K_1^2} \right) (x-a)^2 \\ & + \frac{1}{6} (L_1 - a)^3 \left(- \frac{k(x)}{4} + k^3(x) \right) K^{-3} (x-a) \\ & - \frac{1}{24} (L_1 - a)^4 \left(\frac{k^4(x)}{2} - k^2(x) \right) K^{-4} \end{aligned} \quad 56$$

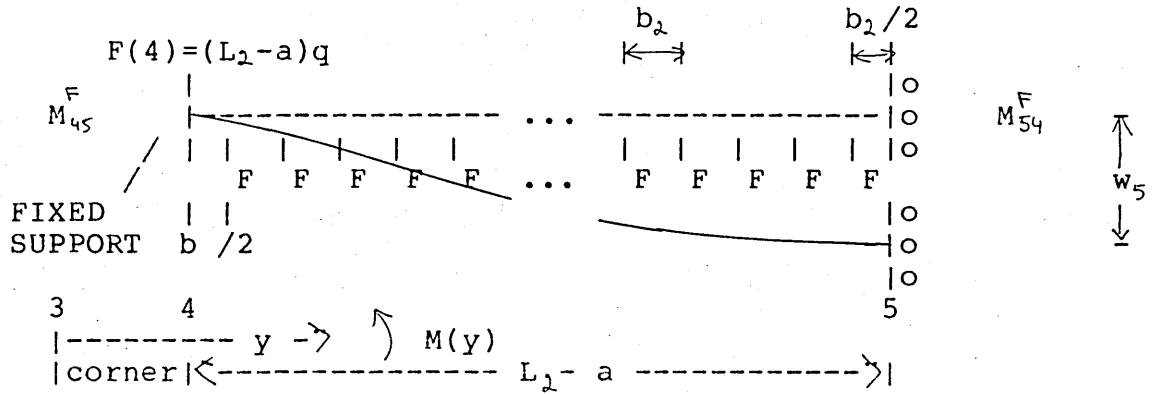
where, $\forall x \in [a, L] = [*1*, *2*]$, $k(x)$ is defined by,

$$\forall x \in [a, a+b/2) \quad k(x) = 0$$

$$\forall x \in [a+b/2, L_1] : \quad k(x) = \left[\frac{(x-a)}{b_1} + \frac{1}{2} \right]_{IN} \quad 57$$

FIXED CORNER DEFLECTION DUE TO ddl

BIMETALLIC SECTION y ,



$$M_{45}^F = \frac{1}{3} q (L_2 - a)^2 \left(1 - \frac{1}{8K_1^2} \right)$$

and $\forall y \in [a, L_2]$,

58

$$\frac{E_2 I_2}{q} \frac{dw^F}{dy} = + \frac{1}{2} (L_2 - a) \left(1 - \frac{k(y)}{K_1} \right) (y - a)^2$$

$$- \frac{1}{3} (L_2 - a)^2 \left(1 - \frac{1}{8K_1^2} - \frac{3k^2(y)}{2K_1^2} \right) (y - a)$$

$$- \frac{1}{3} (L_2 - a)^3 \left(\frac{1}{2} k^3(y) - \frac{1}{8} k^3(y) \right) K_1^{-3}$$

59

$$\frac{E_2 I_2}{q} w^F = + \frac{1}{6} (L_2 - a) \left(1 - \frac{k(y)}{K_1} \right) (y - a)^3$$

$$- \frac{1}{6} (L_2 - a)^2 \left(1 - \frac{1}{8K_1^2} - \frac{3k^2(y)}{2K_1^2} \right) (y - a)^2$$

$$- \frac{1}{6} (L_2 - a)^3 \left(- \frac{k(y)}{4} + k^2(y) \right) K_1^{-3} (y - a)$$

$$+ \frac{1}{24} (L_2 - a)^4 \left(\frac{k^4(y)}{2} - k^2(y) \right) K_1^{-4}$$

60

where, $\forall y \in [a, L_2] = [*4*, *5*]$, $k(y)$ is defined by,

$\forall y \in [a, a + b/2]$: $k(y) = 0$

$\forall y \in [a + b/2, L]$: $k(y) = [(y - a)/b_2 + 1/2]_{in}$

61

AGREEMENT BETWEEN THE udl AND ddl CASES RESULTS FOR
 THE FIXED-CORNER DEFLECTION OF THE BIMETALLIC SECTIONS
 DUE TO THE LOAD

The ddl case, taken to the limit when the number of forces applied tends to infinity, must agree with the continuous case. If the total load applied is the same, the results must be the same.

This provides us with a good test to check the results obtained,

a.- The moment distribution:

$$\lim_{K \rightarrow \infty} M_{AB}^F = \lim_{K \rightarrow \infty} 1/3 \left(1 - \frac{1}{8K^2} \right) q (L-a)^2 \quad 62$$

 *
 * $\lim_{K \rightarrow \infty} M_{AB}^F = 1/3 q (L-a)^2$ * 63
 *

b.- The derivative of the deflection:

From the definitions of $k(x)$ and b , equations 1 and 2, we have,

$$\lim_{K \rightarrow \infty} \frac{k(x)}{K} = \begin{cases} = 0 & , \forall x \in [0, b/2) \\ = \lim_{K \rightarrow \infty} \left(\left[\frac{x K}{(L-a)} + 1/2 \right]_{\infty} / K \right) & , \forall x \in [b/2, L-a) \end{cases} \quad 64$$

that is,

$$\lim_{K \rightarrow \infty} \frac{k(x)}{K} = \frac{x}{L-a} \quad \forall x \in [0, L-a) \quad 65$$

then,

$$\lim_{K \rightarrow \infty} E I \frac{dw^F}{dx} = + 1/2 q (L-a) \left(1 - \frac{x}{L-a} \right) (x-a)^2$$

$$- 1/3 q (L-a)^2 \left(1 - 3/2 \frac{x^2}{(L-a)^2} \right) (x-a)$$

$$- 1/3 q (L-a)^3 \left(1/2 \frac{x^3}{(L-a)^3} \right)$$

66

*
*
* $\lim_{K \rightarrow \infty} E I \frac{dw^F}{dx} = 1/3 q(L-a)^2 x - 1/2 q(L-a) x^2 + 1/6 q x^3$ * 67
*
*

c.- The deflection:

$$\lim_{K \rightarrow \infty} E I w = + 1/6 q (L-a) \left(1 - \frac{x}{L-a} \right) (x-a)^3$$

$$- 1/6 q (L-a)^2 \left(1 - 3/2 \frac{x^2}{(L-a)^2} \right) (x-a)^2$$

$$- 1/6 q (L-a)^3 \left(\frac{x^3}{(L-a)^3} \right) (x-a)$$

$$+ 1/24 q (L-a)^4 \left(\frac{x^4}{(L-a)^4} \right)$$

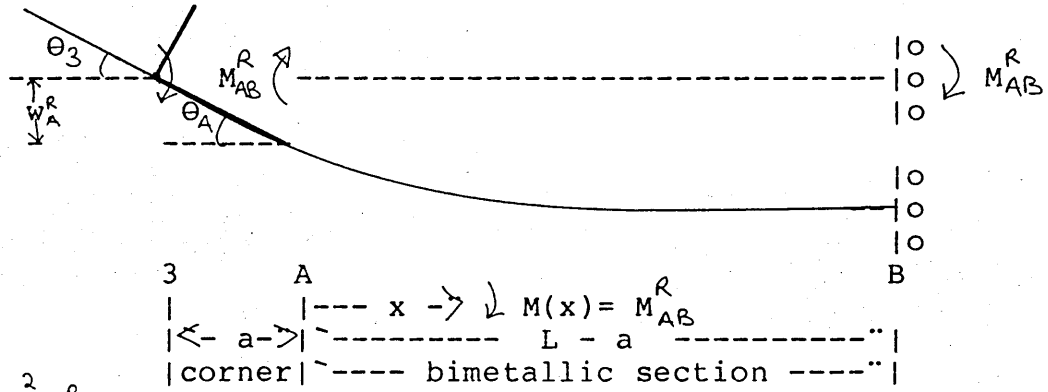
68

*
* $\lim_{K \rightarrow \infty} E I w^F = 1/6 q(L-a)^2 x^2 - 1/6 q(L-a) x^3 + 1/24 q x^4$ * 69
*
*

That is, when the ddl case is taken to the limit, the same results than in the udl case are obtained.

DEFLECTION OF THE BIMETALLIC SECTIONS DUE TO CORNER ROTATION (DUE TO THE LOAD) BOTH udl AND ddl CASES

BIMETALLIC SECTIONS,



$$E I \frac{d^2 w^R}{dx^2} = + M_{AB}^R \quad 70$$

$$E I \frac{dw^R}{dx} = + M_{AB}^R x + C_1 \quad 71$$

$$E I w^R = + 1/2 M x^2 + C_1 x + C_2 \quad 72$$

boundary conditions:

$$w^R = a \frac{dw^R}{dx} \quad \text{at } x = 0 \quad 73$$

$$\frac{dw^R}{dx} = 0 \quad \text{at } x = L - a \quad 74$$

we have, by definition, $\left. \frac{dw^R}{dx} \right|_{x=0} = -\theta_A; \quad \left. u^R \right|_{x=0} = w^R \quad 75$

then, at $x = 0$,

$$E I (-\theta_A) = + M_{AB}^R (0) + C \quad 76$$

$$E I (-a\theta_A) = + 1/2 M_{AB}^R (0) + C_1 (0) + C_2 \quad 77$$

and at $x = L-a$,

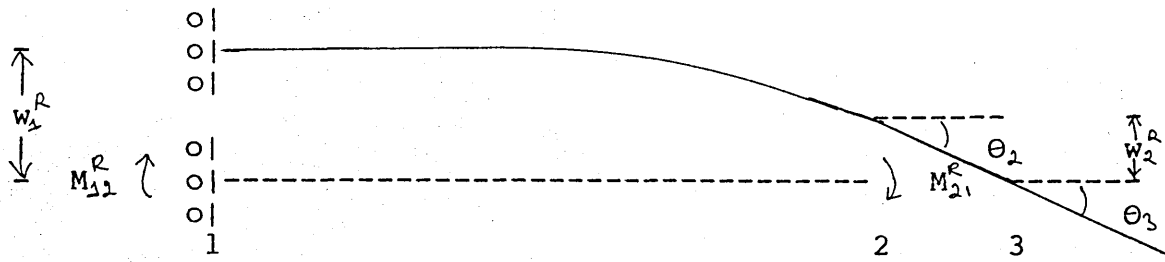
$$E I (0) = + M_{AB}^R (L-a) + (-E I \theta_A) \quad 78$$

we have, ***** and, *****

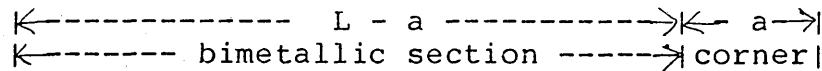
$$* M_{AB}^R = + \frac{E I}{L-a} \theta_A * \quad * w^R = \theta_A \left(-\frac{1}{2} \frac{x^2}{L-a} + x + a \right) * \quad 79$$

If the x-y reference system defined is used, then,

BIMETALLIC SECTION x ,



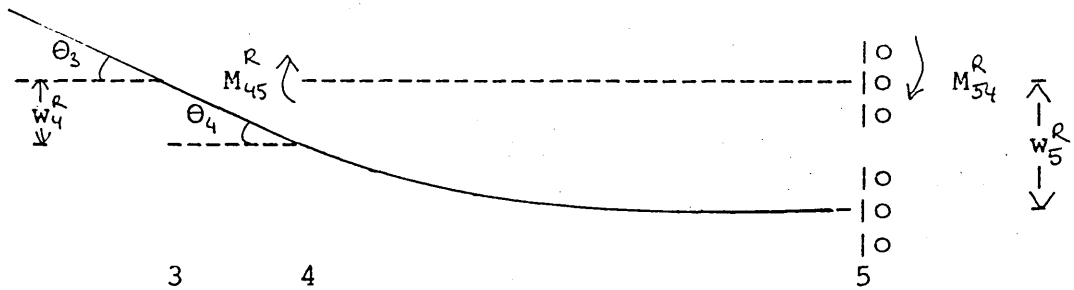
$$M(x) = - M_{12}^R \left(\leftarrow x \right)$$



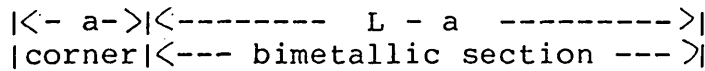
we have, ***** and, $\forall x \in [a, L]$, *****

$M_{21}^R = - \frac{E_1 I_1}{L_1 - a} \theta_2$	$w^R = - \theta_2 \left(-1/2 \frac{(x-a)^2}{L_1 a} + x \right)$	80
---	--	----

BIMETALLIC SECTION y ,



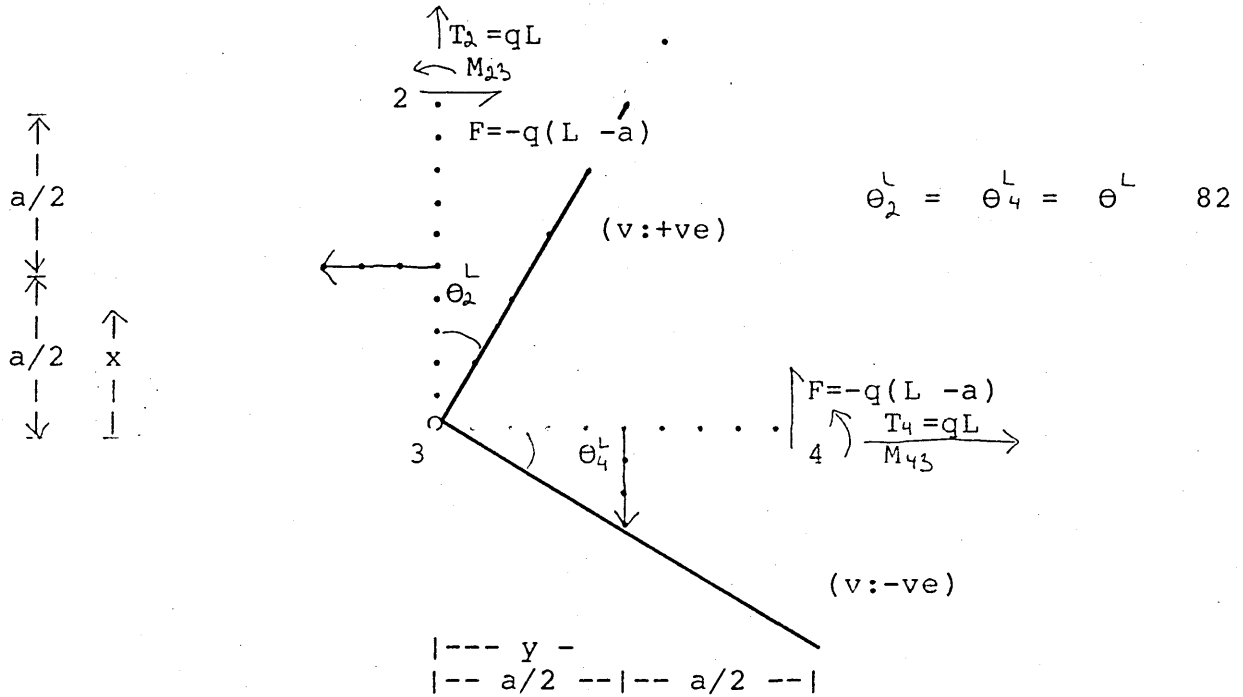
$$M(y) = M$$



we have, ***** and, $\forall y \in [a, L]$, *****

$M_{45}^R = - \frac{E_2 I_2}{L_2 - a} \theta_4$	$w^R = \theta_4 \left(-1/2 \frac{(y-a)^2}{L_2 a} + y \right)$	81
---	--	----

RESULTANT DEFLECTION OF THE CORNER DUE TO THE LOAD
 BOTH udl AND ddl CASES



Taking moments about any of the three nodes,

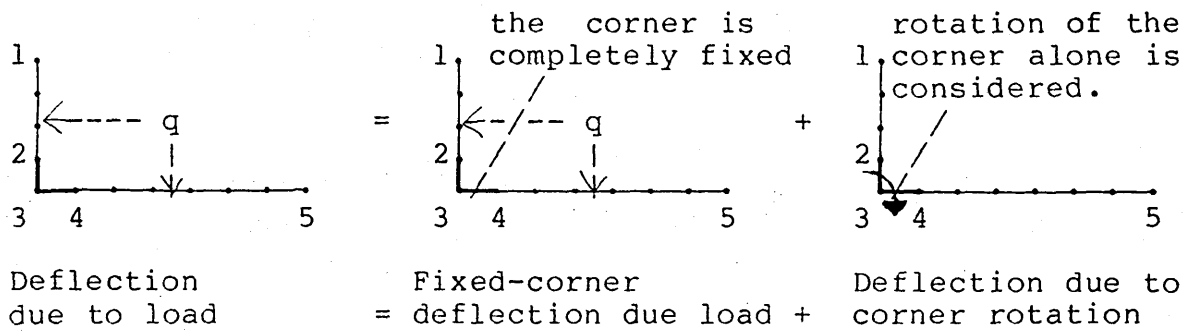
 *
 * $M_{23}^L = -M_{43}^L + q(L_2 - L_1)a$ * 83
 *

and we have,

 *
 * $v^L = \theta^L x \quad \forall x \in [0, a] = [*2*, *3*]$ * 84
 *
 *
 * $v^L = \theta^L y \quad \forall y \in [0, a] = [*3*, *4*]$ * 85
 *

RESULTANT DEFLECTION OF THE BIMETALLIC SECTIONS DUE TO THE LOAD, BOTH udl AND ddl CASE

SUPERPOSITION

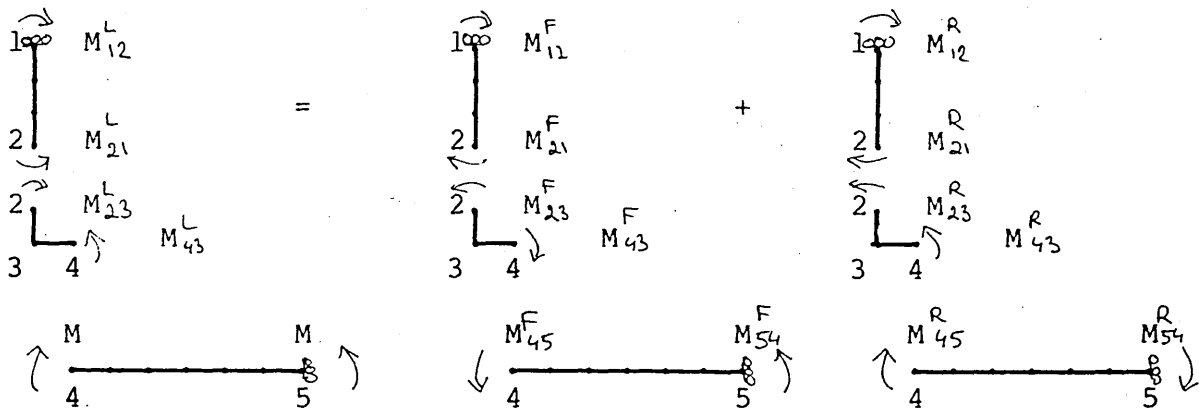


$$v^L = v^F + v^R$$

86

As explained in the introduction to this chapter, the total deflection due to the load, udl or ddl, is found by the superposition of an hypothetical deflection due to the load while the corner is fixed (no rotation), with the deflection due to the rotation of the corner, that is the interaction between the beams.

Signs can be checked by representing the moments,



Using the adopted sign convention we have,

$$M_{21}^L = - M_{21}^F - M_{21}^R \quad 87$$

$$M_{45}^L = - M_{45}^F + M_{45}^R \quad 88$$

The equilibrium condition at the corner requires,

$$M_{21}^L + M_{45}^L + q (L_2 - L_1) = 0 \quad 89$$

we then have, substituting from equations (1) and (2),

$$\begin{aligned} & \text{*****} \\ & * \\ & * \quad (M_{21}^F + M_{21}^R) + (M_{45}^F - M_{45}^R) + q (L_2 - L_1) = 0 \quad * \quad 90 \\ & * \\ & \text{*****} \end{aligned}$$

and as the corner is a rigid right angle corner, we also have,

$$\begin{aligned} & \text{*****} \\ & * \\ & * \quad \theta_2^L = \theta_4^L = \theta^L \quad * \quad 91 \\ & * \\ & \text{*****} \end{aligned}$$

the rotation at the corner must be the same for both beams.

This equation ensures the compatibility of the results.

For the udl case,

$$M_{21}^F = - 1/3 q (L_1 - a) \quad [A1.3] (13)$$

$$M_{45}^F = 1/3 q (L_2 - a) \quad [A1.3] (16)$$

$$M_{21}^R = - \frac{E_1 I_1}{L_1 - a} \theta_2 \quad [A1.3] (80)$$

then,

$$1/3 q [-(L_1 - a)^2 + (L_2 - a)^2 + 3(L_2 - L_1) a] - \left(\frac{E_1 I_1}{L_1 - a} + \frac{E_2 I_2}{L_2 - a} \right) \theta^L = 0 \quad 92$$

and, reordering,

ROTATION OF THE CORNER DUE TO udl :

$$\begin{aligned} & \text{*****} \\ & * \\ & * \quad \theta^L = \left(\frac{E_1 I_1}{L_1 - a} + \frac{E_2 I_2}{L_2 - a} \right)^{-1} 1/3 q [L_2^2 - L_1^2 + (L_2 - L_1) a] \quad * \quad 93 \\ & * \\ & \text{*****} \end{aligned}$$

we have, $\forall x \in [a, L_1]$

$$\begin{aligned} \frac{E_1 I_1}{q} w^F &= -1/6 (L_1 - a) \left(1 - \frac{k(x)}{K} \right) (x-a)^3 \\ &\quad + 1/6 (L_1 - a)^2 \left(1 - \frac{1}{8K} - \frac{3 k^2(x)}{2 K^2} \right) (x-a)^2 \\ &\quad + 1/6 (L_1 - a)^3 \left(-k^3(x)/4 + k^2(x) \right) K^{-3} (x-a) \\ &\quad - 1/24 (L_1 - a)^4 \left(k^4(x)/2 - k^2(x) \right) K^{-4} \end{aligned}$$

where, $\forall x \in [a, a+b_1/2)$: $k(x) = 0$

$\forall x \in [a+b_1/2, L_1]$: $k(x) = [(x-a)/b_1 + 1/2]_{iN}$

[A1.3] (56-57)

and, we have $\forall x \in [a, L_1]$,

$$w^R = -\theta_2 \left(-1/2 \frac{(x-a)^2}{L_1 - a} + x \right) \quad [A1.3] (80)$$

we have, $\forall y \in [a, L_2]$,

$$\begin{aligned} \frac{E_2 I_2}{q} w^F &= +1/6 (L_2 - a) \left(1 - \frac{k(y)}{K_1} \right) (y-a)^3 \\ &\quad - 1/6 (L_2 - a)^2 \left(1 - \frac{1}{8K_1} - \frac{3 k^2(y)}{2 K_1^2} \right) (y-a)^2 \\ &\quad - 1/6 (L_2 - a)^3 \left(-k^3(y)/4 + k^2(y) \right) K^{-3} (y-a) \\ &\quad + 1/24 (L_2 - a)^4 \left(k^4(y)/2 - k^2(y) \right) K^{-4} \end{aligned}$$

where, $\forall y \in [a, a+b_2/2)$: $k(y) = 0$

$\forall y \in [a+b_2/2, L_2]$: $k(y) = [(y-a)/b_2 + 1/2]_{iN}$

[A1.3] (60-61)

and, we have, $\forall y \in [a, L_2]$,

$$w^R = \theta_4 \left(-1/2 \frac{(y-a)^4}{L_2 - a} + y \right) \quad [A1.3] (81)$$

Then, superposing the fixed-corner deflection, w^F , with the deflection due to the corner rotation, w^R , we have,

RESULTANT DEFLECTION OF THE BIMETALLIC SECTIONS DUE TO ddl

$$\begin{aligned}
 v^L = & \frac{1}{6} \frac{q}{E_1 I_1} \left[(L_1 a)^2 (x-a)^2 - (L_1 a)(x-a)^3 \right. \\
 & + \frac{1}{4} x^4 (4C(x) - 6C^2(x) + 4C^3(x) - C^4(x)) \\
 & - \frac{1}{8} \frac{(L_1 a)^2}{K_1^2} (x-a) (1 + 2C(x) - C^2(x)) \left. \right] \\
 & + \theta^L \frac{(x-a)^2}{L_1 a} \quad \forall x \in [a, L_1] \quad 98
 \end{aligned}$$

$$\begin{aligned}
 v^L = & -\frac{1}{6} \frac{q}{E_2 I_2} \left[(L_2 a)^2 (y-a)^2 - (L_2 a)(y-a)^3 \right. \\
 & + \frac{1}{4} y^4 (4C(y) - 6C^2(y) + 4C^3(y) - C^4(y)) \\
 & - \frac{1}{8} \frac{(L_2 a)^2}{K_2^2} (y-a) (1 + 2C(y) - C^2(y)) \left. \right] \\
 & - \theta \frac{(y-a)^2}{L_2 a} \quad \forall y \in [a, L_2] \quad 99
 \end{aligned}$$

```

PROGRAM CCMOD1
REAL N(2),L(2),LB(2)
DIMENSION W(2),T(2),EI(2),VT(2),VC(2),VD(2),D(2),VTC(2),VID(2),CX
/(2),VTE(7,2,7)

```

```

      VTE(7,2,7),VDE(7,2,7)
      "OUT OF MEMORY" LINK MESSAGE GIVEN WHEN ** 2 ** IS REQUIRED.
      CCMOD1 HAS TO BE RUN IN ** 14 ** STAGES.

```

```

THIS PROGRAM CALCULATES THE DEFLECTION OF A STRUCTURE FORMED BY 4
BIMETALIC STRIPS JOINED TOGETHER BY RIGID CORNERS AND IT COMPARES
THESE PREDICTED RESULTS WITH THOSE OBTAINED EXPERIMENTALLY.

```

```

THE PROGRAM ANALYSES THE EFFECT OF:
1.- TEMPERATURE VARIATION.
2.- LOADING, IN TWO DIFFERENT WAYS:
    2.1 - CONTINUOUS DISTRIBUTION OF LOAD
    2.2 - DISCRETE DISTRIBUTION OF LOAD

```

```

THE LOADS ARE DISTRIBUTED DISCRETELY AT AN EQUAL DISTANCE B OF
EACH OTHER AND AT A DISTANCE B/2 OF THE CORNER END, IN ALL 4 BEAMS

```

```

THE CORNERS LENGTH IS B, ON BOTH SIDES.

```

```

RESULTS ARE GIVEN ONLY FOR THE POINTS WHERE DISCRETE LOADS ARE
APPLIED.

```

```

THE "NORMAL SURFACE" FOR THE ELASTIC BEHAVIOUR OF THE BIMETALIC
BEAMS IS CONSIDERED TO BE AT THE CENTER OF THE CROSSECTION OF
EACH BEAM, THEN:

```

$$I = w \cdot t^3 / 12$$

```

WHERE:

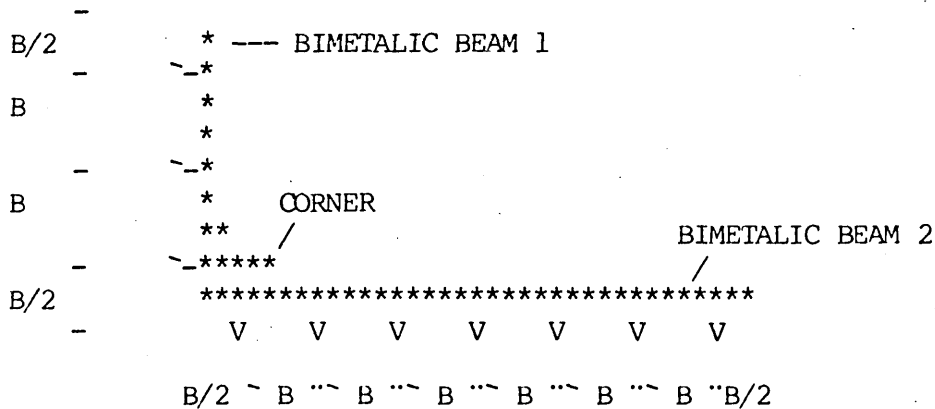
```

- "I" IS THE "SHAPE FACTOR"
- "w" IS THE WIDTH OF THE BIMETALIC BEAM
- "t" IS THE THICKNESS OF THE BIMETALIC BEAM

```

AS THE STRUCTURE IS SYMETRIC, THE ANALYSIS IS SIMPLIFIED TO THE
CONSIDERATION OF 1/4 OF IT, THAT IS, ONE CORNER AND HALF LENGTH OF
EACH BIMETALIC BEAM:

```



C

VTE(2,2,1)=- (0.0+0.5)/2
VTE(2,2,2)=- (2.5+2.5)/2
VTE(2,2,3)=- (3.0+3.0)/2
VTE(2,2,4)=- (3.5+3.0)/2
VTE(2,2,5)=- (3.5+4.0)/2
VTE(2,2,6)=- (3.5+4.0)/2
VTE(2,2,7)=- (4.0+4.0)/2

C

VDE(2,1,1)=0
VDE(2,1,2)=0
VDE(2,1,3)=0

C

C

C

C

VDE(2,2,1)=0

C

VDE(2,2,2)=0

C

VDE(2,2,3)=0

C

VDE(2,2,4)=0

C

VDE(2,2,5)=0

C

VDE(2,2,6)=0

C

VDE(2,2,7)=0

C

C

C

C

C

3: TEMPERATURE = 38,30,39 : DELTA T= APROX.25 (DEG C)

VTE(3,1,1)=(1.0+0.5)/2

VTE(3,1,2)=(3.0+4.0)/2

VTE(3,1,3)=(5.5+5.5)/2

C

VTE(3,2,1)=- (0.5+1.0)/2

VTE(3,2,2)=- (3.0+3.0)/2

VTE(3,2,3)=- (3.5+4.0)/2

VTE(3,2,4)=- (4.0+5.0)/2

VTE(3,2,5)=- (4.0+5.0)/2

VTE(3,2,6)=- (4.5+5.0)/2

VTE(3,2,7)=- (4.5+4.5)/2

C

VDE(3,1,1)=0

C

VDE(3,1,2)=0

C

VDE(3,1,3)=0

C

VDE(3,2,1)=0

C

VDE(3,2,2)=0

C

VDE(3,2,3)=0

C

VDE(3,2,4)=0

C

VDE(3,2,5)=0

C

VDE(3,2,6)=0

C

VDE(3,2,7)=0

C

C

C

C

4: TEMPERATURE = 30,30,30 : DELTA T = 30 (DEG C)

VTE(4,1,1)=(1.0+1.0)/2

VTE(4,1,2)=(3.0+4.0)/2

VTE(4,1,3)=(5.5+5.5)/2

C

VTE(4,2,1)=- (0.5+1.0)/2
 VTE(4,2,2)=- (3.0+3.0)/2
 VTE(4,2,3)=- (3.5+3.5)/2
 VTE(4,2,4)=- (5.0+5.0)/2
 VTE(4,2,5)=- (4.5+4.5)/2
 VTE(4,2,6)=- (4.5+5.0)/2
 VTE(4,2,7)=- (5.0+5.0)/2

C

C

VDE(4,1,1)=0

C

VDE(4,1,2)=0

C

VDE(4,1,3)=0

C

C

VDE(4,2,1)=0

C

VDE(4,2,2)=0

C

VDE(4,2,3)=0

C

VDE(4,2,4)=0

C

VDE(4,2,5)=0

C

VDE(4,2,6)=0

C

VDE(4,2,7)=0

C

C

C

C

C

5: TEMPERATURE = 25,25,25 : DELTA T = 35 (DEG C)

VTE(5,1,1)=(1.0+1.0)/2

VTE(5,1,2)=(3.0+4.0)/2

VTE(5,1,3)=(5.5+5.5)/2

C

VTE(5,2,1)=- (1.0+1.0)/2

VTE(5,2,2)=- (4.0+4.0)/2

VTE(5,2,3)=- (5.0+5.0)/2

VTE(5,2,4)=- (6.0+6.0)/2

VTE(5,2,5)=- (6.0+6.0)/2

VTE(5,2,6)=- (6.5+6.5)/2

VTE(5,2,7)=- (6.5+7.0)/2

C

C

VDE(5,1,1)=0

C

VDE(5,1,2)=0

C

VDE(5,1,3)=0

C

C

VDE(5,2,1)=0

C

VDE(5,2,2)=0

C

VDE(5,2,3)=0

C

VDE(5,2,4)=0

C

VDE(5,2,5)=0

C

VDE(5,2,6)=0

C

VDE(5,2,7)=0

C

C

C

C

6: TEMPERATURE = 20,20,20 : DELTA T = 20 (DEG C)

VTE(6,1,1)=(1.5+1.0)/2

VTE(6,1,2)=(4.0+4.0)/2

VTE(6,1,3)=(6.5+6.5)/2

C

VTE(6,2,1)=- (1.0+1.5)/2
VTE(6,2,2)=- (4.5+4.5)/2
VTE(6,2,3)=- (5.5+6.0)/2
VTE(6,2,4)=- (7.0+7.5)/2
VTE(6,2,5)=- (8.0+8.5)/2
VTE(6,2,6)=- (9.0+9.5)/2
VTE(6,2,7)=- (9.5+9.5)/2

C

C VDE(6,1,1)=0
C VDE(6,1,2)=0
C VDE(6,1,3)=0

C

C VDE(6,2,1)=0
C VDE(6,2,2)=0
C VDE(6,2,3)=0
C VDE(6,2,4)=0
C VDE(6,2,5)=0
C VDE(6,2,6)=0
C VDE(6,2,7)=0

C

C

C

C

C

C

7: TEMPERATURE = 15,15,15 : DELTA T = 45 (DEG C)

VTE(7,1,1)=(1.5+1.5)/2
VTE(7,1,2)=(5.0+5.0)/2
VTE(7,1,3)=(7.0+7.0)/2

C

VTE(7,2,1)=- (1.5+1.5)/2
VTE(7,2,2)=- (5.0+5.0)/2
VTE(7,2,3)=- (6.5+7.0)/2
VTE(7,2,4)=- (8.5+9.0)/2
VTE(7,2,5)=- (9.5+10.5)/2
VTE(7,2,6)=- (10.5+11.5)/2
VTE(7,2,7)=- (11.5+12.0)/2

C

C VDE(7,1,1)=0
C VDE(7,1,2)=0
C VDE(7,1,3)=0

C

C VDE(7,2,1)=0
C VDE(7,2,2)=0
C VDE(7,2,3)=0
C VDE(7,2,4)=0
C VDE(7,2,5)=0
C VDE(7,2,6)=0
C VDE(7,2,7)=0

C

DO 99 KDT=1,7
DT=5*(KDT+2)
K1=2
K2=10
K3=DT
K=K1*10000+K2*100+K3

```

C      TIN=60.0
C      WRITE(2,20)K,K1,CS,CS,E,E,B,B,L(1),L(2),W(1),W(2),T(1),T(2),K2,Q,K
/3,DT,TIN
C
C
C      INITIAL CALCULATIONS:
C
C      CST=2*CS*DT
C      DO 2 I=1,2
C      N(I)=L(I)/B
C      LB(I)=L(I)-B
C      EI(I)=E*W(I)*T(I)**3/12
2 CONTINUE
C
C      WRITE(2,21)CST,N(1),N(2),LB(1),LB(2),EI(1),EI(2)
C
C
C      CORNER ROTATION ANGLES:
C
C      TT=CST*LB(1)*LB(2)*(EI(2)/T(2)-EI(1)/T(1))/(EI(1)*LB(2)+EI(2)*LB(1
/))
C
C      TL=Q*LB(1)*LB(2)*(L(1)**2*(N(1)**2-1)+B*L(1)*(N(1)-1))/3/(EI(1)*LB
/(2)+EI(2)*LB(1))
C
C      WRITE(2,22)TT,TL
C
C
C      DEFLECTION TABLE
C
C      WRITE(2,23)
C
C
C      DEFLECTION AT HALF CORNER LENGTH
C
C      X=B/2
C      DO 3 I=1,2
C      D(I)=0
C      VT(I)=TT*X*(-1)**I
C      VC(I)=TL*X*(-1)**I
C      VD(I)=VC(I)
C      VTC(I)=VT(I)+VC(I)
C      VTD(I)=VTC(I)
3 CONTINUE
C
C      EXP1=VTE(KDT,1,1)
C      EXP2=VTE(KDT,2,1)
C      VTDE1=0.0
C      VTDE2=0.0
C      IX=X
C      WRITE(2,24)IX,VT(1),EXP1,VC(1),VD(1),D(1),VTC(1),VTD(1),VTDE1,VT(2
/),EXP2,VC(2),VD(2),D(2),VTC(2),VTD(2),VTDE2
C

```

C
C
C

DEFLECTION OF THE BIMETALIC BEAMS:

```
NF=N(2)-1
DO 5 KN=1,NF
DO 4 I=1,2
IF(KN.GE.N(1).AND.I.EQ.1) GO TO 13
X=KN*B-B/2
CX(I)=LB(I)*KN/X/(N(I)-1)
VT(I)=TT*(B+X-X**2/LB(I)/2)*(-1)**I
VC(I)=Q*((LB(I)*X)**2-LB(I)*X**3+X**4/4)/6/EI(I)+TL*(X+B-X**2/2/LB
/(I))*(-1)**I
D(I)=Q*(X**4*(4*CX(I)-1-6*CX(I)**2+4*CX(I)**3-CX(I)**4)/4-(LB(I)*X
//(N(I)-1))**2*(1+2*CX(I)-CX(I)**2)/8)/6/EI(I)*(-1)**I
VD(I)=VC(I)+D(I)
VIC(I)=VT(I)+VC(I)
VTD(I)=VT(I)+VD(I)
GO TO 4
```

C

```
13 VT(1)=0.0
VC(1)=0.0
D(1)=0.0
VD(1)=0.0
VIC(1)=0.0
VTD(1)=0.0
KNC=KN+1
VTE(KDT,1,KNC)=0.0
```

C

4 CONTINUE

C

```
X=X+B
KNC=KN+1
EXP1=VTE(KDT,1,KNC)
EXP2=VTE(KDT,2,KNC)
VIDE1=0.0
VIDE2=0.0
IX=X
WRITE(2,24)IX,VT(1),EXP1,VC(1),VD(1),D(1),VIC(1),VTD(1),VIDE1,VT(2
/),EXP2,VC(2),VD(2),D(2),VIC(2),VTD(2),VIDE2
```

C

```
5 CONTINUE
WRITE(2,25)
9 CONTINUE
```

C

99 CONTINUE

C

C

C

C

```
20 FORMAT(7X,'BIMETALIC BEAMS MODEL PREDICTIONS '/7X,'EXPERIMENT NUM
/BER ',I5//7X,'DATA:',27X,'BEAM 1',15X,'BEAM 2'//8X,I1,' DEFLECTIO
/N CONSTANT',5X,E10.3,' 1/DEG C ',E10.3,' 1/DEG C '/10X,'ELASTICIT
/Y COEFFICIENT',2X,E10.3,' KG/MM**2',1X,E10.3,' KG/MM**2'/10X,'BASI
/C LENGTH MODULE B',5X,F8.1,1X,'MM',9X,F8.1,1X,'MM'/10X,'LENGTH',20
/X,F8.1,1X,'MM',9X,F8.1,1X,'MM'/10X,'WIDTH',21X,F8.1,1X,'MM',9X,F8.
```

```

/1,1X,'MM'/10X,'THICKNESS',17X,F8.1,1X,'MM',9X,F8.1,1X,'MM'//7X,I2,
/' LOAD',16X,E10.3,' KG/MM'/7X,I2,' TEMPERATURE VARIATION',4X,F5.1,
/1X,'DEG C',5X,'(COOLING DOWN FROM ',F4.1,' DEG C)')
21 FORMAT(//7X,'INITIAL CALCULATIONS:          CST =' ,E10.3/35X,'N(1) =
/' ,E10.3/35X,'N(2) =' ,E10.3/35X,'LB(1)=' ,E10.3/35X,'LB(2)=' ,E10.3/3
/5X,'EI(1)=' ,E10.3/35X,'EI(2)=' ,E10.3)
22 FORMAT(//7X,'CORNER ROTATION DUE TO TEMPERATURE VARIATION =' ,F7.4,
/' RADIANS'/7X,'CORNER ROTATION DUE TO LOAD',18X,'=' ,F7.4,' RADIANS
/')
23 FORMAT(//5X,'PREDICTED AND EXPERIMENTAL DEFLECTIONS (ALL RESULTS A
/RE GIVEN IN MILLIMETERS)'/9X,'BEAM 1: ',27X,'BEAM 2:'//6X,'X',2X,'*
/*VT1**',2X,'V1 V1 D1',1X,'VIC1 **VD1*',3X,'**VT2***',1X,'VC2 V
/D2 D2',2X,'VIC2 **VD2**'/9X,'TEO EXP',18X,'TEO EXP  TEO EXP',
/21X,'TEO EXP'/)
24 FORMAT(5X,I3,2F4.1,F5.1,F4.1,F4.1,3F4.1,F6.1,3F5.1,F4.1,3F5.1/)
25 FORMAT(//////////)

```

C
C

```

CALL EXIT
END

```

A3.1 CONTINUOUS CASTING HAZARDS

MOLTEN METAL/SLAG SPLASH

Temperature checks of the molten metal in the ladle while at its casting position produces splashes which put directly at risk the casting operators working below.

The thermocouple lance and in particular the thermocouple tip should be selected so as to reduce the amount of steel splash. Alternative means of measuring the temperature should be considered. In some work stations cover has been provided to stop molten steel splash from reaching the mould operators. The cover provided in these cases, however, aggravates other hazards, such as that of a ladle breakout, because it restricts visibility of the ladle without providing any effective protection against a major molten metal fall. Protective clothing provides some protection against splash, it is at present necessary but cumbersome for working exposed to heat.

Sampling is another source of molten metal splash. The use of suction sampling devices helps to reduce the risk.

Additions to the molten metal during the casting operation should be minimized in as much as alternative procedures exist. Whenever they are necessary their potential to generate molten metal splash should be minimized

Fishing of clogged slag in the mould should again be minimized if not eliminated by improving the casting process.

Cleaning nozzle/sliding gate with an oxygen lance during casting is a major source of splash and other hazards.

Example: A technique used for open pouring involves using a nitrogen shroud. Nitrogen is blown within a double cylinder which is placed surrounding the metal stream. A problem arises because solid metal cleaned out of the nozzle mouth falls into the enclosed cavity below and the only way to clear it is by removing the whole cylinder against the metal stream an operation which is bound to be quite dangerous. In its present form the technique is clearly unsafe

MOLTEN METAL OVERFLOW

Various conditions can lead to an overflow of the tundish or the mould. An overflow tank for the tundish and facilities to divert the molten steel stream at any time during casting must be provided. An emergency container able to hold the full content of the ladle must be ready to receive the molten metal. Manual control must be able to override computer controlled casting at any time as the later will fail under unstable conditions. Sliding gates must fail safe. that is the hydraulic pressure opening the gate must act against springs able to close the gate in case of any failure in the system.

BREAKOUT

The ladle and the tundish can breakout because of wear or defect in the refractory lining. It is essential for the safe life of the refractory lining to be well established. A careful follow up of the use of the ladle must be kept in as much as it affects it's safe life. The ladle must be thoroughly inspected before and after each cast. To prolong the use of a ladle beyond it's safe life can not be justified by cost arguments because there is no way to tell when or where it may breakout.

The mould may breakout because of a failure of the water cooling system, a power failure or other reasons. Adequate emergency supply of water (a gravitation tank) and power (diesel engines starting immediately a power failure occurs) are required. The major risk of a mould breakout is that it can entail a strand breakout of serious consequences.

Average strand breakout rates of up to 8 breakouts per 100 cast are reported in the literature.(1) This is perhaps the major potential hazard involved in the continuous casting of steel as was illustrated by the violent water/metal explosions which followed a mould wall steam explosion some years ago in an industrial continuously casting installation. This incident is considered further in Section A3.2 . Strand breakouts are usually followed by explosions of lesser magnitude than those reported in that incident and the casting crews with whom I had the opportunity to discuss the matter seem to have got used to the "bang" and the flames which follow a breakout. Spray

chambers can be seen to be fortified to a certain extent but I could not avoid feeling quite insecure standing on a bridge on top of the spray chamber while the casting operators told me of their stunt experience

WATER/METAL EXPLOSIONS

Water, even as moisture, represents a serious danger when molten metal has to be handled. The entrapment of water under a mass of molten steel leads to a "vapour explosion", or water/metal explosion, as vapour is produced in times of the order of one-thousandth of a second. The resulting damage is caused by the shock wave which is generated. These vapour explosions are different from so called "steam explosions" when the production of steam over a much longer period of time (measured in tenth of a second) exerts a very strong pressure, without a shock wave. Vapour explosions are much more violent, they are also called "catastrophic explosion" as they have been known to wreck a whole industrial plant.(2)

Water/metal explosions have occurred in many different areas of steel plants from furnaces to floor. An essential measure in the case of a ladle breakout is to take it as quick as possible to a dry and otherwise safe area. It is not surprising that explosions occur inside the spray chamber which is by definition full of water when molten metal pours into it after a strand breakout. What is surprising is that they are not more violent

NOXIOUS FUMES AND DUSTS

The danger to health of substances such as casting powders, lubricating oil, tundish powder, phosphate esters (hydraulic system), spray water additives which are directly used for the continuous casting process and of others which are associated to the plant such as refractory dust and the fumes and dust of the electrical arc furnaces, can not be dismissed. Proper ventilation is required

HEAT

Radiant heat is known to affect the organism in various ways. long term effects on the heart and blood pressure have been reported and ocular cataracts have been associated to infrared radiation. Heat represents a short term hazard in that it reduces the capacity of the individual to react rapidly to danger and also in that it weakens the person. Exposure to heat should be minimized.

NOISE

Continuous casting machines do not tend to be noisy appart from the cutting station where the operator can be protected by a sound proof booth. But it is often the case that the electrical arc furnaces which are extremely noisy are situated close to the casting station.

A3.2 EXPLOSIONS AT A CONTINUOUS CASTING PLANT

A steam explosion occurred within one side of a 1280 mm x 150 mm mould on a continuous casting machine some 7 minutes after start of casting. All men were thrown off the machine and back against the rear wall of the operational platform. The cause of this explosion was later associated to a failure in the water cooling system. Between 5 to 10 seconds after the first explosion there was a second explosion which blew them off their feet and which was followed by a third explosion. The tundish teemer described the incident -

"The first explosion came from the top of the mould and I knew what was coming next. The second explosion blew me into the caster helper and I covered my head and ran. As I ran along the walkway there was a third explosion and molten metal was coming down on us like bullets "

The explosions were heard several miles away. The six tons tundish was lifted out of its stand and moved two feet. Eight men were injured fortunately not too seriously.

The Safety Inspector reported his examination of the remains of the slab: "It was almost exactly 5 metres long. The rear and side walls of the top of the billet was intact but the molten core and front wall was missing."

Further information extracted from the casting charts is given in his report :

Casting Temperature = 1550 'C

Casting speed = 0.75 m/min

Secondary spray water flow increased from 980 min⁻¹ to 1550 min⁻¹ just one minute after start of casting (900-1000 min⁻¹ would be the normal flow)

No flow measurement was recorded for the rear mould cooling wall and temperature difference in/out the mould only just commenced rising (approximately 2'C)

Mould front wall water flow = 4800 min⁻¹

Temperature difference in/out of mould = 5'C

but it is pointed out that the thermometers had only just started recording.

Mould side walls water flow = 2200'C

Temperature difference in/out of mould = 5'C

The initial investigation carried out by the Steel Plant Managers produced the below Theory, but this was not accepted by Senior Management

When the secondary water flow increased the pressure also increased up to 4 BARS. If there was any defect or slag in the wall of the cast billet or any defect in the spray pattern it would be possible for the water to penetrate the billet and this could cause a violent water metal explosion.

The Safety inspector suggests as an alternative explanation that a water cooling fault on the back wall could result in

overheating and a steam explosion which could be followed by a water/metal explosion.(...)

But the cast back wall of the billet is intact and there is no sign of loss of cooling and any loss of cooling should surely cause a breakout or some sort of problems.

The Theoretical model presented in the Thesis suggests an explanation which satisfies the observations made both by the Plant Managers and the Safety Inspector

It seems reasonable to accept that the first explosion was related to a water failure and the 75% increase in the spray cooling water flow was probably related to the reduction of the water flow in the rear face of the mould.

The Theoretical model at its present stage of development is not properly equipped to make proper predictions in a situation as this, but it provides a basic understanding of what could have been involved. The Safety Inspector points out that the cast back wall does not present sign of loss of cooling which he relates to a break out of the back wall. But the loss of cooling needs not be that significant to generate surface cracks on the front face of the slab. A lesser thermal contraction of the rear face results in additional moments on the front face which aggravate the build-up of stresses. As soon as the slab section comes out of the mould, it is subjected to an abnormal cooling from the water sprays. Furthermore the metallostatic pressure is probably reduced

because of the metal blown out by the first explosion. Under these circumstances the moments along the front face could well have been reverted rapidly at mould exit and any surface crack would be closed -with water trapped inside. The fact that the front face was neatly removed from the slab suggests that surface cracks were located near both front corners. This would also explain why the third explosion was the most violent as it implies that the bulk of the core was released suddenly and must have trapped water on its way out.

The conditions of this accident were in many ways special, but the risk of a catastrophic explosion to occur in the spray chamber can not be discarded.

The photographs presented in this and the next pages illustrate something which has already happened at least once.

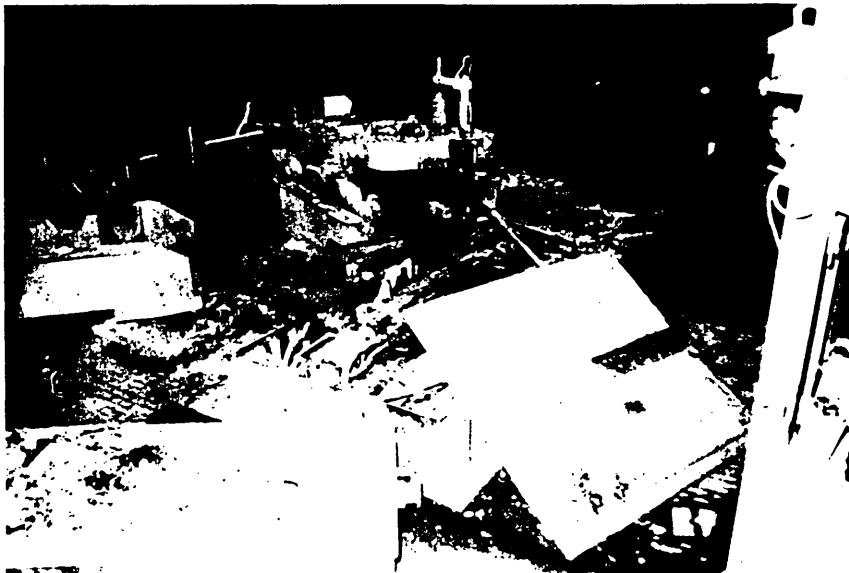


Photo. 1 : CASTING PLATFORM AFTER EXPLOSION



Photo. 2 : CASTER N.2 IN OPERATION

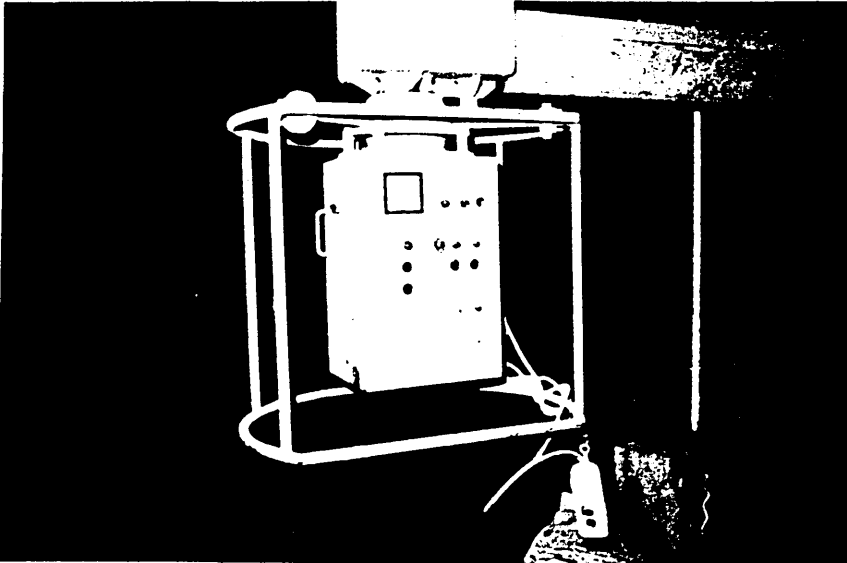


Photo. 3 : CASTER'S CONTROL PANEL



Photo 4 : CAST IN PROGRESS

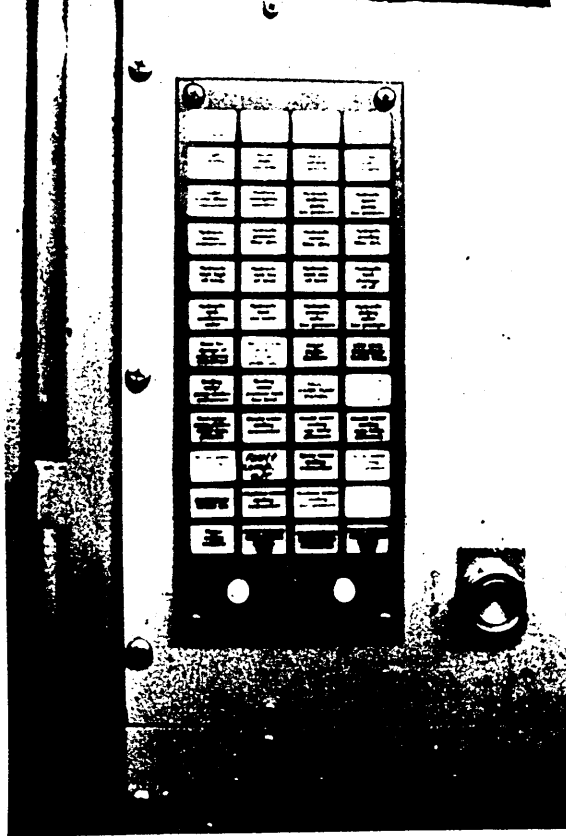


Photo. 5 : ALARM PANEL



Photo. 6 : DAMAGED MOULD.

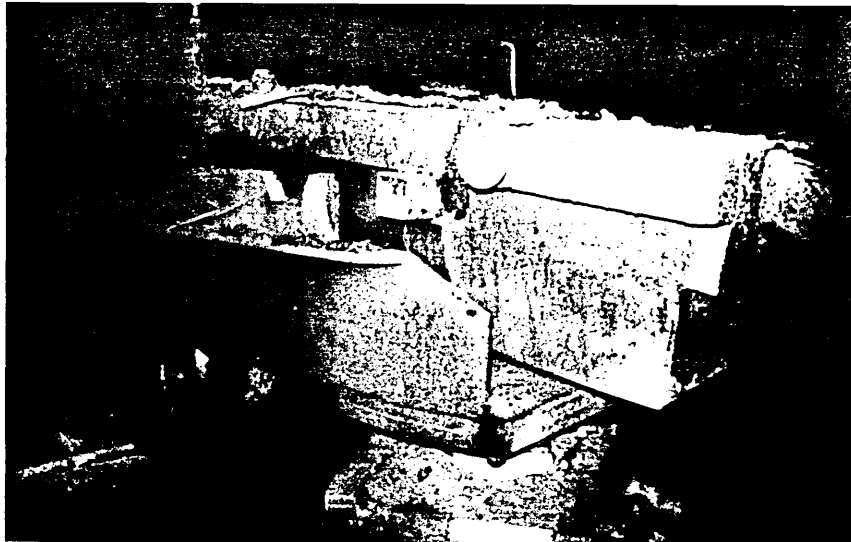


Photo. 7 : TUNDISH BLOWN OUT OF TRUNION SUPPORT FRAME



Photo. 8 : CONTROL ROOM



Photo. 9 : DAMAGED BACK WALL INDICATING INTERNAL STEAM EXPLOSION



Photo. 10 : DAMAGED END OF BILLET SHOWING BACK AND SIDE WALL INTACT

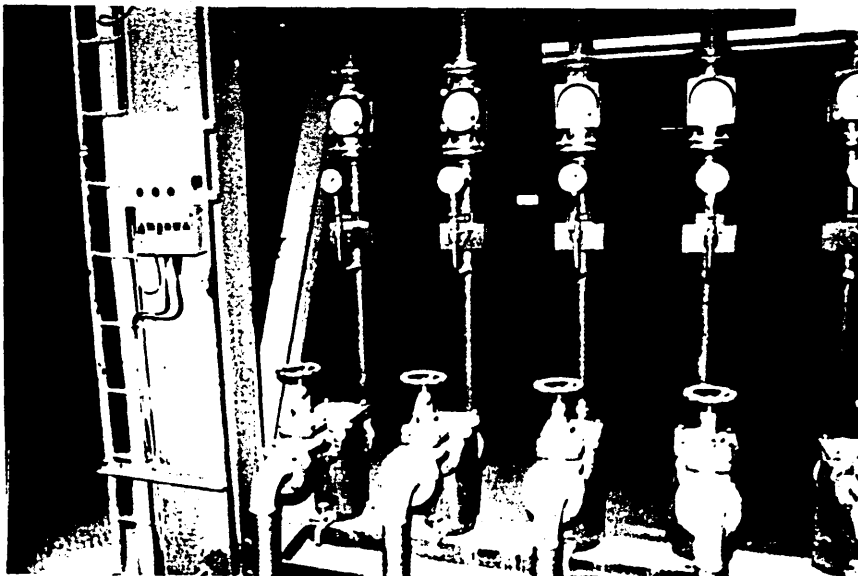


Photo. 11 : WATER VALVES AND LOCAL FLOW METERS

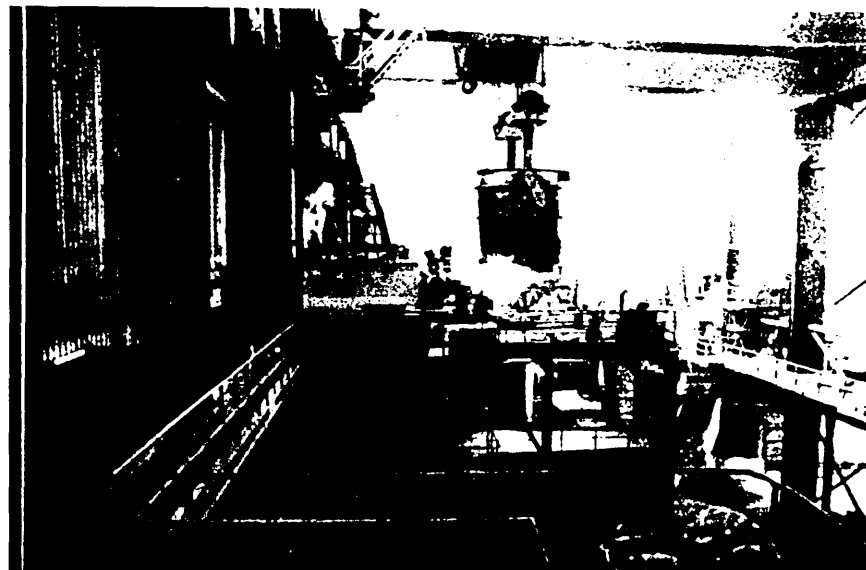


Photo. 12 : CASTER N.2 IN OPERATION (NOTE MEANS OF SCAPE)



Photo. 13 : DAMAGED BACK WALL OF MOULD INDICATING INTERNAL EXPLOSION

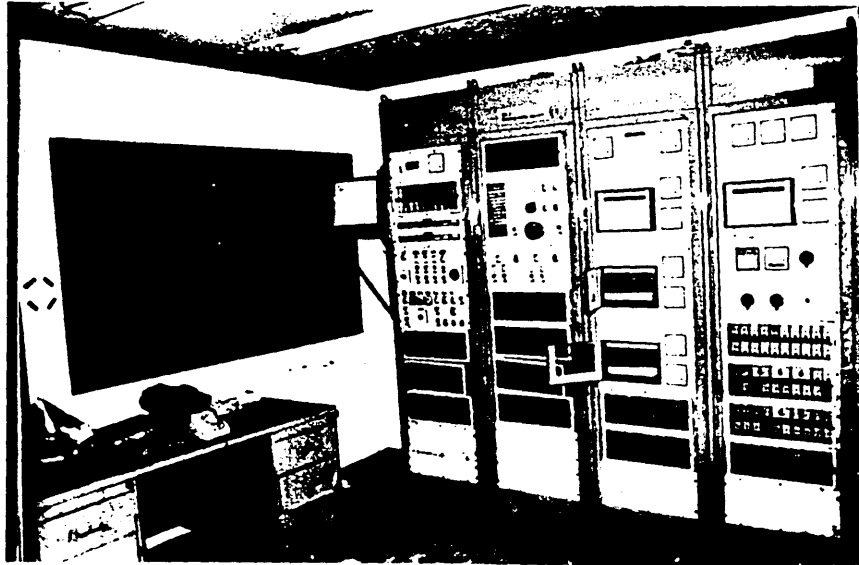


Photo. 14 : CONTROL ROOM PANELS



Photo. 15.: SPRAY FLOW WATER METER